Università degli Studi di Padova

Dipartimento di Scienze Chimiche

CORSO DI DOTTORATO DI RICERCA IN SCIENZE MOLECOLARI

CURRICOLO SCIENZE CHIMICHE

XXX CICLO

Steps forwards to a new type of oncotherapy: from the solution chemistry of Au(III)-dithiocarbamato complexes to the design and development of innovative Au(III)- and Cu(II)-based cancer-targeting agents

Ricerca supportata finanziariamente da T.R.N. Imballaggi S.r.l. (Schio-VI)

Coordinatore: Ch.mo Prof. Leonard Jan Prins

Supervisore: Ch.mo Prof. Dolores Fregona

Valutatori: Ch.mo Prof. Simonetta Geninatti Crich (Università degli Studi di Torino)

Ch.mo Prof. Claudia Pellerito (Università degli Studi di Palermo)

Dottorando: Nicolò Pettenuzzo

Dedicata alla mia famiglia.

"We are all mortal
until the first kiss
and the second glass of wine"
Eduardo Galeano

"England expects that every man will do his duty"
Admiral Lord Horatio Nelson,
just before the Battle of Trafalgar (October 21th, 1805)

INDEX

Abstract

In order to overcome the side effects of the chemotherapy, but remaining firmly convinced in the powerful role of the medicinal inorganic chemistry, Fregona's research group, since 2000, developed a series of metal-based dithiocarbamato molecules, in particular containing Au(III), Ru(III) and Cu(II) metal centers, which are highly active in vitro toward a great number of human tumor cell lines and less toxic in vivo, compared to other chemotherapeutics. Although several insights into the chemistry of these powerful coordination compounds were performed in last years, some aspects remain to be elucidating.
In the first part of this work, we present a comprehensive study concerning the synthesis, the characterization and the solution behavior of eight Au(III) dithiocarbamato complexes, revealing their peculiar and fascinating chemistry. Moreover, seven of them showed interesting biological properties in vitro toward a selected human tumor cell line.
The second part of the Ph.D. research was focused on the synthesis, characterization and biological evaluation of novel bio-conjugated Au(III) and Cu(II) complexes with the aim of improve the accumulation of the anticancer metal payload into malignant cells. In order to reach this goal, carbohydrates were chosen as targeting agents, exploiting the Warburg effect, that stimulates the majority of the neoplastic cells to overexpress the glucose-transporter proteins (in particular GLUTs) in their phospholipid bilayer. We decided to functionalize the dithiocarbamato moiety connecting it to the C-1 position of three different carbohydrates: D-glucose, D-galactose and D-mannose. On the whole, nine different complexes were synthetized and tested as anticancer agents.
Intriguingly, one of them proved a high cytotoxic activity toward a selected human tumor cell line, paving the way to future studies investigating the role of the carbohydrate-functionalization in the selective targeting of the complex toward cancerous tissues.

Sinossi

Al fine di superare gli effetti collaterali della chemioterapia, ma rimanendo fortemente convinti del ruolo potente che può svolgere la chimica inorganica applicata alla medicina, la Prof.ssa Fregona e i suoi collaboratori si sono occupati, fin dai primi anni 2000, dello sviluppo di una serie di molecole a base metallica con leganti ditiocarbammici, in particolare contenenti centri metalli quali Au(III), Ru(III) e Cu(II). Queste si sono rivelate altamente attive *in vitro* verso un gran numero di linee cellulari tumorali umane e meno tossiche, *in vivo*, rispetto ad altri chemioterapici di uso clinico.

Benchè negli ultimi anni siano stati condotti diversi studi approfonditi sulla chimica di questi potenti composti di coordinazione, alcuni aspetti rimangono ancora da spiegare. Nella prima parte di questo lavoro, si presenta uno studio completo sulla sintesi, la caratterizzazione e sulla chimica in soluzione di otto complessi ditiocarbammici di Au(III), che hanno rivelato una reattività peculiare ed affascinante. Inoltre, sette di essi hanno dimostrato interessanti proprietà biologiche *in vitro* verso una linea cellulare tumorale del cancro colon-rettale.

Nella seconda parte del progetto di dottorato, il lavoro si è focalizzato sulla sintesi, la caratterizzazione e la valutazione biologica di nuovi complessi ditiocarbammici di Au(III) e Cu(II), bioconiugati con una funzione molecolare targettante, con l'obiettivo di migliorare l'accumulo di questa classe di molecole all'interno delle cellule cancerose. Al fine di raggiungere questo obiettivo, sono stati scelti i carboidrati come agenti di targeting, sfruttando l'effetto Warburg che stimola la maggior parte delle cellule neoplastiche a sovrapresprimere le proteine trasportatrici del glucosio (in particolare le cosiddette GLUT) sulla loro membrana cellulare. Si è deciso di funzionalizzare il legante ditiocarbammico collegandolo, tramite spacer, al carbonio C-1 di tre diversi carboidrati: D-glucosio, D-galattosio e D-mannosio. Nel complesso, sono stati sintetizzati nove diversi composti di coordinazione che sono stati testati come agenti antitumorali *in vitro*. Fra questi, uno di loro ha dimostrato un'elevata attività citotossica contro una linea cellulare tumorale, aprendo la strada a futuri studi che indagheranno il ruolo della funzionalizzazione dei carboidrati nel targeting selettivo del complesso verso i tessuti cancerosi.

Introduction

Nowadays, literature is still silent on a general comprehensive model of neoplasia that incorporates deep and complicate issues as etiology, mechanisms of action and morphological changes from a normal to a malignant cell. Cancer epidemiologists studying cancer etiology, scientists studying carcinogenesis, molecular biologists studying cell mutations, and histopathologists studying malignant transformation, have until recently been largely working in isolation, hence a unified and complete model describing the nature of neoplasia and its causes has never been developed yet. Considering the dictum of Ockham (1300-1348), usually referred to as "Ockham's razor", stating that "Entities should not be multiplied beyond necessity" (*Quodlibeta Septem,* 1320),[1] the concept of identifying common characteristic between diverse types of neoplasia and of using an economy of hypotheses in determine cancer causes is undoubtedly spreading into modern scientific thinking. The application of this doctrine is hampered by the complexity of human nature, which is composed by an enormous number of intricated and multifaceted chemical transformations, making the human knowledge perennially limited and too focused to be able to understand the thousands of reasons triggering a single symptom, particularly in cancer.

1. The hallmarks of cancer: the identification of common characteristics

Taking into account the previous considerations, cancer is usually defined as the neo-formation of somatic cells without the control of their own development and with the capacity of un-limited growth.[2]

It is currently believed that cancer is a multistep process involving the interaction between genes and their environment and is caused by a series of genetic mutations, inherited during cell replication, in different genes of a single somatic cell. In spite of the great variety of known neoplasm, scientists have determined some traits (hallmarks) that are common to all of them (**Figure 1**).[3]

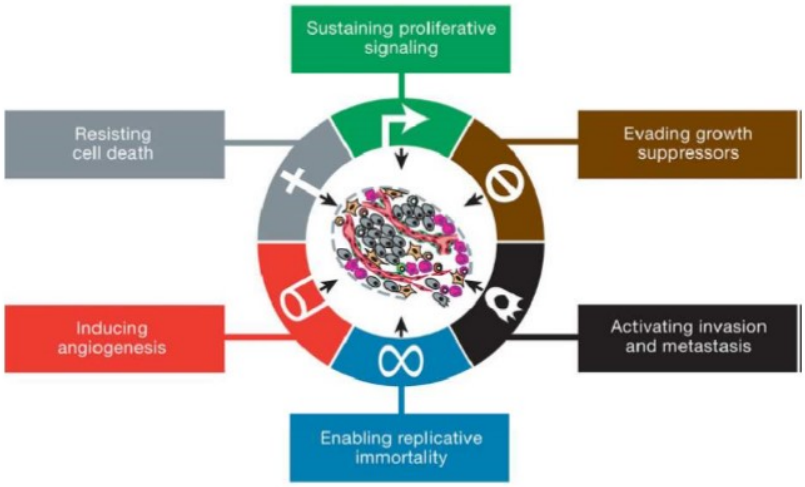

Figure 1: of six hallmarks characteristic of all cancer types.

As a matter of facts, the most common fundamental trait of cancer cells is their ability to sustain chronic proliferation. Contrarily to normal cells, malignant counterparts lose the control on the production and release of growth-promoting signals, thus entering and progressing through the cell life cycle in an unregulated way. The unbalanced homeostasis is largely due to the release of mitogenic signals and the conveyance of growth factors to neighboring cells. In the extracellular matrix, growth factors bind to cell-surface receptors, which trigger intracellular signaling pathways involved in cell growth and function. Likewise, these stimuli may be sent to normal cells within the supporting cancer-associated stroma, which reciprocate by supplying the neoplastic cells with several growth factors. Interestingly, some somatic mutations are known to enhance receptor signaling by either up-regulating the receptor proteins at the cancer cell surface or structurally changing the receptor molecule, thus making such cells hyper-responsive to growth factors.[4,5]

Moreover, to induce and sustain positive growth-stimulatory signals, tumor cells must also circumvent programs that negatively regulate cell proliferation. In this regard, the silencing of many tumor suppressor genes which operate in various ways to limit cell growth and proliferation have been discovered in different cancers. For example, the silencing of the *TP53* and *RB1*, the two main onco-suppressor genes, leads to the subexpression of p53 (tumor protein 53) and pRb (retinoblastoma-associated) proteins. The latter is involved in the regulation of the cell growth-and-division cycle, and it is known to inhibit the cell from replicating damaged DNA, by preventing its progression along the cell cycle through G1 (first gap phase) into S (synthesis phase). When the genes encoding for these proteins are

mutated, the translated protein is dysfunctional, causing a persistent cell proliferation.[3] Similarly, TP53 is a tumor suppressor protein that plays a crucial role in regulating cell cycle, and has been also described as "the guardian of the genome" because of its role in conserving stability by preventing genome mutation functioning, thus acting as a tumor suppressor.

Another important common characteristic among different tumors, is the remarkable ability of neoplastic cells to resister to cell death, in particular apoptosis. In fact, functional studies conducted over the last decades proved apoptosis to be a natural barrier to cancer development in normal cells.[6] Various physiological stresses experienced during their tumorigenesis or as a result of anticancer therapy, trigger the programmed-cell-death process. The main apoptosis-inducing stresses derive from signal imbalances as high levels of oncogene signaling and DNA damage associated with hyperproliferation. The apoptotic machinery is composed by both upstream and downstream effector components, whilst the regulators can be divided in those receiving and processing extracellular death-inducing signals (extrinsic apoptotic pathway involving, for example, Fas ligand/receptor) and those sensing and integrating a variety of signals of intracellular origin (the intrinsic program).[3]

Furthermore, malignant transformation can trigger the enabling of the replicative immortality. Actually, normal cells can pass only through a defined number of subsequent cell growth and division cycles. At the end of its life, the cell enters into a phase of senescence, characterized by the entrance in a non-proliferative but viable state, and ultimately passes to a crisis condition, which results in cell death. Nonetheless, it is possible that cells, when in the crisis phase, revert to a proliferating state with an unlimited replicative potential. This transition is called immortalization[3] and depends strictly from the action of telomeres, hexanucleotide repeats protecting the ends of chromosomes.[7,8] In normal cells they serve as "clocking" device, since are progressively shorten during duplication until leaving chromosomal DNA unprotected from end-to-end fusions, thus triggering apoptosis. In neoplastic cells this control is lost, since they are able to maintain telomeric DNA long enough to avoid the induction of senescence or of apoptosis, usually upregulating the expression of telomerase. This enzyme is almost absent in normal cells, but was found expressed at functionally significant levels in cancer cells. By lengthening telomeric DNA, the tumor cell will not experience the progressive telomere erosion.

Another characteristic of cancer cell is the ability of stimulate the sprouting of new blood vessels from existing ones (called angiogenesis) to absorb more oxygen and nutrients, as well

as discharging metabolic wastes and carbon dioxide. In normal adult cells, angiogenesis is activated transiently only for wound healing and female reproductive function cycle. Instead, during malignancy the angiogenesis is always activated and consists in the continuous developing of new vessels from the existing vasculature.[9]

However, one of the most impressive feature of a neoplastic cell is the enhanced capability in inducing metastasis. In fact, the process of invasion and metastasis comprehends a series of discrete biological changes, starting with local invasion, intravasation of malignant cells into neighboring blood and lymphatic vessels and transit of the cells through the lymphatic and circulatory systems. These processes are followed by escape of cells from the lumina of such vessels into the parenchyma of distant tissues (extravasation), formation of small nodules of cancer cells, called micrometastases, and ultimately by growth of their lesions to yield macroscopic tumors (colonization).[3]

2. Causes of cancer: the multi-causal model

In **Figure 2** is shown the schematic explanation of the Multi-causal model in a simple form. This model indicates the main causes which might act on one or more mechanisms of neoplasia, and these mechanisms are responsible for shifting a normal cell into a malignant cell.

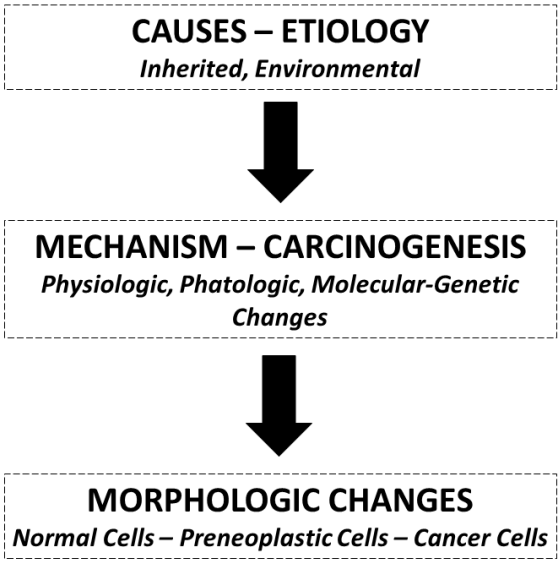

Figure 2: A general model of cancer causes, mechanisms of action and morphologic changes.

Causes – Etiology

The causes triggering cancer can be divided into inherited causes and causes acquired during life. The inherited causes are genetically expressed and are therefore the primary cause of the molecular genetic changes. The acquired causes are environmental factors such as smoking, alcohol consumption, exposure to asbestos, radiation, dietary factors, drugs, chemicals, and others.[10]

Mechanisms of Action - Carcinogenesis

The various causal factors can be depicted as being responsible for several pathophysiologic alterations in the environment of the target cell. This altered milieu is then responsible for a series of distinct genetic changes or mutations of the dividing cell, which results in progression from a normal cell to a malignant cell. For example, the demonstration of mutations in the tumor-suppressor gene p53 among tobacco users who develop oral cancer and oral precancer was the first time in which a cause was connected with a tumor gene mutation.[11-13]

Morphological Changes

An increase in the number of cells, and an intensification in the rate of cell division has been postulated to be definitely related to carcinogenesis in general.[3] Morphological changes have been well correlated with a series of mutations in a number of cancers, and in particular, in colorectal cancer. Morphologic changes imply a sequence of events from a normal cell to a hyperplastic cell, to a dysplastic cell, to a carcinoma, and then to invasion and metastasis. A second pathway of changes may be from a normal cell to a benign tumor, such as an adenoma, and then to a carcinoma.[14]

3. Cancer: an epidemic disease

Nowadays, from the epidemiological point of view, cancer is the first leading cause of death worldwide followed by strokes and ischemic attacks, which compose the two main cardiovascular diseases. As a matter of fact, 32.5 million adults in the world will be diagnosed with cancer in 2017 (around 2 of them in the U.S.), and 8.2 million deaths for malignancies were counted in the same year.[15] According to the last report (2014) of the World Health Organization,[16] cancer deaths will keep rising to an estimated 10 million people dying from cancer in 2017 (among them, 600 hundred in the United States only), and more than 13

million dying in 2030[17]. In particular, Europe seems to be one of the most affected area, inasmuch has around one-quarter of the global cancer cases, even though it comprises only one-eighth of the total world population (**Figure 3**). In fact, approximately 20% of all deaths in the European Union are caused by neoplastic diseases,[18] with an increase of 3.2 million new patients per year. In Italy in 2016 the malignancies have been diagnosed in around 365.000 people, approximately 1.000 new cases/day. In particular, in the same year, breast neoplasia was the most frequent cause of cancer death in women (17% of total deaths), whereas trachea, bronchus, lung cancers were the leading causes of tumor deaths in men (26% of total). For both sexes, the colon and rectum were the second most commonly malignancy-affected organs. Cancer of prostate and respiratory apparatus ranked third in males and females, respectively.[19]

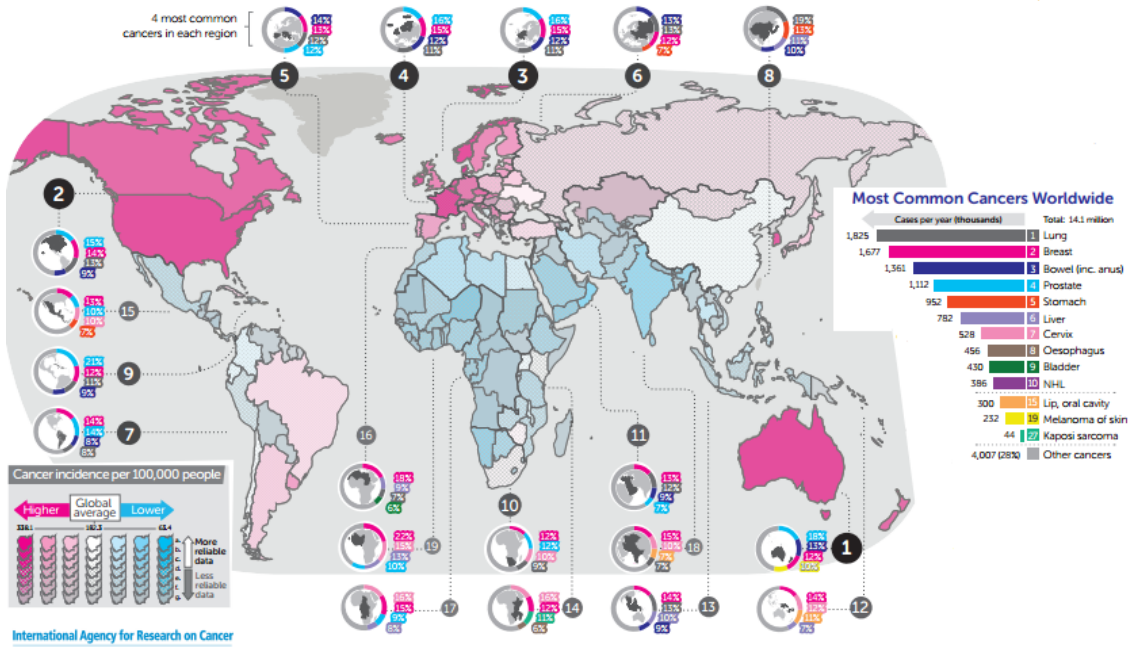

Figure 3: Schematic map of the worldwide cancer incidence in 2012. This image is provided by Cancer Research Organization, UK.[15]

However, through screening, early detection and adequate treatment many cancers can be cured. Traditional cancer treatments are surgery (to remove solid tumors), radiotherapy and chemotherapy, the latter killing the rapidly dividing cancerous cells by radiation or using drugs, respectively. A major drawback of traditional anticancer agents is the onset of serious side-effects (*e.g.*, nausea, weight loss, hair loss and severe fatigue), due to the destruction of

healthy cells that normally divide at a fast rate, including cells in the intestinal mucosa, follicle hair cells, and bone narrow cells.[20]

4. The life-driving contribution and the medicinal potentialities of inorganic chemistry

In the last century, some key discoveries have unlocked a new era for the research of the inorganic compounds in biological field, ranging from paleo-biological interests to medicinal applications.[21-25] To date, twenty-five elements are thought to be essential for mammalian biochemistry, namely H, C, N, O, F, Na, Mg, Si, P, S, Cl, K, Ca, V, Mn, Fe, Co, Ni, Cu, Zn, As, Se, Mo, Sn and I.[21,26,27] However, the biochemistry of some elements, such as Si, V, Mn, Ni, As and Sn, is poorly understood.[28] Remarkably, essentiality is not associated only with the element itself, but with specific compounds of that element. The vitamin B12 is an example as it possesses a Co(I) ion in its core. On the other hand, at the physiological level, the xanthine oxidase enzyme, whose dysfunctions are related to gout, is another interesting metal-containing biomolecule which can oxidize xanthine to uric acid via the catalytic properties of the Mo(VI) complex in its active site.[29]

With respect to the medicinal chemistry, the first commercially-available inorganic molecule with therapeutic properties was the arsenic-based antisyphilis drug Arsphenamine (Salvarsan®), discovered in 1910 by Paul Ehrlich (awarded with Nobel Prize in 1908 for studied in immunology).[30] Salvarsan® (**Figure 4A**), and the related drug Neosalvarsan®, became soon the most widely prescribed drugs, remaining the most incisive cure for syphilis until penicillin became available in the 1940s. This successful story is an effective example of the Paul Ehrlich's "Magic Bullet" theory. In other words, it is possible to fight infectious diseases through a systematic search for drugs that kill invading micro-organisms without damaging the host.[31] More recently, another arsenic-containing agent, As_2O_3 (Trisenox®-**Figure 4B**), has been clinically exploited and it is one of the most effective drugs for the treatment of acute promyelocytic leukemia.[32,33]

Remaining in the field of p-block metal derivatives exploited in the treatment of human diseases, it is important to mention the antimony complex with Meglumine (N-Methyl Glucamine, **Figure 4C**), that is the first-in-class treatment against Leishmania parasites infections,[34] and the Bismuth hydroxide derivative of salicylic acid (Pepto-Bismol), common in treating temporary discomforts of the stomach and gastrointestinal tract.[35]

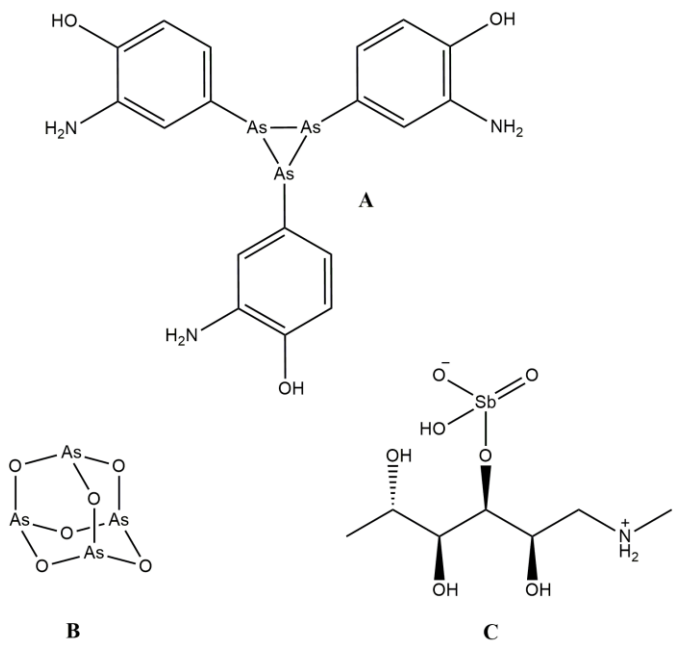

Figure 4: structural representation of three important p-block metal-containing drugs: A) the trimeric form of Salvarsan, B) arsenic trioxide (trisenox) and C) meglumine antimoniate (glucantime).

On the other hands, transition metal complexes receive the lion's share on the field of medicinal inorganic chemistry, in particular those containing noble metals, that have played a role of paramount importance in treating oncological malignancies.[36] In the first scenario, cisplatin ([cis-[$Pt^{II}Cl_2(NH_3)_2$], Platinol®) is the archetype of metal-based anticancer agents and is widely prescribed worldwide (alone or in combination therapy) as much as 70% of treatments against many types of malignancies, including testicular cancer, melanoma, bladder and non-small-cell-lung carcinomas and, in combination therapy, it is considerably active against ovarian neoplasm.[37,38] Concerning the use of inorganic chemistry for diagnostic purposes, many compounds containing radioactive isotopes are daily produced and immediately administered in large or medium-sized hospitals. The two main diagnostic techniques, PET (positron emission tomography) and SPECT (single photon emission computed tomography), allow to obtain several scans of the human internal tissues via the i.v. administration of a radioactive compound followed by detection of its decay products (γ rays, both for PET and SPECT).

The most common radionuclide-containing compound, with applications in high resolution PET, is 2-Deoxy-2-[^{18}F]fluoroglucose (described in detail in **Section 7**) whereas, in SPECT imaging, the salts of the radioactive iodine isotope ($Na^{131}I$), the water soluble complexes of

the gamma-emitter ^{99m}Tc(II) ion (e.g.,^{99m}Tc sestamibi – Cardiolite®) and of the thirteen-group metal ions, such as ^{67}Ga(III), ^{111}In(III) and ^{201}Tl(III), are widely employed.[21-23,39,40] Another application of inorganic compounds in medical diagnostics is provided by the Gd(III) complexes as contrast agents in magnetic resonance imaging (MRI).[41-43]

5. Platinum complexes in tumor treatments: an overview

Nowadays, a significant number of clinical trials involve anticancer agents which interfere with metabolic pathways.[44-46] In this context, the use of metal-based drugs offers potential for peculiar mechanisms of action based on the choice of the metal, its oxidation state, the type and the number of coordinated ligands and the resulting coordination geometry (**Figure 5**).

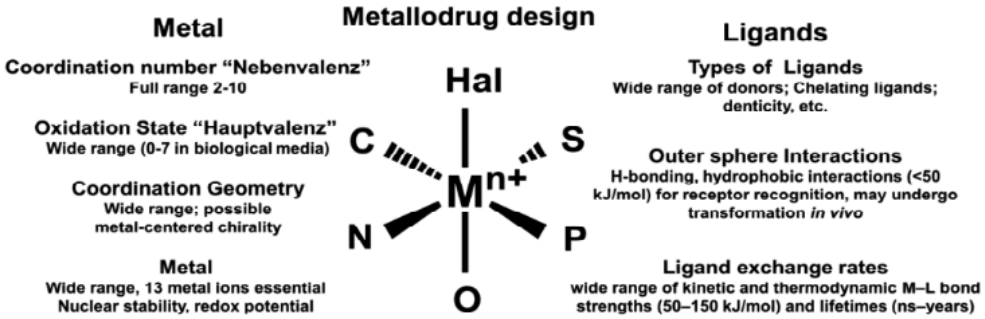

Figure 5: Schematic representation of a metal complex in octahedral geometry (central figure) and description of the principal chemical advantages in using metals in drug-design.[44]

The success of platinum pharmaceuticals in the last forty years has stimulated this research area, whose starting point was the discovery of the biological activity of cisplatin around fifty years ago.[47,48]

The light-yellow *Cis-di*amino*di*chloro platinum(II) (hereinafter *cis*-DDP or cisplatin) had its first appearance in chemistry in 1844, when it was synthesized by Michele Peyrone, an Italian chemist, and was referred to as Peyrone's Chloride. Its discovery was classified as very significant by the XIX century scientific community because, until then, only few examples of platinum(II) complexes bearing amino ligands were known.[49] One of them was the Magnus' Green Salt (**Figure 6A**), synthetized by the German chemist Heinrich Gustav Magnus in 1833.[50] Although the two platinum salts differ in color, melting point and chemical reactivity, they had the same formula bruta and identical elemental analysis, which

was the most exploited characterization method for that time. Therefore, their differences in structure and chemical formula remained unknown for many years. Only fifty years later Alfred Werner, in his theory of coordination chemistry, correctly assigned to these compounds the real structure and determined a *cis* geometry for the Peyrone's salt distinguishing it from its *trans* isomer (as reported in **Figure 6B** and **Figure 6C**, respectively). Such a structure was eventually unambiguously confirmed by *X*-ray determination in 1966.[51]

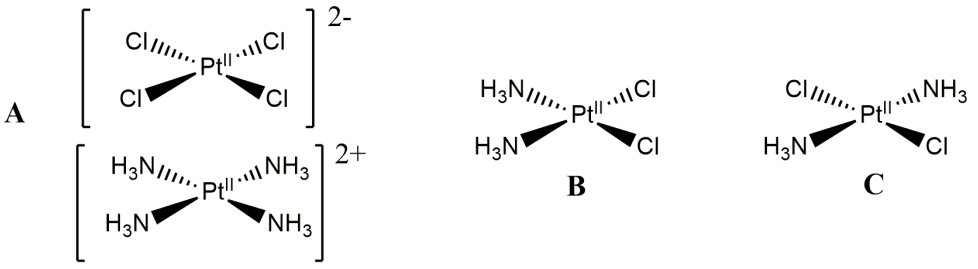

Figure 6: Molecular structures of A) Magnus' green salt, B) *cis*-platin or Peyrone's chloride and C) *trans*-platin.

In 1965, the two scientists Barnett Rosenberg and Loretta VanCamp, a physicist and a microbiologist respectively, discovered an unexpected and surprising phenomenon during their studies on the effect of electric fields on cell division in *Escherichia-coli* bacteria.[52,53] In fact, after the microbial population reached a steady state, a pair of platinum electrodes were included in the growth chamber (platinum was chosen as the material for the electrodes because of its well-known chemical inertness) and an electric field was applied. They observed the bacterial cells stopped dividing one to two hours after the voltage had been applied and that the cells started to elongate forming filaments. After the voltage was removed, the bacteria continued to increase in length for one to two hours, then the cell division started to occur again. It must be underlined that filamentous growth takes place when mitosis is inhibited but cell growth continues to occur. In fact, during filamentous growth, *Escherichia-coli* bacteria are still able to develop, but since they cannot divide, they form long filaments (**Figure 7-right**).[54] On the contrary, under normal conditions, *Escherichia-coli* forms short rods (**Figure 7-left**). Since the electric field seemed to affect bacterial cell division, Rosenberg and co-workers carried out more experiments to clarify the exact cause of this effect at the molecular level. Thus, it was serendipitously discovered that the application of the electric field was not itself responsible of the observed effects on

bacterial growth, but rather that the electric current, with the concomitant presence of oxygen, ammonium and chloride ions and light in the electrolysis chamber, led to the formation of new chemical species able to affect bacterial elongation.[55]

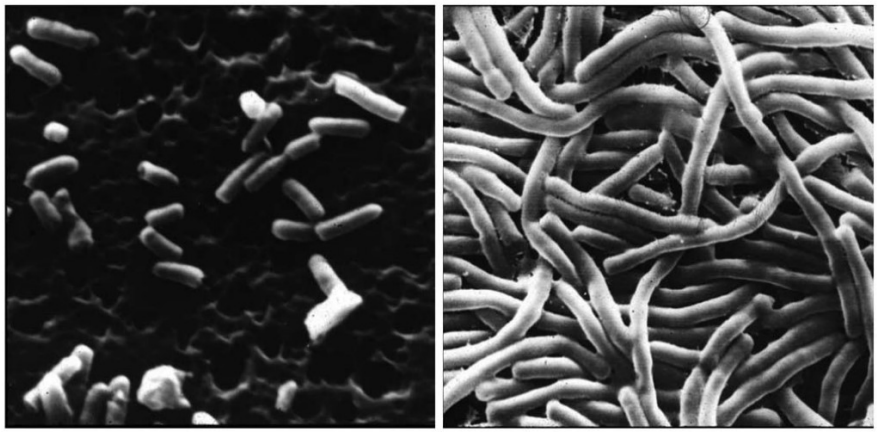

Figure 7: Different shapes of *Escherichia-Coli* bacteria, before (left) and after (right) application of electric field using Pt electrodes. This image is provided by Ref 53.

These agents were subsequently identified as platinum-containing complexes, either in oxidation states +2 (square planar geometry) or +4 (octahedral) with general formula $[Pt^{II}Cl_{4-n}(NH_3)_n]^{(2-n)-}$ or $[Pt^{IV}Cl_{6-n}(NH_3)_n]^{(2-n)-}$, respectively.[55] The property of inhibiting the mitotic division, suggested that this class of compounds would be effective against the fast-growing neoplastic cells. In this regard, c*is-di*amino*di*chloro platinum(II) complex turned out to be more effective with respect to the Pt(IV) derivatives and, thereafter, the Peyrone's Chloride came to be known as cisplatin (Platinol®). After several *in vitro* and *in vivo* studies, the drug received the FDA approval in 1978. Nowadays, Cisplatin is still an effective cure for testicular cancer, one of the most useful against melanoma, bladder and non-small-cell-lung carcinomas, and in combination therapy, it is considerably active against ovarian cancer (**Table 1**).[37,56]

Table 1: combination therapy of cisplatin with other cancer drugs.

Combination drug(s)	Cancer type
Paclitaxel	Ovarian carcinoma, breast carcinoma, lung carcinoma, melanoma, head and neck carcinoma
Paclitaxel and 5-FU	Gastric and esophagogastric adenocarcinoma
UFT	Non small lung carcinoma
Doxorubicin	Diffuse malignant pleural mesothelioma
Cyclophosphamide and doxorubicin	Salivary gland advanced carcinoma
Gemcitabine	Biliary cancer
Osthole	Lung cancer
Honeybee venom	Ovarian cancer
Anvirzel	Breast, colon, lung, prostate, melanoma and pancreatic cancer
Bevacizumab	Non small lung carcinoma
Vinbalstine and bleomycin	Metastatic granulosa cell tumors in ovary
Methotrexate and bleomycin	Advanced squamous cell carcinoma of the male genital tract
Everolimus	Urothelial bladder cancer
Fluorouracil, doxorubicin and cyclophosphamide	Salivary gland carcinoma
Metformin	Lung adenocarcinoma
Oxaliplatin, quercetin and thymoquinone	Ovarian cancer
Olaparib	PTEN deficient lung cancer
Tetra arsenic oxide	Cervical cancer
Vindesine	Non small lung carcinoma
β-galactosyl-pyrrolidinyldiazeniumdiolate	Glial cells of brain Human cervical cancer Gliosarcoma cell lines

Cis-DDP is administered to tumor-affected patients intravenously, upon dissolution in a sterile saline solution. As long as the drug is in the bloodstream and in the extra-cellular fluids, it keeps its original coordination sphere due to the relatively high concentration of chloride ions (~100 mM). Thus, the neutral compound enters the cell preferentially by passive diffusion across the lipid bilayer. Inside the cell, the chloride ion concentration drops from ~100 to ~3-20 mM, and the neutral cisplatin complex undergoes hydrolysis wherein a chloride ligand is replaced by a water molecule, thus generating the positively charged species *cis*-$[Pt^{II}Cl(NH_3)_2(H_2O)]^+$ and *cis*-$[Pt^{II}(NH_3)_2(H_2O)_2]^{2+}$.[56,57] Being 1.000 times more reactive than cisplatin itself, these hydrolyzed forms are able not only to coordinate DNA (so far known as the main target) and other biomolecules, but also to act through the inhibition of mitochondrial respiration by uncoupling oxidative phosphorylation.[58] On the other hand, the *trans*-platin isomer also manages to form coordination complex with DNA but, unlike *cis*-platin, *trans*-DDP is not an effective chemotherapeutic agent. In fact, due to the difference in coordination geometry, the monodentate *transDDP*-complexes with DNA are less stable than the corresponding ones with the *cis*-isomer: in fact, while the latter acts as a cytotoxic agent, the former is only cytostatic.[59] Considering this behavior, the structural features of all

the platinum(II)-based drugs showing antitumor activity have been associated to the possibility to form a specific type of platinum(II)-DNA adduct. Briefly, these features are summarized as follows:

- platinum(II) complexes must contain two labile leaving groups and two inert ligands (that is, chloride ions and ammonia molecules respectively, in cisplatin);
- both labile and inert ligands must be in reciprocal *cis* position, in order to interact with DNA through two adjacent coordination sites.[60]

The coordination interaction between cisplatin and the nitrogen bases of DNA, which is up to now recognized as its main targets in cell, results in a kink on the double-stranded supramolecular structure (**Figure 8**).[61] In particular, in double-stranded DNA, the primary site of platination derives from the metal coordination by two neighboring deoxyguanosines, d(GpG) (47-50 % cis-GG and 23-28 % cis-AG).[62] This alteration gives rise to a reduction in binding capability of the DNA polymerase enzyme, turning out the inhibition of cell division and, hence, induction of cell death *via* apoptosis or necrosis.[47]

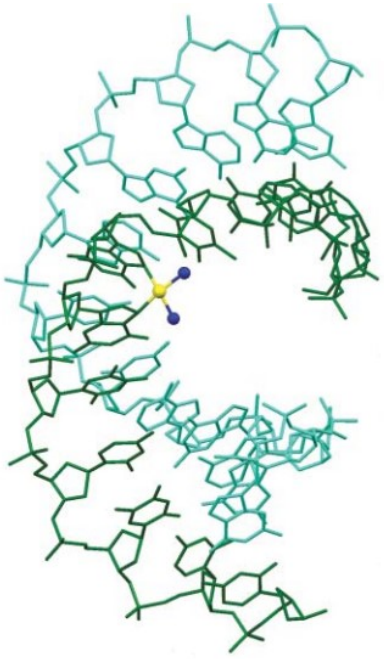

Figure 8: Crystal structure of *cis*platin bounded to two purine bases through intra-strand cross link. To be noted the kink caused in DNA helix (PDB entry: 1AIO).

As mentioned before, once inside the cell, in addition to DNA, *cis*-DDP has a number of other possible targets including RNA, sulfur- and thiol-containing enzymes or small molecules (*e.g.,* metallothionein and other targets).[63] Treatment with cisplatin inhibits

antioxidant enzymes, including superoxide-dismutase (SOD), glutathione peroxidase, glutathione *S*-transferase[54,64] and glutathione reductase,[54,65] through coordination of the Pt(II) metal center - described as soft acid by Pearson - by their sulfur- and selenium-containing residues, such as methionine, selenium-methionine and cysteine (*e.g.*, cysteinyl-glycine). In addition, because of the high affinity between cisplatin and glutathione, the concentration of the tripeptide itself (that is a major thiol-containing reducing agent into the cell) drastically reduced after the treatment, leading to a ROS over-production.[66] As a consequence, the excessive formation of ROS species causes cellular and mitochondrial oxidative stress, including damage to DNA, proteins and lipids, which are associated with cell death.[67] Moreover, cells-exposure to cisplatin induces the activation of an intrinsic apoptotic pathway.

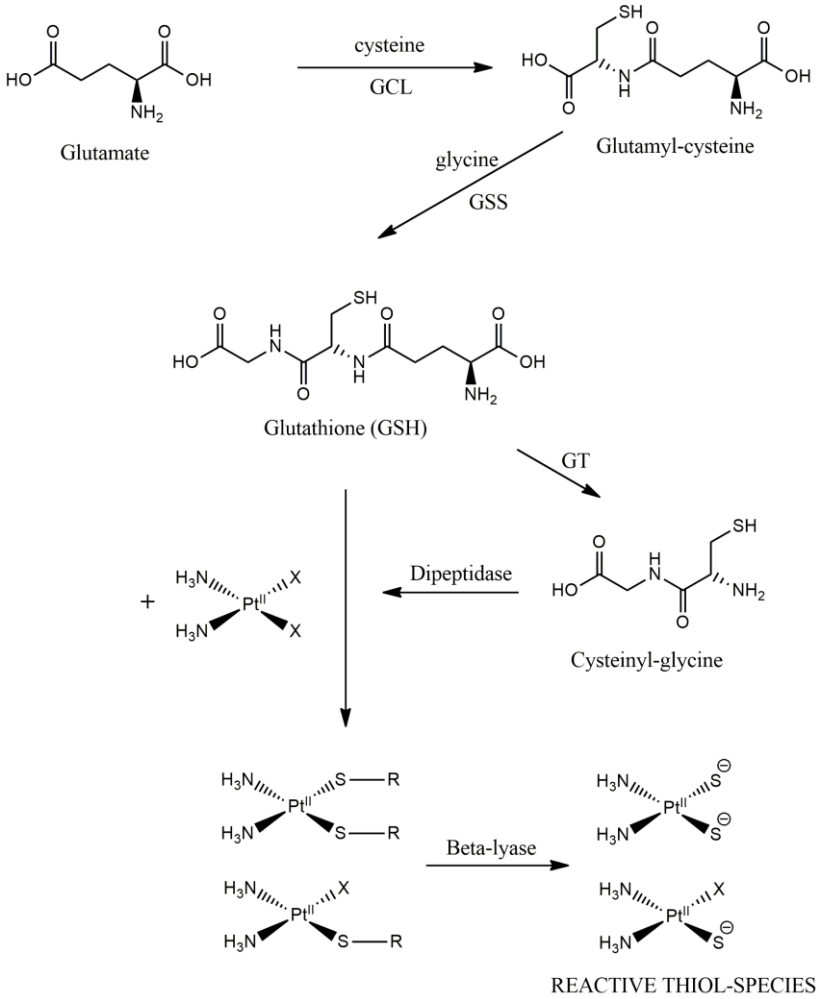

Figure 9: Biosynthesis of glutathione (GSH) and its reactions with cisplatin. The process leads to the formation of reactive thiol-species from Glutathione and cysteinyl-glycine (GCL: glutamate-cysteine ligase; GSS: glutathione synthetase; GT: glutamate transferase; X=Cl, H_2O).

Despite of its important antiproliferative properties, cisplatin causes several side effects, in particular it is very nephrotoxic. In fact, as cisplatin is cleared by the kidney by both glomerular filtration and tubular secretion,[68] renal toxicity can mainly result from the accumulation of the water-soluble Pt(II)-containing complexes (cisplatin itself, aqua-complex or inactivated Pt(II) species) in renal environment.[69] In this context, it is worth highlighting that the cisplatin concentration in proximal tubular epithelial cells is about five times the serum concentration. This phenomenon can be due to the high expression of Ctr1 transporter (copper transporter protein) and energy-dependent Na^+-K^+-ATPase transporters in tubular cells: in fact, there are recent and notable evidences these proteins might play an important role in cisplatin active uptake.[70-75] Once there, the drug, as well as inducing cell apoptosis by coordination of the nuclear DNA of renal cells, undergoes metabolic activation in the kidney to a more potent toxin (reactive thiol-species in **Figure 9**). This process begins with the formation of glutathione conjugates perhaps mediated by glutathione-S-transferase.[76,77] As the GSH-complexes pass through the kidney, they are cleaved to cysteinyl-glycine-derivatives by gamma glutamyl-transpeptidase (GGT) expressed on the surface of the proximal tubule cells.[78,79] Those are further metabolized to cysteine-conjugates by aminodipeptidases, also expressed on the surface of the cells.[78] In turn, the cysteine-conjugates are transported into the cytoplasm, where they are further metabolized by cysteine-S-conjugate beta-lyase to highly reactive thiols (**Figure 9**).[78-80]

Other cisplatin-induced side effects are ototoxicity, neurotoxicity, described as peripheral neuropathy, myelosuppression, nausea and alopecia, all ascribable to an accumulation of the drug in the selected tissues, dues to specific transporters or favorable plasmatic efflux.

Another severe problem of cisplatin is related to the onset of resistance of neoplastic cells that become tolerant to the effectiveness of the drug.[81,82] In this regard, the specific mechanisms involved in cisplatin resistance are several, and the most important ones are discussed below.

Reduced intracellular drug accumulation

There are important evidences indicating that the reduction of the drug accumulation in cancerous tissues is a significant mechanism of cisplatin resistance. A decrement of the order of 20-70% has been documented in a variety of cell lines displaying resistance to cisplatin by a factor of 3-40-fold.[83] Although reduction in drug accumulation is not always directly

proportional to the level of resistance,[84] in some cancer cells the reduction in intracellular cisplatin accumulation is the principal mechanism of resistance, accounting for 70–90% of total resistance.[85]

The cause of the reduced cisplatin accumulation in cells may be ascribed to either an inhibition in drug uptake or an increase in drug efflux, or both. A defect in the uptake process appears to be prevalent, but the mechanism for this remains obscure. Since reduced uptake can be demonstrated over a wide range of extracellular cisplatin concentrations, it is likely that resistance occurs as a result of changes in the process of passive drug diffusion.[86,87] Moreover, as described below, also an alteration in the cisplatin Ctr1- and Na^+-K^+-ATPase-mediated uptake as a causative factor in drug resistance, cannot be totally ruled out.

Increased inactivation by thiol-containing molecules

As described at the beginning of this chapter, the lower chloride concentration (around 4mmol/l) in the cytoplasm facilitates aquation reactions, which enable cisplatin to react with a number of cytoplasmic constituents, including the abundant GSH and the cysteine-rich metallothioneins, making it inactive towards DNA. Concentrations of these thiol-containing molecules increase following chronic cisplatin exposure, and induce resistance by decreasing the level of the antitumor agent available for interaction with the target DNA. Increases in GSH have been demonstrated in a number of cisplatin-resistant tumor models, and confirmed in clinical studies.[88] Furthermore, in a panel of resistant ovarian tumor models, prominent elevations in GSH levels have been correlated directly with resistance. Such elevations may occur as a result of increased expression of the γ-glutamylcysteine ligase (GCL – **Figure 9**) gene, the translational product of which is a rate-limiting enzyme involved in GSH biosynthesis (**Figure 9**).[89]

Undoubtedly, the increased conjugation reaction between GSH and cisplatin is generally accepted as a significant factor in resistance, but other explanations for the effects of GSH are also of interest. These include, among others, the role of elevated GSH levels in increasing DNA repair[84] and increasing the inhibitory effect on apoptosis by buffering an endogenous drug-induced oxidative stress.[90]

Increase in DNA damage repair

Formation and persistence of cisplatin-DNA adducts are essential in inducing apoptosis. Therefore, an enhanced rate of adduct repair will reduce the apoptotic process. This is supported by the demonstration that an increased rate of repair is associated with an inhibition of drug-induced cytotoxicity in several human tumor cell lines.[91,92] As with other mechanisms, repair is not universally present in all cisplatin-resistant cell lines. However, when present, the contribution of increased repair to resistance is low, and usually results in resistance of the order of 1.5-2.0-fold. Nevertheless, this limited increase is considered as significant and highlighted by the understanding that the inactivity of the *trans*-platin congener is largely due to the rapid de-coordination of the metal ion from the DNA, that acts as monodentate ligand.[93]

After the success of cisplatin, many researchers have tried to overcome its drawbacks, studying second-generation platinum drugs.[23] Its analogs should be able (i) to improve the efficacy of the original drug, meaning that lower doses can produce the same beneficial effects; (ii) to cause fewer toxic effects than cisplatin; (iii) to treat cases that have become resistant to the archetype and (iv), to be possibly administered orally.

In 1973, Cleare and co-workers reported a new second-generation injectable di-amino platinum(II) compound,[96-98] analog to cisplatin, that was approved for clinical use by FDA in 1989 and named carboplatin (Paraplatin®), *cis*-diamminedicyclobutane-1,1-dicarboxylato-platinum (II). The chelate effect of the six-membered ring reduces its chemical reactivity and possible side effects as well as damages to the ear (ototoxicity) and the kidneys (nephrotoxicity). After, also Oxaliplatin (Lipoxal®), (*1R,2R*)(*N,N'*-1,2diamminocyclohexane)(*O−O'*)ethanedioato) platinum(II) (**Figure 10c**),[99-100] received European approval in 1999 and approval by the FDA in 2002.

Metallo-drugs with a similar design are nedaplatin, lobaplatin, and heptaplatin (**Figure 10d**, **e, f**), which are currently in clinical trials in the U.S. but are already in clinical use in Japan, China, and South Korea, respectively. In addition, novel liposomal formulations of cisplatin (Lipoplatin®) and oxaliplatin are currently undergoing clinical trials, and seem to diminish the onset of serious adverse reactions, resulting in a better chemotherapeutic index.[101,102]

The first platinum orally-dispensed pharmaceutical was satraplatin (**Figure 10g**), bis(acetato)-amminedichloro(cyclohexylamine) platinum(IV). It was synthetized in 1993

and has been considered as the first example of third-generation Pt-based antitumor drugs. Satraplatin can be administered in pill form, which is convenient for the patient and reduces health care costs. It contains a core of mononuclear platinum(IV), that is reduced by metal-containing proteins within the bloodstream[103] to the active Pt(II) complex.[104] To date, this drug is still under clinical evaluation against various common cancers.[105]

In spite of these encouraging results, advances in anti-cancer research have shown that even the most successful targeted therapies tested so far lose potency with time.[106] This is imputable to the tumor-cell acquired resistance, due to mutations and epigenetic events, that limits efficacy, even if an initial response to chemotherapy occurs.

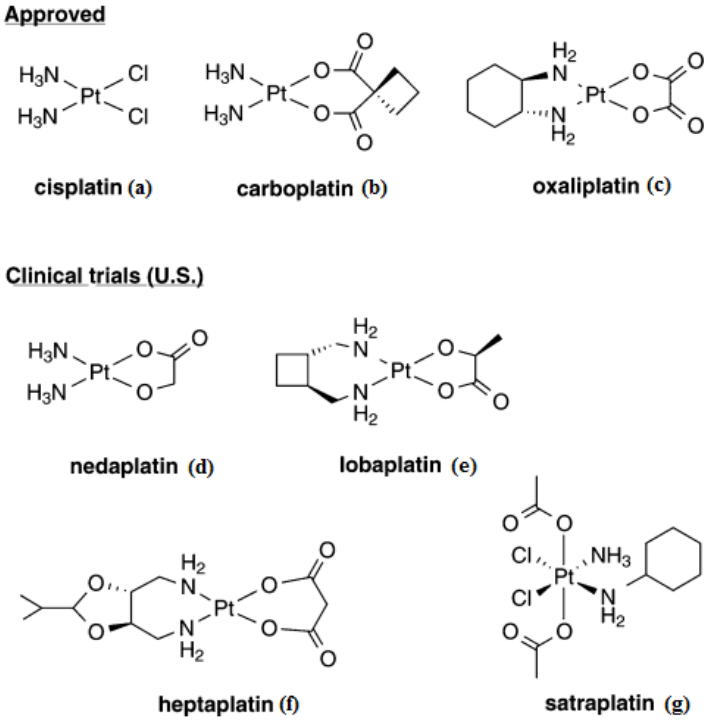

Figure 10: Anticancer platinum-based drugs approved and in clinical trials. Open-Access image from Ref 22.

6. The Warburg Effect

In multicellular organisms, most cells are exposed to a constant supply of nutrients. Survival of the organism requires control systems that prevent aberrant individual cell proliferation when nutrient availability exceeds the levels needed to support cell division. Uncontrolled proliferation is prevented because mammalian cells do not normally take up nutrients from their environment unless stimulated to do so by growth factors. Cancer cells overcome this growth factor dependence by acquiring genetic mutations that functionally alter receptor-initiated signaling pathways. Oncogenic mutations can result in the uptake of nutrients, particularly glucose, that meet or exceed the bioenergetic demands of cell growth and proliferation. This realization has brought renewed attention to Otto Warburg's observation in 1924 that cancer cells metabolize glucose in a manner that is distinct from that of cells in normal tissues.[107,108] By examining how Louis Pasteur's observations about fermentation of glucose to ethanol might apply to mammalian tissues, Warburg found that unlike most healthy cells, cancerous ones tend to catabolize glucose into lactate even in the presence of sufficient oxygen to support mitochondrial oxidative phosphorylation. In order to move deeply inside the scientific evidences of the metabolism of cancerous cells, it is necessary to briefly retrieve some concepts about the most significant human metabolic pathways that are oxidative phosphorylation and anaerobic glycolysis (respiration and lactic fermentation, respectively).

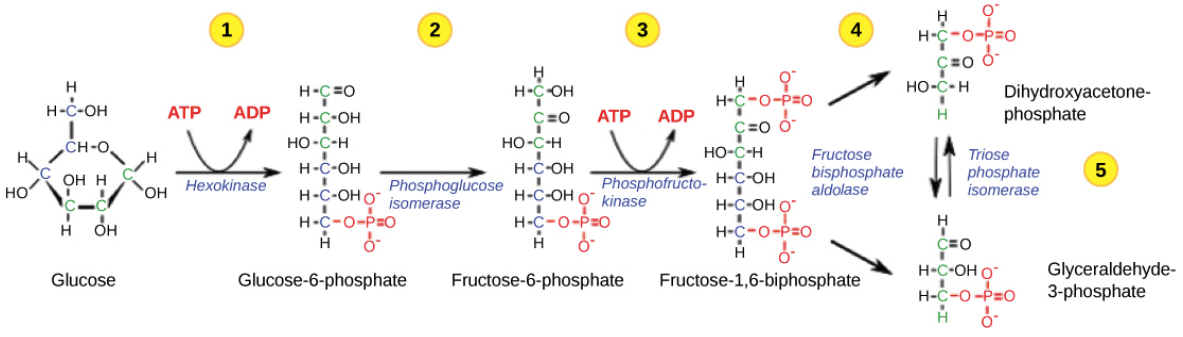

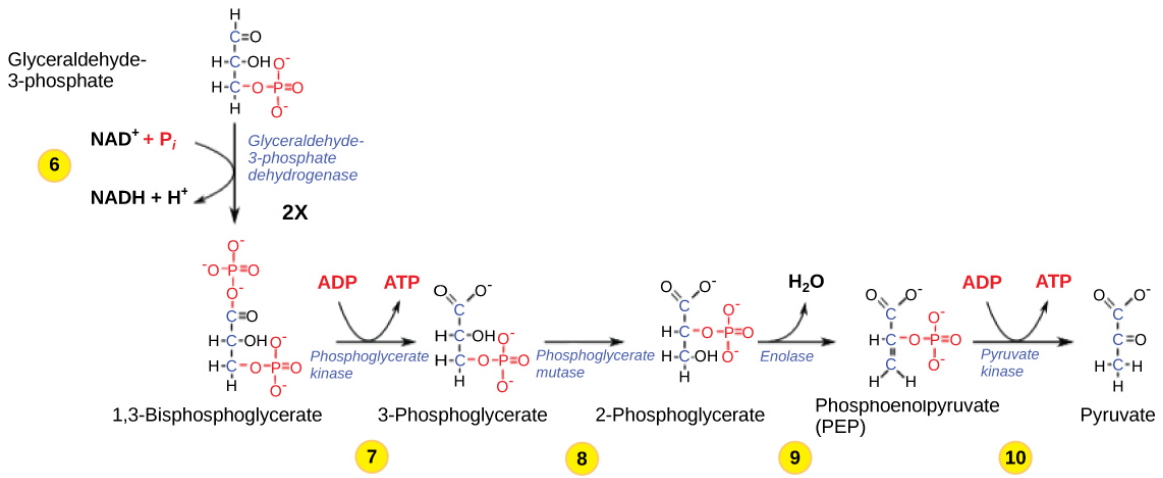

Figure 11: representation of the ten different reactions involved in the glycolysis representation of the ten different reactions involved in the glycolysis. In particular, each mole of D-glucose provides 2 equivalents of Glyceraldehyde-3-phosphate (Product of step 5) and the step sequence 6 - 10 have to be repeated twice. To sum up, the glycolysis pathway produces one mole of NADH and two of ATP (4 moles of ATP formed and 2 consumed) for each metabolized mole of D-glucose. Image credit: https://cnx.org/contents/GFy_h8cu@9.85:tYtpI6rX@6/Glycolysis (last accessed: December 18, 2017)

First, it is important to note that most differentiated non-malignant cells primarily metabolize glucose *via* the enzymatic oxidation, called *glycolysis* (**Figure 11**). Through this process, each mole of glucose is transformed into two moles of pyruvate that diffuse into the mitochondrion, reacting in the tricarboxylic acid cycle (Krebs Cycle).

In turn, each equivalent of pyruvate is processed into other carboxylic derivatives leading to the formation of four moles of the reduced coenzymes NADH and $FADH_2$ which are successively involved, in presence of oxygen, in the oxidative phosphorylation pathway. The latter exploits the activity of the ATP-synthase enzyme (the fifth respiratory-chain complex) to obtain ATP from ADP and a phosphate anion (P). It is worth noting that the Gibbs Free Energy (ΔG) of this phosphorylation step alone is a positive value, meaning that it is not energetically favored. As a consequence, energetic balancing for the phosphorylation reaction of ADP is ensured by the catalytic activity of four different enzymatic complexes in the inner mitochondrial membrane. These enzymes play a crucial role in the process exploiting the oxidation of NADH, formed in the Krebs cycle, piling up the energy demand by a proton pumping from the inner to the outer mitochondrial membrane. To sum up, the overall amount of ATP produced by a mole of reduced coenzyme is around 4 moles which

means, considering other ATP formation during glycolysis, that each equivalent of catabolized glucose in oxidative phosphorylation provides 30-36 of ATP.[109]

On the contrary, when oxygen supply is insufficient, typically during intense muscular activity, energy must be released through anaerobic metabolism, since the oxidative phosphorylation become inactive. In this simpler process, pyruvate, rather than initiating the Krebs Cycle, is reduced to lactate by lactate-dehydrogenase enzyme (LHD) and a catalytic equivalent of NADH, which is converted to NAD+.[110] In turn, NAD+ is re-introduced into the glycolysis pathway (see **Figure 12**) that, overall produces only 2 moles of ATP from each mole of glucose.

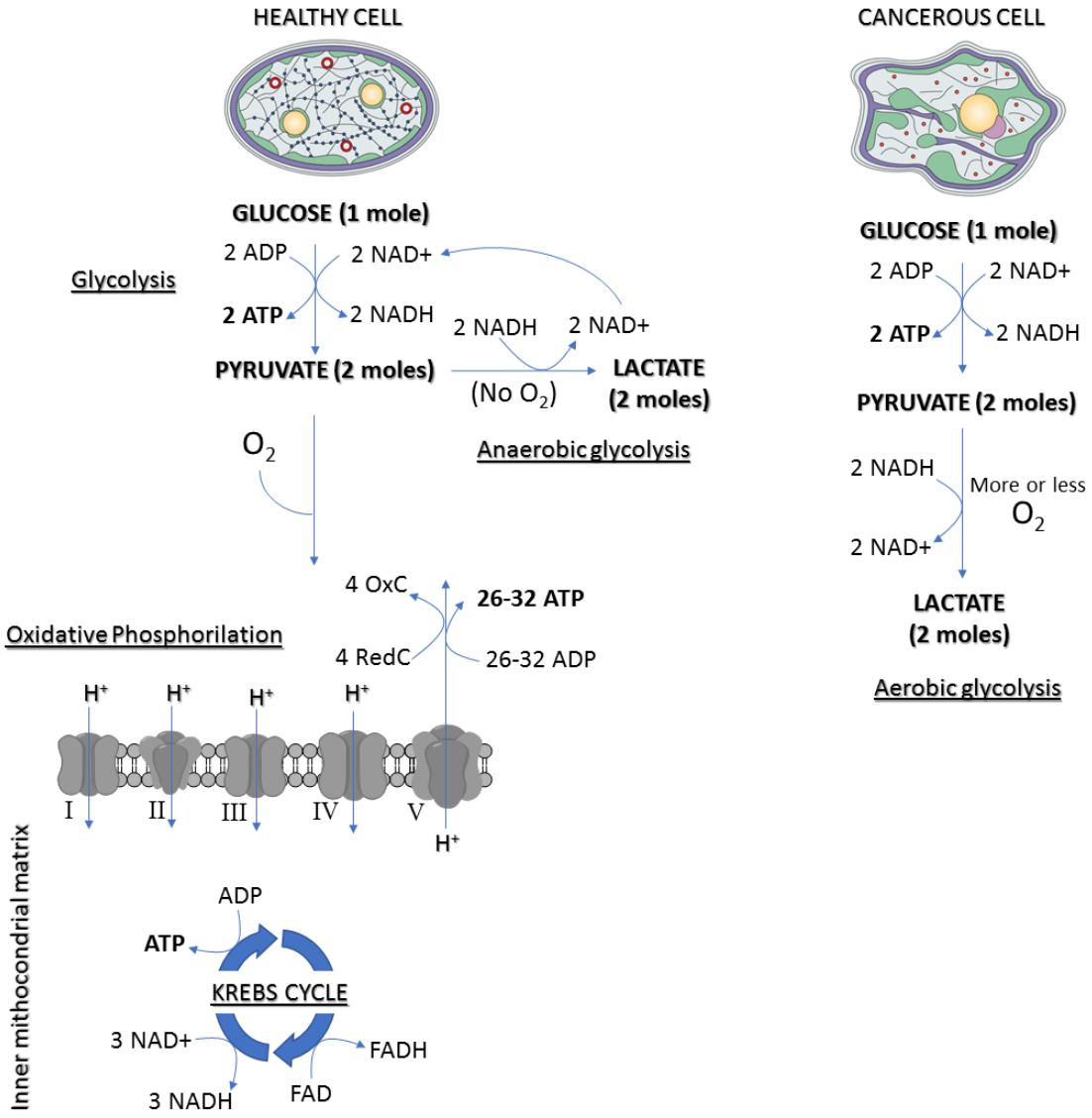

Figure 12: Comparison of glucose metabolism between normal tissues (left) and malignant cells (right).

In this context, most cancer cells produce large amount of lactate regardless of the availability of oxygen and hence their metabolism is often referred to as "aerobic glycolysis." Warburg originally hypothesized that cancer cells develop a defect in mitochondria that leads to impaired aerobic respiration and a subsequent reliance on glycolytic metabolism. However, subsequent works showed that mitochondrial function is not impaired in most cancerous cells,[112,113] suggesting an alternative explanation for their aero-glycolytic metabolism. One possible explanation is that inefficient ATP production is a problem only when resources are scarce. This is not the case for proliferating mammalian cells, which are exposed to a continual supply of glucose and other nutrients in vascularized angiogenetic tissues. Metabolic pathways and their regulation have only recently been studied in actively proliferating cells, and there is evidence that ATP may never be limiting. No matter how much they are stimulated to divide, cells using aerobic glycolysis also exhibit high ratios of ATP/ADP and $NADH/NAD^+$.[113,114] Further, even minor perturbations in the ATP/ADP ratio can impair growth. In this regard, healthy cells deficient in ATP often undergo apoptosis[115] and can also undergo cell cycle arrest and reactivate catabolic metabolism when their ability to produce ATP from glucose is compromised.[116]

One of the most interesting explanation proposed in 1924 for Warburg's observation is that malignant cells could be prompted to anaerobic metabolism because of tumor hypoxia.[107,117] However, further evidences suggested that cancer cells appear to use glycolytic metabolism before exposure to hypoxic conditions. For example, leukemic cells are highly glycolytic,[109,118] even these cells reside within the bloodstream at higher oxygen tensions than cells in most normal tissues. Similarly, lung tumors arising in the airways exhibit aerobic glycolysis even though these tumor cells are exposed to a great amount of oxygen that would account for a phosphorylation metabolism. Thus, although tumor hypoxia is clearly important for other aspects of cancer biology, the available evidence suggests that it is a late-occurring event that may not be a major contributor in the switch to aerobic glycolysis by cancer cells.[110]

Today, it is clear that cancer cells exhibit aerobic glycolysis due to activation of oncogenes, loss of tumor suppressors, and up-regulation of the PI3K pathway, and that one advantage of high glycolytic rates is the availability of precursors for anabolic pathways.[110]

7. The GLUTS' Protein Family

As a major product of the carbon fixation carried out by photosynthetic organisms, glucose is undoubtedly one of the most abundant molecules on the earth, existing mostly in various polymerized forms such as cellulose and starch. Mechanisms have consequently evolved to utilize glucose as a major catabolic and anabolic substrate for most of the organisms in all three kingdoms.

As well as being a source of energy, glucose performs various regulatory functions such as regulating the glucosamine pathway, modulating the activity of the Sirt1 deacetylase (an enzyme involved in cellular stress-regulation and longevity) through glycolysis and controlling the insulin secretion. On the other hand, these glucoregulatory functions are usually secondary to glucose uptake, a step that, in most tissues (with the notable exception of hepatocytes and pancreatic β-cells), is controlled by the level of glucose transporter expression at the cell surface.[119]

In an attempt to explain the isomeric specificity and saturability of glucose uptake into human red blood cells that had been observed 30 years previously, LeFevre[120] in 1948 was the first to postulate that a specific component within the cellular plasma membrane was required for the transfer of glucose across the lipid bilayer. In the early 1950s, Widdas[121] proposed a mobile carrier mechanism to explain the observed kinetics of glucose transport across sheep placenta, but only in the in 1985, thanks to the cDNA cloning technology, there were early evidences on the existence of specific glucose transporter proteins, that paved the way to the subsequently identification of two distinct protein family in human.[122]

In facts, it is recognized that the movement of monosaccharides across plasma membrane is controlled by proteins encoded from two structurally and functionally distinct gene families, namely the facilitative glucose passive transporters, called GLUT and encoded by the SLC2A gene, and Na^+-dependent glucose transporters, SGLT, that are encoded by the SLC5A gene.[123]

The former proteins, that are members of the major facilitator superfamily (MFS) (see **Table 2**),[119,124] are more expressed than the latter and exist in multiple isoforms (GLUT1-14), with different kinetic properties and cell surface expression. Their major activity is to provide the basis for the fine tuning of glucose uptake, metabolism, and signal generation in order to preserve cellular and whole body metabolic integrity shifting glucose down its concentration

gradient without expenditure of energy (passive transport).[125] As a matter of fact, the deficiency in their expression leads to the onset of serious genetic diseases, such as De Vivo syndrome (associated to GLUT1 deficiency in brain tissue).[126]

It is important to note that these classes of proteins can transport not only D-glucose as a unique substrate, but most of them are able to bind D-glucosamine, xylose, fructose, other glucose stereoisomers such as D-galactose and D-mannose, and disaccharides as D-maltose. In a recent paper, it was demonstrated with an experiment exploiting the signal of tritium-containing 2-[^{3}H]-D-glucose, that the uptake of this radioactive substrate by GLUT3 is inhibited in the presence of several carbohydrates with D-configuration, acting as competitors, in the medium (**Figure 13**).[127] Intriguingly, while the protein shows selectivity and high binding constant for the D-isomers, the uptake-competitiveness of non-natural L-isomers is almost nothing.

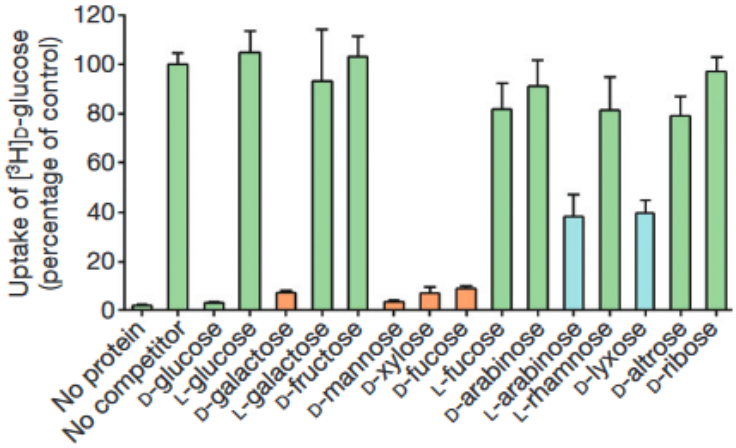

Figure 13: Substrate specificity of GLUT3 studied by evaluating the transport of D-[2-^{3}H]glucose by recombinant GLUT3(N43T) protein with proteoliposome-based counterflow assays.[127]

From the structural point of view, there is a high degree of homology between the 14 GLUT isoforms, in particular related to the residues constituting the trans-membrane domains (**Figure 14** shows, by means of blue balls, the homologous residues found both in GLUT1 and GLUT4).[128] Generally speaking, GLUTs are membrane proteins of about 500 amino acids folded in 12 trans-membrane-spanning and 1 cytoplasmic alpha helices. The 12 helices are divided in two distinct domains, C and N, connected each other by the cytoplasmic one, called ICH. As a part of the N-domain, these proteins expose an extracellular loop in which

one single oligosaccharide is coupled to the amino group of asparagine 45 through an N-linked glycosylation.[128]

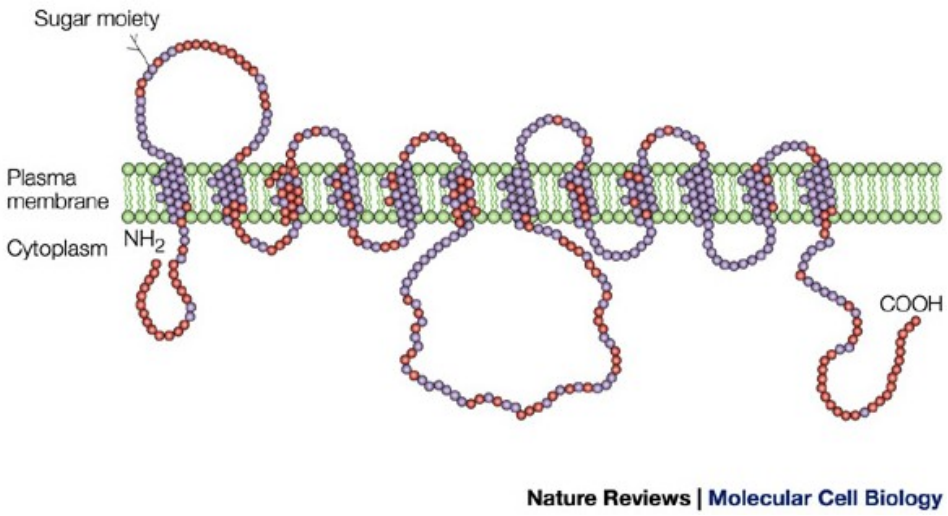

Figure 14: Schematic representation of the GLUT family of proteins.[128] On the bases of crystallographic structures and predictive calculations, proteins span the membrane 12 times with both amino- and carboxyl-termini located in the cytosol.

Moreover, little is known about the precise three-dimensional structure of these proteins and even less concerning how these proteins transport sugars across lipid bilayer membranes. Recently, a crystal structures of human isoform GLUT1 (without the glycosylated site, in order to prevent heterogenicity) and GLUT3 have been obtained and some important aspects of their similar functional mechanisms partially clarified.[129]

In particular, it seems that GLUT1 and GLUT3, exploiting the two connected N and C domains, can display two main stable structural conformations called "outward-open" and "inward-open" and two transition ones in which the substrate is occluded (**Figure 15**).[127,129] In the outward-open conformation, due to the relative distance of the two membrane domains, the protein can accept glucose binding (or other carbohydrates) from the extracellular matrix. Substrate binding at the primary site on the C domain may provide extra contacts with the N domain, inducing closure of the N and C domains on the extra-cellular side and leading to rearrangement of interactions on both sides of the bound substrate. When the binding affinity between the N and C domains on the extracellular side surpasses that of the intracellular side, the protein may switch to the inward-open conformation (**Figure 15**). Once GLUT1 and GLUT3 adopt the inward-open structure, the substrate is exposed to a low concentration environment; then the equilibrium is shifted towards substrate dissociation. The substrate-

free uniporter is able to return to the outward-facing state. This model predicts that substrate-free protein has a preferred open conformation, and substrate association and dissociation drive the conformational switches.

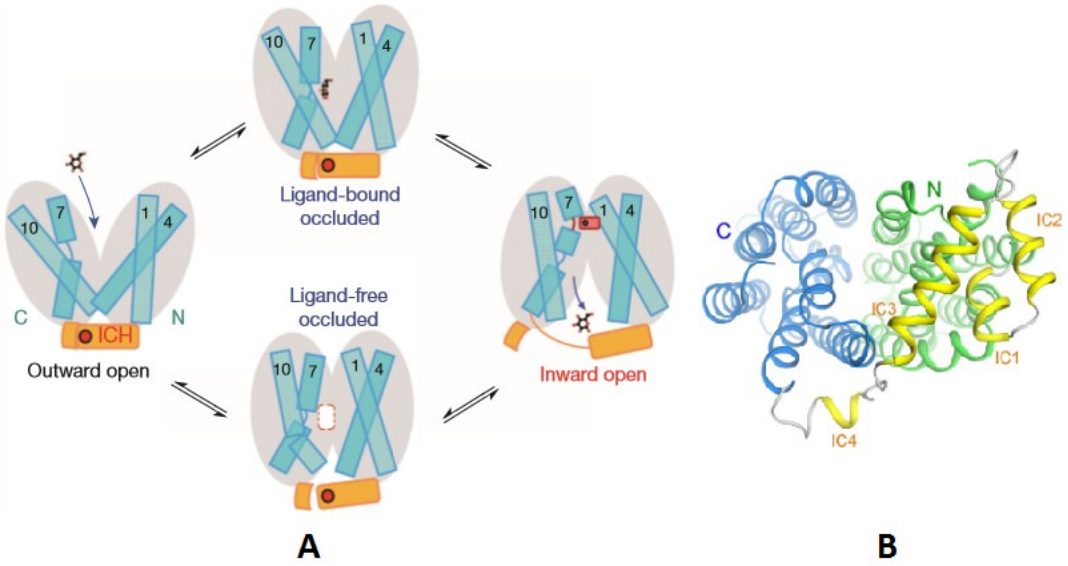

Figure 15: A) pictorial representation of the proposed working model for GLUT1. Shown here are the predicted conformations - outward-open, ligand-bound and occluded, inward-open, and ligand-free and occluded - required for a complete transport cycle according to the alternating access model. The ICH domain is illustrated as a latch that strengthens the intracellular gate in the outward-facing conformations; B) bottom view of the GLUT1 crystal structure, showing the ICH (yellow motif), the C- (blue) and the N- domains (green). The two terminal domains consist of 6 trans-membrane α-helices each.[129]

As reported previously, the GLUT family is composed by 14 different isoforms, each of them are expressed preferentially in one or more tissues (in particular GLUT1) and have high affinity for different substrates. These characteristics are summarized in **Table 2**.

Table 2: list of the known GLUT protein subtypes, reporting the predominant substrates and tissue distribution for each of them.

HUMAN GENE NAME	PROTEIN NAME	PREDOMINANT SUBSTRATES (D-enantiomers)	TISSUE DISTRIBUTION AND CELLULAR EXPRESSION
SLC2A1	GLUT 1	glucose, galactose, mannose, glucosamine	erythrocytes, brain, blood-brain barrier, blood-tissue barrier, many fetal
SLC2A2	GLUT 2	glucose, galactose, fructose, mannose, glucosamine	liver, islet of Langerhans, intestine, kidney, brain
SLC2A3	GLUT 3	glucose, galactose, mannose, xylose	brain (neurons), testis
SLC2A4	GLUT 4	glucose, glucosamine	adipose tissue, skeletal, cardiac muscle
SLC2A5	GLUT 5	fructose	small intestine, kidney
SLC2A6	GLUT 6	glucose	brain, spleen, leucocytes
SLC2A7	GLUT 7	glucose, fructose	small intestine, colon, testis, prostate
SLC2A8	GLUT 8	glucose, galactose, fructose	testis, brain, adrenal gland, liver, spleen, brown adipose tissue, lung (intracellular)
SLC2A9	GLUT 9	fructose	kidney, liver, small intestine, placenta, lung and leucocytes
SLC2A10	GLUT 10	glucose, galactose	heart, lung, brain, liver, skeletal muscle, pancreas, placenta and kidney
SLC2A11	GLUT 11	glucose, fructose	heart, muscles
SLC2A12	GLUT 12	glucose	heart, prostate, skeletal muscle, placenta
SLC2A13	GLUT 13	myo-inositol	brain, adipose tissue
SLC2A14	GLUT 14	-	testis

As a consequence of the Warburg Effect, most types of human tumor cells increase the expression of GLUT proteins in their phospholipidic membrane in order to have a continuous supply of carbohydrate nutrients. As a matter of facts, Medina and co-worker discovered that GLUT proteins (in particular 1, 2, 3, 4, and 5 isoforms) are highly overexpressed in neoplastic cells derived from different kind of tissues. Moreover, this remarkable increment is often associated with the ability of cancer cells to metastasize and with poor prognosis. In other words, the greater is the GLUT overexpression in tumor cells, the higher will be the severity of the malignancies in most cases.[130]

8. Targeting GLUT proteins with carbohydrate-bioconjugation

Due to Warburg effect, targeting GLUT proteins as an anticancer strategy has garnered a great deal of interest in recent years. This strategy is inspired by the widespread clinical use of 2-deoxy-2-(^{18}F)fuoro-D-glucose (^{18}F-FDG; **Figure 16**), a radiolabeled glucose analog, firstly synthetized in 1968, in Positron Emission Tomography (PET) imaging. ^{18}F-FDG has been used to visualize tumors and their metastases due to the tendency of these cancerous tissues to take up glucose at a higher rate than most normal tissues.[131] Once entered in the cancer cell by glucose transport proteins, the C6-position of the carbohydrate is phosphorylated by Hexokinase II enzyme that is overexpressed in cancers and effectively trapped inside the cells.

The ^{18}F nucleotide must be obtained initially as the fluoride anion in a cyclotron. Synthesis of complete FDG radioactive tracer begins with synthesis of the unattached fluoride radiotracer. Cyclotron production of ^{18}F may be accomplished in high yield by bombardment of ^{20}Ne with deuterons, but usually is done by proton bombardment of ^{18}O-enriched water, causing a "knockout reaction"-a common type of nuclear reaction with high probability) at the ^{18}O isotope. This produces ^{18}F-fluoride ($^{18}F^-$) ions in water which have a 109.8-minute half-life. At this point, a substitution reaction between the nucleophile ^{18}F nucleotide and the mesylate group in a 2-deoxy-2-mesylate-1,3,4,6-acetyl-D-mannose leads to formation of the ^{18}FDG molecule in a rapid and effective manner.

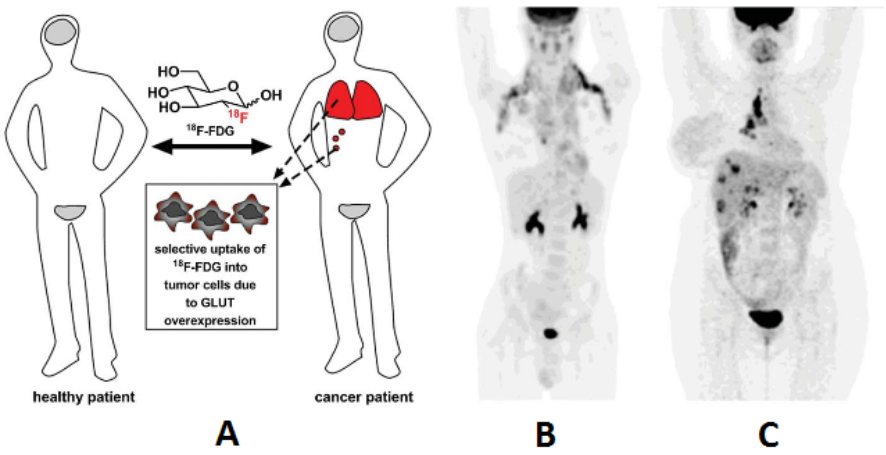

Figure 16: Positron emission tomography (PET) imaging using the radiolabeled glucose analog 18F-FDG is a widely used clinical tool for the diagnosis and staging of many types of cancer. A) In a healthy patient, 18F-FDG will be taken up only by tissues that constitutively consume glucose, such as the brain and bladder (grey). In a cancer patient, tumor cells will preferentially uptake 18F-FDG, allowing clinicians to identify sites of tumors and metastases (red), as well as stage cancer and monitor response to treatment; B) ^{18}F-FDG PET scan of a patient with metastatic Hodgkin's lymphoma; C) ^{18}F-FDG PET scan of a patient with metastatic breast cancer.[131]

It is important to note that, in recent studies it was shown that FDG uptake had no statistically significant correlation with GLUT1 and GLUT3 expression in all tumor. As examples, while positive relationship was seen in adenocarcinomas, the correlation is not linear for squamous-cell carcinomas (SCC).[131] These evidences imply that GLUT protein expression might be not the only key factors influencing glucose accumulation, and other elements, such as hexokinase enzyme activity, glucose-6-phosphatase expression, cell proliferation rates, and tumor cell density may play a more important role in the FDG uptake mechanism.[132]

Nevertheless, some important proofs of concept in targeting glucose transporter proteins through carbohydrate-conjugation were carried out in recent years and these studies provided much mechanistic insight into how future glucose-conjugated drugs might be assessed. For instance, in 2007 and 2008, Chen and coworkers reported the synthesis and cell culture evaluation of several glucose- and glucuronic acid-conjugates of paclitaxel, one of the most clinically-employed anticancer drug.[133,134] These glycoconjugates were designed to improve upon the poor water solubility of paclitaxel, as well as to target it more to cancer versus normal cells. The study reveals that the introduced glucose moiety in position 2' of paclitaxel does not interfere with the mechanism of action of the parent drug and the activity towards

tumor cells (IC_{50}) is comparable to that of the taxane alone. Moreover, it was shown by fluorescence-microscopy studies that the activity of 2-D-glucose conjugated paclitaxel could be selectively inhibited by co-treatment with the SGLT (the transmembrane glucose-sodium cotransporter) inhibitor phloretin (**Figure 17A**), suggesting that translocation into the cells is at least partially protein mediated.

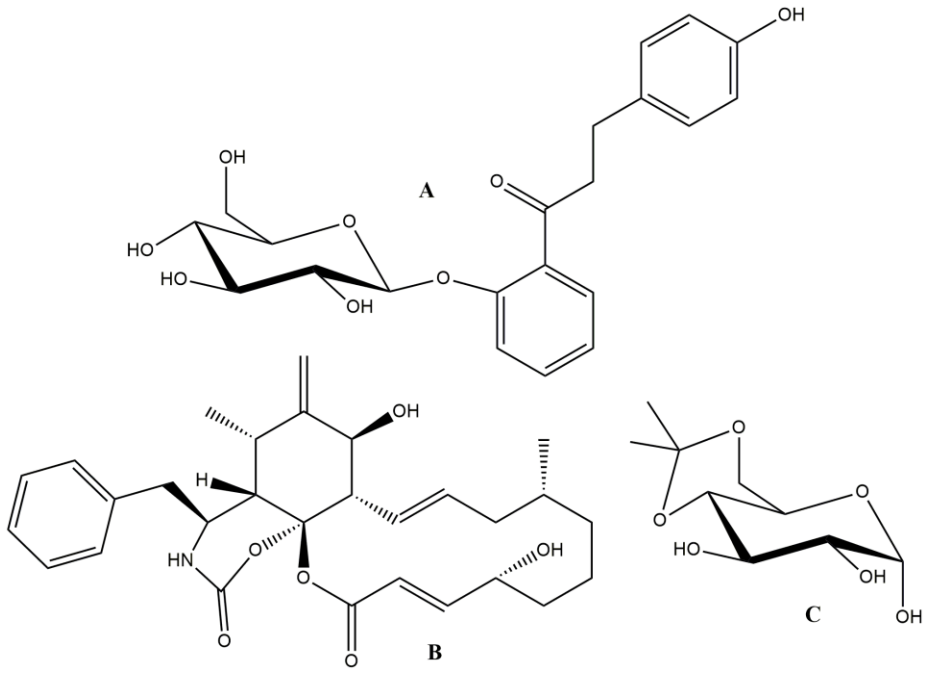

Figure 17: chemical structure of phlorizin (A), Cytochalasin B (B) and 4,6-O-Ethylidene-α-D-glucose (EDG, C). These three molecules are exploited for their inhibitory properties toward SGLT1/2, GLUT1/2/3/4 and GLUT1 proteins, respectively.

Another first-in-class glucose-conjugated organic mustard (DNA alkylating agents), called glufosfamide, is nowadays in phase-III clinical trials against metastatic pancreatic cancer. It consists of ifosfamid mustard linked via a glycosidic bond to β-D-glucose. Several studies demonstrate that the cellular uptake of this conjugated derivative is mediated by SGLT1.[135] On the contrary, the field of sugar metal complexes was largely unexplored for many years. Historically, the synthesis and evaluation of inorganics-sugar conjugated, in particular that of sodium ion, was firstly reported in literature in 1947[136] and, in the initial period, the ligand (that could be mono or multidentate, even in close or open conformation) was chosen only for improving water solubility and mere academical interest. Nowadays, this field has grown markedly, and even more bioinorganic scientists point the attention on the targeting of the cytotoxic metal center with carbohydrate functionalization. Obviously, because of the

importance of cisplatin and its derivatives in modern therapies, the first cytotoxic choice in this research falls on Pt(II) metal ion.

In this regard, very recently, Gao and co-workers synthetized a series of different oxaliplatin analogs, in which the oxalyl ligand is linked to a carbohydrate molecule, by means of a glycosylation reaction and a subsequent substitution (**Figure 18**). All the targeting functions consist in C1 functionalized monosaccharides, in particular, for galactose, mannose and 2-deoxy-glucose, as β-anomer, whereas for glucose, both the α- and β-anomers were investigated.[137-142]

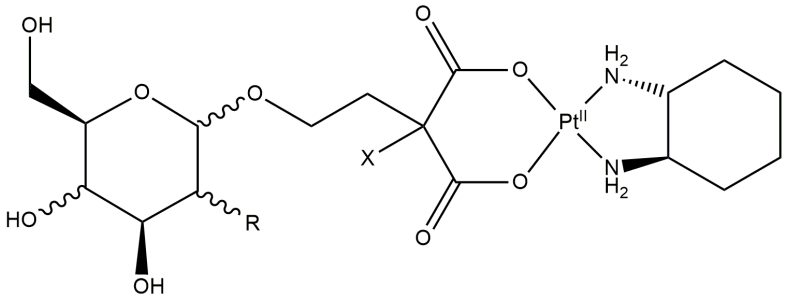

Figure 18: general structure of the complexes synthetized by Gao and co-workers.[136-140] The glycosil moiety could be α- or β-D-glucoside, β-D-galactoside, β-D-mannoside and 2-deoxy-β-D-glucoside (X= F, Cl, Me; R= OH, H).

The authors stated that the carbohydrate functionalization improves not only the solubility of the compound itself, that jumps to 6.2 mg/ml for oxaliplatin to 531.0 mg/ml for the β-glucosyl derivative, but also the cytotoxic activity in vitro toward several human tumor cell lines is maintained similar to the reference drug. In this case, it is clear that an increasing in hydrophilicity of the conjugated-complex do not alter the antineoplastic efficiency. Moreover, in vivo studies have led to the identification of the LD_{50} value for these derivatives, that is considerably lower than clinically-established platinum compounds. In particular, the safe dose for the complex Glucose-Me-Pt (with respect to the Figure 18, X=Me) was found to be 255.1 μmol/kg (for cisplatin 23.3 μmol/Kg).

More specific researches exploring the role of the glucose functionalization in targeting GLUTs were carried out by Lippard and co-workers in 2016.[142,143] They were able to obtain six oxaliplatin- monosaccharide -conjugated, similar to those synthetized by Gao, in which the glucose pendant was connected to the malonate moiety, via a propyl linker, in different positions of the backbone (C1α-anomer, C1β-anomer, C2, C3, C4 and C6 position). Thanks to several experiments exploiting the GLUT1 inhibitor cytochalasin-B (**Figure 17B**), they

found that, in these conditions, the cellular uptake of the complex with C2 substitution was most significantly inhibited (more than 57%), indicating the C2 functionalization as the most favorable for GLUT1 recognition of this class of glycoconjugates. Aside from C2, also the functionalization in C1, both in α or β anomerization, provides a good selectivity for the transporter protein. In fact, the order of specific uptake found by Lippard is: $2 > 1\alpha \geq 1\beta > 3 = 4 = 6$.[143] Moreover, they detected a good cytotoxic activity in vitro, compared to that of oxaliplatin, and a preferential accumulation of Pt-C2-glycoconjugated in tumor tissue in a mouse model, with respect to the reference drug. On the contrary, a docking study on bacterial xylose transporter XylE (PDB 4GBZ), a GLUT1 homolog, published in another paper by the same authors,[142] reveals that the more GLUT-recognizable Pt-glycoconjugated complex must have the glucose moiety functionalized in position C6, linked to the Pt-ligand via a shorter spacer. In particular, the C6-Pt compound, shows a high activity against A2780 cells (IC_{50}= 0.1μM) and a good cellular uptake. It is worth highlighting that the complex uptake strongly reduces (up to 50%) if EDG (**Figure 17C**), an inhibitor of GLUT1, is present in the medium. Similar results are obtained when D-glucose, in 100mM concentration as competitor, is added to cell-culture solution. On the contrary, the addition of non-natural isomer L-glucose, not effects the bio-conjugated complex uptake.

To sum up, linking metal complexes to sugars usually results in improved solubility in biologically compatible media (compared to established anticancer drugs and drug candidates in advanced stages of development). They are suitable for intravenous applications, and result in compounds with a reduced general toxicity, which might be related to a kind of targeted approach. This feature allows the drug candidates to be applied at much higher doses and endows them with a broader therapeutic window.[144] Notably, many examples have been reported with higher anticancer activity, both in vitro and in vivo, than standard chemotherapeutics, but no clear-cut structure-activity relationships were found. Also, the mechanism of action of the sugar complexes is not clear yet.[144,145]

9. Metal dithiocarbamato complexes: state of the art of our researches

As previously mentioned, the side toxicity, limits the clinical use of cisplatin and related platinum-based therapeutics. In addition to nephrotoxicity, the high affinity of Pt(II) center for sulfur-containing ligands, such as cysteine, methionine, glutathione, metallothionein and albumin, is a paramount importance in drug deactivation and ROS overproduction.[87,89,91]

Since sulfur is involved in the whole metabolic process of platinum drugs, several sulfur-containing ligands have been tested as chemoprotectants to modulate cisplatin side effects. In this context, positive outcomes were achieved with sodium diethyldithiocarbamate (NaDEDT), that provides with protection against renal, gastrointestinal and bone marrow toxicity induced by cisplatin without decreasing its antitumor activity. The chemoprotective effect results from its capability to remove platinum from thiol groups in proteins and oligopeptides, without any reversal of platinum-DNA adducts, responsible for its antineoplastic activity.[146,147] Interestingly, platinum-DNA adducts (1,2-intrastrand cross-links) were shown to decrease by ca. 50% upon treatment with NaDEDT soon after cisplatin administration, causing a loss of therapeutic effect, whereas no change in anticancer activity was observed when NaDEDT was administered 3 h after the drug. In particular, DEDT-cisplatin reaction, resulting in the drug-inactivation, is 40,000-fold faster than hydrolysis, leading to the direct chloride substitution. Conversely, when NaDEDT is administered 3 h later, the drug is on his way to the cell nucleus. In this case, the DTC is not able to cleave platinum-DNA adducts, wherein chlorides have been replaced by two guanine *N*-donor atoms, but it can remove platinum centers from a variety of other sulfur-containing molecules and, as a consequence, increases the amount of drug available to interact with DNA. Hence, the controlled use and dosing of NaDEDT as chemoprotectant reduces nephrotoxicity of cisplatin chemotherapy without decreasing their antitumor properties.[148-150] However, up to now, few data showed the DEDT ability to significantly reduce other non-renal toxicities, particularly the cumulative neuropathies, associated with cisplatin treatment. It should be highlighted that the overall benefits of NaDEDT are somewhat limited by its inherent acute hepatic toxicity that excludes the possibility to treat patients with a dose-intensive program. In fact, other potential health hazards associated with free (*i.e.*, not

coordinated) DTCs are still under investigation, including genotoxicity.[151] However, during cisplatin treatment, clinical use of chemoprotectants has been forsaken and replaced by aggressive hydration, together with antiemetic prophylaxis. In the meantime, a continuous effort is still being made by researchers in order to reduce cisplatin-induced toxicity.

On the basis of these considerations, our research group has been designing novel DTC complexes potentially able to combine the cytotoxic activity of the related metal centers (*e.g.*, Pt(II), Pd(II), Au(III), Ru(III), Ru(II), Zn(II), Cu(II), Rh(III), Bi(III), Sb(III)) with the lack of nephrotoxicity due to the inherent chemoprotective action of the ligand (**Figure 19**).[152,153] The rationale of our strategy is based on the peculiar chemical features of the dithiocarbamato moiety (-NCSS$^-$). DTCs are bidentate ligands that can form very stable complexes, due to the chelating effect. Thus, the decomposition with subsequent loss of the dithiocarbamato ligand is unlikely to occur.

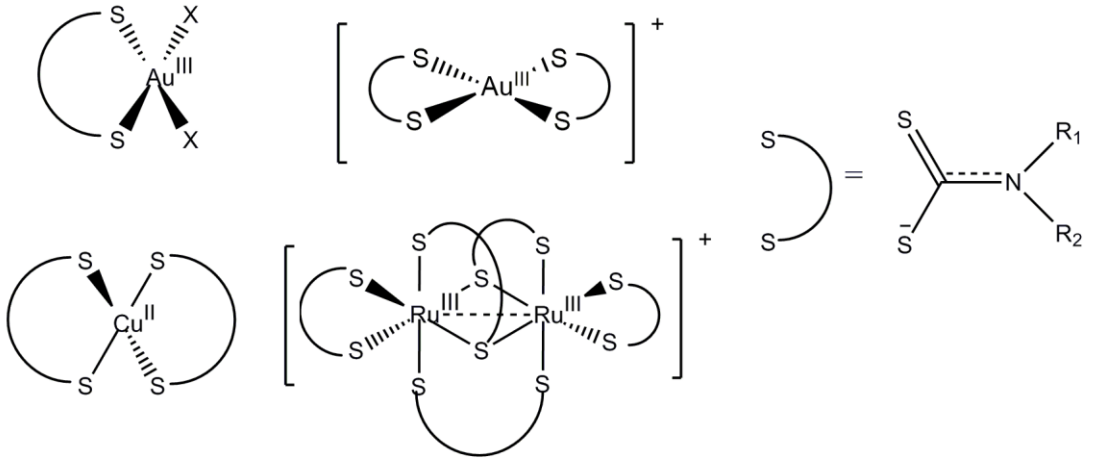

Figure 19: General structures of metal-DTC complexes synthetized by our group. X= halide (Cl$^-$, Br$^-$); R_1= R,(R, Ar), R_2= R', R,,, H.

To date, the toxicological profile along with the anticancer activity of our compounds points out the success of our design strategy, both in stabilizing the heavy metal center and in avoiding the uncontrolled reactivity of the compound, responsible for systemic toxicity.

The most promising results in term of cytotoxicity toward a huge amount of cancer cell lines were obtained with dinuclear-Ru(III)DTC and Cu(II)DTC derivatives, but also the Au(III)-DTC complexes show interesting properties. In particular, both the Ru(III)

compounds with piperidine dithiocarbamato ligand and the Au(III)-sarcosine dithiocarbamate were tested *in vivo*, detecting a safe concentration dose up to 15 mg/kg.

10. The dithiocarbamates as ligands

Dithiocarbamates $(R_2NCS_2)^-$ are a versatile class of anionic (LX) sulfur-chelating (bidentate) ligands (**Figure 20**) widely used in synthesis and a lot of chemistry has been developed around them.[154,155] The first synthesis of a transition metal-DTC (DTC: dithiocarbamato ligand) complex is undefinable but, in a pioneering paper of 1907,[156] Delepine reported the synthesis of a range of aliphatic DTC salts and also the derivatives of di-isobutyl-dithiocarbamate with transition metals including chromium, molybdenum, iron, manganese, cobalt, nickel, copper, zinc, platinum, cadmium, mercury, silver, and gold. Contrary to the DTC salts of the alkali and alkali-earth elements which are water soluble, the transition metal counterparts an also the salts of the p-block metals and lanthanides precipitate in water soon after the synthesis, yielding species soluble in most common organic solvents, and even in some cases, in benzene and carbon disulfide.

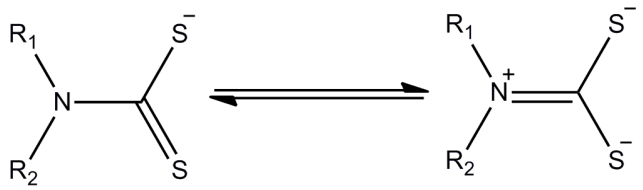

Figure 20: Resonance formulae of a generic DTC ligand; R_1=R'(R, Ar), R_2=R', R'', H. Many authors[157,158] affirmed that there is a strong character of double bond between carbon and nitrogen atoms.

From these early studies, DTCs and their transition metal complexes soon found a host of applications. For example, as a result of their insoluble nature in water solution they are widely used in analytical titrations for the determination of many metals in aqueous samples.[159,160] They can also be used to separate different metal ions by high-performance liquid chromatography and capillary gas chromatography.[161] It is also worth noting that the free ligand and its dimeric form (see below) can act as fungicides[162] and pesticides.[163] In the same time, the properties of the DTC-compounds containing transition metals are receiving a burgeoning interest in inorganic chemistry.

Dithiocarbamates are generally formed by the exothermic reaction between carbon disulfide and a primary or a secondary amine in the presence of a base, in methanol, ethanol or water as solvent.[164] The base may be an alkali, such as sodium hydroxide (**Figure 21a**), or an excess

of the amine. In the latter case the ammonium salt of the ligand ($[R_2NH_2]^+[S_2CNR_2]^-$) is formed (**Figure 21b**). As described previously, the sodium and potassium DTCs are only very poorly soluble (if not at all) in common organic solvents. In contrast, the corresponding ammonium salts generally show higher solubility in organic media. Moreover, some preparations recommend that the reaction is carried out at low temperature (0 °C), but in most cases room temperature is not troublesome.

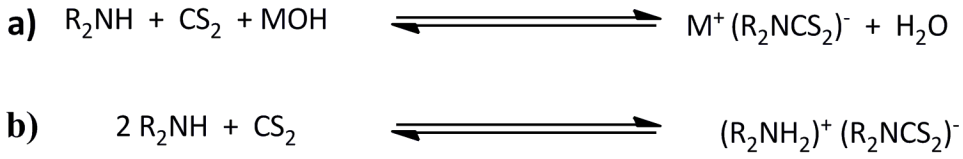

Figure 21: Reactions of formation of DTC salts of amine (secondary or primary), in presence of alkali base (a) or of excess of the aminic reagent (b).

According to Miller and Latimer, the reaction of dithiocarbamate formation occurs as reported in **Figure 22**. The crucial step in this synthesis (likewise in the decomposition) is the hydrogen-transfer from nitrogen to sulfur atoms and *vice-versa*, which takes place in the second equilibrium.[165]

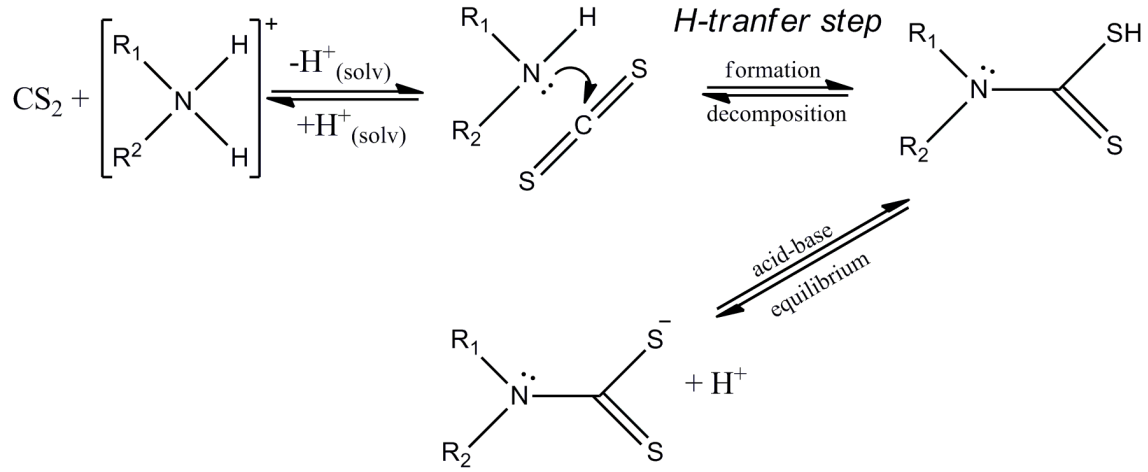

Figure 22: Mechanistic pathway for the formation of DTC in protic solvents. The aminic reagent is protonated by the solvent to ammonium ion in a previous acid-base equilibrium (not reported).

It should be noted that the acid form (hereinafter DTCH), which is obtainable from DTC anion in acidic media, is generally unstable due to its low-energy decomposition trails following the protonation of either nitrogen or sulfur atom. For mono- and di-substituted DTCs, two mechanisms of decomposition have been proposed, each pathway being

dependent on the acid dissociation constant of the parent amine (pK_N).[166-168] If pK_N<10.5, they decompose *via* fast intermolecular (solvent-promoted) *N*-protonation to form the zwitterion [$R_2NH^+CSS^-$] species, which is followed by carbon-nitrogen bond breakdown. In particular, *N*-protonation is slower than the C-N bond cleavage in the case of ammonia, whereas for DTC-derivatives of primary amines (pK_N value between 9.5 and 10.5), the C-N bond breaking is the rate determining step. In contrast, for secondary amines with pK_N>10.5 a slow intramolecular *S*-to-*N* proton transfer occurs, leading the carbon-nitrogen bond DTC-derivatives breakdown. The latter mechanism can be explained taking into account the character of C-N bond, stronger (*i.e.,* higher double-bond character) for secondary amine DTC-derivatives than for the primary counterpart, thus resulting in higher stability of the di-substituted DTCs in acidic media. As a consequence, many authors suggest that the DTCH species should be considered in a steady-state kinetic condition and the determination of pK_a values of DTCHs are necessarily non-trivial. The DTCs derived from secondary amines are stable in alkaline solution, while mono-substituted analogues can undergo a reaction with hydroxide ions, forming isothiocyanates (R-N=C=S) and elemental sulfur. Isothiocyanates, if formed, may further react[164] to yield unstable monothiocarbamates (MTCs). These statements clear up why metal-complexes containing mono-substituted DTC ligands are less common than their secondary counterparts. Also upon coordination, these mono-substituted DTC derivatives show a certain degree of lability (due to decomposition) leading to, in principle, a reduction of their biological activity of the corresponding complexes.

On the other hand, di-substituted DTCs can form the dimer thiuram disulphide molecule containing inter-ligand S-S bonds after bi-electronic oxidation with iodine, bromine, iron(III) chloride, solutions containing Au(III) ions or permanganate (MnO_4^-).[164] (**Figure 23**).

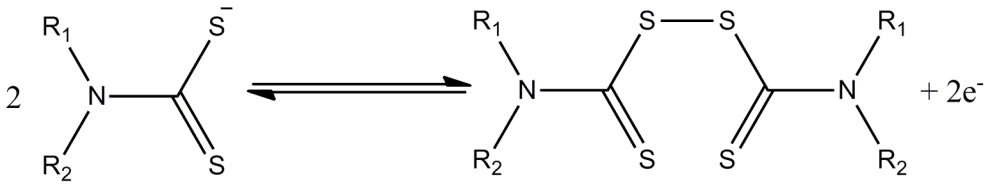

Figure 23: Oxidation reaction yielding thiuram disulphide involving two DTC^- molecules.

Bibliography

1. Glass, H.D. Science, God and Ockham's razor. *Phil. Stud.*, **2017**, *174(5)*, 1145-1161.
2. National Cancer Institute; http://www.cancer.gov/cancertopics/cancerlibrary/what-is-cancer; (last accessed: June 14, 2014).
3. Hanahan, D.; Weinberg, R. Hallmarks of Cancer: The Next Generation. *Cell* **2011**, 144, 646-674.
4. Bhowmick, N. A.; Neilson, E. G.; Moses, H. L. Stromal fibroblasts in cancer initiation and progression. *Nature* **2004**, 432, 332-337.
5. Cheng, N.; Chytil, A.; Shyr, Y.; Joly, A.; Moses, H. L. Transforming growth factor-ß signaling-deficient fibroblasts enhance hepatocyte growth factor signaling in mammary carcinoma cells to promote scattering and invasion. *Mol. Cancer Res.* **2008**, 6, 1521-1533.
6. Junttila, M. R.; Evan, G. I. P53 a Jack of all trades but master of none. *Nat. Rev. Cancer* **2009**, 9, 821-829.
7. Shay, J. W.; Wright, W. E. Hayflick, his limit, and cellular ageing. *Nat. Rev. Mol. Cell Biol.* **2000**, 1, 72-76.
8. Blasco, M. A. Telomeres and human disease: Ageing, cancer and beyond. *Nat. Rev Genet* **2005**, 6, 611-622.
9. Hanahan, D.; Folkman, J. Patterns and emerging mechanisms of the angiogenic switch during tumorigenesis. *Cell* **1996**, 86, 353-364.
10. *Stewa*rt, B.W.; Wild, C.P. eds. *"Cancer etiology". World Cancer Report 2014. World Health Organization.*
11. Kaur, J.; Srivastava, A.; Ralhan, R. Overexpression of p53 protein in betel and tobacco-related human oral dysplasia and squamous-cell carcinoma in India. *Int. J. Cancer,* **1994**, 58, 340-345.
12. Lazarus, P.; Garewal, H.S.; Sciubba, J.; et al. A low incidence of p53 mutations in pre-malignant lesions of the oral cavity from non-tobacco users. *Int. J. Cancer,* **1995**, 60, 458-463.
13. Brennan, J.A.; Boyle, J.O.; Koch, W.M.; et al. Association between cigarette smoking and mutation of the p53 gene in squamous-cell carcinoma of the head and neck. *N. Engl. J. Med.,* **1995**,332, 712-717.
14. Tanaka, T. Colorectal carcinogenesis: Review of human and experimental animal studies. *J. Carcinog.,* **2009**, 8(5), doi: 10.4103/1477-3163.49014
15. http://www.cancerresearchuk.org/cancer-info/cancerstats; (last accessed: June 14, 2014).
16. World Health Organization, *World Health Statistics 2013;* World Health Organization **2013**.
17. Mathers, C. D.; Loncar, D. Projections of global mortality and burden of disease from 2002 to 2030. PLoS Medicine 2006, 3, 2011-2030.
18. http://www.euro.who.int/en/health-topics/noncommunicable-diseases/cancer/data-and-statistics; (last accessed: June 14, 2014).
19. AIOM and AIRTUM Associations; I Numeri del Cancro in Italia; Intermedia Editore: Roma, 2016.
20. http://www.drugs.com/sfx/platinol-side-effects.html; (last accessed: June 14, 2014).
21. Alessio, E. Bioinorganic Medicinal Chemistry; Wiley-VCH Verlag & Co.: Weinheim, 2011.
22. Mjos, K.D.; Orvig, C. Metallodrugs in medicinal inorganic chemistry. *Chem. Rev.*, **2014**, 114(8), 4540-4563.
23. Barry, N.P.; Sadler, P.J. Exploration of the medical periodic table: towards new targets. *Chem. Commun.* **2013**, 49(45), 5106-5131.

24. Martin, W.; Russell, M.J. On the origins of cells: a hypothesis for the evolutionary transitions from abiotic geochemistry to chemoautotrophic prokaryotes, and from prokaryotes to nucleated cells. *Philos. Trans. R. Soc. Lond. B Biol. Sci.*, **2003**, 358(1429), 59-83.
25. Russell, M.J.; Hall, A.J. The emergence of life from iron monosulphide bubbles at a submarine hydrothermal redox and pH front. *J. Geol. Soc. London*, **1997**, 154(3), 377-402.
26. World Health Organization (WHO). Trace Elements in Human Nutrition and Health, WHO, 1996, p. 361.
27. Zhang, Y.; Gladyshev, V.N. Comparative genomics of trace elements: emerging dynamic view of trace element utilization and function. *Chem. Rev.*, **2009**, 109(10), 4828-4861 [and references therein].
28. Mertz, W. The essential trace elements. *Science*, **1981**, 213(4514), 1332-1338.
29. Hille, R.; Hall, J.; Basu, P. The mononuclear molybdenum enzymes. *Chem. Rev.*, **2014**, 114(7), 3963-4038.
30. Drews, J. Paul Ehrlich: magister mundi. *Nat. Rev. Drug Discov.*, **2004**, 3(9), 797-801.
31. Strebhardt, K.; Ullrich, A. Paul Ehrlich's magic bullet concept: 100 years of progress. *Nat. Rev. Cancer*, **2008**, 8(6), 473-480.
32. Ralph, S.J. Arsenic-based antineoplastic drugs and their mechanisms of action. *Met. Based Drugs*, **2008**, 260146.
33. Watts, J.M.; Tallman, M.S. Acute promyelocytic leukemia: what is the new standard of care? *Blood Rev.*, **2014**, 28(5), 205-212.
34. Haldar, A.K.; Sen, P.; Roy, S. Use of Antimony in the Treatment of Leishmaniasis: Current Status and Future Directions. *Mol. Biol. Int.,* **2011**, Article-ID 571242.
35. Tillman, L.A.; Drake, F.M.; Dixon, J.S.; Wood, J.R. Review article: safety of bismuth in the treatment of gastrointestinal diseases. *Aliment Pharmacol. Ther*. **1996**, 10(4), 459-467.
36. Medici, S.; Peana, M.; Nurchi, V.M.; Lachowicz, J.I.; Crisponi, G.; Zoroddu, M.A. Noble metals in medicine: Latest advances. *Coord. Chem. Rev.*, **2015**, 284, 329-350.
37. Kelland, L. The resurgence of platinum-based cancer chemotherapy. *Nat. Rev. Cancer*, **2007**, 7(8), 573-584.
38. Jayson, G.C.; Kohn, E.C.; Kitchener, H.C.; Ledermann, J.A. Ovarian cancer. *Lancet*, **2014**, 384(9951), 1376-1388.
39. Cutler, C.S.; Hennkens, H.M.; Sisay, N.; Huclier-Markai, S.; Jurisson, S.S. Radiometals for combined imaging and therapy. *Chem. Rev.*, **2013**, 113(2), 858-883.
40. Wadas, T.J.; Wong, E.H.; Weisman, G.R.; Anderson, C.J. Coordinating radiometals of copper, gallium, indium, yttrium, and zirconium for PET and SPECT imaging of disease. *Chem. Rev.*, **2010**, 110(5), 2858-2902.
41. Guglielmo, F.F.; Mitchell, D.G.; Gupta, S. Gadolinium contrast agent selection and optimal use for body MR imaging. *Radiol. Clin. North Am.*, **2014**, 52(4), 637-656.
42. Bottrill, M.; Kwok, L.; Long, N.J. Lanthanides in magnetic resonance imaging. *Chem. Soc. Rev.*, **2006**, 35(6), 557-571.
43. Pierre, V.C.; Allen, M.J.; Caravan, P. Contrast agents for MRI: 30+ years and where are we going? J. *Biol. Inorg. Chem.*, **2014**, 19(2), 127-131.
44. Mjos, K. D.; Orvig, C. Metallodrugs in medicinal inorganic chemistry. *Chem. Rev.*, **2014**, 114, 4540-4563.
45. Barry, N. P. E.; Sadler, P. J. Exploration of the medical periodic table: Towards new targets. *Chem. Comm.*, **2013**, 49, 5106-5131.
46. Hannon, M. J. Metal-based anticancer drugs: From a past anchored in platinum chemistry to a post-genomic future of diverse chemistry and biology. *Pure Appl. Chem.*, **2007**, 79, 2243-2261.

47. Lippert, B. Impact of Cisplatin on the recent development of Pt coordination chemistry: A case study. *Coord. Chem. Rev.* **1999**, *182,* 263-295.
48. Rosenberg, B.; Van Camp, L.; Krigas, T. Inhibition of cell division in Escherichia coli by electrolysis products from a platinum electrode. *Nature,* **1965**, *205,* 698-699.
49. Kauffman, G. B.; Pentimalli, R.; Doldi, S.; Hall, M. D. Michele Peyrone (1813-1883), discoverer of Cisplatin. *Platinum Metals Rev.;* **2010**, 54, 250-256.
50. Kauffman, G. B. Gustav Magnus and his Green Salt. *Platinum Metal Rev.*, **1976**, 20(1), 21-24.
51. Millburn, G. H. W.; Turter, M. R., The crystal structure of cis- and trans-dichlorodiammineplatinum(II); *J. Chem. Soc. (A)*, **1966**, 1609-1616.
52. Rosenberg, B.; Van Camp, L.; Krigas, T. Inhibition of cell division in Escherichia coli by electrolysis products from a platinum electrode. *Nature,* **1965**, *205,* 698-699.
53. Muggia, F.; Leone, R.; Bonetti, A. Platinum and other heavy metal coordinating compounds in cancer chemotherapy: overview of Verona ISPCC XI. *Anticancer Res.* **2014**, *34,* 417.
54. Eastman, A. in *Cisplatin: Chemistry and Biochemistry of a Leading Anticancer Drug;* Lippert, B. ed.; Verlag Helvetica Chimica Acta, Zurich; Wiley-VCH: Weinheim, Germany, **1999**, 111-134.
55. Rosenberg, B.; Van Camp, L.; Grimley, E. B.; Thomson, A.J. The inhibition of growth or cell division in Escherichia Coli by different ionic species of Platinum (IV) complexes. *J. Biol. Chem.*, **1967**, 242(6), 1347-1352.
56. Dasari, S.; Tchounwou, P. B. Cisplatin in cancer therapy: Molecular mechanisms of action. *Eur. J. Pharmacol.* **2014**, 740, 364-378.
57. Lippard, S. J. The inorganic side of chemical biology. *Nat. Chem. Biol.,* **2006**, *2,* 504-507.
58. Aggarwal, S. K. A histochemical approach to the mechanism of action of cisplatin and its analogs. *J. Histochem. Cytochem.,* **1993**, 41, 1053-1073.
59. Beck, D. J.; Popoff, S. Toxic effects of *cis*- and *trans*-diamminedichloroplatinum(II) in *uvr*D mutans of *Escherichia Coli*. *Ohio Journal of Science* **1994**, 94, 4, 99-104.
60. Howe Grant, M. E.; Lippard, S. J. Binding of platinum(II) intercalation reagents to deoxyribonucleic acid. Dependence on base-pair composition, nature of the intercalator, and ionic strength; *Biochemistry*, **1979**, 18, 26, 5762-5769.
61. Hannon, M. J. Supramolecular DNA recognition. *Chem. Soc. Rev.,* **2007**, *36,* 280-295.
62. Ratanaphan, A.; Wasiksiri, S.; Canyuk, B.; Prasertsan, P. Cisplatin-damaged BRCA1 exhibits altered thermostability and transcriptional transactivation. *Cancer Biol. Ther.,* **2009**, *8,* 890-898.
63. Stefanopoulou, M.; Kokoschka, M.; Sheldrick, W. S.; Wolters, D. A. Cell response of Escherichia coli to cisplatin-induced stress. *Proteomics,* **2012**, *11,* 4174-4188.
64. Greggi Antunes, L. M.; D'arc C. Darin, J.; Bianchi, M. D. L. P. Protective effects of vitamin C against cisplatin-induced nephrotoxicity and lipid peroxidation in adult rats: A dose-dependent study. *Pharmacol. Res.,* **2000**, *41,* 405-411.
65. Kadikoylu, G.; Bolaman, Z.; Demir, S.; Balkaya, M.; Akalin, N.; Enli, Y. The effects of desferrioxamine on cisplatin-induced lipid peroxidation and the activities of antioxidant enzymes in rat kidneys. *Hum. Exp. Toxicol.,* **2004**, *23,* 29-34.
66. Siddik, Z. H. Cisplatin: mode of cytotoxic action and molecular basis of resistance. *Oncogene*, **2003**, *22*, 7265-7279.
67. Masgras, I.; Carrera, S.; De Verdier, P. J.; Brennan, P.; Majid, A.; Makhtar, W.; Tulchinsky, E.; Jones, G. D. D.; Roninson, I. B.; Macip, S. Reactive oxygen species and mitochondrial sensitivity to oxidative stress determine induction of cancer cell death by p21. *J. Biol. Chem.,* **2012**, *287,* 9845-9854.

68. Yao, X.; Panichpisal, K.; Kurtzman, N.; Nugent, K. Cisplatin nephrotoxicity: A review. *Am. J. Med. Sci.,* **2007**, *334*, 115-124.
69. Waud, W. R. Differential uptake of cis-diamminedichloroplatinum(II) by sensitive and resistant murine L1210 leukemia cells. *Cancer Res.,* **1987**, *47,* 6549-6555.
70. Kuhlmann, M. K.; Burkhardt, G.; Kohler, H. Insights into potential cellular mechanisms of cisplatin nephrotoxicity and their clinical application. *Nephrol. Dial. Transplant*., **1997**, 12, 2478-2480.
71. Lin, X.; Okuda, T.; Holzer, A.; Howell, S.B. The Copper Transporter CTR1 regulates cisplatin uptake in Saccharomyces Cerevisiae. *Mol. Pharmacol.*, **2002**, *62*, 1154-1159.
72. Kuo, M.T.; Chen, H.H.W.; Song, I.S.; Savaraj, N.; Ishikawa, T. The roles of copper transporters in cisplatin resistance. *Cancer Metastasis Rev.,* **2007**, *26*, 71-83.
73. Howell, S.B.; Safaei, R.; Larson, C.A.; Sailor, M.J. Copper Transporters and the cellular pharmacology of the platinum-containing cancer drugs. *Mol. Pharmacol.*, **2010**, *77*, 887-894.
74. Akerfeldt, M.C.; Tran, C.M.; Shen, C.; Hambley, T.W.; New, E.J. Interactions of cisplatin and the copper transporter CTR1 in human colon cancer cells. *J. Biol. Inorg. Chem.,* **2017**, DOI 10.1007/s00775-017-1467-y.
75. Eljack, N.D.; Ma, H.Y.; Drucker, J.; Shen, C.; Hambley, T.W.; New, E.J.; Friedrich, T.; Clarke, R.J. Mechanisms of cell uptake and toxicity of the anticancer drug cisplatin. *Metallomics*, **2014**, *6(11)*, 2126-2133.
76. Townsend, D. M.; Tew, K. D.; He, L.; King, J. B.; Hanigan, M. H. Role of glutathione S-transferase Pi in cisplatin-induced nephrotoxicity. *Biomed. Pharmacother*., **2009**, *63*, 79-85.
77. Sadzuka, Y.; Shimizu, Y.; Takino, Y.; Hirota, S. Protection against cisplatin-induced nephrotoxicity in the rat by inducers and an inhibitor of glutathione S-transferase. *Biochem. Pharmacol*., **1994**, *48*, 453-459.
78. Townsend, D. M.; Deng, M.; Zhang, L.; Lapus, M. G.; Hanigan, M. H. Metabolism of Cisplatin to a nephrotoxin in proximal tubule cells. *J. Am. Soc. Nephrol.,* **2003**, *14*, 1-10.
79. Townsend, D.M.; Hanigan, M.H. Inhibition of gamma-glutamyl transpeptidase or cysteine S-conjugate beta-lyase activity blocks the nephrotoxicity of cisplatin in mice. *J. Pharmacol. Exp. Ther.,* **2002**, *300*, 142-148.
80. Zhang, L.; Hanigan, M. H. Role of cysteine S-conjugate β-lyase in the metabolism of cisplatin. *J. Pharmacol. Exp. Ther.*, **2003**, *306*, 988-994.
81. Ozols, R. F.; Corden, B. J.; Jacob, J.; Wesley, M. N.; Ostchega, Y.; Young, R. C. High-dose cisplatin in hypertonic saline. *Ann. Intern. Med.*, **1984**, *100*, 19-24.
82. Ozols, R. F.; Hamilton, T. C.; Reed, E.; Poirier, M. C.; Masuda, H.; Lai, G.; Young, R. C. *Platinum and Other Metal Coordination Compounds*, in Cancer Chemotherapy. Nicolini M. ed.; Martinus Nijhoff: Boston, 1988, 197-206.
83. Schilder, R.J.; Ozols, R.F. New therapies for ovarian cancer. *Cancer Invest.*, **1992**, *10*, 307-315.
84. Kelland, L.R. New platinum antitumor complexes. *Crit. Rev. Oncol. Hematol.*, **1993**, *15*, 191-219.
85. Johnson, S.W.; Laub, P.B.; Beesley, J.S.; Ozols, R.F.; Hamilton, T.C. Increased platinum-DNA damage tolerance is associated with cisplatin resistance and cross-resistance to various chemotherapeutic agents in unrelated human ovarian cancer cell lines. *Cancer Res.*, **1997**, *57*, 850-856.
86. Yoshida, M.; Khokhar, A.R.; Siddik, Z.H. Biochemical pharmacology of homologous alicyclic mixed amine platinum(II) complexes in sensitive and resistant tumor cell lines. *Cancer Res.*, **1994**, *54*, 3468-3473.
87. Kelland, L.R. Preclinical perspectives on platinum resistance. *Drugs*, **2000**, *59*(Suppl4), 1-8.

88. Chen, H.H.W.; Kuo, M.T. Role of Glutathione in the regulation of cisplatin resistance in cancer chemotherapy. *Met. Based Drugs,* **2010**, ID 430939.
89. Kotoh, S.; Naito, S.; Yokomizo, A.; Kohno, K.; Kuwano, M.; Kumazawa, J. Enhanced expression of gamma-glutamylcysteine synthetase and glutathione S-transferase genes in cisplatin-resistant bladder cancer cells with multidrug resistance phenotype. *J. Urol.,* **1997**, 157(3), 1054-1058.
90. Slater, A.F.; Nobel, C.S.; Maellaro, E.; Bustamante, J.; Kimland, M.; Orrenius, S. Nitrone spin traps and a nitroxide antioxidant inhibit a common pathway of thymocyte apoptosis. *Biochem. J.*, **1995**, *306*, 771-778.
91. Adams, M.N.; Ashton, N.W.; Paquet, N.; O'Byrne, K.J.; Richard, D.J. *Mechanisms of cisplatin resistance: DNA repair and cellular implications.* In Advances in Drug Resistance Research. Morais, Christudas, Ed.; Nova Science Publishers, New York, 2014, 1-37.
92. O'Grady, S.; Finn, S.P.; Cuffe, S.; Richard D.J.; O'Byrne K.J.; Barr, M.P. The role of DNA repair pathways in cisplatin resistant lung cancer. *Cancer Treat. Rev*., **2014**, *40(10)*,1161-1170.
93. Heiger-Bernays, W.J.; Essigmann, J.M.; Lippard, S.J. Effect of the antitumor drug cis-diamminedichloroplatinum(II) and related platinum complexes on eukaryotic DNA replication. *Biochemistry*, **1990**, *29*, 8461-8466.
94. Lee, K.B.; Parker, R.J.; Bohr, V.; Cornelison, T.; Reed, E. Cisplatin sensitivity/resistance in UV repair-deficient Chinese hamster ovary cells of complementation groups 1 and 3. *Carcinogenesis*, **1993**, *14*, 2177-2180.
95. Koberle, B.; Masters, J.R.; Hartley, J.A.; Wood, R.D. Defective repair of cisplatin-induced DNA damage caused by reduced XPA protein in testicular germ cell tumours. *Curr. Biol.*, **1999**, *9*, 273-276.
96. Cleare, M. J.; Hoeschele, J. D. Studies on the antitumor activity of group VIII transition metal complexes. I. Platinum (II) complexes. *Bioinorg. Chem.,* **1973**, *2*, 187-210.
97. Cleare, M. J.; Hoeschele, J. D. anti-tumour platinum compounds. relationship between structure and activity; *Platinum Metals Review.* **1973**, *17*, 2-13.
98. Cleare, M. J.; Hoeschele, J. D.; Rosenberg, B.; VanCamp, L. Malonato platinum anti-tumor compounds. U.S. Patent Office, 4,140,707, 1979.
99. Kidani, Y.; Noji, M.; Tashiro, T. Antitumor activity of platinum(II) complexes of 1,2-diamino-cyclohexane isomers. Gann, *The Japanese Journal of Cancer Research*, **1980**, *71*, 637-643.
100. Kidani, Y.; Masahide, N. Cytostatic platinum organic complexes. U.S. Patent Office 4, 710, 577, 1987.
101. Charest, G.; Sanche, L.; Fortin, D.; Mathieu, D.; Paquette, B. Optimization of the route of platinum drugs administration to optimize the concomitant treatment with radiotherapy for glioblastoma implanted in the Fischer rat brain. *J. Neurooncol.,* **2013**, *115,* 365-373.
102. Stathopoulos, P. G.; Rigatos, S.; Stathopoulos, J.; Batzios, S. Liposomal cisplatin in cancer patients with renal failure. *Journal of Drug Delivery & Therapeutics*, **2012**, 2(3), 106-109
103. Carr, J. L.; Tingle, M. D.; McKeage, M. J. Satraplatin activation by haemoglobin, cytochrome C and liver microsomes in vitro. *Cancer Chemother. Pharmacol.,* **2006**, *57,* 483-490.
104. Hall, M. D.; Hambley, T. W. Platinum(IV) antitumour compounds: Their bioinorganic chemistry. *Coord. Chem. Rev.,* **2002**, *232,* 49-67.
105. http://www.drugs.com/history/satraplatin.html (last accessed: June 9, 2017)
106. Stewart, D. J. Mechanisms of resistance to cisplatin and carboplatin. *Crit. Rev. Oncol.,* **2007**, *63,* 12-31.

107. Warburg, O.; Posener, K.; Negelein, E. Üeber den Stoffwechsel der Tumoren *Biochem. Z.*, **1924**, *152*, 319-344.
108. Warburg, O. On the origin of cancer cells. *Science,* **1956**, *123*, 309-314.
109. Zheng, J. Energy metabolism of cancer: Glycolysis versus oxidative phosphorylation. *Oncol. Lett.,* **2012**, *4(6)*, 1151-1157.
110. DeBerardinis, R.J.; Chandel, N.S. Fundamentals of cancer metabolism. *Sci. Adv.*, **2016**, *2*, e1600200
111. Weinhouse, S. The Warburg Hypothesis fifty years later. *Cancer Res. Clin. Oncol.,* **1976**, *87*, 115.
112. Fantin, V.R.; St-Pierre, J.; Leder, P. Attenuation of LDH-A expression uncovers a link between glycolysis, mitochondrial physiology, and tumor maintenance. *Cancer Cell*, **2006**, *9*, 425.
113. Deberardinis, R.J.; Lum, J.J.; Hatzivassiliou, G.; Thompson, C.B. The biology of cancer: metabolic reprogramming fuels cell growth and proliferation. *Cell Metab*., **2008**, *7*, 11.
114. Christofk, H.R.; Vander-Heiden, M.G.; Harris, M.H.; Ramanathan, A.; Gerszten, R.E.; Wei, R.; Fleming, M.D.; Schreiber, S.L.; Cantley, L.C. The M2 splice isoform of pyruvate kinase is important for cancer metabolism and tumor growth. *Nature*, **2008**, *452*, 230-233.
115. Vander Heiden, M.G.; Chandel, N.S.; Schumacker, P.T.; Thompson, C.B. Bcl-xL prevents cell death following growth factor withdrawal by facilitating mitochondrial ATP/ADP exchange. *Mol. Cell*, **1999**, *3*, 159.
116. Lum, J.J.; Bauer, D.E.; Kong, M.; Harris, M.H.; Li, C.; Lindsten, T.; Thompson, C.B. Growth factor regulation of autophagy and cell survival in the absence of apoptosis. *Cell,* **2005**, *120*, 237-248.
117. Koppenol, W.H.; Bounds, P.L.; Dang, C.V. Otto Warburg's contributions to current concepts of cancer metabolism. *Nat. Rev. Cancer,* **2011**, *11*, 325-337.
118. Suganuma, K.; Miwa, H.; Imai, N.; Shikami, M.; Gotou, M.; Goto, M.; Mizuno, S.; Takahashi, M.; Yamamoto, H.; Hiramatsu, A.; Wakabayashi, M.; Watarai, M.; Hanamura, I.; Imamura, A.; Mihara, H.; Nitta, M. Energy metabolism of leukemia cells: glycolysis versus oxidative phosphorylation. *Leukemia & Lymphoma,* **2010**, *51(11)*, 2112-2119.
119. Thorens, B.; Mueckler, M. Glucose transporters in the 21st Century. *Am. J. Physiol. Endocrinol. Metab.*, **2010**, *298*, E141-E145.
120. LeFevre, P.G. Evidence of active transfer of certain non-electrolytes across the human red cell membrane. *J. Gen. Physiol.*, **1948**, *31*, 505-527.
121. Widdas, W.F. Inability of diffusion to account for placental glucose transfer in the sheep and consideration of the kinetics of a possible carrier transfer. *J. Physiol.*, **1952**, *118*, 23-39.
122. Uldry, M.; Thorens, B. The SLC2 family of facilitated hexose and polyol transporters. *Pflügers Arch.*, **2004**, *447*, 480-489.
123. Szablewski, L. Glucose Homeostasis and Insulin Resistance. Bentham e-book, 2011, 25-27.
124. Mueckler, M.; Thorens, B. The SLC2 (GLUT) Family of Membrane Transporters. *Mol. Aspects Med.*, **2013**, *34*, 121-138.
125. Carruthers, A. Facilitated diffusion of glucose. *Physiol. Rev.*, **1990**, *70*, 1135-1176.
126. Wang, D.; Pascual, J.M.; De Vivo, D. Glucose Transporter Type 1 Deficiency Syndrome. *Gene-Reviews,* **2002** (internet version: https://www.ncbi.nlm.nih.gov/books/NBK1430/ - last accessed June 8, 2017).
127. Deng, D.; Sun, P.; Yan, C.; Ke, M.; Jiang, X.; Xiong, L.; Ren, W.; Hirata, K.; Yamamoto, M.; Fan, S.; Yan, N. Molecular basis of ligand recognition and transport by glucose transporters. *Nature,* **2015**, *526*, 391-396.

128. Bryant, N.J.; Govers, R.; James, D.E. Regulated transport of the glucose transporter GLUT4. *Nat. Rev. Mol. Cell Bio.*, **2002**, *3*, 267-277.
129. Deng, D.; Xu, C.; Sun, P.; Wu, J.; Yan, C.; Hu, M.; Yan, N. Crystal structure of the human glucose transporter GLUT1. *Nature*, **2014**, *510*, 121-125.
130. Medina, R.A.; Owen, G.I. Glucose transporters: expression, regulation and cancer. *Biol. Res.*, **2002**, *35(1)*.
131. Calvaresi, E.C.; Hergenrother, P.J. Glucose conjugation for the specific targeting and treatment of cancer. *Chem. Sci.,* **2013**, *4*, 2319-2333.
132. Choi, W.E.; Yoo, I.E.; O, J.H.; Kim, T.J.; Lee, K.Y.; Kim, Y.K. Is the Glut expression related to FDG uptake in PET/CT of non-small cell lung cancer patients? *Technol. Health Care,* **2015**, *23*, S311-S318.
133. Lin, Y.S.; Tungpradit, R.; Sinchaikul, S.; An, F.M.; Liu, D.Z.; Phutrakul, S.; Chen, S.T. Targeting the delivery of glycan-based paclitaxel prodrugs to cancer cells via glucose transporters. *J. Med. Chem.,* **2008**, *51*, 7428-7441.
134. Liu, D.Z.; Sinchaikul, S.; Reddy, P.V.; Chang, M.Y.; Chen, S.T. Synthesis of 2'-paclitaxel methyl 2-glucopyranosyl succinate for specific targeted delivery to cancer cells. *Bioorg. Med. Chem. Lett.,* **2007**, *17*, 617-620.
135. Mazur, L.; Opydo-Chanek, M.; Stojak, M. Glufosfamide as a new oxazaphosphorine anticancer agent. *Anti-Cancer Res.,* **2011**, *22*, 488-493.
136. Beevers, C.A.; Cochran, W. The crystal structure of sucrose sodium bromide dihydrate. *Proc. Roy. Soc. (London), Ser. A*, **1947**, *190(1021)*, 257-272.
137. Liu, P.; Lu, Y.; Gao, X.; Liu, R.; Zhang-Negrerie, D.; Shi, Y.; Wang, Y.; Wanga, S.; Gao, Q. Highly water-soluble platinum(II) complexes as GLUT substrates for targeted therapy: improved anticancer efficacy and transporter-mediated cytotoxic properties. *Chem. Commun*.,**2013**, *49*, 2421-2423.
138. Li, H.; Gao, X.; Liu, R.; Yu, W.; Zhang, M.; Fu, Z.; Mi, Y.; Wang, Y.; Yao, Z.; Gao, Q. Glucose-conjugated platinum(II) complex: Antitumor superiority to oxaliplatin, combination effect and mechanism of action. *Eur. J. Med. Chem.*, **2015**, *101*, 400-408.
139. Mi, Q.; Ma, Y.; Gao, X.; Liu, R.; Liu, P.; Mi, Y.; Fu, X.; Gao, Q. 2-Deoxyglucose conjugated platinum (II) complexes for targeted therapy: design, synthesis, and antitumor activity. *J. Biomol. Struct. Dyn.,* **2015**, DOI: 10.1080/07391102.2015.1114972.
140. Wu, M.; Li, H.; Liu, R.; Gao, X.; Zhang, M.; Liu, P.; Fu, Z.; Yang, J.; Zhang-Negrerie, D.; Gao, Q. Galactose conjugated platinum(II) complex targeting the Warburg effect for treatment of non-small cell lung cancer and colon cancer. *Eur. J. Med. Chem.*, **2016**, *110*, 32-42.
141. Gao, X.; Liu, S.; Shi, Y.; Huang, Z.; Mi, Y.; Mi, Q.; Yang, J.; Gao, Q. Mechanistic and biological characteristics of different sugar conjugated 2-methyl malonatoplatinum(II) complexes as new tumor targeting agents. *Eur. J. Med. Chem.*, **2017**, *125*, 372-284.
142. Patra, M.; Johnstone, T.C.; Suntharalingam, K.; Lippard, S.J. A potent glucose-platinum conjugate exploits glucose transporter and preferentially accumulates in cancer cells. *Angew. Chem. Int. Ed.,* **2016**, *55,* 2550-2554.
143. Patra, M.; Awuah, S.G.; Lippard, S.J. Chemical approach to positional isomers of glucose−platinum conjugates reveals specific cancer targeting through glucose transporter-mediated uptake *in vitro* and *in vivo*. *J. Am. Chem. Soc.*, **2016**, 138, 12541-12551.
144. Hartinger, C.G.; Nazarov, A.A.; Ashraf, S.M.; Dyson, P.J.; Keppler, B.K. Carbohydrate-Metal complexes and their potential as anticancer agents. *Curr. Med. Chem.,* **2008**, *15*, 2574-2591.

145. Pettenuzzo, A.; Pigot, R.; Ronconi, L. Metal-based glycoconjugates and their potential in targeted anticancer chemotherapy. *Metallodrugs*, **2015**, *1*, 36-61.
146. Borch, R.F.; Dedon, P.C.; Gringeri, A.; Montine, T.J. in *Platinum and OtherMetal Coordination Compounds in Cancer Chemotherapy*, Nicolini, M. ed.; Martinus Nijoff Publishing, Boston, **1988**, 216-281.
147. Dorr, R.T. in *Platinum and Other Metal Coordination Compounds in Cancer Chemotherapy*, Pinedo, H.M.; Schornagel, J.H. eds., Plenum Press, New York, **1996**, 131.
148. Borch, R. F.; Pleasants, M.E. Inhibition of cis-platinum nephrotoxicity by diethyldithiocarbamate rescue in rat model. *Proc. Natl. Acad. Sci. USA*, **1979**, *76(12)*, 6611.
149. Borch, R. F.; Katz, J.C.; Lieder, P.H.; Pleasants, M.E. Effect of diethyldithiocarbamate rescue on tumor response to cisplatinum in rat model. *Proc. Natl. Acad. Sci. USA*, **1980**, *77(9)*, 5441.
150. Rybak, L. P.; Ravi, R.; Somani, S.M. Mechanism of protection by diethyldithiocarbamate against cisplatin ototoxicity: antioxidant system. *Fund. Appl. Toxicol*., **1995**, *26*, 293.
151. Segovia, N.; Crovetto, G.; Lardelli, P.; Espigares, M. In vitro toxicity of several dithiocarbamates and structure - Activity relationships. *J. Appl. Toxicol.,* **2002**, *22,* 353-357.
152. Márta, E.; Ronconi, L.; Nardon, C.; Fregona, D. Noble metal-dithiocarbamates precious allies in the fight against cancer. *Mini-Reviews in Medicinal Chemistry* **2012**, *12,* 1216-1229.
153. Ronconi, L.; Fregona, D. The Midas touch in cancer chemotherapy: From platinum- to gold-dithiocarbamato complexes. *Dalton Transactions* **2009**, 10670-10680.
154. Heard, P. J. Main group dithiocarbamate complexes. *Progress in Inorganic Chemistry,* **2005**, *53,* 1-69.
155. Hogarth, G. Transition metal dithiocarbamates: 1978-2003. *Progress in Inorganic Chemistry,* **2005**, *53,* 71-561.
156. Delépine, M. Thiosulfocarbamates métalliques: préparation des sulfocarbimides de la série grasse, *Compt. Rend.*, **1907**, 144, 1125–1127.
157. Paparizos, C.; Fackler Jr., J. P. Kinetic studies by NMR of carbon-nitrogen and carbon-oxygen bond rotations in dithiocarbamate and aryl xanthate complexes of dimethylgold(III). *Inorg. Chem.,* **1980**, *19,* 2886-2889.
158. Lieder, M. Molecular structure and electrochemical properties of alkyldithiocarbamates. *Electrochim. Acta,* **2004**, *49,* 1813-1822.
159. Laghari, A. J.; Ali, Z. M.; Shah, F. A.; Zardari, L. A.; Khuhawar, M. Y. Pyrrolidinedithiocarbamate as a reagent for GC analysis of metal ions. *Journal of Applied Sciences Research*, **2010**, *6*, 6046-6051.
160. Imyim, A.; Daorattanachai, P.; Unob, F. Determination of Cadmium, Nickel, Lead, and Zinc in fish tissue by flame and graphite furnace atomic absorption after extraction with pyrrolidine dithiocarbamate and activated carbon. *Anal. Lett*., **2013**, *46*, 2101-2110.
161. Riekkola, M. Capillary gas chromatography of some metal chelates of dipropyl- and dibutyldithiocarbamic acids. *Mikrochim. Acta,* **1982**, *77,* 327-334.
162. Crnogorac, G.; Schwack, W. Residue analysis of dithiocarbamate fungicides. *TrAC – Trends Anal. Chem.,* **2009**, *28,* 40-50.
163. 111. López-Fernández, O.; Rial-Otero, R.; González-Barreiro, C.; Simal-Gándara, J. Surveillance of fungicidal dithiocarbamate residues in fruits and vegetables. *Food Chem.,* **2012**, *134,* 366-374.
164. Halls, D. J. The properties of dithiocarbamates A Review. *Mikrochim. Acta* **1969**, *57,* 62-77.
165. Miller, D. M.; Latimer, R. A. The kinetics of the decomposition and synthesis of some dithiocarbamates, *Can. J. Chem.*, **1962**, 40, 246-255.

166. Humeres, E.; Debacher, N. A.; Marta de S. Sierra, M.; Franco, J. D.; Schutz, A. Mechanisms of acid decomposition of dithiocarbamates. 1. Alkyl dithiocarbamates. *J. Org. Chem.,* **1998**, *63,* 1598-1603.
167. Humeres, E.; Debacher, N. A.; Sierra, M. M. D. S. Mechanisms of acid decomposition of dithiocarbamates. 2. Efficiency of the intramolecular general acid catalysis. *J. Org. Chem.,* **1999**, *64,* 1807-1813.
168. Humeres, E.; Debacher, N. A.; Franco, J. D.; Lee, B. S.; Martendal, A. Mechanisms of acid decomposition of dithiocarbamates. 3. Aryldithiocarbamates and the torsional effect. *J. Org. Chem.,* **2002**, *67,* 3662-3667.

Aims of this Ph.D. thesis

Nowadays, cancer is one of the most terrible plagues affecting 32.5 million adults worldwide, especially in the developed countries. Although immunotherapies come recently to a burgeoning interest in the international pharmacopoeia, chemotherapy (based on cytotoxic small-molecules) is still either the most effective treatment, after surgery, for almost all neoplastic malignancies and a cure for a restricted group of tumors (*e.g.*, testicular cancers). In this regard, platinums drugs (in particular, cisplatin, carboplatin and oxaliplatin) are among the most powerful chemotherapeutics, used as first-in-class treatments for several cancers, even for orphan ones, in which any other drug is not effective. On the other hand, platinum(II) derivatives causes severe side effects to patients, such as myelosuppression, neurotoxicity and renal failure.

In order to overcome the downsides of platinum drugs, but remaining firmly convinced in the powerful role of the medicinal inorganic chemistry, Fregona's research group, since 2000, developed a series of metal-based dithiocarbamato molecules, in particular containing Au(III), Ru(III) and Cu(II) centers, which are highly active in vitro toward a great number of human tumor cell lines and less toxic in vivo, compared to platinum chemotherapeutics. Although the great amount of data collected by Fregona and co-workers in these last years, some aspects on the chemistry of Au(III) dithiocarbamato complexes remains to be clarified. For this purpose, the first aim of this thesis is to deeply investigate the synthetic processes and the chemistry in solution of this class of compounds, unravelling interesting phenomena never studied in literature before.

An important aspect which triggers the systemic toxicity of the chemotherapeutic agents is their non-selectivity toward the malignant cells. In other words, the bioactive small molecules after the administration, do not accumulate in cancer tissues but, on the contrary, are able to interact either with neoplastic than healthy cells as well. As a consequence, the research for novel drugs that selectively explicate their cytotoxic action preferably toward malignant transformations is of primary important for the development of future and more effective treatments. In this regard, in order to target the cytotoxic metal-compounds into cancerous tissues, we decide to functionalize them with a monosaccharide function, exploiting the overexpression of glucose transporters proteins (GLUTs) in cancer cell membranes. In other words, the second aim of this Thesis is to obtain active dithiocarbamato complexes that act

as GLUT substrates which can exploit the transporter proteins to selectively enter into the cell cytoplasm, triggering cell death. In this context, interesting results were obtained thanks to this preliminary research, paving the way for future investigations.

Materials

Sodium tetrachloro-aurate dihydrate ($Na[AuCl_4]\cdot 2H_2O$, 99%), Potassium tetrabromo-aurate(III) di-hydrate ($K[AuBr_4]\cdot 2H_2O$, 99,9%), N-(Benzyloxycarbonyloxy)succinimide (Z-OSu, 98%) (Alfa Aesar). Copper chloride dihydrate ($CuCl_2\cdot 2H_2O$, ≥99%), anhydrous carbon disulfide (CS_2, >99%), *N*-methyl aminoethanol (97%), D-galactose (≥98%), D-mannose (≥99%), acetic anhydride anhydrous, piperidine (99%), boron trifluoride diethyl etherate ($BF_3\cdot Et_2O$, >46.5% BF_3), dimethyltin dichloride ($SnMe_2Cl_2$, 99%), triphenylphosphine (99%), tetrahydrothiophene (THT, >99%), Na_2SO_3 (>99%), KI (>99%), KBr (>99%), HCl (37% *w/v*) and manganese dioxide (MnO_2, 99%) (Sigma-Aldrich). D-glucose anhydrous (≥99%), pyridine anhydrous (>99%), sodium hydroxide (NaOH), potassium hydroxide (KOH), NaClO (14% Cl_2 in H_2O), bromine and iodine (VWR-Prolabo). Sterile saline solution was purchased by Fresenius-Kabi.

Dimethyl sulfoxide-*d6*, acetone-*d6*, CD_2Cl_2, $CDCl_3$, methanol-*d4*, D_2O were obtained from Aldrich. Anhydrous solvents (used for reactions in Schlenk vacuum line, such as THF, MeOH, CH_2Cl_2, CH_3CN) were obtained by Sigma-Aldrich (Sure-Seal bottle) or by overnight drying with molecular sieves followed by fractional distillation. All other reagents and solvents were of high purity and were used as purchased without any further purification.

For the reactions occurring in aqueous medium, departmental deionized water has been employed.

Regarding biological experiments: HCT-116 cells (American Type Culture Collection, ATCC). Dulbecco Modified Eagle's Medium (D-MEM), Dulbecco Modified Eagle's Medium Low-Glucose (D-MEM low glucose), L-glutamine, penicillin, streptomycin, fetal bovine serum (FBS), trypsin (0.05%, EDTA 0.02% in PBS) (Euro Clone). DMSO (>99.9%, for biological treatments), in vitro toxicology assay kit (resazurin based), paraformaldehyde, ElvanolTM (polyvinyl alcohol) (Aldrich).

Instrumentation

Elemental analysis

Elemental analyses were carried out at the microanalysis lab. (Chemistry Dept., University of Padova) by a Carlo Erba 1108 CHNS-O micro-analyzer.

ESI-MS analysis

ESI-MS spectra were recorded on a Mariner Perspective Biosystem instrument, setting a 5 kV ionization potential and a 20 mL/min flow rate. A mixture of coumarin and 6-methyl-triptophan was used as a standard in positive ionization mode. Samples were dissolved in methanol, and the same solvent was used as eluent. ESI-MS spectra have been processed by the software Data Explorer.

FT-IR spectroscopy

Infrared spectra have been recorded at room temperature in N_2 atmosphere, in solid KBr by a spectrophotometer Nicolet Nexus 5SXC in the range 4000 ÷ 400 cm^{-1} (32 scansions, 2 cm^{-1} resolution) and in nujol between two polyethylene tablets by a spectrophotometer Nicolet Nexus 870 in the range 600 ÷ 50 cm^{-1} (200 scansions, 4 cm^{-1} resolution). Data processing was carried out using OMNIC (version 5.1-Nicolet Instrument Corporation).

NMR spectroscopy

The ^{1}H-NMR monodimensional spectra described in *Chapter One and Two* and all bidimensional (COSY) NMR ones were recorded in $CDCl_3$, methanol-*d4*, or DMSO-*d6* at 298 K on a Bruker Avance DRX600 spectrophotometer equipped with a BBI-5 mm z-field gradient probe-head, and a Silicon Graphics O_2 workstation, operating in Fourier transform. Typical acquisition parameters (^{1}H: 600.13 MHz): 128 transients (for bidimensional acquisition: 512 transients of 32 scans/block), spectral width 7.5 kHz, 2 k data points and a delay time of 7.0 s. Spectra were processed by using sine-square weighting with a resolution of 1.0/3.0 Hz and a line-broadening threshold of 0.3/1.0 Hz. Data processing was carried out by means of MestReNova version 6.2.0 (Mestrelab Research S.L.). Chemical shifts were referred to external tetramethylsilane (TMS). Peak multiplicity has been described as follows: *s* (singlet), *d* (doublet), *dd* (doublet of doublets), *t* (triplet), *q* (quartet) and *m* (multiplet).

UV-Vis spectrophotometry

Electronic spectra were acquired at 25°C without stirring in different wavelength ranges according to the solvent cut-offs (DMSO, 250 nm; CH_2Cl_2, 190 nm; H_2O, 190 nm; octanol, 220 nm; methanol, 220 nm; acetone, 330 nm) with an Agilent Cary 100 UV-Vis double beam spectrophotometer (1 cm optical path, quartz cuvettes), using freshly prepared solutions of the samples.

Incubator

Cell cultures have been incubated at 37 °C in a 5% carbon dioxide controlled atmosphere of a Hera Cell 150i CO_2 incubator (Thermo Scientific).

Optical plate reader

Cellular vitality was determined by absorbance measurements at 595 nm (resazurin test), using a plate reader ELISA Microplate Reader Model 550 (Bio-Rad). Data were obtained and processed by Microplate Manager 4.0, Origin 8.0 or Excel 2016 softwares.

CHAPTER 1

DETAILED CHEMISTRY OF AU(I/III) DITHIOCARBAMATO COMPLEXES

1.1 The chemistry of gold: an overview

Gold is undoubtedly one the first metals known to early civilizations. It is widely distributed and almost always associated with pyrite or quartz. Gold is found as free metal and in tellurides in veins and in alluvial deposits. The metal is also present in seawater in concentrations of 0.1-2 ppb, depending on the location of the sample. In solid state, it appears as yellow nuggets, not very hard and can be indeed easily scratched by a knife.[1] In fact, properties such as ductility, malleability and sectility are some remarkable characteristics of the metal, meaning it can be easily stretched into a wire, crushed into other shapes, and cut into slices, respectively. It is a leading metal also for jewelry because it never tarnishes and is not attacked by exposure to air or to most reagents.[2,3] In the solid state, gold is a yellow-colored element, although it may appear black, ruby or purple when finely divided. In fact, it can be suspended in solution in a metastable colloidal state. It is a good conductor of both electricity ($4.5 \cdot 10^{-7}$ S/m - the third highest value after Cu and Ag) and heat (320 W/m·K - ranking third after Cu and Ag) and it is a good reflector of infrared radiation.[1]

Although the electron affinity for metals is not usually included in textbooks, the process to yield Au(-I) from Au(0) can be easily accomplished, and is, indeed, known since 1930.[2,4]

Gold belongs to 11th group of the periodic table and its most stable oxidation states are *+1* and *+3*. The electronic configurations of gold(0), gold(I) and gold(III) are $[Xe]4f^{14}5d^{10}6s^{1}$, $[Xe]4f^{14}5d^{10}$ and $[Xe]4f^{14}5d^{8}$, respectively. The solution chemistry of these two ions is intriguing. Gold(I) can form linear, trigonal-planar or tetrahedral diamagnetic complexes, in which the hybridization at the gold center may be considered *sp*, sp^2 and sp^3, respectively, involving its *6s* orbital and one or more of the *6p* orbitals. However, this scenario is oversimplified inasmuch as *5d* orbitals of gold are used in bonding to a great extent. Gold(I) is considered a very soft metal center by Pearson's theory, and this property is highlighted when the metal reacts with potentially bidentate ligands. In fact, it almost invariably coordinates the softest donor atoms of the ligand. For example, NCO^-, $S_2O_3^{2-}$ and SO_3^{2-} are bound through *N* or *S* rather than *O* atom.[5] On the other hand, gold(III) is a less soft metal ion than gold(I) and, thus, is able to form many diamagnetic complexes with hard ligands,

containing oxygen donor atoms. However, gold(III) displays higher selectivity toward soft (*e.g.,* sulfur-based) ligands,[6] forming complexes with square planar (D_{4h}) geometry.[3,7] **Figure 1.1** displays the molecular orbital representation for this tetra-coordination, common for d^8 electronic configuration.

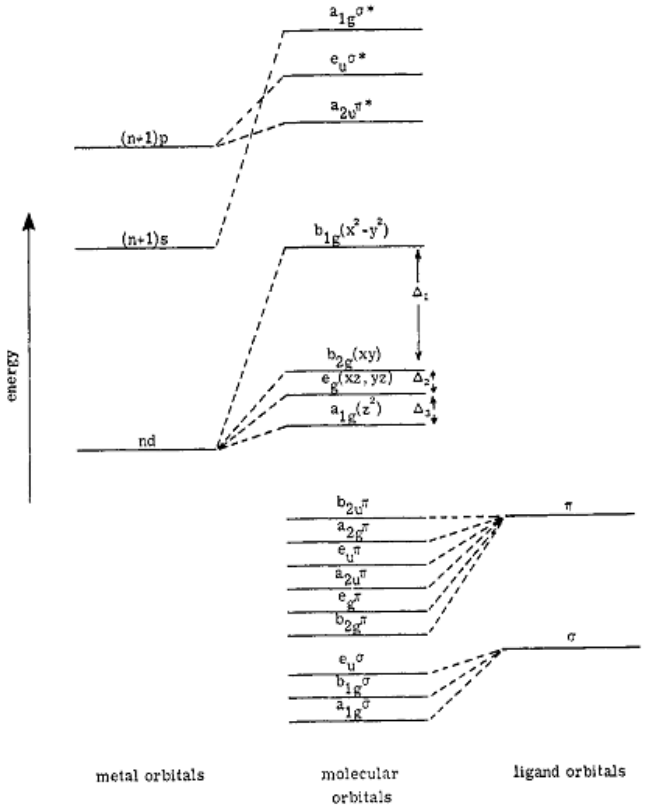

Figure 1.1: Molecular orbital diagram for square planar complexes (with D_{4h} geometry) involving π-basic ligands (*e.g.*, Cl^-, Br^-). For a 32 valence-electron d^8 complex (such as $[Au^{III}Br_4]^-$), b_{1g} (x^2-y^2) orbital can be referred to as LUMO. This image is provided by Ref 7.

The most important gold(III) precursors for chemical syntheses are the corresponding halides both in polymeric form such as the halide-bridged $AuCl_3$, $AuBr_3$ and as aurate anions. The latter group is represented by the $[AuCl_4]^-$, $[AuBr_4]^-$ and $[AuI_4]^-$. In particular, while chloride and bromine derivatives are stable both in solid state and in solution (with Au-Br bond stronger than Au-Cl one) as alkaline metal salts, the tetraiodoaurate can be obtained synthetically as dark solid (especially with bulky cations such as Rb^+ or Cs^+) but decomposes rapidly when solvated.[8] The decomposition leads to the formation of polymeric yellow AuI or $[AuI_2]^-$ complex and I_2 due to the higher reduction potential of gold(III) with respect to

iodide. These peculiar oxidizing properties are due to the so-called "relativistic effect", that is briefly resumed above.

Post-lanthanoid elements (Z>72),[9] such as Au, contain a large number of protons in their nuclei. Therefore, the electrons move around the atomic core in a highly positive electric field (due to the high Z value), which causes them to have velocities approaching that of light and, consequently, they have to be described according to the Einstein's theories of relativity. This is particularly true for electrons in *s* core orbitals, and is less important for *p*, *d* and *f* electrons, being more spatially-diffuse.[10]

Charges moving at a speed close to *c* cannot be treated in terms of classical physics, but they are endowed with a relativistic mass that, for electrons, is higher than the mass of the electron at rest.[11] In the post-lanthanoid elements, the relativistic effect on the *6s* electrons is visible on the contraction of the orbital radius (associated with a stabilization of the 6s orbital – *direct* effect), that results in higher shielding of the positive nuclear charge, thus affecting Z_{eff}. The energy-decrement of the *6s* shell causes also a destabilization and a spatial-expansion of the non-core *5d* orbitals (*indirect* effect). As a consequence, the gap between these two valence levels becomes smaller with respect to all the other elements of the 6th period.[11-14] **Figure 1.2** shows a plot where the ratio of the relativistic radius of the *6s* orbital out of its non-relativistic counterpart is presented as a function of the atomic number (Z). This ratio strongly deviates from unity with increasing of Z and it reaches a pronounced local minimum with gold. Thus, without discussing any further theoretical remark, this relativistic approach points out that gold (and even platinum) actually occupies a unique position among the elements.[2,11]

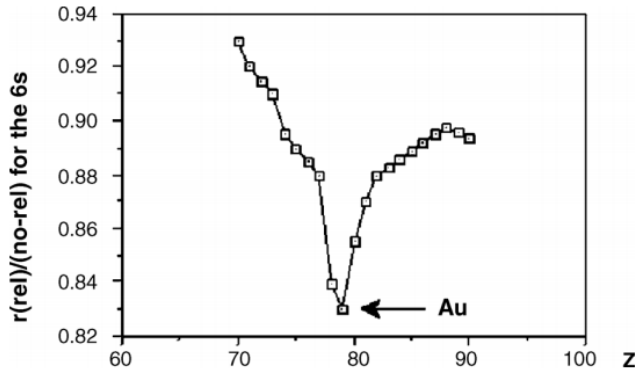

Figure 1.2: Ratio of *r*(relativistic)/*r*(non-relativistic) for the 6s orbitals versus atomic number for various elements. Image provided by Ref 2.

The relativistic effect can pave the way to the understanding of the change in electronic configuration for Au (m=9) and, similarly, for Pt (m=8) from $5d^m6s^2$ to $5d^{m+1}6s^1$. Moving an electron from the *6s* orbital to the *5d* ones increases the value of Z_{eff} sensed by non-core orbitals (additional deshielding by configurational change). As a matter of fact, with a $5d^{10}6s^1$ electronic displacement, the ten electrons in the full *5d* shell of Au atoms result more stabilized compared to the other configuration ($5d^96s^2$) while a further stabilization, because of the *5d* fulfillment-mediated Z_{eff} increase, occurs for the *6s* electron that remains uncoupled. In other words, the closed *5d* shell experiences a weaker *indirect* destabilization effect and, accordingly, an increment of the *direct* stabilization effect occurs for the *6s* orbital. Hence, the maximum of relativistic effect is detectable for gold atoms and not for Hg ($5d^{10}6s^2$).[15]

There are several consequences of this effect in gold chemistry:

- the color of gold. Unlike other metals of the 6th period, its *6s*←*5d* transition starts absorbing at 517 nm (2.4 eV) according to its relatively small band gap. It strongly absorbs blue and violet and it reflects red and yellow light (the analogous absorption for silver lies in the ultraviolet, at around 335 nm, 3.7 eV, accordingly silver is uncolored in solid state);
- the relativistic destabilization (*indirect* effect) of the *5d* orbitals allows the easy formation of the oxidation state *+3*. Conversely, the relativistic stabilization (*direct* effect) of the *6s* orbital accounts for the formation of the pseudo-halogen auride ion, in which the metal is in the oxidation state *-1*. As a consequence of this behavior, gold is the most electronegative transition metal and according to Pauling's scale it possesses a value of electronegativity of 2.54 (comparable to that of iodine; in comparison, Cu and Ag have 1.90 and 1.93, respectively).[1] Likewise, the metal has got a strong electron-affinity (1.1 eV)[1] and high reduction potentials for the different oxidation states. The value of its standard electrochemical potential (E_0) for every reduction, as shown in **Figure 1.3**, is the highest among metals.[3]

$$Au^{3+} \xrightarrow{1.29\,V} Au^{+} \xrightarrow{1.68\,V} Au$$

$$Au^{3+} \xrightarrow{1.42\,V} Au$$

Figure 1.3: Reduction potentials E^0(V) of the most stable gold ions.[1]

Accordingly, gold in any cationic form is able to accept electrons from actually any source (reducing agent) to form neutral gold atoms which can aggregate as a metal bulk;

- as described above, due to the relativistic destabilization, the closed shell $5d^{10}$ is no longer chemically inert and can interact with other gold atoms in molecules or clusters and other elements. Bonding between two gold centers with equal charge (*+1*) and a closed-shell $5d^{10}$ electronic configuration can also be rationalized, although it is difficult in terms of classical bonding. The metal ions approach each other to an equilibrium distance ranging 2.7 to 3.3 Å. This range comprises the distance observed between gold atoms in the metal bulk and it comes closer, or even correspond to, the range of distances found for the authentic Au^{I}-Au^{I} single bonds. Schmidbaur has called this Au(I)-Au(I) interaction *aurophilic-attraction* or *aurophilicity.*[16,17] Many examples of d^{10}-d^{10} interactions have been collected in literature since 1990.[18] It is worth highlighting that other studies have provided support for the hypothesis that the *aurophilic-attraction* can also exist for d^{10}-d^{8} and d^{8}-d^{8} systems, in which one or both gold are in the oxidation state *+3*.[19-21]

In order to achieve a more complete view about the chemistry of this interesting metal, it should be mentioned that many gold compounds with the metal center in the *+2*-oxidation state were described in literature.[22] In fact, the number of complexes with gold in a formal oxidation state of two has increased considerably during the last two decades. In this oxidation state, gold ion has the electronic configuration $[Xe]4f^{14}5d^{9}$ that gives rise to exa-coordinated complexes in distorted octahedral geometry. Gold(II) complexes are generally not stable but they can be isolated and studied (*e.g.*, by EPR spectroscopy) at very low temperature (-78 °C) using chelating soft ligands, such as dithiocarbamates.[23] Intriguingly, an exception was recently reported for gold(II) with chelate di-phosphine ligands, which proved to be stable at room temperature for several hours.[24] The Au(II)-DTC complexes are generally synthetized by oxidative addition from dinuclear Au(I)-DTCs (**Figure 1.4**), treating them at -78 °C with an equivalent of halides or pseudo-halides such as Br_2, I_2, BrCN, $(SCN)_2$ or $(SeCN)_2$.

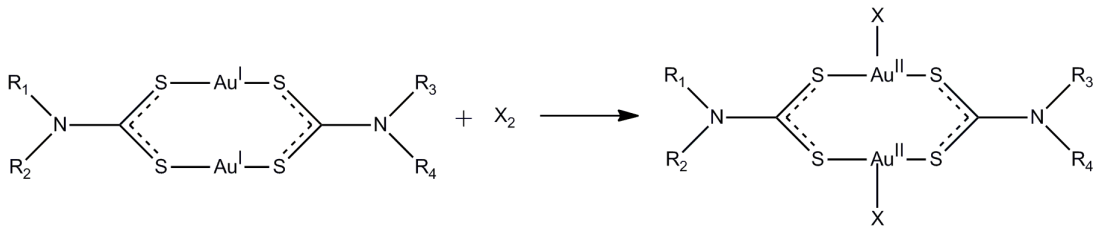

Figure 1.4: This picture describes the oxidative reaction forming an Au(II)-dithiocarbamato complex from an Au(I) dinuclear compound. The product is generally unstable at RT and can be studied spectroscopically at -78°C [X=halide or pseudo-halide, R= alkyl, aryl, H].

As reported in literature,[22] this reaction immediately leads to the precipitation of a green compound which turns into yellow upon warming. This change is probably due to the disproportion reaction involving two Au(II) centers, as reported in below:

$$2\ \text{Au (II)} \longrightarrow \text{Au (I)} + \text{Au (III)}$$

Moreover, this oxidation state could be considered as an intermediate one in the oxidation process of Au(I)-dithiocarbamato complexes to Au(III) ones, in the presence of an excess of strong oxidizing agents.

1.2 Chrysotherapy, an old alchemical milestone reassessed and updated for the modern therapies

Among all elements, gold has always fascinated human beings, leaving a mark on cultures, arts and, also, medicine. The earliest therapeutic uses of gold can be traced back to the ancient Egyptian and Chinese cultures around 3000-2500 BC.[25,26] Following the course of history, in medieval Europe, alchemists developed a number of methods for preparing many elixirs referred to as *aurum potabile*, most of them containing a little quantity of colloidal gold. Later, a liquor drink, known as *cordial*, could be found in the pharmacopoeias of the 17th century and consisted in a suspension of the finely-divided noble metal. Nicholas Culpeper (an English botanist of the XVII century) prescribed it for the treatment of illnesses "caused by a decrease in the vital spirits, including fever, melancholy, fainting, and sickness".[27,28]

In addition to the medical uses of the gold in the native and colloidal states, also its coordination compounds played a key role in the development of the modern medicine. In fact, in the 19th century, an aqueous mixture of $Na[Au^{III}Cl_4]$ and NaCl was used as a

treatment for syphilis.[28] The term chrysotherapy (χρυσός - in Greek stands for gold) was coined for the usage of gold-based compounds in the twentieth-century medicine, and goes back to the pioneering work of the German bacteriologist Dr. Robert Koch (awarded the Nobel Prize in 1905) whose discovery in 1890 was associated with the bacteriostatic activity of gold(I) cyanide $K[Au^{I}(CN)_2]$ against the tubercle bacilli (*mycobacterium tuberculosis*). Gold therapy for tuberculosis was subsequently introduced in the 1920s. The discovery that the tubercle bacillus was also one of the causes of the rheumatoid arthritis led to the use of gold compounds as therapeutic agents for this disease.[29] It should be highlighted that gold-based treatments proved soon to be ineffective for tuberculosis. In contrast, after a thirty-year debate, a clinical study confirmed the effectiveness of chrysotherapy against rheumatoid arthritis. In fact, Auranofin (2,3,4,6-tetraacetyl-β-1-D-thioglucopyranose-S-(triethylphosphine) gold(I)) is nowadays the most effective metal-based treatment against this autoimmune disease and its use is normally recommended when it is necessary to relieve symptoms in adult rheumatoid arthritis poorly controlled with other therapies.[29,30]

Auranofin (Ridaura®), approved for clinical use by oral administration, is a monomeric species with a linear coordination geometry, able to cross the cell membrane due to the lipophilic phosphine ligand. Its in vivo mechanism of action is still unknown, but it is certainly associated with the rapid displacement of the tetra-acetylthioglucose ligand by ligand-exchange reactions on the Au(I) ion.[31] On the contrary, the phosphine is removed more slowly by similar processes after about 24 hours, causing fewer toxic side-effects compared to the forerunner polymeric agents, such as the aurothioglucose (Solganal®) and the sodium aurothiomalate (Myochrysine®). Nevertheless, the slow reactivity influences also the efficacy of the drug, which results generally reduced with respect to the other two compounds, *i.v.* or *i.m.* administered.

Currently-chrysotherapy is clinically addressed not only to inflammatory diseases. In fact, Auranofin is nowadays used, alone or in combination therapy, also for cancer treatment in clinical trials (phase I and II for leukemia, ovarian and lung cancers).[32,33] Additional effects have been recently reported in terms of inhibition of various thiol-containing enzymes and antimicrobial/antifungal activity.[34,35] The first reports of the anticancer activity of gold compounds appeared in the mid-1980s. In this regard, two rationales have been taken into account for the investigation of gold compounds as antineoplastic agents: i) similarities

between gold(III) square-planar complexes and their platinum(II) analogues (their archetype cisplatin approved in 1978 by FDA as antineoplastic drug) and ii) the possibility to synthesize gold(I) and gold(III) complexes functionalized with organic drugs and/or solubilizing agents as ligands, in order to modulate or confer new properties to the metal ion. However, the generally reducing physiological environment allows gold(III) compounds to be reduced *in vivo* to gold(I) species and, in turn, to metallic gold atoms. Consequently, a proper selection of the ligands is required to enhance the stabilization of the metal center in its oxidation state, by lowering its reduction potential.[36] Auranofin proved cytotoxic towards tumor cells *in vitro*, and this led to the identification of other Au(I) phosphines with a broader spectrum of antitumor activity, in particular the bis-chelated Au(I) diphosphine complexes (of the type $[Au^{I}(DPPE)_2]Cl$; DPPE = bis (diphenylphosphino)ethane). They were selected as interesting candidates for therapeutic uses and firstly patented by Berners-Price and co-workers in 1986.[37,38] In addition, some Au(III) complexes with a bidentate ligand, such as $[Au^{III}Cl_2(damp)]$ (damp = dimethyl aminomethylphenyl) and its acetate analogue first reported by Fricker in 1996, showed interesting biological properties.[39,40] These foremost attempts suggested that a higher stability and, hence, an enhanced delivery of gold along with lower toxicity could be obtained with less labile chelating ligands endowed with N-, S- and P-donor atoms. From the chemical point of view, the compounds reported by Berners-Price and Fricker are stabilized against gold reduction under physiological conditions by the di-phosphino ligands.[37,41,42] In last decades, various classes of gold compounds were synthetized and tested from the biological point of view in different laboratories worldwide, exhibiting outstanding therapeutic effects. In addition to chlorides and bromides, these coordination compounds involve N-, O-, P- and S-donor ligands.[37,43] Lately, many organometallic complexes with a pure σ-coordination have been synthesized as well (conversely, the π-Au–C bond counterparts are unstable under most conditions[44]), and have showed interesting biological properties.

1.3 The chemistry of gold dithiocarbamato complexes

A significant part of this work is addressed to the understanding of the chemistry, the equilibria in solution, the reactivity and the biological profile of the gold(III) and gold(I) dithiocarbamates. As described in the Introduction (**Section 8**), several Au(III)-DTC complexes bearing different dithiocarbamato ligands (*e.g.*, either linear or cyclic alkyl

ligands, aromatic ones or peptide-functionalized DTCs) were synthetized and studied by our research group in the last fifteen years. Besides the chemical investigation of these compounds, also the biological activity and biochemical interaction were explored with interesting and promising results. Initially, the attention of our researches was mainly addressed to the neutral complexes bearing one dithiocarbamate and two halogens (chlorine or bromine atoms). The latter ligands are in trans with respect to the bidentate DTC and in cis position each other, miming the features of cisplatin. Thanks to this previous work, additional gold(I/III)-DTC species with different metal-ligand ratios were defined, isolated and characterized, that paved the way to a deeper comprehension about their fascinating chemistry. For rigorousness and convenience, all the complexes described in this first chapter possess the piperidine dithiocarbamato ligand (hereinafter PipeDTC), isolated as potassium or sodium salt (the only exception is shown in the crystal structures of $[Au^{I}(PPh_3)(DTC)]$ complexes in which a methyl-amino or a hydroxy-methyl group is present in the C-4 position of the piperidine ring; **Figure 1.5**). This ligand has shown interesting properties, such as the absence of deliquescence as alkaline metal salt, the high synthetic yield and, due to the stability of the chair conformation of the six-member ring in solution, is able to confer better solubility in organic solvents to the products.

1.3.1 The Au(I)-DTC Complexes and their synthesis

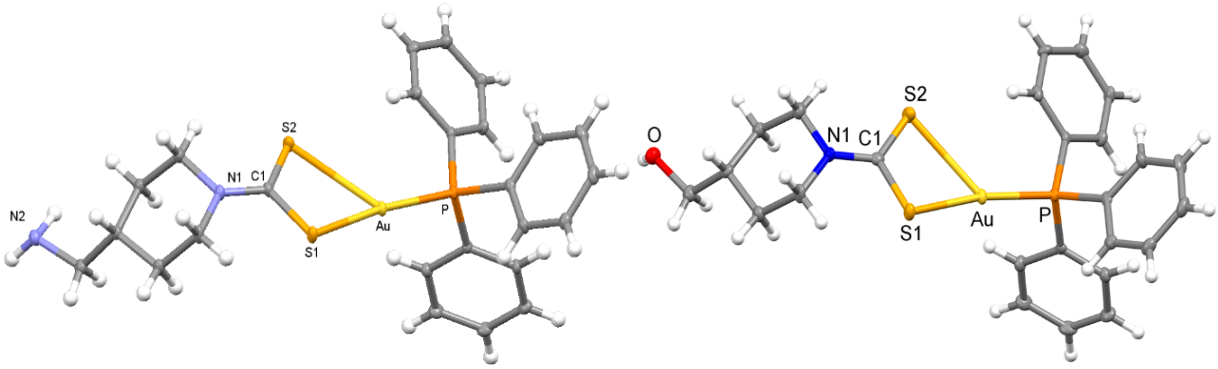

Figure 1.5: crystal structures of the linear pseudo-tricoordinated [Au^{I}PPh$_3$(aminomethyl-PipeDTC)] (*left)* and [Au^{I}PPh$_3$(hydroxymethyl-PipeDTC)] (*right*). The thermal ellipsoids are set at a 50% probability level.

As described in the "Chemistry of Gold" section (**Section 1.1**), Au(I) ion has a d^{10} electronic configuration and forms linear complexes. The most important ligands for gold(I) are those with polarizable donor atoms, such as P, S, As and Se.[45] In light of these considerations, dithiocarbamates establish strong interactions with the soft metal center, either in bidentate or monodentate mode, depending on the nature of the precursor. In fact, if the synthesis is carried out from [Au^{I}(THT)Cl] complex (THT: tetrahydrothiophene ligand) or Na[Au^{I}X$_2$] (X: Cl, Br; that are not stable in solid state and have to be obtained in solution throught the reduction of an Au(III) salt), the addition of one equivalent of PipeDTC leads to the release of the primitive ligands and the formation of a dinuclear Au(I) complex that possesses a 2:2 metal:DTC stoichiometric ratio (**Figure 1.6**). In this case, the dithiocarbamate act as a bidentate bridging coordinating agent between the two metal centers. In this regard, first systematic investigations of N,N-dialkyl-dithiocarbamato derivatives of gold(I) started at the end of the 1950's and, already at that time, it was evident that these compounds appear as dimeric "at least in benzene solution".[46] A subsequent X-ray crystallographic study of N,N-dipropyldithiocarbamato gold(I)[47] revealed a supramolecular structure with gold chains, where the gold ions form pairs linearly coordinated by two sulfur atoms of the dithiocarbamato moiety. It is a common feature of these complexes that the interatomic Au–Au distances inside the dimer units Au$_2$[DTC]$_2$ are comparable with the distance in elemental gold (2.8782 Å)[48], or they are even shorter [e.g., R= 2.76(1)Å[47] or 2.782(1) Å][49], whereas the distances between adjacent chains vary significantly from structure to structure as revealed

during further investigations.[49,50] The nature of the interaction accounting for the short Au-Au distance was strongly debated since the late 1980's,[51,52] and finally led to the terms aurophilic bonding and/or aurophilicity.[16-18]

On the other hand, if the phosphino-gold(I) chloride complex ([$Au^{I}(PR_3)Cl$]) is used as precursor, an heteroleptic product [$Au^{I}(PR_3)DTC$], bearing a phosphine and a dithiocarbamato ligand, is obtained upon the addition of one equivalent of DTC. This phenomenon, in which the phosphino-ligand remains coordinated to the metal and cannot be replaced by a DTC, accounts for the strong interaction between Au(I) center and P-donor substrates, that exceeds that of S-donating ligands (**Figure 1.5** and **Figure 1.6**).

Moving to the crystal structure, the phosphino gold(I) dithiocarbamato complexes show a linear coordination geometry, with a P-Au-S1 angle of around 175° thus accounting for an asymmetrical bonding mode of the DTC ligand. Intriguingly, a long-range Au-S2 interaction can be detected, with the Au-S2 bond length of 2.94 Å compared to the distance of 2.34 Å between Au and S1. The other structural values of the coordinated dithiocarbamate are very similar to those of the free ligand.[53]

Unfortunately, the very low solubility of the 2:2 compounds in all the solvents, limits their chemical biological properties ad their use as precursors in chemical synthesis.

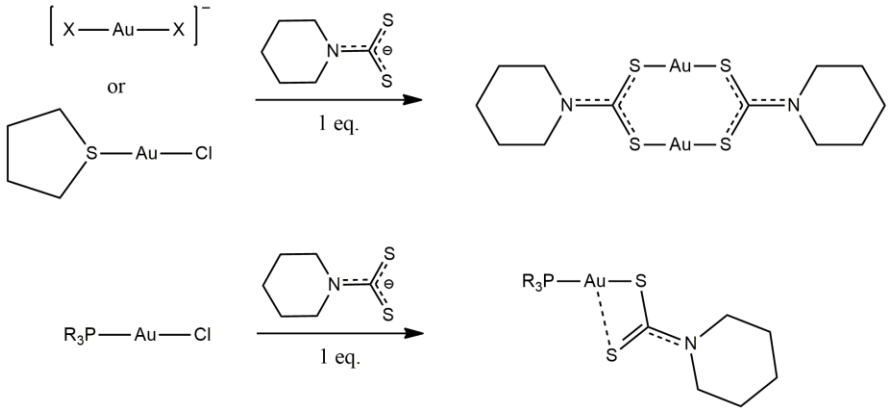

Figure 1.6: Schematic representation of the synthetic pathways of Au(I)-DTC complexes.

- Synthesis of bis(piperidine dithiocarbamate) di-gold(I), [Au^{I}(PipeDTC)]$_2$

From *in-situ* reduced [$Au^{I}X_2]^-$ precursor: To a stirring ice-cold aqueous solution (10 ml), saturated with NaCl, containing 0.5 mmol of $Na[Au^{III}X_4]\cdot 2H_2O$ was added dropwise 1 eq. of Na_2SO_3 pre-dissolved in deionized water (2 mL). The mixture slowly became colorless and,

only at this point, 5 mL of deionized water containing 1 eq. of PipeDTC potassium salt were added in one portion. A flocculent yellowish solid readily precipitated. The product was separated, washed 3 times with water (10 mL) and dried in pump over P_2O_5.

From [Au^I(THT)Cl] precursor: The chloro-tetrahydrothiophene-gold(I) complex was synthetized as reported elsewhere.[54] At this point, 1 mmol of precursor was dissolved in acetone (6 mL), obtaining a colorless solution. To this, 1 eq. of DTC ligand in MeOH (2 mL) was added in one portion leading to the precipitation of the yellowish product that was work upped as described above.

Aspect: green-yellow solid

Yield: 90-95 %

Anal. Calc. for $C_{12}H_{20}Au_2N_2S_4$ (MW = 714.49 g·mol^{-1}): C 20.17; H 2.82; N 3.92; S 17.95. Found: C 20.20; H 2.82; N 3.99; S 17.89.

1H-NMR (DMSO-d6, 600 MHz): δ (ppm) = 0.85 (m, 12H, $H_{(3)}$ + $H_{(4)}$ + $H_{(5)}$), 4.13 (m, 8H, $H_{(2)}$ + $H_{(6)}$).

Medium FT-IR (KBr): $\tilde{\nu}$ (cm^{-1}) = 2934.15, 2846.67 (ν_a, C-H); 1427.69 (ν_a, N-CSS); 967.97 (ν_a, CSS).

Far FT-IR (nujol): $\tilde{\nu}$ (cm^{-1}) = 556.72 (ν_s, CSS); 478.93 (ν_a, Au-S).

- Synthesis of piperidine dithiocarbamate-triphenylphosphine-gold(I), [$Au^I$$PPh_3$(PipeDTC)]

20 mL dichloromethane solution containing 0.5 mmol of [$Au^I$$PPh_3$Cl][55] complex was poured in a 100 mL round-bottom flask and a vigorous stirring was started. At this point, 1.5 eq. of PipeDTC potassium salt dissolved in 20 mL of deionized water was added in one portion into the flask. The mixture was left stirring for one hour. Readily after the addition, the organic phase became greenish yellow. The progress of the reaction was monitored with TLC (eluent: dichloromethane). When the reagent was totally consumed, the organic phase was separated, dried with Na_2SO_4, filtered and the solvent was half-reduced by rotatory evaporator. The addition of diethyl ether lead to the precipitation of a light green solid that was collected and dried in vacuo.

Aspect: light green-yellow solid

Yield: 90-95 %

Anal. Calc. for $C_{24}H_{25}AuNPS_2$ (MW = 619.53 g·mol^{-1}): C 46.53; H 4.07; N 2.26; S 10.35. Found: C 46.10; H 4.30; N 2.28; S 10.49.

^{1}H-NMR ($CDCl_3$, 300 MHz): δ (ppm) = 1.88 (m, 6H, $H_{(3)}$ + $H_{(4)}$ + $H_{(5)}$), 3.05 (m, 8H, $H_{(2)}$ + $H_{(6)}$), 7.50-7.05 (m, 15H, aryl).

Medium FT-IR (KBr): $\tilde{\nu}$ (cm^{-1}) = 2934.15, 2846.67 (ν_a, C-H); 1530.69 (ν_a, N-CSS); 951.97 (ν_a, CSS).

Far FT-IR (nujol): $\tilde{\nu}$ (cm^{-1}) = 556.27 (ν_s, CSS); 439,59 (ν_a, Au-S); 284,77 (ν_a, Au-P).

1.3.2 The Au(III) di-Halo DTC-Complexes (Metal to DTC-ligand ratio 1:1)

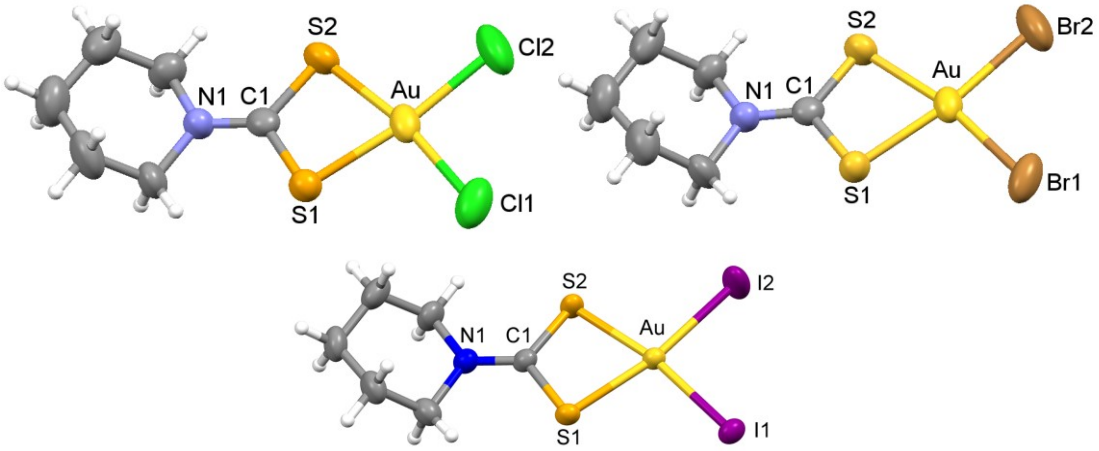

Figure 1.2: crystal structures of the three neutral Au(III) dithiocarbamato di-halo complexes with metal-ligand stoichiometry 1:1 with general formula [$Au^{III}X_2$(PipeDTC)]. The thermal ellipsoids are set at a 50% probability level.

The 1:1 derivatives are neutral tetracoordinated complexes possessing one bidentate dithiocarbamato ligand and two halides saturating the opposite coordination positions. These ones could be Cl, Br and I.

As revealed by the crystal structures (data reported in **Table 1.1**), this class of compounds shows a distorted square planar coordination, with a planarity that includes also the C-N bond. The distortion from a D_{4h} coordination geometry is mainly due to the small S-Au-S angle of 75°, with respect to 90° in the case of perfect square planar complexes.

Table 1.1

	Au-S1 (Å)	Au-S2 (Å)	C1-N1 (Å)	Au-X1 (Å)	Au-X2 (Å)	S1-Au-S2 (°)
[$AuCl_2$(PipeDTC)]	2.289(2)	2.299(2)	1.289(8)	2.323(2)	2.307(2)	75.67(7)
[$AuBr_2$(PipeDTC)]	2.320(5)	2.314(5)	1.300(1)	2.460(4)	2.463(5)	75.60(1)
[AuI_2(PipeDTC)]	2.327(3)	2.321(2)	1.294(13)	2.601(8)	2.595(10)	74.89(10)

Moreover, the distance between the Au center and sulfur atom is around 230 pm, which is longer than the C-S bond (170 pm). The same bite angle, with the addition of the C-N, C-S distances and S-C-S angle value, has been detected in literature also for Ni(II), Cu(II), Zn(II) and Pt(II)-DTC derivatives,[56-59] proving that the ligand itself is not susceptible to considerable structural variations after the metal coordination. On the contrary, a difference is noticed in the Au-X distances in the case of chloro- and bromo-derivatives, with values of ca. 231 pm and 246 pm for Au-Cl and Au-Br bonds, respectively. As a matter of facts, despite the higher orbital affinity of Au(III) for the more polarizable halides, such as Br and I, the Au-X distance in the di-chloro complex is the smallest one, due to the high electronegativity and small Van der Waals radius of chlorine atom.[1]

Concerning the solvating properties, the non-ionic nature of the 1:1 compounds imparts a strong insolubility in water and in polar solvents. On the contrary, they are soluble in most organic aprotic media, such as acetone, acetonitrile and, in particular, dichloromethane and chloroform.

1.3.2.1 Syntheses of 1:1 Au(III)-DTC di-halo complexes

The synthesis of the described di-halo derivatives has been in deeply studied and optimized during this work. In particular, the most efficient synthesis detected, in term of yield, is the oxidative addition of the dinuclear Au(I) compounds with an excess of halogens, such as bromine and chlorine (**Figure 1.7**, Path 1), firstly reported by Steggerda and co-workers in 1968.[60] In this reaction, the oxidation state of gold ions passes from +1 to +3, whereas the halogens formally reduce to -1. Due to the high reduction potential of the metal, the oxidation process is not fast, and the formation of different intermediates can be detected qualitatively: in fact, the reaction mixture, initially an ochre suspension, become brown as soon after the addition of the excess of halogens, then turns to green and, after 10 to 30 minutes becomes yellow or red, in the case of di-chloro or di-bromo compounds, respectively. Several

authors[22, 61] suggested that the intermediate green species formed via oxidative addition reaction could be associated to a tri-coordinated Au(II) complexes, that can be stabilized (but not isolated) if the reaction is carried out at -78°C. However, the excess of oxidant and the instability of the +2-oxidation state for gold, lead to the formation of the more stable Au(III) di-halo derivative in good yield. It is worth highlighting that the oxidative addition reaction cannot be achieved if iodine is used as oxidant, due to the high difference in reduction potential between gold and the halogen ($E^0_{Au(III)/Au} = 1.5$ V; $E^0_{I2/2I-} = 0.54$ V)[1]. Attempts to obtain the di-iodo complex through the oxidative addition cause the precipitation of insoluble yellow AuI with the contemporary oxidation of the dithiocarbamato ligand to thiuram disulfide (**Introduction**, **Figure 23**). In order to obtain the di-iodo derivative, a halogen substitution reaction was carried out by heterogeneously mixing a CH_2Cl_2 solution of the purified di-chloro and di-bromo counterparts with an excess of aqueous sodium iodide (NaI).[62] Soon after the addition, the organic phase becomes strongly purple, indicating the quantitative formation of the di-iodo Au(III) dithiocarbamato complex (**Figure 1.7**, Path 4).

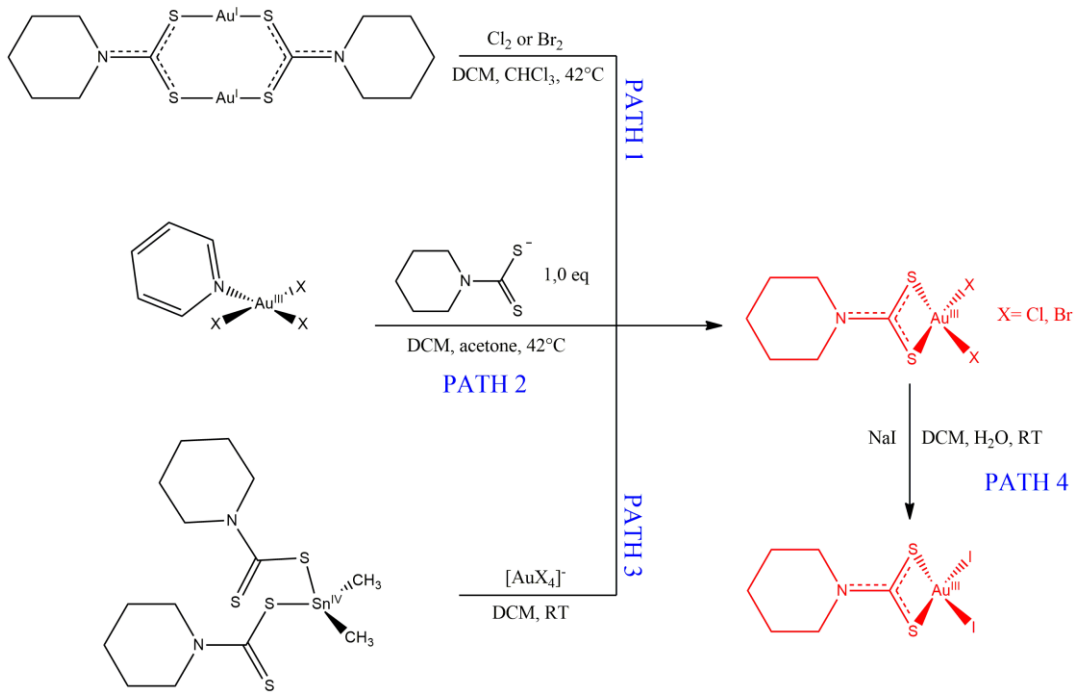

Figure 1.7: description of the main reaction pathways optimized for the synthesis of the 1:1 complexes.

Alternative synthetic routes to obtain the 1:1 compounds are presented in **Figure 1.7** as Path 2 and 3. The first one consists in a complexation reaction between the DTC ligand and the

well-known tri-halo pyridine Au(III) precursor [$Au^{III}X_3(py)$],[63] which is soluble in apolar aprotic solvents. If exactly one equivalent of the ligand is added, the 1:1 complex is formed as majority product. Conversely, if the DTC salt is present in excess, also the complex with 1:2 stoichiometry ($[Au^{III}(DTC)_2]^+$) could be obtained.

Furthermore, the reaction route labelled as Path 3 involves the transmetallation of the dithiocarbamato ligand between the hard Sn(IV) center and the softer Au(III) ion. The reaction exploits the occurrence that sulfur-donating ligands interact stronger with more polarizable metal centers preferably in low oxidation states, such as Pt(II), Au(I/III) and Hg(II), and form less stable complexes with *p*-block metals which are less polarizable and possess a remarkable covalent behavior. As a consequence, the dithiocarbamato ligand is easily transferred from the less stable [$Sn^{IV}Me_2DTC_2$] complex to the Au(III) center (added as $[Au^{III}X_4]^-$ salt), leading to the formation of the 1:1 di-halo complex in good yield and the di-halo, di-methyl tin(IV) as byproduct. It is important to specify that the di-methyl substituted stannane complex has been preferred with respect to the mono-methyl and tri-methyl derivatives thanks to the lower cost of the reagent (that is the [$Sn^{IV}Me_2Cl_2$]) which is also less toxic than its counterparts. Moreover, while the [$Sn^{IV}Me_2DTC_2$] complex is an easy-to-manageable solid, the [$Sn^{IV}MeDTC_3$] and [$Sn^{IV}Me_3DTC$] derivatives appear as a hygroscopic solid and a viscous liquid, respectively.

Such a transmetallation reaction, besides its positive aspects (*i.e.*, high yield, high reaction rate, etc.), has never been described in literature until now.

- Synthesis of di-halo (Cl or Br) piperidine dithiocarbamato gold(III) complex

PATH 1: 0.5 mmol of gold(I)-DTC di-nuclear complex were suspended in 20 mL of halogenated solvent (chloroform or dichloromethane) and the mixture was refluxed under stirring for 10 minutes. Then, in order to obtain the di-chloro derivative, an excess of Cl_2, generated in a separate flask by mixing 300 mg of MnO_2 with 3 mL of concentrated HCl or by adding 4 mL of concentrated HCl to 50 mL of aqueous NaClO (37%), was gurgled for 1 hour. Similarly, in the case of di-bromo counterpart, an excess of bromine was directly added to the Au(I)-DTC suspension (100 equivalents of liquid Br_2 previously dissolved in dichloromethane). In all cases, it was possible to observe that, after some minutes, the solution turned brown with the dissolution of the Au(I) precursor, then turned green and, at the end, became yellow or orange.

After an additional hour, the reaction flask was cooled, the mixture filtered and the volume of the solvent half-reduced. Successively, 40 mL of diethyl ether were added, leading to the precipitation of a yellow-orange solid that was filtered, washed with 2x 4 mL of diethyl ether and 2x 5mL of distilled water, and dried in pump in the presence of P_2O_5. Yield: 91%.

PATH 2: 1 mmol of tri-halo pyridine gold(III) precursor [$Au^{III}X_3(py)$], previously synthetized as reported in literature,[63] were dissolved in 1:3 dichlorometane-acetone mixture. This solution was put at reflux under stirring. After 10 minutes, 1.0 mmol (1.0 eq) of pipeDTC salt dissolved in 2 mL of methanol were added to the Au(III) solution, which in few minutes turned from yellow-red to orange. The reaction was left under stirring at reflux for 2 hours, then the solution was cooled, filtered and reduced to half its initial volume. After the addition of 5 mL of diethyl ether, the flask was left at -10 ° C for two days, leading to the formation of orange needles. Yield 80%.

PATH 3: The reagent [$Sn^{IV}Me_2DTC_2$] was synthetized as follow: to a 10 mL aqueous solution containing 2 mmol of [$Sn^{IV}Cl_2Me_2$] was added 4 mmol (2 eq.) of pipeDTC salt previously dissolved in 5 mL of deionized water. The white flocculent precipitate formed was centrifuged, washed 3 times with distilled water (3x 10 mL) and dried under vacuum in the presence of P_2O_5. Yield: 95%. Afterwards, 1 mmol of the obtained complex were dissolved in 10 mL of dichloromethane and dropwise added, under vigorous stirring, to a 10 mL acetone solution containing 0.5 mmol (0.5 eq.) of $Na[Au^{III}Cl_4]\cdot 2H_2O$ or $K[Au^{III}Br_4]\cdot 2H_2O$. The mixture progressively turned from yellow or red to orange and an orange product started to precipitate. After 20 minutes stirring, the solvent was half-reduced and 40 mL of diethyl-ether added, leading to the precipitation of orange solid, that was filtered, washed with diethyl ether (3x 5 mL) and dried in vacuo. Successively, the solid was portion-wise dissolved in dichloromethane (10 mL) and purified by flash column chromatography using dichloromethane as eluent (Rf: 0.86). Yield: 82%.

Dichloro(piperidine dithiocarbamate)gold(III), [$AuCl_2$(PipeDTC)]

Aspect: dark yellow solid

R.f. (on silica gel, CH_2Cl_2): 0.86

Anal. Calc. for $C_5H_{10}AuCl_2NS_2$ (MW = 428.15 g·mol-1): C 16.83; H 2.35; N 3.27; S 14.98. Found: C 16.86; H 2.37; N 3.21; S 15.02.

^{1}H-NMR (DMSO-d6, 600 MHz): δ (ppm) = 1.72 (s, 6H, $H_{(3)}$ + $H_{(4)}$ + $H_{(5)}$), 3.82 (s, 4H, $H_{(2)}$ + $H_{(6)}$).
^{1}H-NMR ($CDCl_3$, 400 MHz): δ (ppm) = 1.88 (s, 6H, $H_{(3)}$ + $H_{(4)}$ + $H_{(5)}$), 3.77 (s, 4H, $H_{(2)}$ + $H_{(6)}$).
Medium FT-IR (KBr): $\tilde{\nu}$ (cm^{-1}) = 2944.60, 2858.64 (ν_a, C-H); 1581.42 (ν_a, N-CSS); 947.36 (ν_a, CSS).
Far FT-IR (nujol): $\tilde{\nu}$ (cm^{-1}) = 539.66 (ν_s, CSS); 366.20 (ν_a, Au-S); 349.71 (ν_a, Au-Cl); 334.59 (ν_s, Au-S); 315.67 (ν_s, Au-Cl).

Dibromo(piperidine dithiocarbamate)gold(III), [$AuBr_2$(PipeDTC)]
Aspect: orange needles
R.f. (on silica gel, CH_2Cl_2): 0.83
Anal. Calc. for $C_6H_{10}AuBr_2NS_2$ (MW = 517.05 g·mol^{-1}): C 13.94; H 1.95; N 2.71; S 12.40. Found: C 13.99; H 1.98; N 2.73; S 12.42.
^{1}H-NMR (DMSO-d6, 600 MHz): δ (ppm) = 1.72 (s, 6H, $H_{(3)}$ + $H_{(4)}$ + $H_{(5)}$), 3.79 (s, 4H, $H_{(2)}$ + $H_{(6)}$).
^{1}H-NMR ($CDCl_3$, 400 MHz): δ (ppm) = 1.87 (s, 6H, $H_{(3)}$ + $H_{(4)}$ + $H_{(5)}$), 3.73 (s, 4H, $H_{(2)}$ + $H_{(6)}$).
Medium FT-IR (KBr): $\tilde{\nu}$ (cm^{-1}) = 2941.65 (ν_a, C-H); 1573.91 (ν_a, N-CSS); 941.52 (ν_a, CSS).
Far FT-IR (nujol): $\tilde{\nu}$ (cm^{-1}) = 538.90 (ν_s, CSS); 369.79 (ν_a, Au-S); 350.61 (ν_s, Au-S); 239.11 (ν_a, Au-Br); 223.85 (ν_s, Au-Br).

- Synthesis of di-iodo piperidine dithiocarbamato gold(III) complex

PATH 4: 0.25 mmol of di-chloro dithiocarbamato gold(III) complex were dissolved in 30 mL of dichloromethane at room temperature. Successively, 15 mL of deionized water containing 1 mmol of NaI (4 eq.) was added in one portion and the heterogeneous mixture was keep under vigorous stirring for 1 hour while monitoring by TLC (DCM, R_f: 0.95). The color of the organic phase changed progressively from yellow to deep violet. After the completion of the reaction, the aqueous solution was separated and washed with dichloromethane (3x 20 mL). The combined organic phases were dried with Na_2SO_4, filtered and the solvent evaporated until 5 mL. Then, the addition of 40 mL of n-hexane gave the

desired product as violet powder that was centrifuged, washed with n-hexane (2x 4 mL) and dried under P_2O_5. Yield 75%.

Diiodo(piperidine dithiocarbamate)gold(III), [AuI_2(PipeDTC)]

Aspect: violet powder

R.f. (on silica gel, CH_2Cl_2): 0.95

Anal. Calc. for $C_6H_{10}AuI_2NS_2$ (MW = 611.04 g·mol^{-1}): C 11.79; H 1.67; N 2.29; S 10.51. Found: C 11.82; H 1.65; N 2.33; S 10.51.

^{1}H-NMR (DMSO-d6, 600 MHz): δ (ppm) = 1.72 (s, 6H, $H_{(3)}$ + $H_{(4)}$ + $H_{(5)}$), 3.73 (s, 4H, $H_{(2)}$ + $H_{(6)}$).

^{1}H-NMR ($CDCl_3$, 400 MHz): δ (ppm) = 1.82 (s, 6H, $H_{(3)}$ + $H_{(4)}$ + $H_{(5)}$), 3.68 (s, 4H, $H_{(2)}$ + $H_{(6)}$).

Medium FT-IR (KBr): $\tilde{\nu}$ (cm^{-1}) = 2942.08 (ν_a, C-H); 1558.61 (ν_a, N-CSS); 942.62 (ν_a, CSS).

Far FT-IR (nujol): $\tilde{\nu}$ (cm^{-1}) = 504.20 (ν_s, CSS); 359.05 (ν_a, Au-S); 341.44 (ν_s, Au-S).

1.3.3 The Au(III) cationic complexes (Metal to DTC-ligand ratio 1:2)

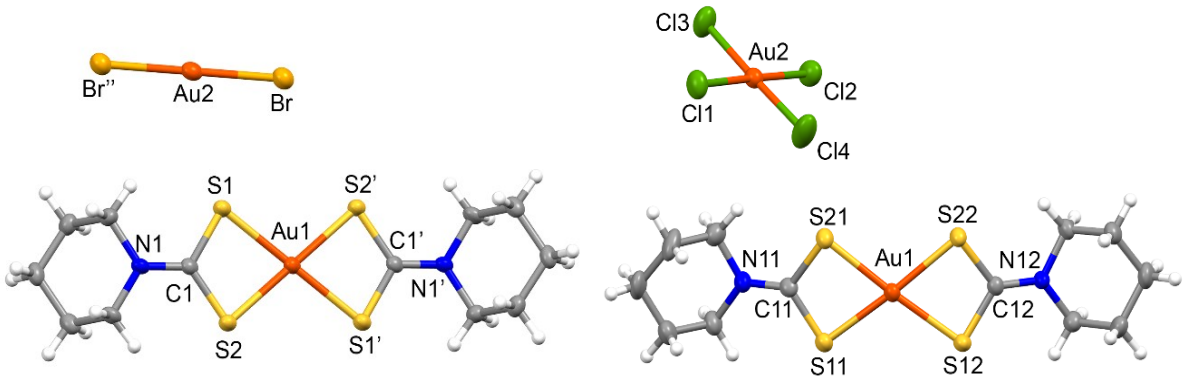

Figure 1.8: Crystal structures of the piperidine dithiocarbamato Au(III) complexes of the type [1:2][$AuBr_2$] (left) and [1:2][$AuCl_4$] (right). The thermal ellipsoids are set at a 50% probability level.

The 1:2 complexes are cationic Au(III)-DTC derivatives in which the metal center is completely saturated by two bidentate dithiocarbamato ligands. These compounds can be easily obtained with different counterions such as halides (in particular, chlorine and bromine), other common anions (e.g., NO_3^-, PF_6^-, BF_4^-, triflate, etc.) or with anionic gold complexes such as $[AuX_4]^-$ or $[AuX_2]^-$. In this last case, the scientific community usually refers to them as double complex salts (DCS) (**Figure 1.8**).[64,65]

The 1:2 dithiocarbamato derivatives were firstly synthetized by Van der Linden, Steggerda and co-workers in 1969,[66,67] paving the way to more detailed studies carried out by Forghieri et. al. in 1988.[68] Moreover, in recent years, the chemistry of such complexes has been investigated by several authors both for pharmaceutical and material-science purposes.[69,70]
Like 1:1 complexes, also this class of compounds shows a distorted square planar coordination, with a S-Au-S bond angle of 75° (**Table 1.2**). Intriguingly, no aurophilic interaction between the cationic and anionic gold ions in the double complex salts is detected as shown by the crystal structures (**Figure 1.8**). In fact, the Au-Au length is 730 pm in the complex $[Au^{III}(PipeDTC)_2][AuCl_4]$ and 550 pm in the $[Au^{III}(PipeDTC)_2][Au^{I}Cl_2]$, proving that the two ions are too far each other to interact.

Table 1.2

	Au-S1 (Å)	Au-S2 (Å)	C1-N1 (Å)	Au-Au (Å)	S1-Au-S2 (°)	S-Au-S (°)
$[Au(pipeDTC)_2][AuCl_4]$	2.337(3) 2.343(3)	2.328(3) 2.315(3)	1.300(1)	7.894(8)	75.36(9) 75.33(9)	176.08(10) 173.23(10)
$[Au(pipeDTC)_2][AuBr_2]$	2.338(0)	2.335(0)	1.323(9)	5.521(0)	75.52(0)	104.48(0)

Concerning the solvating properties, the solubility of the 1:2 compounds is strongly affected by the nature of the counterion. In particular, small anions, such as halides, help to increase the solvation enthalpy and then the hydrophilicity of the entire complex. In fact, the [1:2]Cl compound is readily soluble in a wide range of solvents, passing from halogenated ones to acetone, alcohol and water. On the contrary, the double salt derivatives are more lipophilic, and this effect can be explained by considering a strong lattice energy in solid state between the two paired complexes. Moreover, it is worth highlighting that the $[1:2][AuCl_4]$ double salt is not stable when solubilized in non-coordinating solvents, such as dichloromethane, chloroform and acetone (**Section 1.5**).

1.3.3.1 Synthesis of 1:2 Au(III)-DTC complexes

The synthesis of the gold(III) complexes with stoichiometric ratio 1:2 can be achieved in several ways. For example, Steggerda and co-workers obtained the $[1:2][AuBr_2]$ by simply adding one equivalent of bromine to a suspension of Au(I) dinuclear compound.[67] Furthermore, Isab and collaborators, were able to isolate the $[Au(Me_2DTC)_2]Cl$ complex refluxing an ethanol-water mixture containing a gold(III) precursor and two equivalents of

the ligand.[70] Besides these procedure, the most efficient method in terms of yield has been discovered during this work and consist in the addition of the dithiocarbamato ligand to an equimolar solution of the 1:1 di-halo complex, usually the di-chloro derivative, in aprotic solvent (**Figure 1.9**, path 5). In this case, the substitution of the two halides is favored by the strong trans-effect of the already-coordinated dithiocarbamate.[71] At the best of our knowledge, this experimental procedure has never been reported in literature yet and permits to synthetized also heteroleptic 1:2 complexes containing two different dithiocarbamato ligands in Au(III) coordination sphere.

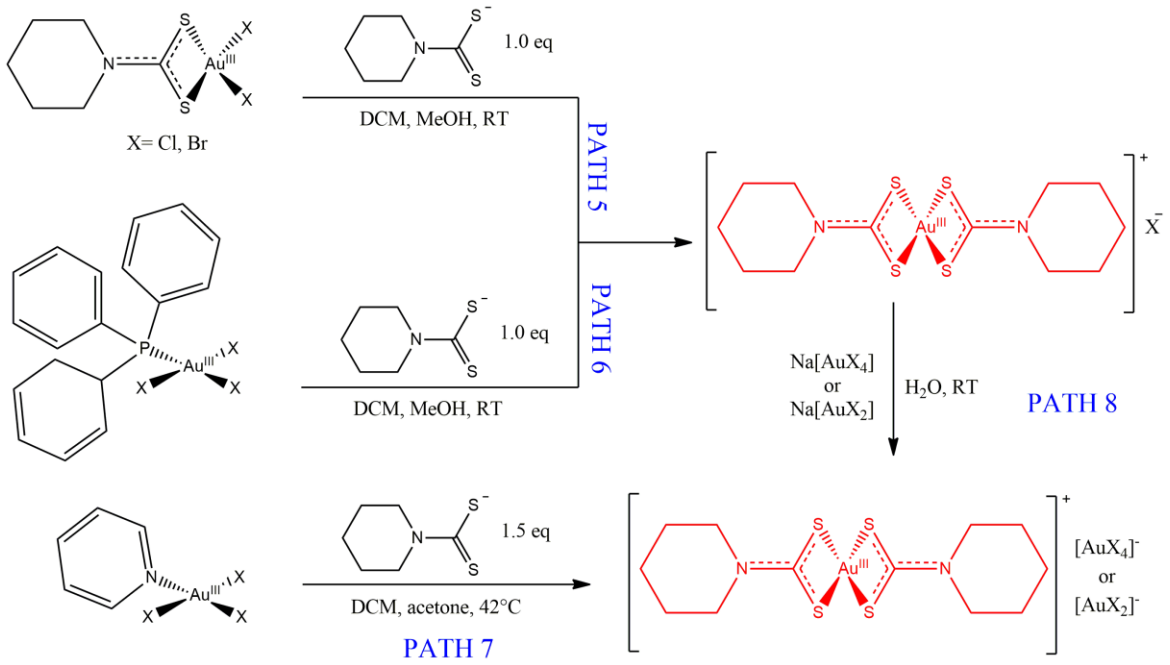

Figure 1.9: description of the main reaction pathways optimized for the synthesis of the 1:2 complexes.

Furthermore, other synthetic routes have been investigated in order to selectively obtain the 1:2 derivative from simple Au(III) precursor, such as $[Au^{III}X_3(PPh_3)]$ and $[Au^{III}X_3(py)]$ (**Figure 1.9**, path 6 and 7). The last procedures were proven to be effective in the synthesis of 1:2 complexes with steric-hindered dithiocarbamates (such as glycoconjugated DTC, see **Chapter 2**), for which the first reaction route did not give any good results. In particular, through the route involving the triphenylphosphino tri-halo Au(III) derivative (path 6), the desired product is formed quantitatively upon the addition of one equivalent of dithiocarbamato ligand, dissolved in methanol-water mixture. From the mechanistic point of view, the coordination of the first DTC ligand to the Au(III) sphere promotes the formation

of the instable $[Au^{III}Cl(DTC)(PPh_3)]^+$ intermediate. Then, the release of the soft triphenylphosphine ligand is prompted thanks to its participation from the redox equilibrium that involves a second equivalent of the $[Au^{III}Cl_3(PPh_3)]$ reagent, forming the stable $[Au^{I}Cl(PPh_3)]$ complex (with the consequent oxidation of PPh_3 to PPh_3O). At that point, the $[Au^{III}Cl(DTC)]^{2+}$ ion, assumed as transition state, can easily chelate a second dithiocarbamato molecule, leading to the formation of the desired product as chloride salt (**Figure 1.10**).

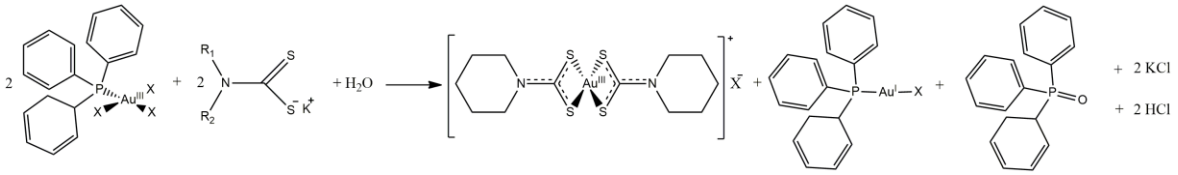

Figure 1.10: Schematic reaction for the synthesis of $[1:2]^+$ compounds starting from the $[Au^{III}(PPh_3)Cl_3]$ precursor.

- Synthesis of bis-(piperidine dithiocarbamato) gold(III) halide complexes

PATH 5: The ionic bis(dithiocarbamato)gold(III) complexes $[Au^{III}(PipeDTC)_2]^+$ with X (X= Cl^-, Br^-) as a counterion were obtained by adding dropwise 1 mmol of the dithiocarbamato salt KPipeDTC dissolved in methanol (2 mL) to a solution containing 1 mmol of $[AuX_2(PipeDTC)]$ dissolved in 10 mL of dichloromethane. The orange solution of the neutral Au(III)-DTC complex became immediately yellow. The progress of the reaction was detected by TLC analysis. Then, the solvent was removed under reduced pressure, the residual solid taken up with 1 mL of anhydrous dichloromethane and the insoluble NaX (X= Cl or Br) was removed by filtration. At this point, the product was collected by precipitation with 10 mL of n-hexane, and dried in vacuum. The product was further purified by means of flash column chromatography on silica gel using DCM-MeOH 9:1 as eluent. These ionic products resulted soluble in halogenated solvents, CH_3CN, acetone, alcohols and water.

PATH 6: 1 mmol of $[Au^{I}X(PPh_3)]$, prepared as reported elsewhere,[55] were dissolved in 15 mL of DCM in a 50 mL two-necked round-bottom flask, equipped with a rubber septum. At this point, chlorine gas was bubbled through a rubber cannula or an excess of bromine was added dropwise (previously diluted in 5 mL of dichloromethane). The mixture, initially colorless, gradually turns bright greenish-yellow in the case of Cl derivative or bright red for

Br, denoting the formation of related Au(III) complex [$Au^{III}X_3(PPh_3)$] in solution.[72] After monitoring the completion of the reaction by TLC, the chlorine flow was then stopped (if present), and Ar was gurgled for 10 minutes in order to remove the excess of halogen. To the resulting solution, 1 mmol of the piperidine dithiocarbamato, potassium salt dissolved in methanol (2 mL) was added while stirring and the mixture quickly turned yellow or light orange. A precipitate (KCl or KBr) was seen fluctuating in both cases. After 15 minutes, the mixture was filtered, the solvent was half-reduced under rotatory evaporator and a yellow solid was collected after the addition of 30 mL of diethyl ether. The product was finally purified by means of flash column chromatography on silica gel using DCM-MeOH 9:1 as eluent.

Bis-(piperidine dithiocarbamate)gold(III) chloride, [Au^{III}(PipeDTC)$_2$]Cl

Aspect: yellow solid

Yield: 82 % (path 5); 80 % (path 6)

R.f. (on silica gel, CH_2Cl_2/MeOH 9:1): 0.12

Anal. Calc. for $C_{12}H_{20}AuClN_2S_4$ (MW = 552.98 g·mol^{-1}): C 26.02; H 3.65; N 5.07; S 23.19. Found: C 26.07; H 3.71; N 5.19; S 23.11.

^{1}H-NMR (DMSO-d6, 600 MHz): δ (ppm) = 1.74 (m, 12H, $H_{(3)} + H_{(4)} + H_{(5)}$), 3.83 (m, 8H, $H_{(2)} + H_{(6)}$).

^{1}H-NMR ($CDCl_3$, 300 MHz): δ (ppm) = 1.88 (s, 6H, $H_{(3)} + H_{(4)} + H_{(5)}$), 3.97 (s, 4H, $H_{(2)} + H_{(6)}$).

Medium FT-IR (KBr): $\tilde{\nu}$ (cm^{-1}) = 2936.83, 2861.75 (ν_a, C-H); 1560.51 (ν_a, N-CSS); 951.13 (ν_a, CSS).

Far FT-IR (nujol): $\tilde{\nu}$ (cm^{-1}) = 511.54 (ν_s, CSS); 414.36 (ν_a, Au-S); 370.15 (ν_s, Au-S).

ESI-MS m/z, $[M-Cl]^+$ found (calc.): 517.03 (517.02).

Bis-(piperidine dithiocarbamate) gold(III) bromide, [Au^{III}(PipeDTC)$_2$]Br

Aspect: yellow-orange solid

Yield: 85 %

R.f. (on silica gel, CH_2Cl_2/MeOH 9:1): 0.12

Anal. Calc. for $C_{12}H_{20}AuBrN_2S_4$ (MW = 597.43 g·mol-1): C 24.12; H 3.37; N 4.69; S 21.47. Found: C 24.23; H 3.52; N 4.78; S 21.60.

1H-NMR (DMSO-d6, 600 MHz): δ (ppm) = 1.74 (m, 12H, $H_{(3)} + H_{(4)} + H_{(5)}$), 3.83 (m, 8H, $H_{(2)} + H_{(6)}$).

^{1}H-NMR ($CDCl_3$, 300 MHz): δ (ppm) = 1.88 (s, 6H, $H_{(3)} + H_{(4)} + H_{(5)}$), 3.98 (s, 4H, $H_{(2)} + H_{(6)}$).

Medium FT-IR (KBr): $\tilde{\nu}$ (cm^{-1}) = 2935.18, 2864.80 (ν_a, C-H); 1558.23 (ν_a, N-CSS); 950.98 (ν_a, CSS).

Far FT-IR (nujol): $\tilde{\nu}$ (cm^{-1}) = 514.51 (ν_s, CSS); 423.38, 410.84 (ν_a, Au-S); 378.55, 367.76 (ν_s, Au-S).

ESI-MS m/z, $[M-Br]^+$ found (calc.): 517.03 (517.02)

- Synthesis of bis-(piperidine dithiocarbamato) gold(III) double complex salts

PATH 7: For $[AuCl_2]$ salt: this Au(III)/Au(I) double complex was obtained starting from the gold(III) precursor $[AuCl_3(py)]$ (py= pyridine; 1 mmol), previously synthetized as reported in literature[63] and then dissolved in 25 mL of dichloromethane. This solution was put at reflux under stirring.

After 10 minutes, 1.5 mmol (1.5 eq) of PipeDTC salt, dissolved in 2 mL of methanol, were added to the Au(III) solution, which in few minutes turned from yellow to orange. The reaction was left at reflux for 2 hours under stirring, then the solution was cooled, filtered and reduced to half its initial volume. After the addition of 5 mL of diethyl ether, the flask was left at -10 ° C for two days, leading to the formation of yellow needles. This product did not result water-soluble.

For $[AuCl_4]$ salt: The synthetic procedure used to obtain the complex $[Au^{III}(PipeDTC)_2]^+[Au^{I}Cl_4]^-$ was the same reported for the previous compound. However, the $[Au^{III}Cl_3(py)]$ precursor was used (py= pyridine), and the ligand PipeDTC was added according to a ligand-to-metal stoichiometry 0.5:1. Also in this case orange needles were obtained, and the product did not result water-soluble.

PATH 8: For $[Au^{I}Cl_2]$ salt: in a 10 mL glass centrifuge tube equipped with a screw cap was added a 3 mL saturated NaCl aqueous solution (brine) containing 1 mmol of $Na[Au^{III}Cl_4]$. To this bright yellow mixture was dropwise added under stirring an equimolar amount of Na_2SO_3, as reducing agent, previously dissolved in 2 mL of deionized water. The solution gradually turns colorless. At this point 1 equivalent of $[Au^{III}(PipeDTC)_2]X$ in 2 mL of

deionized water was added and a light-yellow solid readily precipitated. The product was washed 3 times with deionized water (3x 3 mL) and dried in vacuum in presence of P_2O_5.
For $[Au^{III}Cl_4]$ salt: in a 10 mL glass centrifuge tube equipped with a screw cap was added a 3 mL aqueous solution containing 1 mmol of $[Au^{III}(PipeDTC)_2]X$. Afterwards, to this bright yellow mixture was dropwise added while stirring an equimolar amount of $Na[Au^{III}Cl_4]$ previously dissolved in 2 mL of deionized water. A light orange flocculent solid precipitated immediately, leaving colorless mother liquors on the top. The product was centrifuged, washed with deionized water (3x 3 mL) and dried in pump over P_2O_5.

Bis(piperidine dithiocarbamate)gold(III) dichlorogold(I), $[Au^{III}(PipeDTC)_2][Au^{I}Cl_2]$
Aspect: light yellow needles
Yield: 83 % (path 8); 94 % (path 9)
R.f. (on silica gel, CH_2Cl_2/MeOH 9:1): 0.14
Anal. Calc. for $C_{12}H_{20}Au_2Cl_2N_2S_4$ (MW = 785.40 g·mol-1): C 16.48; H 2.31; N 3.20; S 14.67.
Found: C 16.42; H 2.38; N 3.25; S 14.69.
^{1}H-NMR (DMSO-d6, 600 MHz): δ (ppm) = 1.72 (s, 12H, $H_{(3)} + H_{(4)} + H_{(5)}$), 3.83 (s, 8H, $H_{(2)} + H_{(6)}$).
^{1}H-NMR ($CDCl_3$, 400 MHz): δ (ppm) = 1.88 (s, 6H, $H_{(3)} + H_{(4)} + H_{(5)}$), 3.86 (s, 4H, $H_{(2)} + H_{(6)}$).
Medium FT-IR (KBr): $\tilde{\nu}$ (cm^{-1}) = 2942.27 (ν_a, C-H); 1552.34 (ν_a, N-CSS); 1005.63 (ν_a, CSS).
Far FT-IR (nujol): $\tilde{\nu}$ (cm^{-1}) = 512.63 (ν_s, CSS); 410.06 (ν_a, Au-S); 370.54 (ν_s, Au-S); 228.52 (ν_a, Au-Cl).
ESI-MS m/z, $[M\text{-}AuCl_2]^+$ found (calc.): 517.03 (517.02).

Bis-(piperidine dithiocarbamate) gold(III) tetrachloroaurate, $[Au^{III}(PipeDTC)_2][Au^{III}Cl_4]$
Aspect: light orange powder
Yield: 79 % (path 8); 95 % (path 9).
R.f. (on silica gel): n.a.
Anal. Calc. for $C_{12}H_{20}Au_2Cl_4N_2S_4$ (MW = 856.31 g·mol^{-1}): C 16.83; H 2.35; N 3.27; S 14.98.
Found: C 16.81; H 2.36; N 3.30; S 14.90.
^{1}H-NMR (DMSO-d6, 600 MHz): δ (ppm) = 1.73 (s, 12H, $H_{(3)} + H_{(4)} + H_{(5)}$), 3.83 (m, 8H, $H_{(2)} + H_{(6)}$).

^{1}H-NMR ($CDCl_3$, 400 MHz): δ (ppm) = 1.88 (s, 6H, $H_{(3)}$ + $H_{(4)}$ + $H_{(5)}$), 3.84 (s, 4H, $H_{(2)}$ + $H_{(6)}$).

Medium FT-IR (KBr): $\tilde{\nu}$ (cm^{-1}) = 2936.89 (ν_a, C-H); 1553.33 (ν_a, N-CSS); 1005.32 (ν_a, CSS).

Far FT-IR (nujol): $\tilde{\nu}$ (cm^{-1}) = 509.85 (ν_s, CSS); 411.98 (ν_a, Au-S); 361.10 (ν_s, Au-S); 334.29 (ν_a, Au-Cl).

ESI-MS m/z, $[M\text{-}AuCl_4]^+$ found (calc.): 517.03 (517.02).

1.4 Characterization of Au dithiocarbamato complexes

1.4.1 The ^{1}H-NMR investigation

In order to deeply characterize the discussed classes of compounds, several ^{1}H-NMR spectra were recorded in $CDCl_3$ (other suitable solvents are CD_2Cl_2, acetone-d6 or CD_3CN) and are reported in the **Supporting Information A**. The piperidine-dithiocarbamato ligand possesses eight diastereotopic protons which can be divided in three groups depending on their position on the six-atom carbon ring: the α, β and γ protons (**Figure 1.11**).

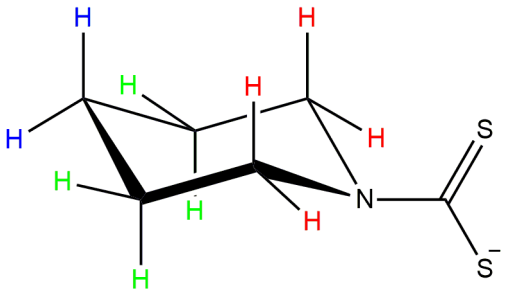

Figure 1.11: Schematic representation of piperidine dithiocarbamato anion with highlighted the diastereotopic hydrogens. In particular, the α protons are depicted in red, while the β and γ are represented in green and blue, respectively.

Each proton couples with the other one of the methylene group through a J^2 interaction and, through a J^3 coupling constant, with the protons bound to adjacent carbon atoms. These couplings between diastereotopic nuclei appear as multiplets-type resonances. On the whole, as the electron density of the β and γ protons are very similar both in the free and coordinated ligand, all the acquired spectra show only two distinct peaks, one at higher chemical shift (usually, around 3.7 ppm), ascribable to the protons in α position and the other one at 1.8 ppm gathering together the resonances of the more shielded β and γ ones.

Comparing the chemical shifts of all the complexes with those of free dithiocarbamato ligands reported in Table 1.3, a lower-field shift of the signals related to the α-protons with respect to the dithiocarbamic nitrogen atom is detected upon coordination. The possible explanation for this phenomenon lies in the metal-to-ligand back-donation, allowed by the presence of low-energy empty *d*-orbitals of sulfur atoms, which makes the DTC-protons more shielded. A similar effect was reported for phosphinogold(I)-dithiocarbamato complexes. Concerning the neutral Au(III)-DTC compounds of the type [$Au^{III}X_2$(DTC)], a relation was found between the resonance of the α protons of the coordinated ligand and the nature of halides in trans position as shown in **Figure 1.12**.

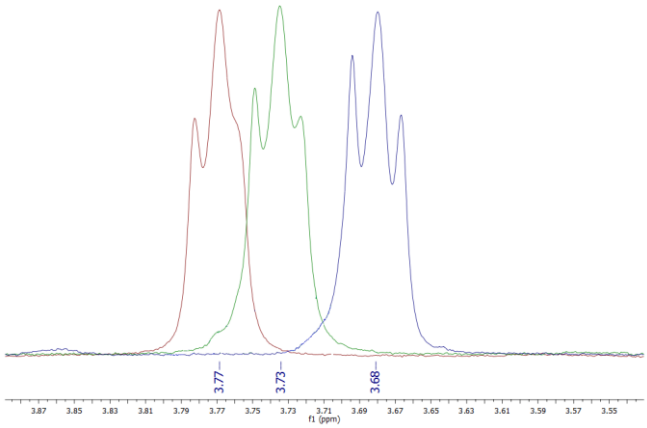

Figure 1.12: enlargement of the α protons resonances on the ^{1}HNMR spectra the [$Au^{III}X_2$(PipeDTC)] compounds. In particular, the red spectrum is referred to the di-chloro complex, while the green and blue ones are related to the di-bromo and di-iodo derivatives, respectively.

In fact, it was discovered that the resonances of the chloro-complex fall in a slightly higher chemical shift with respect to the bromo-counterpart and, in turn, the iodo derivative possess the more shielded α-protons among all. Once again, the metal-to-ligand back-donation theory rationalizes this behavior. In particular, due to the lower electronegativity and higher polarizability of the iodine ($E^0_{I2/2I}$= 0.535 V),[1] a higher electron density insists on the Au(III) metal center in the iodo-complex with respect to the chloro derivative, and this can be traduced in the higher ability of the metal center to interact with the empty anti-bonding molecular orbital of the dithiocarbamato functional group. For this reason, passing from chloro to iodo complexes, the protons of organic backbone of the DTC-ligand result more shielded. This effect can be observed also in the FT-IR characterization (see **Section 1.4.2**)

in which the vibrational stretching frequencies of the N-CSS and CSS bonds are higher in the chloro complex (meaning a stronger bond), thus accounting for a more consistent back-donation from the metal to the N-CSS antibonding orbital (that weakens the intraligand bonds) in the case of the complexes with more polarizable halogens (Br and I).

Finally, on passing from the neutral to the ionic Au(III)-PipeDTC complexes, the α-proton signals are slightly shifted to lower fields. At the same time, the nature of the counter-ion in $[Au^{III}(PipeDTC)_2]X$ compounds seems not to affect the proton resonances.

Table 1.3: ^{1}H-NMR resonances (ppm) of the protons in the piperidine moiety of the dithiocarbamato ligand and in all synthetized Au complexes.

COMPOUND	**α-protons**	**β protons**	**γ protons**
PipeDTC K^+	4.27 (DMSO)	1.39 (DMSO)	1.54 (DMSO)
$[Au^{I}_2(PipeDTC)_2]$	4.13 (DMSO)	0.85 (DMSO)	0.85 (DMSO)
$[Au^{III}Cl_2(PipeDTC)]$	3.82 (DMSO) 3.77 ($CDCl_3$)	1.72 (DMSO) 1.88 ($CDCl_3$)	1.72 (DMSO) 1.88 ($CDCl_3$)
$[Au^{III}Br_2(PipeDTC)]$	3.79 (DMSO) 3.73 ($CDCl_3$)	1.72 (DMSO) 1.87 ($CDCl_3$)	1.72 (DMSO) 1.87 ($CDCl_3$)
$[Au^{III}I_2(PipeDTC)]$	3.73 (DMSO) 3.68 ($CDCl_3$)	1.72 (DMSO) 1.82 ($CDCl_3$)	1.72 (DMSO) 1.82 ($CDCl_3$)
$[Au^{III}(PipeDTC)_2]Cl$	3.83 (DMSO) 3.97 ($CDCl_3$)	1.74 (DMSO) 1.88 ($CDCl_3$)	1.74 (DMSO) 1.88 ($CDCl_3$)
$[Au^{III}(PipeDTC)_2][AuCl_2]$	3.83 (DMSO) 3.86 ($CDCl_3$)	1.72 (DMSO) 1.88 ($CDCl_3$)	1.72 (DMSO) 1.88 ($CDCl_3$)
$[Au^{III}(PipeDTC)_2][AuCl_4]$	3.83 (DMSO) 3.84 ($CDCl_3$)	1.73(DMSO) 1.88 ($CDCl_3$)	1.73 (DMSO) 1.88 ($CDCl_3$)

1.4.2 The FT-IR characterization

The FT-IR spectra have been collected for all the Au(I/III)-DTC derivatives both in the medium (4000-600 cm^{-1}) and far (600-50 cm^{-1}) wavenumber range (**Supporting Information B**), and the diagnostic absorptions are reported in Table 1.4. This spectrophotometric technique is the most useful tool to detect the different chemical features generated by the different oxidation states of the gold metal center, as well as the presence of different stoichiometric metal-ligand ratios. In general, DTC salts possess the ability to be potentially both strong- and weak-field ligands.[73] When coordinated, the contribution of the thioureide resonance form (**Figure 1.13**), for which a positive charge is formally on the nitrogen atom while each sulfur atom carries a negative charge, makes this class of ligands capable to stabilize a wide range of metal ions. Dithiocarbamato metal compounds display a characteristic band at around 1500 cm^{-1} assignable to the ν(N-CSS) which defines the carbon-nitrogen bond order.[74] For the dithiocarbamato form (**Figure 1.13a**), the stretching of single C-N bond can be recognized at ν~1250-1350 cm^{-1} whereas the double C=N bond counterpart in thioureide form (**Figure 1.13b**) is at ν~1600-1690 cm^{-1}.[75]

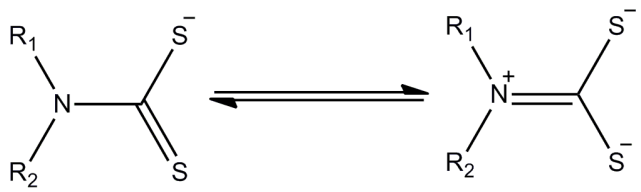

Figure 1.13: Resonance equilibrium between the dithiocarbamic (*left*) and thioureidic (*right*) form of a generic DTC ligand; R_1=R'(R, Ar), R_2=R', R'', H.

Both the 1:1 and [1:2] Au(III) species show an intense band at about 1550 cm^{-1} thus highlighting an intermediate situation between a single and a double C-N bond, while the Au(I) complexes show an absorption band at ν~1420 cm^{-1} thus accounting for a less strong C-N bond. These data are in agreement with the observations of Calabro and co-workers which reported a small increase in the ν(SSC-N) frequency of the DTC ligand as the oxidation state of gold increases.[23]

Moreover, the ν(N-CSS) band position is shifted to higher frequencies following the order $[Au^{III}Cl_2(pipeDTC)] > [Au^{III}Br_2(pipeDTC)] > [Au^{III}I_2(pipeDTC)] \sim [Au^{III}(PipeDTC)_2]Cl > [Au^{III}(PipeDTC)_2][AuCl_4] > [Au^{III}(PipeDTC)_2][AuCl_2]$

due to an increase of electronic density on the DTC moiety in the presence of two trans-coordinated halogens, thus resulting in a greater N-C bond strength. We can conclude that the contribution of the thioureide resonance structure is larger in 1:1 derivatives compared to [1:2]X species.

In order to discern the bonding type of the dithiocarbamato ligands in their complexes, the Bonati-Ugo method is, so far, the most used.[76] It consists of tracing the 940-1060 cm^{-1} spectral region, where the ν(C-S) modes commonly appear. Notably, the bands, due to the -CSS moiety, are very sensitive to the nature of the parent amine and are usually coupled to other vibrations and, hence, they are diagnostic to distinguish between monodentate and chelate coordination.[77] In fact, the presence of only one band in the investigated region (around 950-1000 cm^{-1} both for the 1:1 and the [1:2] complexes – **Table 1.8**), commonly attributed to ν_a(SCS) mode, is assumed to point out a completely symmetrically-bidentate bonding of the dithiocarbamato ligand. Conversely, a split band (behavior not observed in the complexes studied in this work) indicates an asymmetrically-bonded chelate ligand ($\Delta\tilde{\nu}<20$ cm^{-1}) or a monodentate one ($\Delta\tilde{\nu}>20$ cm^{-1}).

Concerning the far-IR spectra, the main recorded resonances are reported in **Table 1.9**. For both compounds, the bands in the range of 350-400 cm^{-1} are assigned to gold(III)-sulfur stretching vibrations.[76] In particular, the 1:1 complexes are associated with two absorptions at ~365 (ν_a) and 345 cm^{-1} (ν_s). Similarly, in the case of [1:2] complexes, the $\nu_{a/s}$ Au-S bands are detectable in closer wavelengths with respect to the 1:1 counterparts (at 370 cm^{-1}) which could suggest a comparable geometry and bond-strength around the metal center.

The two remaining coordination sites in 1:1 complexes are taken up by cis-halides in agreement with the two bands visible at 316-350 cm^{-1} for chloro-derivative and at 224-239 cm^{-1} for bromide ones and can be ascribed to the $\nu_{a/s}$(X−Au−X). It is worth highlighting that the related absorptions for the iodo-complex cannot be detected because of the high molecular weight of iodine that shifts the resonance to lower and non-detectable wavenumbers. As expected, these metal-halide vibrational modes have not been found in the spectrum of [1:2] halide complex, while only a resonance compatible with the ν_a(X−Au−X) vibration of the counterion can be seen for the double salts at 334 cm^{-1} and 340 cm^{-1}, for the $[AuCl_4]$ and $[AuCl_2]$, respectively.[78]

Table 1.4: main IR absorption bands of the Au(III) dithiocarbamato compounds (count: absorption frequency assigned to vibrational mode of the counterion).

COMPOUND	**ν(N-CSS)**	**ν_a(CSS)**	**ν_s(CSS)**	**ν_a(Au-S)**	**ν_s(Au-S)**	**ν_a(Au-X)**	**ν_s(Au-X)**
$[Au^{I}_2(PipeDTC)_2]$	1428	968	557	479	-	-	-
$[Au^{III}Cl_2(PipeDTC)]$	1581	947	540	366	335	350	316
$[Au^{III}Br_2(PipeDTC)]$	1574	942	539	370	351	239	224
$[Au^{III}I_2(PipeDTC)]$	1559	942	504	359	341	-	-
$[Au^{III}(PipeDTC)_2]Cl$	1561	951	512	414	370	-	-
$[Au^{III}(PipeDTC)_2]$ $[Au^{I}Cl_2]$	1552	1005	510	412	361	340 count.	-
$[Au^{III}(PipeDTC)_2]$ $[Au^{III}Cl_4]$	1553	1005	513	410	371	334 count.	-

1.4.3 The UV-Vis characterization

Electronic spectra were acquired in $CHCl_3$ (800-190 nm) at 25 °C for all the synthetized gold(III)-DTC derivatives, and in DMSO (800-270 nm) at 25 °C for the Au(I) counterparts (**Supporting Information C**), and the diagnostic absorptions are summarized in **Table 1.5**. Concerning the Au(III)-DTCs, it is worth reminding that both neutral and ionic derivatives are square planar (SP) complexes. Consequently, the five-degenerate *d*-orbitals of the free Au(III) d^8 ion split into four different levels. In particular, Gray and Ballhausen described the molecular orbital theory for SP complexes, discussing two distinct cases.[79] The first is related to SP compounds in which the ligands themselves have a π-orbital system, whereas the second is associated with SP complexes with no intra-ligand π-orbital system. For both cases, there are three spin-allowed *d-d* transitions, corresponding to the one electron transitions $^1A_{1g}\rightarrow{}^1A_{2g}$, $^1A_{1g}\rightarrow{}^1B_{1g}$ and $^1A_{1g}\rightarrow{}^1E_g$. Moreover, considering DTC ligands as moieties containing a π-orbital system three charge-transfer (CT) transitions are foreseen, namely $^1A_{1g}\rightarrow{}^1E_u$, $^1A_{1g}\rightarrow{}^1A_{2u}$, and $^1A_{1g}\rightarrow{}^1B_{1u}$. However, only the first and second are allowed, with the $^1A_{1g}\rightarrow{}^1E_u$ transition expected to have considerably greater intensity. On the other hand, halo ligands belong to the second case presented, and in general generate two allowed charge transfer transitions of the type $^1A_{1g}\rightarrow{}^1E_u$ (more intense) and $^1A_{1g}\rightarrow{}^1A_{2u}$.[79-81]

In particular, observing the electronic spectra for the 1:1 di-halo complexes, three different major bands can be recognized, which are well-resolved for the di-bromo and di-iodo complexes and partially overlapped for the di-chloro analogues. The band I, the strongest one in the spectrum of the di-iodo complex, has not been undoubtedly ascribed in the literature to a particular electronic transition and it is still the subject of debate: sometimes, it has been assigned either to an intra-ligand $\pi^* \leftarrow \pi$ transition located in the -NCSS moiety[82] or to intra-ligand $p \leftarrow d$ transitions between the levels originated by sulfur atoms, and it has even been not ascribed in most cases.[83] On the contrary, band II and band III, which display very great molar extinction coefficients ($\varepsilon \sim 10^4$ $M^{-1} \cdot cm^{-1}$), have been ascribed in the literature[68] to DTC intra-ligand $\pi^* \leftarrow \pi$ transitions mainly located in the -NCS and -CSS moieties, respectively. Notably, these transitions are overlapped in DMSO solvent for the same compounds. The weaker band IV has been attributed to either an intramolecular L ← M charge transfer, involving the *nd* orbitals of the metal center and the dithiocarbamato π* system, or an electron transfer of the type u ← g from a *4p* orbital (σ symmetry) of the halide ligands to the lowest unfilled *5d* orbital (d_{x2-y2}).[84] The second hypothesis is more conceivable taking into account the high oxidizing power of the Au(III) center and the presence of band IV only in the spectrum of the 1:1 complexes. In this regard, it is interesting to note that all bands are gradually shifted to higher wavelengths on passing from chloride to bromide and then to iodide. In particular, the band IV seems to be the most affected by the nature of the halide. On the other hand, an overall red-shift is also observed in the ionic PipeDTC complexes of the type $[Au(PipeDTC)_2]X$, especially for the band III that shifts from around 270 nm for the 1:1 complexes to around 310 nm in 1:2 derivatives. This effect, reveals a higher electron delocalization in the -C<$_S^S$>Au<$_S^S$>C- moiety. It is worth noting that, on passing from DMSO (dielectric constant, ε = 47.24, 25 °C) to $CHCl_3$ (ε = 4.81, 20 °C)[1], a blue shift is detected for the $\pi^* \leftarrow \pi$ transitions, namely bands II and III, due to the greater stabilization of π* orbitals compared to π orbitals in a more polar solvent. Moreover, it is generally difficult to observe $d \leftarrow d$ transitions (spin allowed but symmetry forbidden) in electronic spectra of coordination compounds relying on their low extinction coefficient.[85] Notwithstanding, in more concentrated solutions, an absorption is visible for both 1:2 and 1:1 species at 399.5 nm and 430.4 (shoulder) nm, respectively (**Supporting Information C**). It is likely that the slightly distorted square-planar geometry for both compounds makes these $d \leftarrow d$ transitions visible.

Table 1.5: wavelengths (nm) of the most important UV-Vis absorptions of the Au(III) dithiocarbamato complexes (bold value) with related molar extinction coefficients (ε°) at 25°C (*: overlapped band, sh: shoulder).

COMPOUND	Band I	Band II		Band III		Band IV	
	$CHCl_3$	$CHCl_3$	DMSO	$CHCl_3$	DMSO	$CHCl_3$	DMSO
$[Au^{I}_2$ (PipeDTC)$_2]$	-	-	279	-	317	-	
$[Au^{III}Cl_2$(PipeDTC)]	**243** 20447	**265*** 42123	**266*** 20381	**265*** 42123	**266*** 20381	**328** 3513	**318** 5621
$[Au^{III}Br_2$(PipeDTC)]	**254** 28243	**269** 31480	**280*** 21321	**285** 41853	**280*** 21321	**384** 2933	**365** 3167
$[Au^{III}I_2$(PipeDTC)]	**259** 31336	**286** 30246	**277** 22453	**307** 40824	**308** 22666	**500** 2098	**485** 3368
$[Au^{III}$(PipeDTC)$_2]$Cl	**242** (sh) 11233	**277** 34400	**278** 30333	**318** 31440	**319** 25333	-	-
$[Au^{III}$(PipeDTC)$_2]$ $[Au^{I}Cl_2]$	**243** (sh) 9330	**277** 31600	**277** 27305	**318** 30117	**320** 22289	-	-
$[Au^{III}$(PipeDTC)$_2]$ $[Au^{III}Cl_4]$	**243** 21703	**276** 36253	**272** 31082	**319** 37233	**318** 21000	-	-

1.4.4 Overall considerations about the syntheses

The kinetic of complexation of Au(III) halides, such as $[AuCl_4]^-$ and $[AuBr_4]^-$, with dithiocarbamates is usually very fast, also due to the strong interaction between the metal center with sulfur-donating ligands.[86] Therefore, adding a DTC salt to a solution containing a gold(III) precursor lead to the co-formation of different species which possess various metal to ligand stoichiometry independently of the added equivalents of the ligand. Moreover, the composition of this mixture strongly depends on the solvent used for the synthesis. For example, the low solubility in water of the 1:1 and [1:2][AuX_4] DTC-complexes drives the equilibrium toward the precipitation of these two insoluble compounds in aqueous medium. On the contrary in organic solvents, in particular halogenated ones, the 1:1 species (thermodynamically stable) is obtained fairly quantitatively when one equivalent of the ligand is added. In this case, due to the insolubility of the aurate-alkaline metal salts in dichloromethane or chloroform, a different gold(III) precursor (usually the pyridine-trihalo derivatives, with formula $[Au^{III}X_3(py)]$) must be used. The various synthetic pathways described in this chapter were designed and optimized in order to avoid the formation of a mixture of different stoichiometric species and to obtain selectively the pure compounds for

the subsequent biological evaluations. In the case in which some byproducts were formed during the synthesis, purification by column chromatography was always performed.

1.5 Solution chemistry of Au(III) dithiocarbamates

One of the aims of this work was to investigate and understand the unusual chemistry in solution involving the 1:1 [$Au^{III}X_2$(DTC)] complexes and the 1:2 [Au^{III}(DTC)$_2$][AuX_4] ones. A rearrangement phenomenon in solution were first hypothesized by Van der Linden and co-workers in the 1969,[66] who simply reported that the [1:2][$AuBr_4$] dibutyl-dithiocarbamato derivative transforms into two equivalents of the related 1:1 di-bromo compound if refluxed in dichloromethane solution. Remarkably, no additional explanation was given by the authors and other mentions about this interesting behavior was not possible to found in literature since then. Afterwards, in 2015, Isab and colleagues, while discussing the instability of the 1:1 complexes in MeOH and DMSO over time by means of UV-Vis kinetic studies, suggested that the di-chloro compounds might be involved in an equilibrium forming the corresponding more stable [1:2][$AuCl_4$] derivatives once solvated.[70]

Apparently, the two papers seem to be in contradiction to each other, the former asserting a "direct equilibrium" which drives the ionic [1:2][AuX_4] species to the neutral 1:1 ones and the latter an "inverse equilibrium" that is exactly the opposite of the first.

In order to deeply investigate this interesting phenomenon, the experimental conditions for the two rearrangement equilibria detected by Van der Linden and Isab were repeated and several kinetic and spectroscopic studies were carried out.

The UV-Vis 72 h kinetic analyses are reported in **Figure 1.14** and **Figure 1.15**. The direct equilibrium can be detected even in chloroform and at room temperature and as soon after the dissolution of [1:2][$AuCl_4$] complex in $CHCl_3$, the UV-Vis spectrum changes gradually. In particular, the band II of the ionic compound at 276 nm is shifted to lower wavelengths and, as two equivalents of 1:1 derivative are formed through the inverse equilibrium, the absorbance value progressively increases. This band continues to growth until reaching a maximum at 265 nm after 72 hours, that correspond exactly to the intra-ligand $\pi^* \leftarrow \pi$ transitions (band II) of the -NCS moiety of the neutral 1:1 di-chloro compound. Conversely, in the same time lapse, the strong absorption at 319 nm (band III) of the double-complex salt decreases over time until a minimum. In this case is also visible a pseudo-isosbestic point at 351 nm, in which the reduction of the strong absorbance of the reagent at 319 nm is matched

with the growth of the broad and weak band IV of the 1:1 complex (that has a maximum at 328 nm).

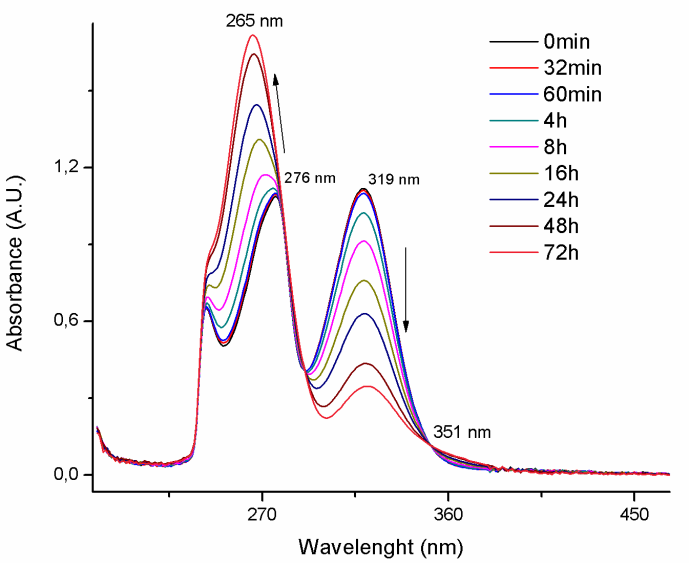

Figure 1.14: UV-Vis 72 h kinetic analysis of the rearrangement process involving the [1:2][$AuCl_4$] complex in $CHCl_3$ at RT.

On the other hand, if the 1:1 complex is dissolved in pure DMSO or DMSO-H_2O mixture (for example in 1:9 v/v ratio), the opposite equilibrium is observed. In fact, the absorbance of N-CSS band of the neutral compound falls drastically in few minutes when the compound is dissolved in DMSO-H_2O, followed by a redshift from 258 nm to 274 nm. Moreover, the weak absorbance of the band at 318 nm, referred initially to metal-halogen charge transfer for the 1:1 neutral derivative (328 nm in $CHCl_3$, see **Figure C1** in **Supporting Information C**) gradually increases, giving rise to the C-SS absorption (band III) of the [1:2][$AuCl_4$] complex. In this case a complete interconversion to the ionic counterpart is reached after 48 h. Intriguingly, this inverse equilibrium could be detected only after UV-Vis irradiation, as demonstrated by the absorption spectrum of a DMSO-water solution of the 1:1 complex protected from light for 72 h (**Figure 1.16**).

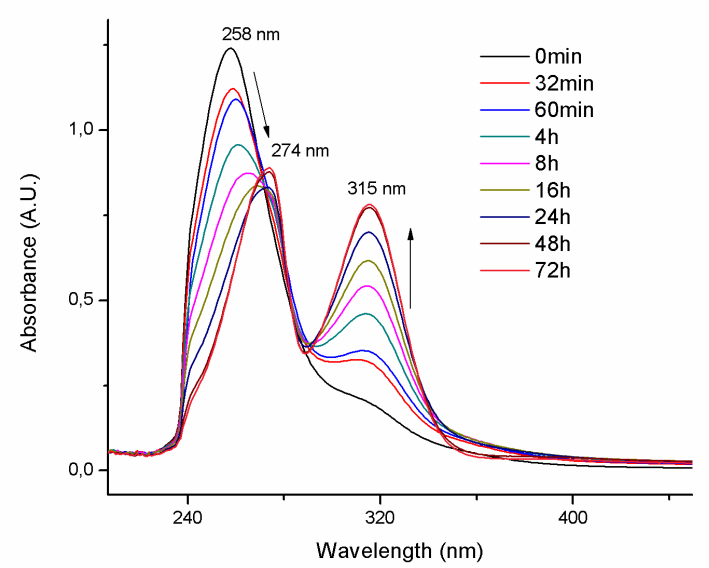

Figure 1.15: UV-Vis 72 h kinetic analysis of the rearrangement process involving the [$Au^{III}Cl_2$(PipeDTC)] complex in DMSO-H_2O (1:9 *v/v*) at RT.

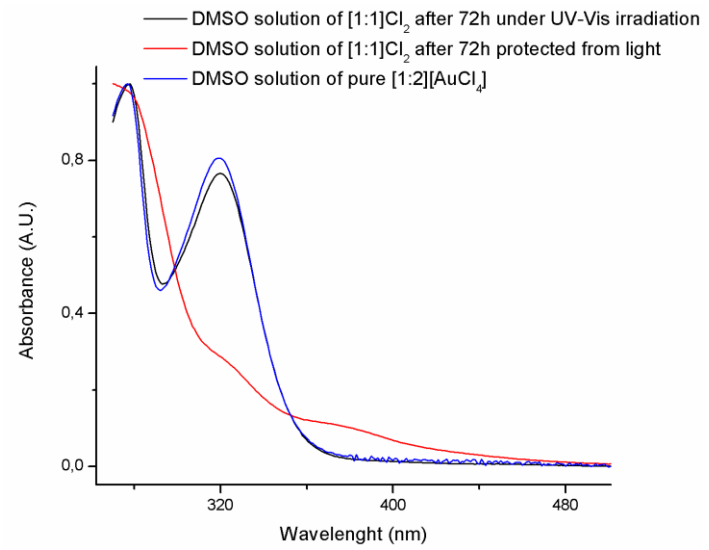

Figure 1.16: UV-Vis investigation of the role of the light irradiation on the rearrangement process.

After these studies in solution, it seems clear that the polarity of the solvent can drive the equilibrium toward the neutral species, or the double salt complex (in the latter case also the light excitation is necessary). In other words, the driving force of the whole phenomenon is the ΔH_{solv} of the product in the medium. In the case of polar solvents such as DMSOwater and alcohol, the hydrophobic 1:1 complexes are poorly solvated, and the system tends to convert the solute into the ionic double salt. On the contrary, when the ionic derivatives are dissolved in apolar medium, for example halogenated solvents, the low ΔH_{solv} does not

stabilize the complex in solution and drives the systems to the neutral counterparts. In particular, more polar is the solvent in which the 1:1 is dissolved and more rapid is the interconversion process, as denoted by the UV-Vis kinetic analysis (**Figure 1.17**) recorded in pure DMSO. In this case, the evolution of the bands in terms of absorbance and wavelength over time is slower than the data recorded in DMSO-H_2O medium, and only minor modification could be detected in 72h.

The latter spectrum, gives some information regarding the mechanistic insights into the rearrangement process. In fact, it is important to note that when the 1:1 complex is dissolved in pure DMSO at 25 °C, a sudden increase on the absorbance of the main UV absorption bands can be observed during the first 60 minutes. Whereupon, a behavior similar to that seen in Figure 1.15 (even if less pronounced due to the absence of H_2O) could be recognized.

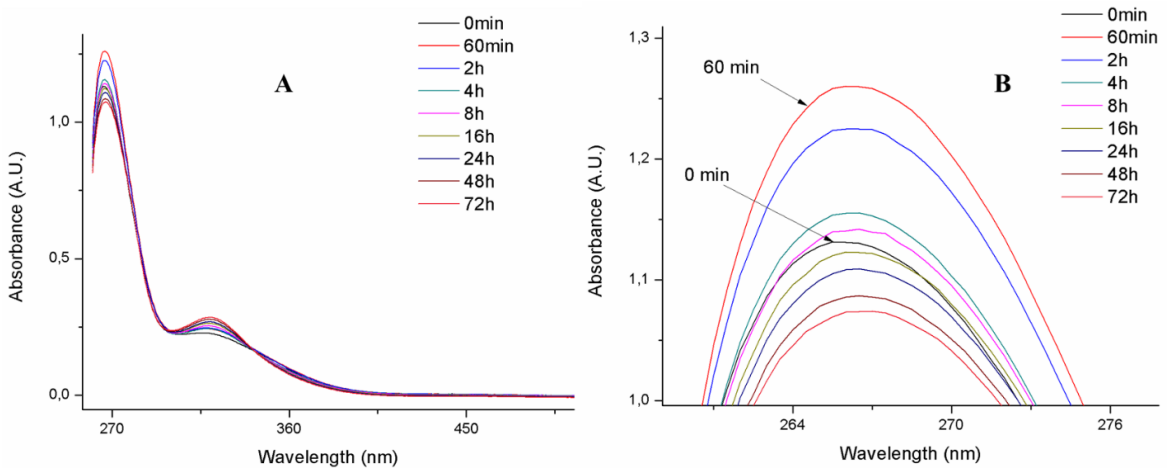

Figure 1.17: A) Full and B) zoomed UV-Vis kinetic spectrum at 25 °C of [$Au^{III}Cl_2$(PipeDTC)] compound in pure DMSO over 72 h. The sudden increase of the absorbance of the absorption band at 266 nm can be observed during the first 60 minutes.

This effect might be related to the apical coordination of the sulfur atom of the DMSO molecule in the Au(III) coordination sphere, exploiting the free $6p_z$ orbital (LUMO) of the metal ion (**Figure 1.18**). In fact, pseudo five-coordinated Au(III) complexes containing four coordination bonds and a longer apical interaction are already reported in literature and isolated.[87] Under solvent coordination, the main bands of the UV-Vis spectrum slightly change.

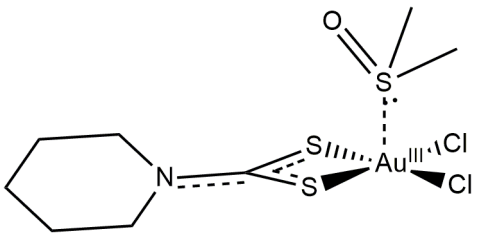

Figure 1.18: proposed structure for the first intermediate in the rearrangement process. The solvent molecule, in this case DMSO, interacts with the $6p_z$ free orbital of the Au(III) center.

This complex might evolve to a square planar reactive intermediate in which the dithiocarbamato ligand acts as monodentate substituent (intermediate V, **Figure 1.20**). At this point, the free sulfur atom can interact with the Au(III) center of another 1:1 molecule leading to the formation of the 1:2 cation by a DTC transfer process. Similarly, the halides cleaved by the entrance of the migrating dithiocarbamate, are transferred to the second gold(III) ion to saturate its coordination sites, forming the well-solvated $[AuCl_4]$ anion.
Before describing the proposed mechanism at issue, a brief overview about the substitution reactions within a d^8 square planar complex is necessary (**Figure 1.19**).

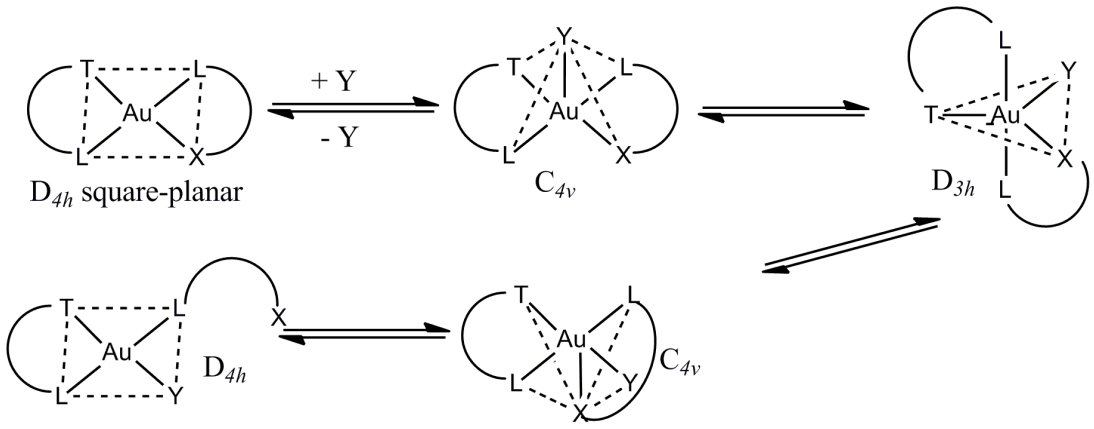

Figure 1.19: Example of substitution cycle in a Au^{III} square planar complex by an incoming group (Y) of one coordination site of a chelating ligand (X). Charges are omitted for clarity reasons.

First of all, the coordination of the entering ligand (Y) takes place through the overlap with the $6p_z$ metal orbital in apical position. The interaction leads to the formation of a square pyramidal intermediate with a C_{4v} geometry, subsequently evolving to a high energy trigonal bi-pyramidal complex (D_{3h}).[88] The latter step can be favored by the trans-ligand stabilization, called *trans*-effect. Afterwards, the exit of the living group (X) is preceded by an internal geometrical reorganization, resulting in a second C_{4v} intermediate with the X substituent in

apical position.[88] It must be taken into account that a complex with a chelating ligand needs to pass through two independent substitution cycles involving two distinct incoming molecules in order to completely release the bidentate substituent.[89] In this regard, it is worth highlighting that when a chelate ligand passes from a bidentate coordination to a monodentate one, the potentially coordinating sulfur, which has just acted as a leaving group, may easily approach either the same metal center or another one, as an incoming ligand. The first process is favored by the high local effective molarity (*chelate effect*), thus re-establishing the initial complex. On the other hand, the free coordination site can bind intermolecularly the Au(III) center of another [$Au^{III}Cl_2$(pipeDTC)] complex, fostering the rearrangement reaction.

On the basis of the mechanistic pathways previously described (**Figure 1.19**), it is possible to hypothesize a conversion to the 1:2 double salt starting with the formation of an intermolecular intermediate with a DTC and a chloride as bridging ligands between the two metal centers (Intermediate II, **Figure 1.20**). This step can be rationalized as two concerted directed attacks from a sulfur donor atom and a chlorine, respectively, to two opposite electrophilic Au(III) ions (Lewis-acid site). On the basis of the different conversion-rates observed in various media, the solvent entrance into the coordination sphere of the metal is likely to occur. The following steps of the rearrangement correspond to a series of high energy intermediates in which the various coordination geometries taken by the metal centers, are in agreement with the theoretical assumptions about the substitution reaction in square planar complexes described before.

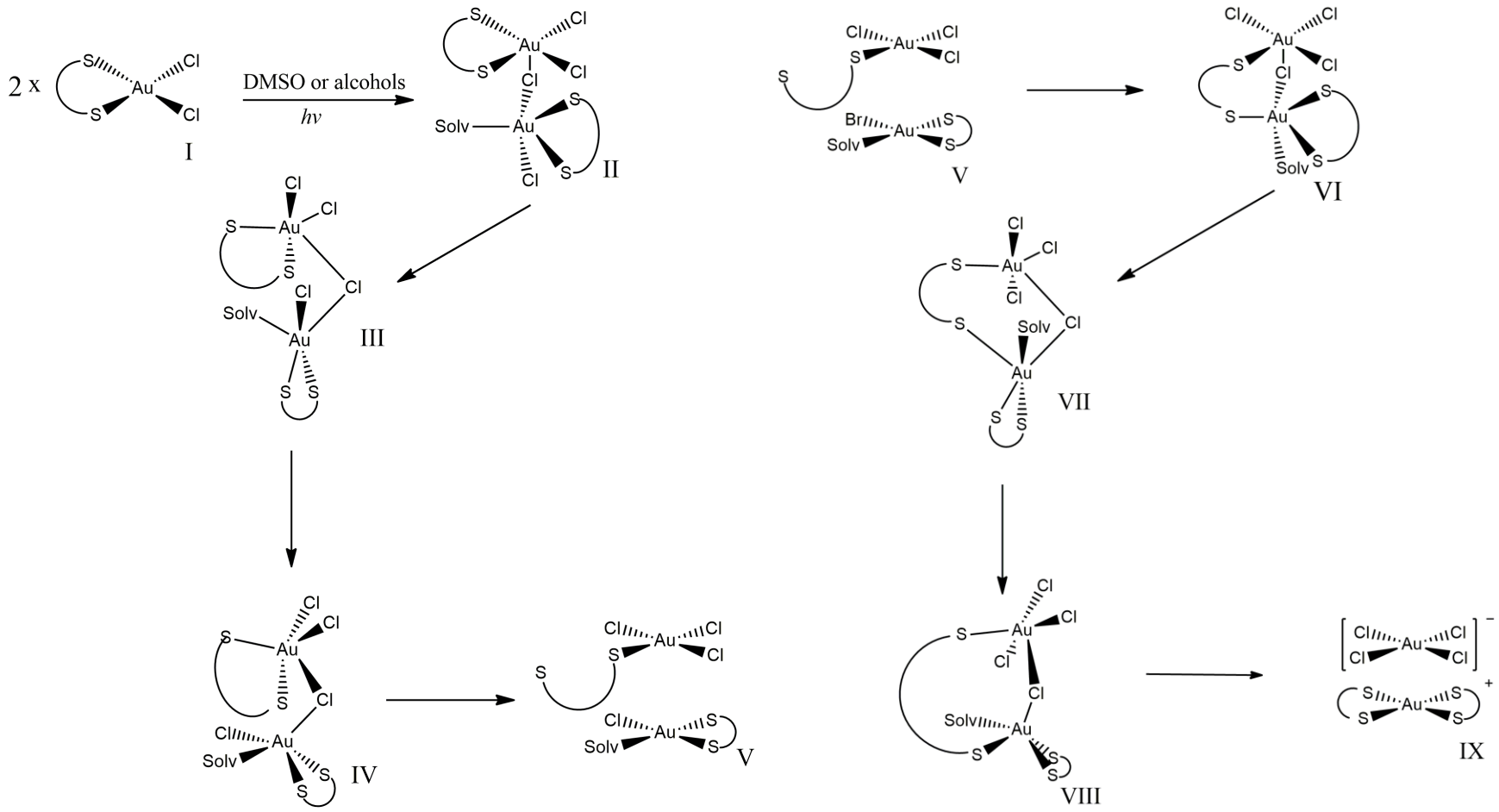

Figure 1.20: Detailed representation of the hypothesized rearrangement equilibrium carried out by two molecules of 1:1 complex forming 0.5 equivalents of [1:2][$AuCl_4$] compound in coordination solvent and after UV-Vis irradiation. It is worth pointing out that the coordination geometries for each intermediate are D_{4h} for I, V, IX, C_{4v} for II, IV, VI, VIII and D_{3h} for III, VII. The incoming and leaving groups can be a chlorine or a sulfur-coordination site of the dithiocarbamato moiety and, in most of the intermediates, they can act as a bridging ligand between the two metallic centers. The coordinating solvent (Solv) plays an important role in the saturation of the coordination sphere of the metal. In particular, at the VIII-step, the solvent molecule is the leaving group. Charges are omitted for clarity reasons. In the case of "direct equilibrium", the representation should be read from step IX to I.

To some up, it is possible to stabilize the 1:1 species by dissolving it in an apolar and non-coordinating medium whereas the system could be driven to the [1:2][$AuCl_4$] form by dissolution in a coordinating solvent (*e.g.*, MeOH or DMSO), followed by UV-light irradiation with an UV-lamp at 254 nm for few minutes and stirred for at least 72 h. After the complete conversion, the solvent can be removed and the neutral 1:1 compound re-obtained by dissolution in a halogenated solvent at refluxing (**Figure 1.21**). At the best of our knowledge, this is one of the few examples of dynamic and tunable inorganic system ever detected.[90]

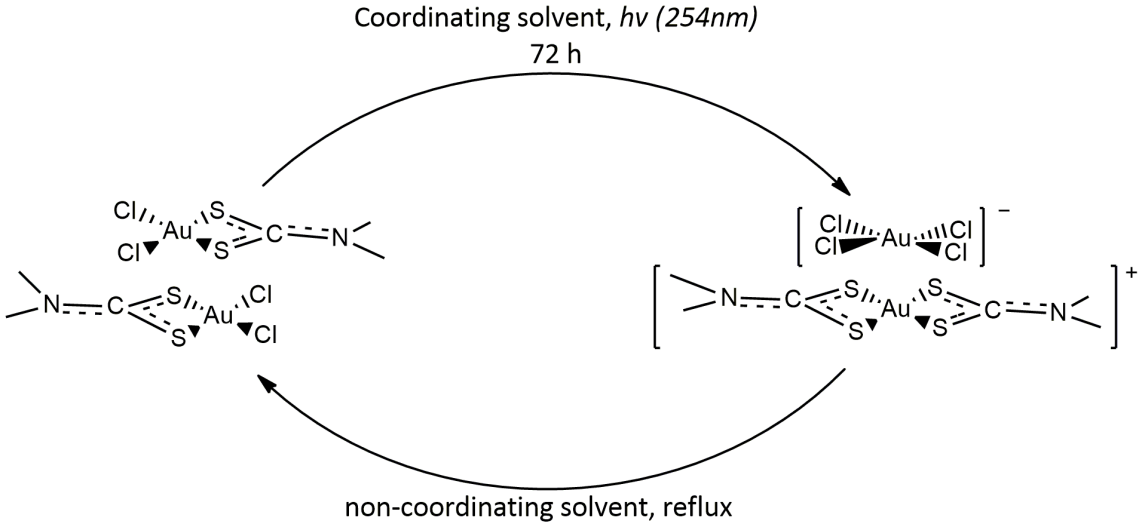

Figure 1.21: schematic representation of the dynamic equilibria involving the Au(III) dithiocarbamato specie described above.

Moreover, it is important to highlight that, in the case of di-bromo compounds, the same behavior of the di-chloro derivatives can be observed. Conversely, the UV-Vis kinetic analysis of the di-iodo complex shows an inhibition of the rearrangement process in coordinating polar solvents in 72h (**Figure 1.22**). This characteristic might be due to the stronger interaction between the polarizable iodine and the gold(III) center resulting in a higher electron density on the metal that prevent the apical interaction of the latter with the lone pairs of the solvent molecules.

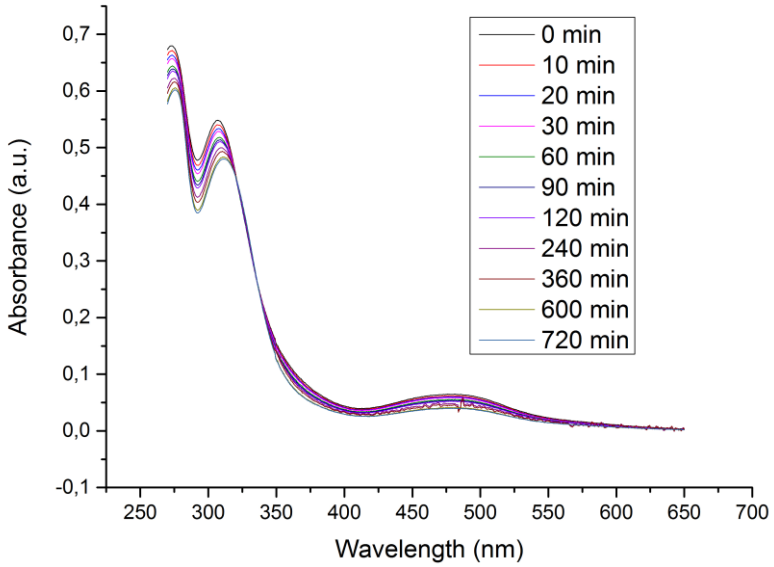

Figure 1.22: UV-Vis kinetic analysis over 72 h of the $[Au^{III}I_2(PipeDTC)]$ dissolved in DMSO.

1.6 Organometallic 1:1 Au(III) dithiocarbamato compounds

In light of the previous considerations, modifications of the mono-anionic ligands on the 1:1 structure were taken into account to prevent the rearrangement equilibrium in coordinating polar solvents and under UV-Vis irradiation. In particular, as the interconversion process was found to be independent by the nature of the dithiocarbamato ligand, the unique plausible solution to stabilize the complex is to replace the trans halides with strong non-migrating substituents. In other words, changing the chlorine and bromine ligands with other less-leaving substituents, from the coordination sphere of the Au(III) ion make possible, at least in theory, to prevent the formation of the stable $[Au^{III}X_4]^-$ anion in polar solvent. In this regard, is it interesting to note that the 1:1 dithiocarbamato complexes showed a great stability toward harder ligands, such as O- and N-donating molecules or anions both monodentate and bidentate. Several experimental attempts to obtain the di- or mono-hydroxyl or aquo-complex were tried and failed without any detectable substitution. Similarly, the efforts to replace the halogens with ammonia, ethylenediamine or imidazole did not give any interesting results. Moreover, forcing the precipitation of the halides with a Ag(I) salts or using S-donating ligands lead to the subsequent reduction of Au(III) to Au(I) dimeric species. At this point, we addressed our attention to the organometallic chemistry of gold(III), in particular with σ-type bond. As other compounds synthetized previously, organogold(III) derivatives with one to four organic groups are four coordinated and assumed

as square planar. Complexes having a lower coordination number appear to be inherently unstable. Moreover, as the alkyl R^- anion is extremely strong ligands, an electronic configuration of d^8 low-spin state for Au(III) is obtainable, which accounts very well for the diamagnetism and stability observed in all organogold(III) compounds present in literature.[60,91] Like gold(I), also gold(III) is a weak π-acceptor, and R-Au^{III} bonds are probably of pure σ-character.[91] As a matter of facts, the most common organometallic Au(I/III) compounds are cyano-derivatives as $[Au^{I}(CN)_2]^-$ and $[Au^{III}(CN_2)X_2]^-$, that possesses a primary importance in gold mining since the XIX century, while the alkyl-complexes, in particular with methyl ligand, were firstly synthetized by Pope and Gibson in 1907.[92] These latter compounds were obtained by reacting a gold(III) salt solution with the appropriate Grignard Reagent, leading to the formation of the quite stable dimeric precursor $[Au^{III}(Me)_2X]_2$ in very low yield. This compound, crystallized many years later,[93] is the more convenient starting point for the Au(III) organometallic chemistry. In facts, upon mixing it with a O-, N- or S-donor ligand, either mono or bidentate, the bridging halide acts as leaving group forming the desired di-methyl mononuclear complexes quantitatively. After, in the 1994, Schmidbaur and co-worker purposed a novel yield-saving synthesis for the same precursor exploiting the transmetalation reaction between a gold(III) polymeric halide $Au^{III}X_3$ and the $Sn^{IV}(CH_3)_4$ in aprotic apolar solvent at -40°C.[94] Anyway, several attempts to follow Schmidbaur's procedure in our laboratory failed. The precursor was then prepared according to Pope and Gibson.

In the light of these considerations, two different organogold(III) dithiocarbamato complexes were synthetized and characterized, the first obtained by the substitution of only one halide with a cyanide group, the second possessing two trans-methyl ligands.

Moreover, two crystals suitable for *X*-ray diffraction analysis were obtained by means of slow evaporation of a dichloromethane or acetone solution of the complexes (**Figure 1.23**). The main structural parameters are reported in **Table**

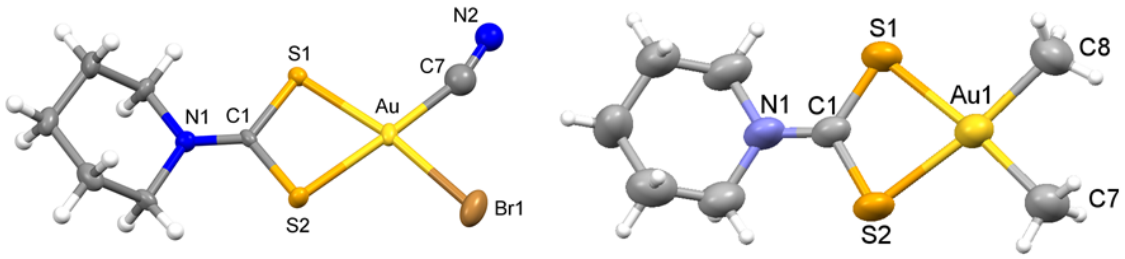

Figure 1.23: Crystal structures of the organometallic derivatives synthetized in this work: [Au^{III}CNBr(PipeDTC)] (*left*) and the [$Au^{III}Me_2$(PipeDTC)] (*right*). The thermal ellipsoids are set at a 50% probability level.

Table 1.6

	Au-S1 (Å)	Au-S2 (Å)	C1-N1 (Å)	Au-Br (Å)	Au-C7 (Å)	S1-Au-S2 (°)
[AuBrCN(pipeDTC)]	2.305(2)	2.324(2)	1.287(11)	2.445(12)	1.952(3)	75.59(7)
[$AuMe_2$(pipeDTC)]	2.391(3)	2.384(3)	1.318(14)	-	2.050(13)	74.59(8)

1.6.1 Syntheses

To obtain the 1:1 organometallic complexes, two different approaches were followed. For the synthesis of the cyano-bromo derivative an oxidative addition of the non-symmetrical pseudohalogen Br-CN to Au(I) dimeric dithiocarbamate was carried out. The reagent BrCN was chosen for its low toxicity and easy-to-handle formulation (3M in CH_2Cl_2). Due to the lower reduction potential of BrCN with respect to chlorine and bromine the oxidative addition reaction to obtain the 1:1 cyano-bromo derivative was slower if compared to the others, and in 48 hours at 40°C the major amount of Au(I) was oxidized.

The second approach aimed to obtain a fully substituted organometallic dithiocarbamato complex, started from the synthesis and isolation of the dimeric precursor [$Au^{III}(Me)_2I]_2$, followed by the addition of two equivalent of PipeDTC potassium salt. All the compounds were purified by means of column chromatography.

- Synthesis of Cyano, Bromo (piperidine dithiocarbamato) gold(III), [AuCNBr(PipeDTC)]

To a stirring dichloromethane suspension of [Au^{I}(PipeDTC)]$_2$ (0.5 mmol) was added an excess of cyanogen-bromide (BrCN, 3M solution in CH_2Cl_2) and the resulting mixture was refluxing for 48h. The initially clear solution become orange-yellow over time. Then the suspension was cooled (Ar was bubbled for 10 minutes, in order to eliminate the excess of

BrCN) and filtered. After the evaporation of the solvent by rotatory evaporator, an orange powder was obtained. The crude product was then re-dissolved in DCM and purified by means of flash column chromatography with DCM as eluent. Two final products were separated: one with R_f 0.8, corresponding to the 1:1 dibromo derivative, and one with R_f 0.3 that was half-dried and precipitated with diethyl ether. A yellow solid, soluble in halogenated solvents, acetone, acetonitrile and slightly in alcohols, was obtained (Yield: 65 %).

Aspect: light yellow solid
R.f. (on silica gel, CH_2Cl_2): 0.3
Anal. Calc. for $C_7H_{10}AuBrN_2S_2$ (MW = 463.17 g·mol-1): C 18.15; H 2.18; N 6.05; S 13.85. Found: C 18.84; H 2.28; N 5.89; S 13.74.
^{1}H-NMR ($CDCl_3$, 400 MHz): δ (ppm) = 1.80-1.95 (m, 6H, $H_{(3)} + H_{(4)} + H_{(5)}$), 3.70-3.83 (m, 4H, $H_{(2)} + H_{(6)}$).
Medium FT-IR (KBr): $\tilde{\nu}$ (cm^{-1}) = 2947.58 (ν_a, C-H); 2863,74 (ν_a, C-N); 1575.89 (ν_a, N-CSS); 1006.00 (ν_a, CSS).
Far FT-IR (nujol): $\tilde{\nu}$ (cm^{-1}) = 543.78 (ν_s, CSS); 415,79 (ν_a, Au-C); 366.60 (ν_a, Au-S); 349.71 (ν_a, Au-Br).

- Synthesis of Dimethyl(piperidine dithiocarbamate)gold(III), [$AuMe_2$(PipeDTC)]

In a 2-necked round-bottom flask equipped with stirring bar, nitrogen flow and a rubber septum, 0.5 mmol of $[Au^{III}IMe_2]_2$, synthetized as reported elsewhere,[92] were dissolved in a dry acetone (10 mL) through syringe. To this solution were added 1.25 mmol of potassium piperidine dithiocarbamate dissolved in dry MeOH. As soon after the addition, the uncolored mixture became clear yellow. After 10 minutes stirring, the nitrogen flux was stopped, the solution was filtered, and the solvent evaporated, obtaining a white deliquescent solid. The crude product was then re-dissolved in DCM and purified by means of flash column chromatography with DCM as eluent (R_f: 0.91). The purified white solid is soluble in all solvents, including halogenated ones, alkanes, alcohols, except water.

Aspect: white solid
R.f. (on silica gel, CH_2Cl_2): 0.91
Anal. Calc. for $C_8H_{16}AuNS_2$ (MW = 387.32 g·mol^{-1}): C 24.81; H 4.16; N 3.62; S 16.56. Found: C 24.70; H 4.05; N 3.21; S 15.98.

^{1}H-NMR ($CDCl_3$, 400 MHz): δ (ppm) = 1.04 (s, 6H, -CH_3), 1.62-1.84 (m, 6H, $H_{(3)}$ + $H_{(4)}$ + $H_{(5)}$), 3.84 (m, 4H, $H_{(2)}$ + $H_{(6)}$).
Medium FT-IR (KBr): $\tilde{\nu}$ (cm^{-1}) = 2938.38-2801.25 (ν_a, C-H); 1509.80 (ν_a, N-CSS); 1005.85/980.50 (ν_a, CSS).
Far FT-IR (nujol): $\tilde{\nu}$ (cm^{-1}) = 556.66 (ν_s, CSS); 439,59 (ν_a, Au-C).

1.6.2 The ^{1}H-NMR characterization

Any information about the nature of resonances of the piperidine protons, could be found in **Section 1.4.1**. Concerning the cyano-bromo organometallic complex described above, a normal pattern for the α protons and β-γ ones of the ligand was detected, consisting of multiplets at about 3.85 ppm and 1.88 ppm in $CDCl_3$, respectively (**Supporting Information A**). Intriguingly, in the case of the dimethyl derivative the β and γ protons resonate at 1.77 ppm, meaning that they are more shielded with respect to the other 1:1 complexes. This behavior can be explained considering the electron-donating nature of the methyl group, the opposite with respect to halogens. However, the resonances of the α protons of the piperidine moiety generate a multiplet at 3.84 ppm (in $CDCl_3$), a higher value compared to that of the non-organometallic 1:1 complexes whose maximum value was registered at 3.77 ppm for the dichloro derivative. This effect suggests the presence of a lower electron density on the N-CSS moiety, which reflects on the de-shielding of the α protons.
Moreover, as shown in **Figure 1.24**, in the case of the α protons of the cyano-bromo derivative dissolved in $CDCl_3$, a double resonance is visible, meaning that the two groups of α protons are not equivalent to each other. This effect is in agreement with the presence of two different trans substituents on gold(III) coordination sphere, taking into account the slow rotation rate of the N-C bond of the dithiocarbamato moiety.[95,96] The multiplet centered at 3.75 ppm can be associated to the two protons nearest to the bromide substituent (position 2 of piperidine), according to the resonance of the di-bromo 1:1 complex, while the two protons in position 5 experience a greater withdrawing effect due to the presence of the cyanide group.

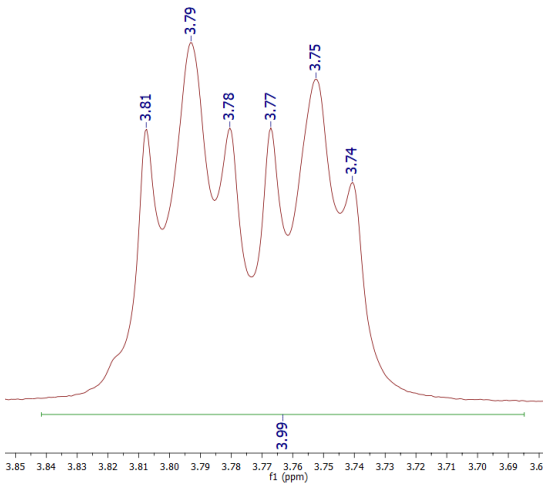

Figure 1.24: Zoom on the α-protons resonances of the 1:1 cyano-bromo gold(III)dithiocarbamato derivative in $CDCl_3$ (400 MHz, 25°C).

1.6.3 The FT-IR characterization

The FT-IR spectra have been collected for all the Au(III)-DTC metallorganic derivatives both in the medium (4000-600 cm^{-1}) and far (600-50 cm^{-1}) wavenumber range (**Supporting Information B**), and the main absorptions are reported in **Table 1.5**. Interestingly, while the medium FT-IR spectra are very similar to those of the di-halo derivatives, the most important diagnostic absorptions are present in the Far-FT-IR acquisitions. In particular, for both compounds, a strong band is visible at ca. 415-440 cm^{-1} assignable to the ν(Au-C) vibration.[97] As a matter of facts, such absorption cannot be found in the spectra of the di-halo complexes. Moreover, in the case of bromo-cyano derivative, the band related to the ν(Au-Br) is detectable at 237 cm^{-1}, accounting for the presence of the two different anionic ligands saturating the trans positions of the Au(III) coordination sphere with respect to the dithiocarbamate.[78] For the 1:1 Me_2 complex, the ν(N-CSS) absorption band is at 1510 cm^{-1} that is a considerable smaller value if compared to the same peak in the di-halo and bromo-cyano counterparts (in which it is usually visible at around 1570-1580 cm^{-1}). Moreover, the ν(CSS) vibration band is at 1005 cm^{-1}, higher than the usual energy values (960 cm^{-1} ly). This behavior can be explained considering the pure σ-donor nature of the methyl ligand which, as it is not able to accept back-donation from the metal center, contributes to increase the electronic density in the dithiocarbamato moiety.[91] As a consequence, while the strength

of the C-S bounds growths, the N-CSS one is depleted of electronic density, leading to the stabilization of the dithiocarbamic form of the ligand instead of the thioureidic one.

1.6.4 The UV-Vis characterization

The UV-Vis absorption spectra of the organometallic complexes were acquired in $CHCl_3$ at 25°C and do not show important differences if compared to the previously registered ones, in particular to that of dichloro-complex (**Supporting Information C**).

As a matter of fact, it is possible to note a strong absorption at 251 nm and 262 nm, for the dimethyl and cyano-bromo dithiocarbamates, respectively, that can be ascribable to the overlapped bands I, II and III (**Figure 1.25**). In the case of the cyano-bromo complex, a weak shoulder can be seen at 244 nm, that corresponds to the band I of the 1:1 dihalo derivatives, in particular to the di-chloro one.

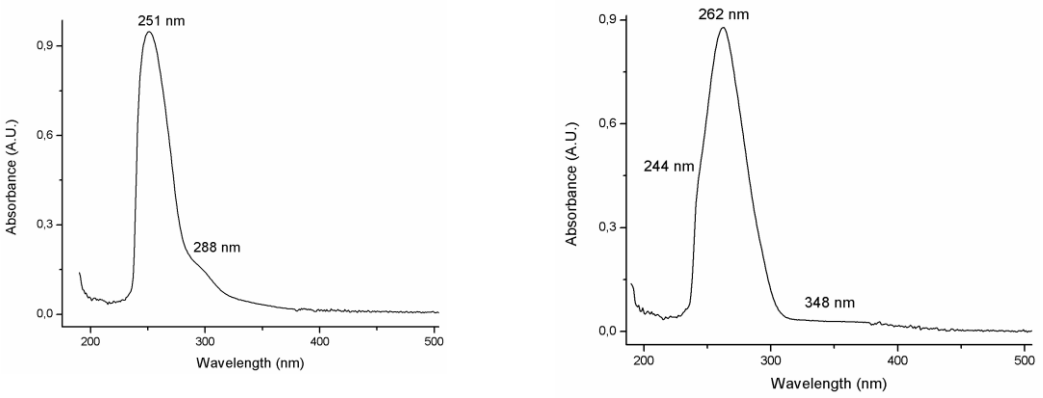

Figure 1.25: UV-Vis absorption spectra of the [$Au^{III}Me_2$(PipeDTC)] complex at 1 μM (left) and [Au^{III}BrCN(PipeDTC)] at 30 μM (right) registered in $CHCl_3$ at 25°C.

Moreover, for the dimethyl complex, a weaker band at 288 nm can be observed, and could be ascribable to the charge transfer between Au-Me (band IV), thus accounting for a stronger M-C bond with respect to the di-halo derivatives. Similarly, for the cyano-bromo compound a weak absorption is detected at 348 nm, probably related to the Au^{III}-Br charge transfer, as the same band for Au^{III}-CN is not visible at energies higher than 185 nm.[80]

It is important to highlight that the band at 251 nm of the dimethyl piperidine dithiocarbamato gold(III) complex possesses the highest molar extinction coefficient ever measured in our laboratory, that is 947700 $L \cdot mol^{-1} \cdot cm^{-1}$. This huge constant value could pave the way for novel applications of this class of organometallic compounds, for example in optics and in other technologies in which a strong UV absorption in required.

1.6.5 Solution chemistry of Au(III) organometallic dithiocarbamates

One of the aims of this Chapter is to understand the role of the trans ligands in the Au(III) 1:1 dithiocarbamato complexes on the rearrangement process that, in the case of chloro- and bromo-derivatives, leads to the formation of the corresponding [1:2][AuX_4] compounds in polar coordinating solvents. In this regard, the novel organometallic dithiocarbamates showed interesting results which let us to deeper understand the interconversion equilibrium. Intriguingly, when the cyano-bromo derivative is dissolved in DMSO and irradiated by means of UV-Vis waves, a reaction similar to that observed for the di-halo derivatives has been detected. In other words, the presence of the high-field cyano ligand do not prevent the interconversion process that occurs in the same time scale and produces a double-salt product as in the other cases described in previous chapters. The only difference is that, in this particular situation, the counterion of the [1:2] bis-dithiocarbamato cation is not the tetrahaloaurate ion but the stable *trans*-[$Au^{III}Br_2(CN)_2]^-$ anion.[98] At this point, it is possible to state that the interconversion process may occur only if (i) an adequate UV irradiation is maintained, if (ii) the Au(III) center owns a sufficient electronic density to interact with the solvent molecule and if (iii) the related counterion of the $[1:2]^+$ complex is stable and well solvated in the reaction medium.

Moreover, it is likely to expect that the [$Au^{III}(Me)_2$(PipeDTC)] complex, as the related $[Au(CH_3)_4]^-$ anion is not stable in solution in presence of O_2,[99,100] may not experience the rearrangement equilibria in DMSO. In fact, this compound is perfectly stable in such solvent over 72 h as shown in **Figure 1.26**.

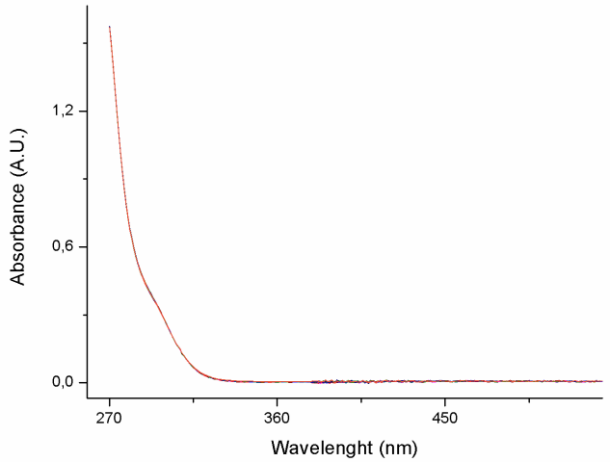

Figure 1.26: UV-Vis kinetic study proving the stability of [$Au^{III}Me_2$(PipeDTC)] complex dissolved in DMSO over 72h.

Bibliography

1. David R.L, ed. CRC *Handbook of Chemistry and Physics,* 89th edition, (Internet Version 2009), CRC Press/Taylor and Francis, Boca Raton, FL.
2. Conception-Gimeno, M. *The Chemistry of Gold-Modern Supramolecular Gold Chemistry: Gold-Metal Interactions and Applications*. Ed. Laguna A. **2008,** Wiley-VCH Verlag GmbH & Co. KGaA, Weinheim, pp. 1-50.
3. Greenwood, N.N.; Earnshaw, A. *The Chemistry of the Elements*, Second Volume, **1984**, Pergamon Press, Ltd.
4. Mohr, F. in *Gold Chemistry: Applications and Future Directions in the Life Sciences.* Verlag Helvetica Chimica Acta, Zurich; Wiley-VCH: Weinheim, Germany, **1999**, 111-134.
5. Hydes, P. C.; Middleton, H. The sulphito complexes of gold - Their chemistry and applications in gold electrodeposition. *Gold Bulletin* **1979**, *12,* 90-95.
6. Skibsted, L. H.; Bjerrum, J. Studies on Gold Complexes. III. The Standard Electrode Potentials of Aqua Gold Ions. *Acta Chem. Scand*., Ser. A, **1977**, 31, 155.
7. Mason III, W. R.; Gray, H. B. Electronic structures of square-planar complexes. *J. Am. Chem. Soc.* **1968**, *90,* 5721-5729.
8. Das Gupta, S. The double auric iodides of substituted ammonium bases. *J. Am. Chem. Soc.* **1914**, *36(4),* 747-751.
9. International Union of Pure and Applied Chemistry. Nomenclature of Inorganic Chemistry, IUPAC RECOMMENDATIONS 2005, The Royal Society of Chemistry, Thomas Graham House, Science Park, Milton Road, Cambridge CB4 0WF, UK, pag.336.
10. Doll, K.A., Pyykkö, P., Stoll, H. Closed-shell interaction in silver and gold chlorides, *J. Chem. Phys.,* 109, 6, **1998**, 2339-2345.
11. Pyykkö, P. Theoretical chemistry of gold. *Angew. Chem. Int. Ed.,* **2004**, *43,* 4412-4456.
12. Pyykkö, P. Theoretical chemistry of gold. II. *Inorg. Chim. Acta* **2005**, *358,* 4113-4130.
13. Pyykkö, P. Theoretical chemistry of gold. III. *Chem. Soc. Rev.* **2008**, *37,* 1967-1997.
14. Hutchings, G. J.; Brust, M.; Schmidbaur, H. Gold: an introductory perspective. *Chem. Soc. Rev.* **2008**, *37,* 1759-1765.
15. Autschbach, J.; Siekierski, S.; Seth, M.; Schwerdtfeger, P.; Schwarz, W. H. E. Dependence of relativistic effects on electronic configuration in the neutral atoms of d- and f-block elements. *J. Comput. Chem.*, **2002**, *23,* 804-813.
16. Schmidbaur, H.; Schier, A. A briefing on aurophilicity. *Chem. Soc. Rev.* **2008**, *37,* 1931-1951.
17. Schmidbaur, H.; Schier, A. Aurophilic interactions as a subject of current research: An up-date. *Chem. Soc. Rev.* **2012**, *41,* 370-412.
18. Schmidbaur, H. The aurophilicity phenomenon: A decade of experimental findings, theoretical concepts and emerging applications. *Gold Bull.* **2000**, *33,* 3-10.
19. Hayoun, R.; Zhong, D. K.; Rheingold, A. L.; Doerrer, L. H. Gold(III) and platinum(II) polypyridyl double salts and a general metathesis route to metallophilic interactions. *Inorg. Chem.* **2006**, *45,* 6120-6122.
20. Klapötke, T. M.; Krumm, B.; Galvez-Ruiz, J.; Nöth, H. Highly sensitive ammonium tetraazidoaurates(III). *Inorg. Chem.* **2005**, *44,* 9625-9627.
21. Doerrer, L. H. Steric and electronic effects in metallophilic double salts. *Dalton Trans.* **2010**, *39,* 3543-3553; and references therein.
22. Laguna, A.; Laguna, M. Coordination chemistry of gold(II) complexes. *Coord. Chem. Rev.* **1999**, *193-195,* 837-856.
23. Calabro, D. C.; Harrison, B. A.; Todd Palmer, G.; Moguel, M. K.; Rebbert, R. L.; Burmeister, J. L. Thiocyanation, selenocyanation, and halogenation reactions of dithiocarbamate

complexes of gold(I) and silver(I). Generation of gold(II) and silver(II) complexes. *Inorg. Chem.* **1981**, *20,* 4311-4316.
24. Schmidbaur, H. Inorganic chemistry with ylides. *Acc. Chem. Res.* **1975**, *8,* 62-70.
25. Sutton, B.M. Gold compounds for rheumatoid arthritis. *Gold Bull*. **1996**, *19*, 15-16.
26. Messori, L.; Marcon, G. *Gold Complexes in the Treatment of Rheumatoid Arthritis in: Metal Ions in Biological Systems*, Marcel Dekker. Inc., **2004**, *41*, 279-304.
27. Smith-Kline & French Labor. Anti-arthritic compositions comprising a trialkylphosphinegold complex of a 1-β-D-glucopyranoside and methods of producing anti-arthritic activity. US Patent US3708579, **1973**.
28. Glenna, A.; Kvien, T.K.; Andrup, O.; Clarke-Jenssen, O.; Karstensen, B.; Brodin, U. Auranofin is safe and superior to placebo in elderly-onset rheumatoid arthritis. *Br. J. Rheumatol*. **1997**, *36(8)*, 870-877.
29. Shaw, C.F. Gold-based therapeutic agents. *Chem. Rev.*, **1999**, *99(9)*, 2589-2600.
30. Takahashi, K.; Griem, P.; Goebel, C.; Gonzalez, J.; Gleichmann, E. The antirheumatic drug gold, a coin with two faces: Au(I) and Au(III). Desired and undesired effects on the immune system. *Met. Based Drugs*, **1994**, *1(5-6)*, 483-496.
31. Snyder, R.M.; Mirabelli, C.K.; Crooke, S.T. Cellular association,intracellular distribution, and efflux of auranofin via sequential ligand exchange reactions. *Biochem. Pharmacol*., **1986**, *35(6)*, 923-932.
32. a) University of Kansas. Phase I and II study of auranofin in chronic lymphocytic leukemia (CLL). US National Institutes of Health, Available from: ClinicalTrials.gov/ct2/show/ NCT01419691; b) Majo Clinic Cancer Center. Auranofin in Treating Patients with Recurrent Epithelial Ovarian, Primary Peritoneal, or Fallopian Tube Cancer. US National Institutes of Health, Available from: ClinicalTrials.gov identifier NCT 01747798.
33. Roder, C.; Thomson, M.J. Auranofin: repurposing an old drug for a golden new age. *Drugs R D*. **2015**, *15(1)*, 13-20.
34. Glišić, B.D.; Djuran, M.I. Gold complexes as antimicrobial agents: an overview of different biological activities in relation to the oxidation state of the gold ion and the ligand structure. *Dalton Trans.* **2014**, *43(16)*, 5950-5969.
35. Harbut, M.B.; Vilchèze, C.; Luo, X.; Hensler, M.E.; Guo, H.;Yang, B.; Chatterjee, A.K.; Nizet, V.; Jacobs, W.R., Jr; Schultz, P.G.; Wang, F. Auranofin exerts broad-spectrum bactericidal activities by targeting thiol-redox homeostasis. *Proc. Natl. Acad. Sci. USA*, **2015**, *112(14)*, 4453-4458.
36. a) Nardon, C.; Boscutti, G.; Fregona, D. Beyond platinums: gold complexes as anticancer agents. *Anticancer Res*. **2014**, *34(1)*, 487-492; b) Nardon, C.; Fregona, D. Gold(III) complexes in the oncological preclinical arena: From aminoderivatives to peptidomimetics. *Curr. Top. Med. Chem.* **2016**, *16(3)*, 360-380.
37. Berners-Price, S.J.; Barnard, P.J. *Therapeutic Gold Compounds in: Ligand Design in Medicinal Inorganic Chemistry*; John Wiley & Sons, Ltd: Chichester, **2014**, pp. 227-256.
38. McKeagea, M.J.; Maharaj, L.; Berners-Price, S.J. Mechanisms of cytotoxicity and antitumor activity of gold(I) phosphine complexes: the possible role of mitochondria. *Coord. Chem. Rev.* **2002**, *232*, 127-135.
39. Parish, R.V.; Howe, B.P.; Wright, J.P.; Mack, J.; Pritchard, R.G.; Buckley, R.G.; Elsome, A.M.; Fricker, S.P. Chemical and biological studies of dichloro(2-((dimethylamino) methyl)phenyl)gold(III). *Inorg. Chem.* **1996**, *35(6)*, 1659-1666.
40. Abram, U.; Mack, J.; Ortner, K.; MA1/4ller, M. Reactions of dichloro [2-(dimethylaminomethyl)phenyl-C1,N] gold(III), [Au(damp-C1,N)Cl_2], with heterocyclic

thiols. Evidence for Au-N bond cleavage and protonation of the dimethylamino group. *J. Chem. Soc. Dalton Trans.* **1998**, 1011-1019.
41. Ott, I. On the medicinal chemistry of gold complexes as anticancer drugs. *Coord. Chem. Rev.* **2009**, *253*, 1670-1681.
42. Ronconi, L.; Fregona, D. The Midas touch in cancer chemotherapy: from platinum- to gold-dithiocarbamato complexes. *Dalton Trans.* **2009**, *48*, 10670-10680.
43. Maia, P.I.; Deflon, V.M.; Abram, U. Gold(III) complexes in medicinal chemistry. *Future Med. Chem.* **2014**, *6(13)*, 1515-1536.
44. Schier, A.; Schmidbaur, H. *Gold: Organometallic Chemistry in: Encyclopedia of Inorganic Chemistry*; John Wiley & Sons Ltd, **2006**.
45. Pearson, R. G. Hard and soft acids and bases. *J. Am. Chem. Soc.* **1963**, *85,* 3533-3539.
46. Åkerström, S. *Arkiv Kemi*, **1959**, *14*, 387-401.
47. Hesse R.; Jennische, P. The Crystal and Molecular Structure of the Gold(I) Dipropyldithiocarbamate Dimer. *Acta Chem. Scand.* **1972**, *26*, 3855-3864.
48. Pearson, W.B. *A Handbook of Lattice Spacings and Structures of Metals and Alloys*, Part II, Pergamon Press, London, **1964**, pp. 124.
49. Jennische, P. *The Crystal Structure of Gold(I) Dibutyldithiocarbamate*, Report UUIC-B20–02. Institute of Chemistry, University of Uppsala, Uppsala, **1975**.
50. Heinrich, D.D.; Wang, J.C.; Fackler J.P. Structure of $Au_2[S_2CN(C_2H_5)_2]_2$, bis (diethyldithiocarbamato) digold(I). *Acta Crystallogr. Sect. C,* **1990**, *46*, 1444-1447.
51. Jiang, Y.; Alvarez, S.; Hoffmann, R. Binuclear and polymeric gold(I) complexes. *Inorg. Chem*. **1985**, *24,* 749-757.
52. Jansen, M. Homoatomic d^{10}–d^{10} Interactions: Their Effects on Structure and Chemical and Physical Properties. *Angew. Chem. Int. Ed.* **1987**, *11*, 1098-1110.
53. Teske, L.C.; Bensch, W. On Crystal Structure Investigations of α- and β-Ammoniumdithiocarbamate $NH_4CS_2NH_2$ and the Role of Hydrogen Bonding. *Z. Anorg. Allg. Chem*. **2010**, *636*, 356-362.
54. Whittall, I.R.; Humphrey, M.G.; Samoc, M.; Luther-Davies, B.; Hockless, D.C.R. Organometallic complexes for non-linear optics XII. Syntheses and second-order susceptibilities of (neomenthyldiphenylphosphine) gold σ-arylacetylides: X-ray crystal structures of Au(C≡CPh) (nmdpp) and Au((E)-4,4′-C≡CC_6H_4CH=CH$C_6H_4NO_2$)(nmdpp). *J. Organomet. Chem.* **1997**, *544(2)*, 189-196.
55. Baenziger, N.C.; Bennett, W.E.; Soboroff, D.M.; O'Donnell, P.F.; Doyle, J.R. Synthesis, crystal structure and a spectroscopic study of bistriphenylphosphine)gold$(I)^+$ $TCNQ^-$. *Polyhedron,* **1998**, *17*, 2379-2410.
56. Srinivasan, N.; Valarmathi, P.; Thirumaran, S.; Ciattini, S. Synthesis and spectral studies on NiS_4, NiS_2PN, NiS_2P_2 chromophores: Single-crystal X-ray structure of [Ni(dbpdtc)$_2$] (dbpdtc = benzyl(4-(benzylamino)phenyl)dithiocarbamate). *Transition Met. Chem.* **2010**, *35*, 815-819.
57. de Lima, G.M.; Menezes, D.C.; Cavalcanti, C.A.; dos Santos, J.A.F.; Ferreira, I.P.; Paniago, E.B.; Wardell, J.L.; Wardell, S.; Krambrock, K. Synthesis, characterisation and biological aspects of copper(II) dithiocarbamate complexes, [Cu{S_2CNR(CH_2CH_2OH)}$_2$], (R = Me, Et, Pr and CH_2CH_2OH). *J. Mol. Struct.* **2011**, *988*, 1-8.
58. Shahid, M.; Ruffer, T.; Lang, H.; Awan, S.A.; Saeed, A. Synthesis and crystal structure of a dinuclear zinc(II)-dithiocarbamate complex, bis{[(μ^2-pyrrolidinedithiocarbamato-S,S')(pyrrolidinedithiocarbamato-S,S')zinc(II)]}. *J. Coord. Chem.* **2009**, *62(3)*, 440-445.

59. Onwudiwea, D.C.; Mugo, J.N.; Hrubaru, N.; Hosten, E. Bis diallyl dithiocarbamate Pt(II) complex: synthesis, characterization, thermal decomposition studies, and experimental and theoretical studies on its crystal structure. *J. Sulfur Chem.* **2015**, *36(1)*, 36-47.
60. Beurskens, P.T.; Cras, J.A.; Steggerda, J.J. Structure and properties of dibromo-*N,N*-dibutyldithiocarbamato complexes of copper(III) and gold(III). *Inorg. Chem.* **1968**, *7(4)*, 810-813.
61. Bardaji, M.; Laguna, A.; Laguna, M. Phosphoniodithioformate gold derivatives. Synthesis of tricationic gold(II)complexes. *J. Organomet. Chem.* **1995**, *496*, 245-248.
62. Cordon, J.; Jimenez-Oses, G.; Lopez-De-Luzuriaga, J.M.; Monge, M.; Olmos, M.E.; Pascual, D. Experimental and theoretical study of gold(III)-catalyzed hydration of alkynes. *Inorg. Chem.* **2014**, *33(14)*, 3823-2830.
63. Chen, H.W.; Paparizos, C.; Fackler, J.P. Dimethylgold(III) complexes. Synthesis of several compounds with AuC_2S_2 coordination. The crystal and molecular structure of $[(CH_3)_2AuSC_2H_5]_2$. *Inorg. Chim. Acta*. **1985**, *96(2)*, 137-149.
64. Bobrovnikova, A.A.; Cherkasova, T.G.; Shirokolobova, A.G.; Bolsunovskaya, L.M. Preparation and Structure of Double Complex Compounds $[La(HMPA)_4(NO_3)_2][Cr(NH_3)_2(NCS)_4]$. *Procedia Chem.* **2014**, *10*, 530-534.
65. Domonov, D.P.; Kuratieva, N.V.; Pechenyuk, S.I. Structure and properties of double complex salts $[Co(NH_3)_6][Fe(CN)_6]$ and $[Co(NH_3)_6]_2[Cu(C_2O_4)_2]_3$. *J. Struct. Chem.* **2011**, *52(2)*, 358-364.
66. Beurskens, P.T.; Cras, J.A.; Van der Linden, J.G.M. Preparation, structure, and properties of bis(N,N-di-n-butyldithiocarbamato)gold(III) bromide and bis(N,N-di-n-butyldithiocarbamato) gold(III) tetrabromoaurate(III). *Inorg Chem.* **1969**, *9(3)*, 475-479.
67. Beurskens, P.T.; Blaauw, H.J.A.; Cras, J.A.; Steggerda, J.J. Preparation structure, and properties of bis(N,N-dibutyldithiocarbamato)gold(III) dihaloaurate(I). *Inorg. Chem.* **1968**, *7(4)*, 805-810.
68. Forghieri, F.; Preti, C.; Tassi, L.; Tosi, G. Preparation, properties and reactivity of gold complexes with some heterocyclic dithiocarbamates as ligands. *Polyhedron*, **1988**, *7(14)*, 1231-1237.
69. Serpe, A.; Marchiò, L.; Artizzu, F.; Mercuri, M.L.; Deplano, P. Effective one-step gold dissolution using environmentally friendly low-cost reagents. *Chem. Eur. J.* **2013**, *19(31)*, 10111-10114.
70. Altaf, M.; Isab, A.A.; Vančo, J.; Dvořák, Z.; Trávníček, Z.; Stoeckli-Evans, H. Synthesis, characterization and in vitro cytotoxicity of gold(III) dialkyl/diaryldithiocarbamato complexes. *RSC Advances*, **2015**, *5(99)*, 81599-81607.
71. Hynes, M. J.; Brannick, P. F. Rates and mechanisms of substitution reactions of square-planar dithiocarbamate and dithiophosphate complexes of the nickel triad in methanol. *Journal of the Chemical Society, Dalton Trans.* **1977**, 2281-2285.
72. Leyva, A.; Zhang, X.; Corma, A. Chemoselective hydroboration of alkynes *vs* alkenes over gold catalysts. *Chem. Commun.* **2009**, *33*, 4947-4949.
73. Scintilla, S.; Brustolin, L.; Gambalunga, A.; Chiara, F.; Trevisan, A.; Nardon, C.; Fregona, D. Ru(III) anticancer agents with aromatic and non-aromatic dithiocarbamates as ligands: Loading into nanocarriers and preliminary biological studies. *J. Inorg. Biochem.* **2016**, *165*, 159-169.
74. Colthup, N. B.; Daly, L. H.; Wiberley, S. E. *Introduction to Infrared and Raman Spectroscopy*; Academic Press: New York, **1990**.

75. Brown, D. A.; Glass, W. K.; Burke, M. A. The general use of IR spectral criteria in discussions of the bonding and structure of metal dithiocarbamates. *Spectrochim. Acta, Pt. A: Mol. Spectrosc.* **1976**, *32,* 145-147.
76. Bonati, F.; Ugo, R. Organotin(IV) *N,N*-disubstituted dithiocarbamates. *J. Organomet. Chem.* **1967**, *10,* 257-268.
77. Kellner, R.; St. Nikolov, G.; Trendafilova, N. Detecting the bonding type of dithiocarbamate ligands in their complexes as inferred from the asymmetric CS mode. *Inorg. Chim. Acta* **1984**, *84,* 233-239.
78. Nakamoto, K. *Infrared and Raman Spectra of Inorganic and Coordination Compounds,* 4th Ed., John Wiley & Sons, **1986**.
79. Gray, H.B.; Ballhausen, C.J. A molecular orbital theory for square planar metal complexes. *Inorg. Chem.* **1963**, *85(5)*, 260-265.
80. Mason III, W.R.; Gray, H.B. Electronic structures and spectra of square-planar gold(III) complexes. *Inorg. Chem.* **1968**, *7(1)*, 55-58.
81. Brown, D.H.; McKinlay, G.C.; Smith, W.E. The electronic spectra of some gold(III) complexes, *Inorg. Chim. Acta*, **1979**, *32*, 117-121.
82. Hadjikostas, C.C.; Katsoulos, G.A.; Shakhatreh, S.K. Synthesis and spectral studies of some new palladium(II) and platinum(II) dithiocarbimato complexes. Reactions of bases with the corresponding N-alkyldithiocarbamates. *Inorg. Chim. Acta*, **1987**, *133,* 129-132.
83. Pallacani, G.C. Gold(III) complexes with dithiocarbimides, *Inorg. Chim. Acta*, **1982**, *58*, 193-200.
84. Gangopadhayay, A.K.; Chakravorty, A. Charge Transfer Spectra of some Gold(III) Complexes, *J. Chem. Phys.* **1961**, 35, 2206-2209.
85. Laporte, O.; Meggers, W.F. Some rules of spectral structure. *J. Opt. Soc. Am.* **1925**, *11(5)*, 459-463.
86. Baddley, W.H.; Basolo, F. A Kinetic Study of Substitution Reactions of Some Gold(III) Complexes. *Inorg. Chem.* **1968**, *3(8)*, 1087-1091.
87. Zhu, S.; Gorski, W.; Powell, D.R.; Walmsley, J.A. Synthesis, Structures, and Electrochemistry of Gold(III) Ethylenediamine Complexes and Interactions with Guanosine 5'-Monophosphate. *Inorg. Chem.* **2006**, *45*, 2688-2694.
88. Hopmann, K.H.; Conradie, J. Density function theory study of substitution on square-planar acetylacetonato-dicarbonyl-rhodium(I) complex. *Organometallics*, **2009**, *28*, 3710-3715; and references therein.
89. Billo, E. J. Mechanisms of ligand replacement in square-planar nickel(II) complexes. I. Reaction of cyanide with bis(1,5-diazacyclooctane)nickel(II) ion. *Inorg. Chem.* **1973**, *12,* 2783-2787; and references therein.
90. Pitteri, B.; Bortoluzzi, M.; Bertolasi, V. Chelate polypyridine ligand rearrangement in Au(III) complexes. *Transition Met. Chem.* **2008**, *33*, 649-654.
91. Schier, A.; Schmidbaur, H. *Gold: Organometallic Chemistry: Encyclopedia of Inorganic Chemistry*, John Wiley & Sons, Ltd, **2006**.
92. Pope, W.J.; Gibson, C.S. The alkyl compounds of gold. *J. Chem. Soc., Trans.* **1907**, *91*, 2061-2066.
93. Zharkova, G.I.; Baidina, I.A.; Igumenov, I.K. Synthesis, Properties, and Structure of Dimethylgold(III) Complexes $[(Me_3)_2AuI]_2$ and $(CH_3)_2AuS_2CN(C_2H_5)_2$. *J. Struct. Chem.* **2007**, *48(1)*, 108-113.
94. Paul, M.; Schmidbaur, H. A New Synthesis of Dimethylgold(III) Chloride Using Tetramethyltin. *Z. Naturforsch., B: Chem. Sci.* **1994**, *49*, 647-649.

95. Heard, P.J.; Kite, K.; Nielsen, J.S.; Tocher, D.A. Trimethylplatinum(IV) complexes of dithiocarbamato ligands: an experimental NMR study on the barrier to C–N bond rotation. *J. Chem. Soc., Dalton Trans.* **2000**, *0*, 1349-1356.
96. Moriyasu, M.; Hashimoto, Y.; Endo, M. Kinetic Studies of Fast Equilibrium by Means of High-performance Liquid Chromatography. IV. Separation of Rotamers of Palladium(II) Dithiocarbamates. *Bull. Chem. Soc. Jpn.* **1983**, *56*, 1972-1977.
97. Cattalini, L.; Orio, A.; Tobe, L.M. The cis effect of the cyanide group in substitution reactions of square-planar gold(III) complexes. *Inorg. Chem.* **1967**, *6(1)*, 75-78.
98. Ovens, J.S.; Leznoff, D.B. Thermally triggered reductive elimination of bromine from Au(III) as a path to Au(I)-based coordination polymers. *Dalton Trans.* **2011**, *40*, 4140-4146.
99. Komiya, S.; Albright, T.A.; Hoffmann, R.; Kochi, J.K. The Stability of Organogold Compounds. Hydrolytic, Thermal and Oxidative Cleavages of Dimethylaurate(I) and Tetramethylaurate(III). *J. Am. Chem. Soc.* **1977**, *99(26)*, 8440-8447.
100. Rice, G.W.; Tobias, S. Synthesis of Tetramethylaurate(III). Studies on the Structures of $Li[(CH_3)_2Au]$ and $Li[(CH_3)_4Au]$ in Solution. *Inorg. Chem.* **1975**, *14(10)*, 2402-2407.

CHAPTER TWO

CARBOHYDRATE-CONJUGATED DITHIOCARBAMATO COMPLEXES

The second Chapter of this Ph.D. thesis is focused on the synthesis of a novel class of Au(III) and Cu(II) dithiocarbamato complexes, functionalized with monosaccharides, in order to obtain a selective delivery of the cytotoxic metal complex into the tumor tissue. In fact, as described in the **Introduction** (**Section 5**), cancer cells require a higher supply of nutrients, in particular carbohydrates, compared to the healthy tissues, due to the Warburg effect and other metabolic mutations. As a consequence, the major parts of neoplastic cells overexpress glucose-transporter proteins (GLUTs) in their phospholipid membrane.[1] The novel bioinorganic compounds described in this chapter should act as substrates for such proteins to be carried into the cytoplasm through an active transport. Reaching this goal, we aim to recognize a significant difference in uptake between the malignant tissues and the healthy ones, leading to the accumulation of the anticancer drug selectively into the former.

Concerning the nature of the monosaccharides, we chose D-glucose and other two diastereomers: D-galactose and D-mannose.[2] While D-glucose is the most common monosaccharide in the body, the other two carbohydrates were selected for comparison purposes, thanks to their affinity for GLUT proteins (see **Introduction**, **Figure 13**).

2.1 The choice of the carbohydrate functionalization position

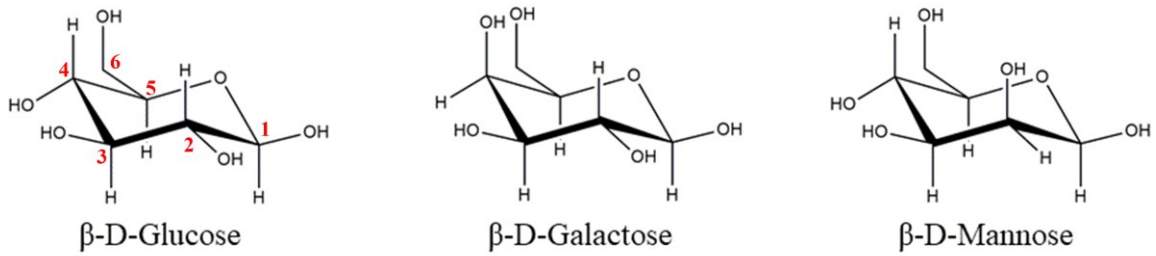

Figure 2.1: Structure of the main stable anomers (β-form) of the three D-monosaccharides used in this work. It is important to note that they are three stereoisomers, in particular D-galactose differs from D-glucose because of the inverted stereocenter in position 4, while D-mannose differs from D-glucose for the stereocenter in C-2.[2]

As shown in **Figure 2.1**, each monosaccharide possesses 5-hydroxyl group which could be modified via organic chemistry techniques. Some of the them are quite easy to functionalize, such as the hydroxyl in position 1, which is more activated as part of the hemiacetalic group, and the primary alcohol in position 6. On the other hand, functionalizing the secondary hydroxyl-groups in position 2, 3 and 4 is highly challenging due to their proximity and very similar reactivity.[3] In literature, the most common functionalized hydroxyl group is that bound to the C-1: it can be transformed into a bromide, an amino or a thiol groups in few chemical passages, or can be converted to an acetal via the reaction with an alcohol and a proper activating reagent.[3] In particular, when the acetal is obtained, the whole molecule is generally called *O*-glycoside (glucoside for glucose, galactoside and mannoside for galactose and mannose, respectively) and the reaction to form it is an *O*-glycosylation. The first glucose-derived glycoside, the methyl-glucoside, was synthetized by Hermann Emil Fischer in 1893. It is worth highlighting that, contrary to the hemiacetals, glycosides cannot open to their linear aldehydic form and, hence, they can be "locked" in one of the two anomeric structure, the α or β form, depending on the reaction conditions.[3] If the reaction is not stereoselective the most stable anomer will be obtained that is the α form, in the case of glucosides. In this work have exploited only stereoselective procedures we to prevent the formation of an anomeric mixture.

One of the mayor problem in the design of the carbohydrate metal-DTC complexes is the choice of the proper functionalization position, in order to obtain a good GLUT substrate. As a matter of fact, is well-known that even a minor modification on the molecular structure can change enormously its binding constant with the target protein.[4] In this regard, literature sources agree in affirming that the best positions to functionalize monosaccharides maintaining their GLUT recognition, are the C-1, C-2 and C-6, as shown in **Figure 2.2**.[5]

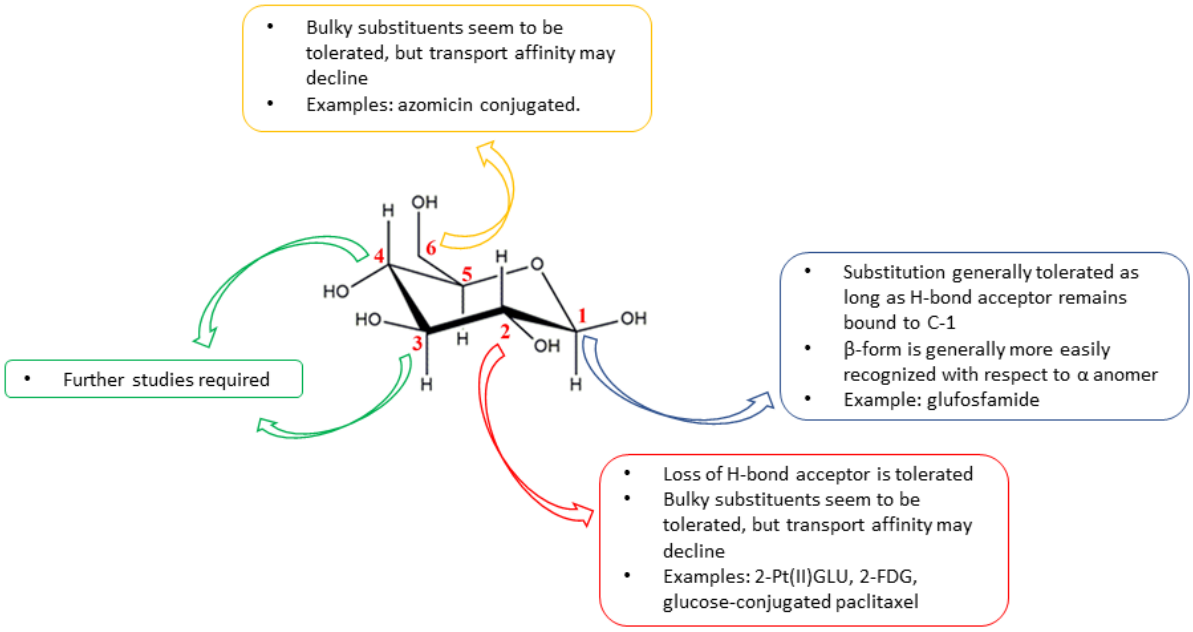

Figure 2.2: Representation of the positions for glycoconjugation with general comments regarding the efficacy of the functionalized product on GLUT recognition[5].

In this work, only the syntheses and characterizations of the Au(III) and Cu(II) glycoside complexes, that are functionalized at C-1, will be presented. First synthetic attempts to obtain a dithiocarbamato ligand conjugating the monosaccharide through the C-2 and C-6 positions of the backbone failed. However, the research on other synthetic pathways to obtain the C-2 and C-6 carbohydrate-metal-DTC conjugates are still ongoing.

2.2 The glycosylation reaction

One of the most interesting method reported in literature for the transformation of the hemiacetal hydroxyl group is the glycosylation reaction, that is arguably the most important reaction in the field of glycochemistry.[3] Briefly, the reaction consists in the functionalization of a carbohydrate, a glycosyl donor, bonding it to a hydroxyl, or other functional groups, of another molecule (a glycosyl acceptor). If the glycosyl acceptor is an alcohol, a O-glycoside will be formed, otherwise, also N- or C-glycosides can be obtained through the reaction with amines or carbanions. The first O-glycosylation was originally accomplished by Fisher in 1893, named Fischer Glycosylation, by dissolving fully unprotected D-glucose in methanol in presence of trimethylsilyl chloride (Cl-Si(CH_3)$_3$) as promoter of acidic catalysis.[6] This

promoter plays a paramount role in the activation of the entering alcoholic function as shown in **Figure 2.3**.

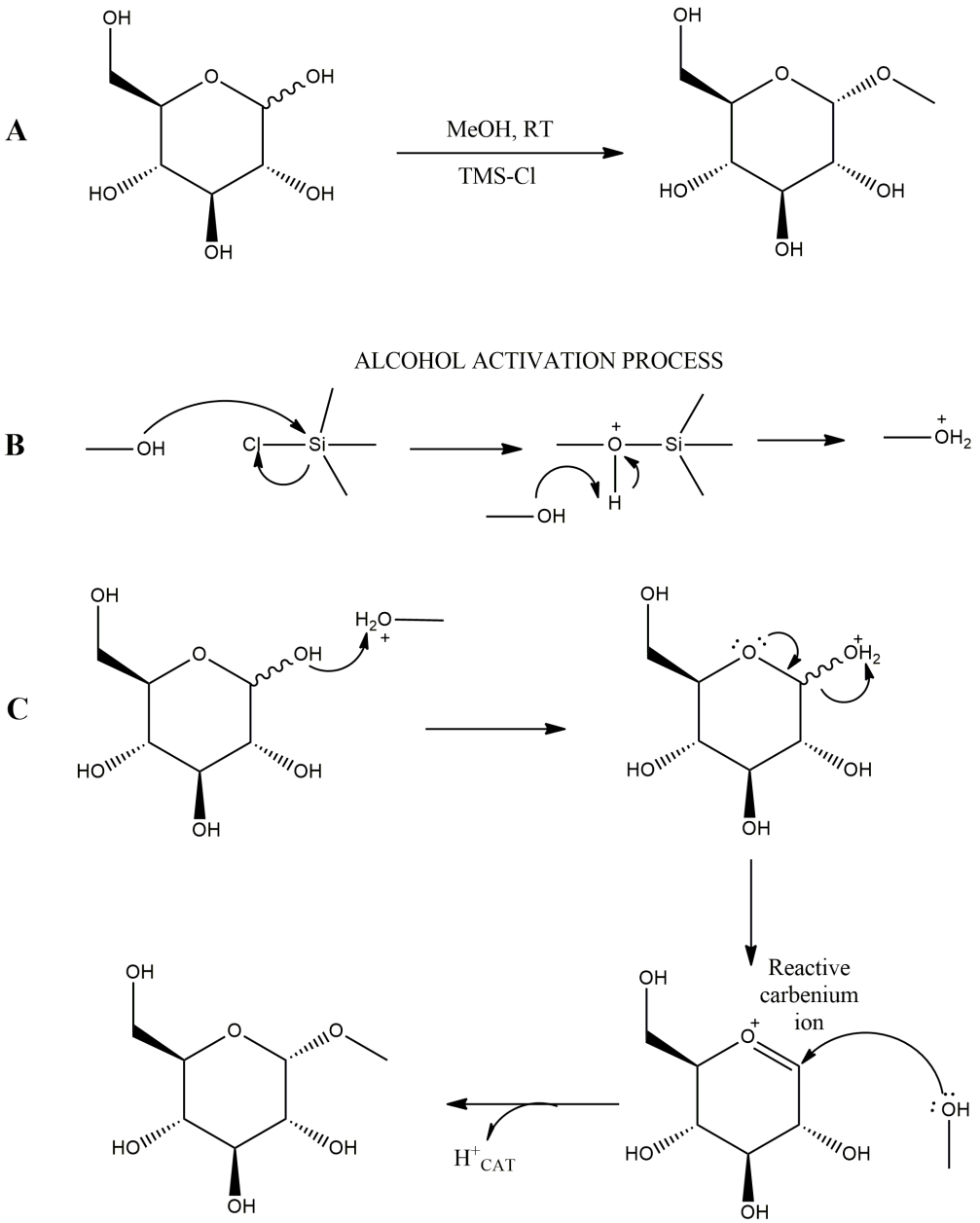

Figure 2.3: (A) General procedure of Fischer Glycosylation of D-glucose in methanol that leads to the formation of the more stable α-methyl glucoside. The reaction takes place only in the presence of an alcohol activator reagent or promoter (B), in this case trimethylsilyl chloride, that facilitates the formation of the protonated methanol species in solution. Then (C) the protonation of the anomeric hemiacetal is provided with the subsequent formation of the reactive carbenium ion. In turn, this charged intermediate reacts with another methanol molecule to obtain the major product and catalytic H^+.

After the research of Fischer, other chemists gave their contribution to the field of glycosylation from the early years of the XX century.[7] Moreover, they started to consider the advantages on the use of protected monosaccharides in organic synthesis, instead of unprotected ones, due to their higher solubility in apolar solvents and the easier handling. They optimized several types of glycosylation reactions, most of them evolving from a per-acetylated glycosyl-halide as reagent or intermediate. In particular, the discovery of the first controlled general glycosylation procedure, involving the nucleophilic displacement of chlorine or bromine at the anomeric center, is credited to Koenigs and Knorr in 1901.[7] The glycosylations were performed in the presence of Ag_2CO_3, which acted both as an acid (HCl or HBr) scavenger and as a promoter that prompts the formation of the carbenium ion. At that early stage, glycosylations of poorly nucleophilic acceptors such as sugar hydroxyls were sluggish and inefficient; hence, even the synthesis of disaccharides represented a notable challenge. The first attempts to solve this problem gave rise to the development of new catalytic systems that were thought to be actively involved in the glycosylation process.[8] Zemplen and Gerecs[9] and, subsequently, Helferich and Wedermeyer[10], assumed that the complexation between the anomeric bromides or chlorides with more reactive heavy-metal-based catalysts, would significantly have improved their leaving-group ability. This approach, that has become a valuable expansion of the classic Koenigs–Knorr method, made it possible replacing Ag_2CO_3 or Ag_2O by more active mercury(II)salt catalysts (**Figure 2.4**).

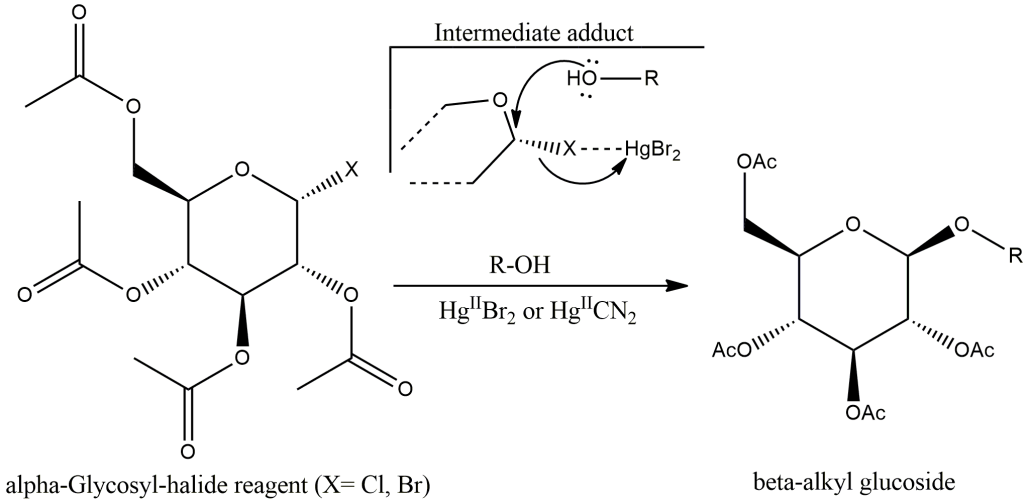

Figure 2.4: Representation of the Helferich glycosylation involving the action of the mercury(II) salt for improving the leaving ability of the halide.

Another commonly used Lewis acid in Helferich-glycosylations is the boron trifluoride diethyl-etherate adduct ($BF_3 \cdot OEt_2$), reported for these synthetic purposes as early as 1949.[11,12] The first complete description about the role of this promoter and about the reaction optimization was published in 1981 by Magnusson and co-workers,[12] in which they were managed to conjugate several pentaacetylated monosaccharides with a simple alkyl alcohol using a five-fold excess of $BF_3 \cdot OEt_2$ in dry CH_3CN and CH_2Cl_2. In particular, the role of the Lewis acid was to force the leaving of the acetyl group of the anomeric carbon with the subsequent formation of the well-known carbenium ion.[13] Contrary to the Fischer glycosylation, in which unprotected carbohydrates are used, in the case of acetylated sugars an important assistance in the stabilization of the carbenium intermediate is given by the carbonyl oxygen of the acetyl group in C-2 position. If the stabilizing group is present, the reaction become highly stereoselective. Regarding D-glucose and D-galactose, in which the C-2 substituent is in equatorial position, the glycosylation reaction leads to the selectively formation of β-anomeric products, because of the assisted stabilization of the adjacent acetyl group that prevent the axial nucleophilic attack of the glycosyl acceptor. Conversely, in the case of D-mannose, an α-mannoside is obtained as product, due to the different stereocenter at C-2 (**Figure 2.5**).

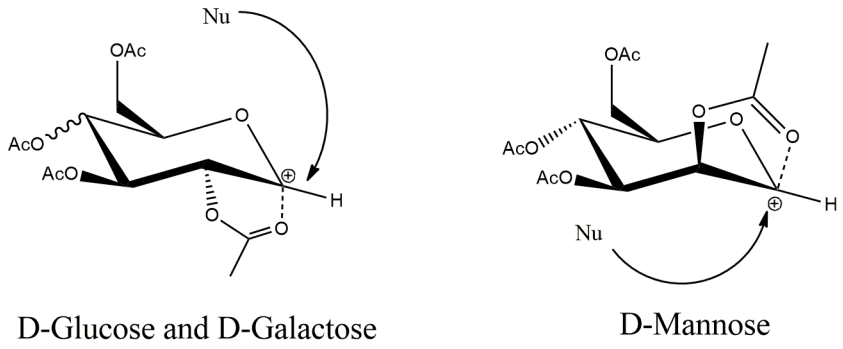

Figure 2.5: depiction representing the different stabilization of the carbenium intermediate upon changing the stereocenter in C-2. The nucleophile (*i.e.*, the glycosyl acceptor) can interact with the electrophilic carbon only from the top of the backbone plane in the case of D-Glucose and D-galactose and from below for D-Mannose.

In addition, $BF_3 \cdot OEt_2$ drives efficiently the glycosylation reaction between phenols and per-acetyl donors.[14,15] A distinct application of the $BF_3 \cdot OEt_2$ was demonstrated by Kihlberg and coworkers in a convenient method for glycopeptide fragments by glycosylation of an amino

acid alcohol acceptor that incorporates an unprotected C-terminal carboxylate.[16,17] In this reaction, excess $BF_3 \cdot OEt_2$ (3 equiv) was added to a solution of pentaacetyl galactose and N-Fmoc-serine acceptor (1 equiv.) to provide the glycoconjugated product in 53% yield after 1h at room temperature.[18]

To sum up, it is possible to state that $BF_3 \cdot OEt_2$ is an efficient Lewis acid activator, which tolerates a wide spectrum of glycosyl acceptors. Thanks to these considerations, it was used as promoter for all the glycosylation reactions performed in this work.

2.3 The design of the glyconjugated ligands

As reported in the **Introduction** (**Section 9**), the most stable dithiocarbamates are those derived from secondary amines. In this regard, it is essential to design a molecule which conjugates this functional group with the glycoside moiety through a linker of appropriate length. Taking as example the most active Pt(II) complexes synthetized by Gao (see **Introduction**, **Section 7**), we decided to exploit an aliphatic ethyl linker bearing a hydroxyl group, necessary for the glycosylation reaction, and a secondary amine, such as the 2-(N-Methylamino) ethanol, as shown below (**Figure 2.6**).

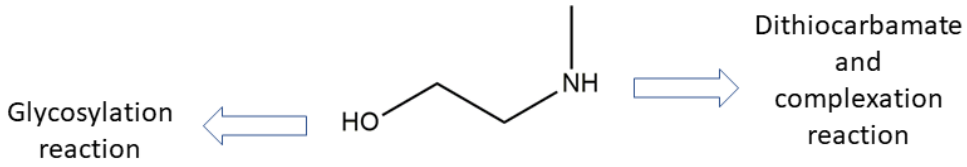

Figure 2.6: Structure of 2-(*N*-Methylamino) ethanol, the double-carbon spacer used in this work. It possesses an alcoholic group that can be conjugated to the monosaccharide by a glycosylation reaction, and a secondary amine useful for the formation of a stable dithiocarbamato and, successively, for the complexation with the metal ions.

It is important to note that, as the presence of the Lewis acid is necessary in this type of glycosylation reactions, a free amine in the reaction medium will disactivate the reactive promoter species forming an acid-base adduct. To avoid this situation, the secondary amine has to be modified with a protecting group before the glycosylation reaction, transforming it into a benzyl carbamate derivative, for example with a benzyloxy-carbonyl (CbZ) group, that is stable both in acidic and basic media.

2.4 Synthesis of the glycoconjugated dithiocarbamato ligands

The first step of the synthesis of dithiocarbamato ligands conjugated with D-glucose, D-galactose and D-mannose consists in the glycosylation reaction between the pentaacetylated glycosyl donor and the Z-protected 2-(*N*-methylamino) ethanol as glycosyl acceptor in dry CH_2Cl_2 or dry acetonitrile (**Figure 2.7**). As described above, this step is accomplished thanks to the activating process promoted by the Lewis acid $BF_3 \cdot Et_2O$ and provides β-anomer in case of D-glucose and D-galactose and α-isomer for D-mannose. Unfortunately, although the reaction is fast and highly stereoselective, a lot of sub-products are formed in solution due to the reactivity of the carbenium ion that can interact with other nucleophiles present in solution (*e.g.,* water and acetate anion). For this reason, a very low yield from 10% to 28% was registered in all cases after the chromatographic purification. Conversely, the deacetylation and the hydrogenation processes, that are the second and the third synthetic steps, respectively, provide the unprotected glycosides almost quantitatively. During the process-optimization studies, we observed that, if dry acetonitrile is replaced by freshly-distilled dichloromethane as reaction solvent, the final yield of the acetylated glycoside increases of 10 percentage points. Moreover, it was also discovered that, if the column purification is performed only after the second step, instead of immediately after the glycosylation reaction, a further increment of 10-15% yield of the deacetylated product can be obtained. In this case, as the deacetylated products (the second step product) holds four hydroxyl groups, a more polar eluent is necessary to elute it through silica column. Concerning the nucleophilic attack of the glycosyl-conjugated secondary amine toward CS_2 during the dithiocarbamate synthesis, we observed that the reaction (in water) is slower (5-6 h) if compared with the same process using less substituted amines (usually 1-2 h), such as piperidine or diethylamine, in the same solvent. The reason can be found by considering the steric hindrance of the amines under investigation, that possess a huge and linear free-to-rotate substituent, thus accounting for a decrement of their nucleophilic power.

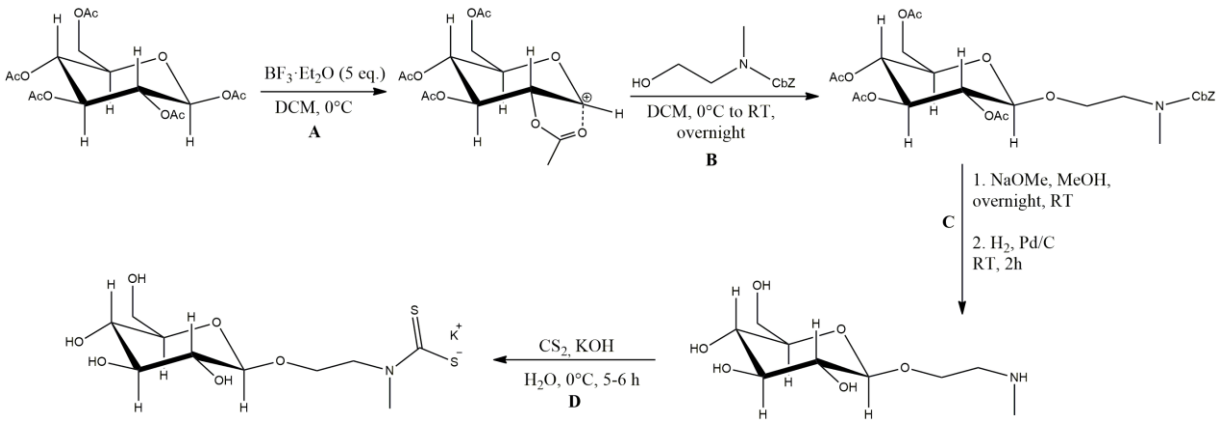

Figure 2.7: Schematic representation of the synthesis of the D-glucoside-conjugated dithiocarbamato ligand as potassium salt. For the D-galactoside and D-mannoside derivatives, the reaction steps are the same as for D-glucoside.

- Synthesis of 2-(N-benzyloxy carbonylamino)ethanol

To an ice-cold freshly distilled dichloromethane solution (100 mL) containing 1 mmol of 2-(*N*-methylamino) ethanol was added, portion-wise and under stirring, 2 eq. of Z-OSu (N-benzyloxy carbonyloxy succinimide) and 2 eq. of triethylamine. Two hours later, the mixture was warmed at room temperature and left under vigorous stirring for 72 h. After the completion of the reaction (monitored with TLC by means of ninhydrin colorimetric detection), the solution was diluted with 50 mL of deionized water and transferred in a separatory funnel. The organic fraction was separated and successively washed with HCl 1N (3 x 25 mL), $NaHCO_{3\,(sat)}$ (3 x 25 mL) and brine (2 x 25 mL). The combined organic fractions were dried with Na_2SO_4, filtered and the solvent evaporated, obtaining a crude mixture in the form of viscous oil. The product was then re-dissolved in EtOAc and purified by means of flash column chromatography on silica gel (eluent EtOAc:ligroin, 7:3 *v/v*). The pure product was isolated as clear oil.

Aspect: clear oil

Yield: 85 %

R.f. (on silica gel): 0.26

^{1}H-NMR ($CDCl_3$, 300 MHz): δ (ppm) = 2.99 (s, 3H, -CH_3); 3.43 (m, 2H, -CH_2OH); 3.54 (br, 1H, -OH); 3.72 (m, 2H, -CH_2N); 5.13 (s, 2H, -CH_2Ph); 7.35 (m, 5H, -Ph).

- Synthesis and characterization of pentaacetyl β-D-glucopyranoside and pentaacetyl β-D-galactopyranoside

For the synthesis of fully protected monosaccharides a procedure similar to that reported by Yamada and co-workers were exploited.[19] Briefly, a 100 mL round bottom flask were filled with 50 mL of acetic anhydride and 0.15 moles of anhydrous NaOAc. The suspension was gently brought to reflux and, when the temperature was reached, 30 mmol of D-glucose or D-galactose were added in one portion. After 3-5 minutes from the addition of the carbohydrate, the solution started to boil vigorously and the suspended solid suddenly went into solution. Then the clear yellow mixture was cooled, poured into 400 mL of ice and left under vigorous stirring overnight in order to neutralize the excess of acetic anhydride. Finally, the obtained white suspension was filtered, the solid was washed with cold water (2 x 50mL) and dried under reduced pressure in presence of P_2O_5. In the case of D-mannose, the solution readily turns dark brown after the addition of the mono-saccharide into boiling acetic anhydride, probably due to the decomposition of the substrate.

Penta-O-acetyl β-D-glucopyranoside
Aspect: white amorphous powder
Yield: 95 %
^{1}H-NMR (400 MHz, $CDCl_3$): 5.71 (d, 1H), 5.24 (dd, 1H), 5.16−5.10 (m, 2H), 4.29 (dd, 1H), 4.11 (dd, 1H), 3.84 (ddd, 1H), 2.11 (s, 3H), 2.09 (s, 3H), 2.03 (s, 6H), 2.01 (s, 3H).

Penta-O-acetyl β-D-galactopyranoside
Aspect: white amorphous powder
Yield: 96 %
^{1}H-NMR (400 MHz, $CDCl_3$): 2.05, 2.07, 2.10, 2.11 (s, 12H), 4.44 (m, 1H), 5.18 (d, 1H), 5.41 (s,1H), 5.43 (s, 1H), 5.44 (s, 1H), 5.47 (s, 1H), 5.80 (s, 1H), 7.32 (m, 1H).

- Synthesis and characterization of pentaacetyl D-mannopyranoside as mixture of anomers

50 mL of dry pyridine and 40 mL of acetic anhydride were added to 30 mmol of D-mannose in a 100 mL round-bottom flask. The mixture was kept at RT for four days. In the meantime, the carbohydrate slowly went into solution. Then, the mixture was diluted with 100 mL of ethyl acetate and transferred into a separatory funnel. The organic fraction was separated and

washed 3 times with deionized water (50 ml), 1M HCl_{aq} (3 x 25 mL), saturated aqueous $NaHCO_3$ (3 x 25 mL) and with an aqueous 5% *w/v* solution of $CuSO_4$ (5 x 25 mL) in order to remove the excess of pyridine from the organic layer. All the obtained organic fractions were combined and dried and the solvent evaporated obtaining a clear viscous oil in good yield. In one circumstance, white crystalline needles of the pure product were obtained by triturating the syrup with diethyl ether and cooling.

Penta-O-acetyl D-mannopyranoside
Aspect: clear oil/white crystals
Yield: 85 %
^{1}H NMR (400 MHz, $CDCl_3$, mixture of anomers): signals of β-anomer δ (ppm) = 1.98 (s, 3H), 2.07 (s, 3H), 2.08 (s, 3H), 2.15 (s, 3H), 2.19 (s, 3H), 3.99–4.05 (m, 1H), 4.07 (dd, 1H), 4.26 (dd, 1H), 5.23 (dd, 1H), 5.31–5.34 (m, 2H), 6.06 (d, 1H); signals of α-anomer δ (ppm) = 1.98 (s, 3H), 2.03 (s, 3H), 2.07 (s, 3H), 2.15 (s, 3H), 2.16 (s, 3H), 3.79 (ddd, 1H), 4.11 (dd, 1H), 4.28 (dd, 1H), 5.11 (dd, 1H), 5.27 (t, 1H), 5.46 (dd, 1H), 5.84 (d, 1H).

- *O*-glycosylation reaction

For all three penta-acetylated sugar derivatives, the same procedure was used.
To a cold, freshly distilled dichloromethane solution (70 mL) containing 1.0 mmol of fully acetylated carbohydrate and 1.2 mmol of 2-(N-benzyloxycarbonyl, methylamino) ethanol, 5.0 mmol of $BF_3 \cdot Et_2O$ were added dropwise under stirring in inert atmosphere. The yellow mixture was maintained at 0 °C for 1h and overnight at RT. Then, the organic solution was firstly neutralized by the dropwise addition of a saturated aqueous $NaHCO_3$ and then washed with $NaHCO_3$ (2 x 30 mL), HCl 1N (3 x 30 mL) and brine (3 x 30 mL). The combined organic fractions were dried with Na_2SO_4, filtered and the solvent removed by rotatory evaporation, obtaining a yellow oil that was used in the next step without further purification.

- De-acetylation reaction

The syrupy residue obtained in the previous step was dissolved in dry MeOH and transferred in a 50 mL round-bottom flask and added at RT of 0.33 equivalents (with respect to a hypothetic 100% yield in the first step) of NaOMe. The solution was then kept in inert atmosphere overnight. After the completion of the reaction monitored by TLC, the mixture

was neutralized with Amberlite IR-120 H^+-resin, filtered and dried in rotatory evaporator obtaining a yellow oil. The crude product was then re-dissolved in EtOAc, the solution was filtered, and the pure glycosylated product was purified by means of flash column-chromatography on silica, obtaining a clear oil (eluent gradient: EtOAc 100%, then EtOAc-MeOH 85:15).

- CbZ-cleavage reaction and characterization of the unprotected glycosylated amines

The deacetylated glycoside was dissolved in EtOAc-MeOH mixture (2:1). Successively, in a 50 mL round-bottom flask equipped with a gas bubbler, H_2 was bubbled in presence of Pd/C (10% *w/w*) for 2h under stirring. After the completion of the reaction, the mixture was filtered over a pad of Celite and the solvent evaporated until dryness, obtaining a clear oil that solidified in a fluffy white solid when dried in vacuum-pump.

O-ethyl,2-(N-methylamino)-β-glucopyranoside

Aspect: white solid

Total final yield: 25 %

^{1}H-NMR (400 MHz, MeOD): δ (ppm) = 2.84–2.86 (m, 2H, CH_2NH), 3.15 (dd, 1H, C2-H), 3.21–3.24 (m, 2H, C4-H, C5-H), 3.31 (dd, 1H, C3-H), 3.58–3.63 (m, 2H, C6-H, CH_2CH_2NH), 3.81 (dd, 1H, C6-H), 3.88 (ddd, 1H, CH_2CH_2NH), 4.22 (d, 1H, C1-H).

O-ethyl,2-(N-methylamino)-β-galactopyranoside

Aspect: white solid

Total final yield: 28 %

^{1}H-NMR (400 MHz, MeOD): δ (ppm) = 2.80 (ddd, 1H, CH_2NH), 2.84 (ddd, 1H, CH_2NH), 3.45 (dd, 1H, C3-H), 3.49 (ddd, 1H, C5-H), 3.52 (dd, 1H, C2-H), 3.61 (ddd, 1H, CH_2CH_2NH), 3.69 (dd, 1H, C6-H), 3.73 (dd, 1H, C6-H), 3.80 (dd, 1H, C4-H), 3.91 (ddd, 1H, CH_2CH_2NH), 4.21 (d, 1H, C1-H).

O-ethyl,2-(N-methylamino)-α-mannopyranoside

Aspect: white solid

Total final yield: 30 %

^{1}H NMR (400 MHz, MeOD): δ (ppm) = 2.82–2.86 (m, 2H, C*H*$_2$NH), 3.48 (ddd, 1H, C*H*$_2$CH$_2$NH), 3.56 (ddd, 1H, C5-*H*), 3.63 (t, 1H, C4-*H*), 3.73 (dd, 1H, C6-*H*), 3.74 (dd, 1H,

C3-*H*), 3.79 (ddd, 1H, C*H*$_2$CH$_2$NH), 3.86 (dd, 1H, C2-*H*), 3.86 (dd, 1H, C6-*H*), 4.80 (d, 1H, C1-*H*).

- Synthesis and characterization of the glycosylated-dithiocarbamato salts

To a cold aqueous solution (10 mL) containing the free amine (0.5 mmol), was added KOH (1 eq.), followed by an excess of CS_2. After 5-6 h of stirring, Ar was bubbled for few minutes to eliminate the excess of carbon disulfide still present. Then, the solution was freezed in an $CO_{2(s)}$/acetone bath and lyophilized under reduced pressure, leading to the formation of a yellow viscous oil. The oil was re-dissolved in anhydrous methanol and precipitated with diethyl ether obtaining a white flocculent solid.

O-ethyl,2-(N-methylamino)-β-D-glucopyranosyl dithiocarbamato potassium salt

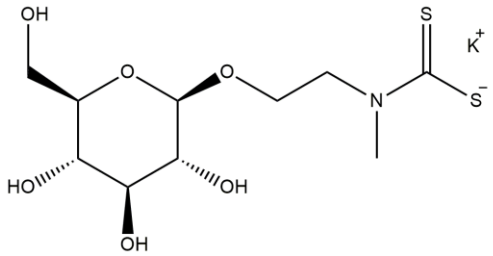

Chemical Formula: $C_{10}H_{18}KNO_6S_2$
Exact Mass: 351,02
Molecular Weight: 351,48

Aspect: white solid

Yield: 65 %

Anal. Calc. for $C_{10}H_{18}KNO_6S_2$ (MW = 351.48 g·mol^{-1}): C 34.17; H 5.16; N 3.99; S 18.25. Found: C 33.83; H 5.57; N 3.90; S 17.94.

^{1}H-NMR (DMSO-d6, 600 MHz): δ (ppm) = 2.93 (m, 1H, C2-H); 3.05 (m, 2H, C4-H, C5-H); 3.11 (m, 1H, C3-H); 3.40 (s, 3H, N-CH$_3$); 3.44, 3.65 (m, 2H, C6-H, C7-H); 3.67, 3.93 (m, 2H, O-CH$_2$); 4.14 (d, 1H, C1-H); 4.20-4.26 (m, 2H, N-CH$_2$); 4.50 (t, 1H, C6-OH); 4.87 (d, 1H, C4-OH); 4.83 (d, 1H, C2-OH); 4.95 (d, 1H, C3-OH).

Medium FT-IR (KBr): $\tilde{\nu}$ (cm^{-1}) = 2926 (ν_a, C-H); 1481 (ν_a, N-CSS); 953 (ν_a, CSS); 898 (ν, OCO).

ESI-MS m/z, [DTC-CS$_2$]$^-$ found (calc.): 236.11 (236.11).

O-ethyl,2-(N-methylamino)-β-D-galactopyranosyl dithiocarbamato potassium salt

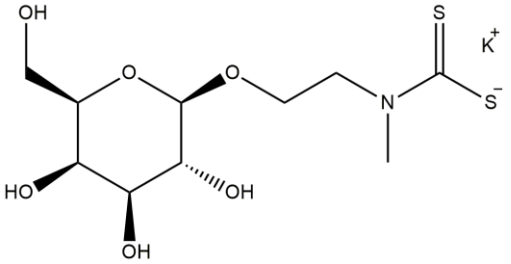

Chemical Formula: $C_{10}H_{18}KNO_6S_2$
Exact Mass: 351,02
Molecular Weight: 351,48

Aspect: white solid

Yield: 61 %

^{1}H-NMR (DMSO-d6, 600 MHz): δ (ppm) = 3.25 (m, 2H, C2-H, C3-H); 3.31 (m, 1H, C5-H); 3.40 (s, 3H, N-CH_3); 3.49 (m, 2H, C6-H, C7-H); 3.62 (m, 1H, C4-H); 3.67, 3.90 (m, 2H, O-CH_2); 4.10 (d, 1H, C1-H); 4.21-4.24 (m, 2H, N-CH_2); 4.31 (d, 1H, C4-OH); 4.56 (t, 1H, C6-OH); 4.64 (d, 1H, C3-OH); 4.80 (d, 1H, C2-OH).

Medium FT-IR (KBr): $\tilde{\nu}$ (cm^{-1}) = 2931-2890 (ν_a, C-H); 1481 (ν_a, N-CSS); 952 (ν_a, CSS); 892 (ν, OCO).

ESI-MS m/z, $[DTC\text{-}CS_2]^-$ found (calc.): 236.11 (236.11).

O-ethyl,2-(N-methylamino)-α-D-mannopyranosyl dithiocarbamato potassium salt

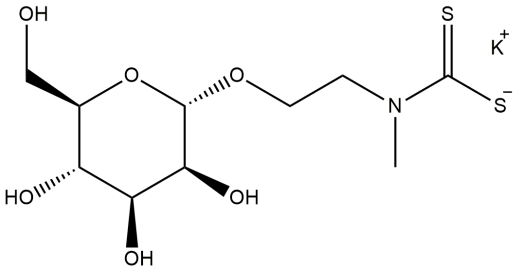

Chemical Formula: $C_{10}H_{18}KNO_6S_2$
Exact Mass: 351,02
Molecular Weight: 351,48

Aspect: white solid

Yield: 74 %

^{1}H-NMR (DMSO-d6, 600 MHz): δ (ppm) = 3.30 (m, 1H, C3-H); 3.38 (m, 2H, C4-H); 3.40 (s, 3H, N-CH_3); 3.45 (m, 1H, C5-H); 3.45, 3.63 (m, 2H, C6-H, C7-H); 3.63, 3.75 (m, 2H, O-CH_2); 4.16-4.26 (m, 2H, N-CH_2); 4.38 (t, 1H, C6-OH); 4.52 (d, 1H, C4-OH); 4.61 (d, 1H, C1-H); 4.65 (d, 1H, C3-OH); 4.67 (d, 1H, C2-OH).

Medium FT-IR (KBr): $\tilde{\nu}$ (cm^{-1}) = 2929 (ν_a, C-H); 1480 (ν_a, N-CSS); 955 (ν_a, CSS); 882 (ν, OCO).

ESI-MS m/z, $[DTC\text{-}CS_2]^-$ found (calc.): 236.11 (236.11).

2.5 Characterization of the glycoconjugated dithiocarbamato ligands

2.5.1 ^{1}H-NMR characterization

The ^{1}H-NMR spectra of the glycosyl-functionalized ligands are characterized by the presence of several multiplets, due to the high number protons in the pyranose ring and in the spacer. In fact, each glycosylic substrate holds 11 protons of the carbohydrate backbone (7 aliphatic and 4 hydroxylic protons) and 7 related to the amino-alcohol, numbered as shown in **Figure 2.8**.

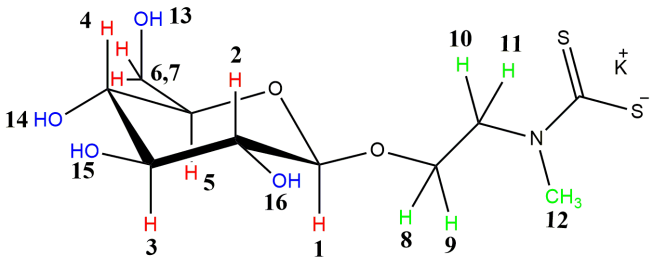

Figure 2.8: schematic representation of the β-D-Glucosyl, O-Ethyl dithiocarbamato ligand with numbered protons. The 7 protons of the pyranose ring are highlighted in red, while the alcoholic ones (4) and those related to the spacer (7) are written in blue and green, respectively. The same progressive numeration is used for the β-D-galactoside and α-D-mannoside ligands.

It is worth noting that 11 of the 18 total protons, such as the methynic ones of the pyranose ring and those of the ethylic spacer (excluding the methyl protons), are diastereotopic and each of them give rise to a multiplet in different fields of the spectrum. For these reasons, a monodimensional ^{1}H-NMR investigation does not always provide sufficient information to assign undoubtedly every resonance to its corresponding proton. Bidimensional ^{1}H^{1}H-COSY 2D spectra were required to better elucidate the exact position of each protons in the structure. In this paragraph, only the 1D and 2D spectra of the glucoside ligand will be presented (**Figure 2.9** and **Figure 2.10)**, whereas those related to the D-galactoside and D-mannoside derivatives are reported in the **Supporting Information C**. All the spectra were acquired in DMSO-*d6*. This is a very good aprotic solvent that permits the revelation of the resonances related to the alcoholic functions of the monosaccharides. Moreover, spectra recorded in DMSO-d6 show better resolved peaks that resonate in a range spanning from 2.9 ppm to 4.9

ppm. On the contrary, acquisitions in D_2O or MeOD are characterized by closer peaks, thus affecting an appropriate integration process.

As shown in the 1D ^{1}H-NMR spectrum in **Figure 2.9**, the groups of protons in α position with respect to the dithiocarbamato moiety resonate at 3.40 and 4.23 ppm for the *N*-methyl and the *N*-methylene protons, respectively. These values are in agreement with data reported for other dithiocarbamates bearing similar substituents surrounding the dithiocarbamic nitrogen (for example, the sarcosine-DTC ligand). The protons of the hydroxyl groups of the pyranose ring are at 4.59-4.95 ppm and are coupled with the adjacent methynic protons, giving rise to three doublets and a triplet, assigned to the alcoholic protons in position 3, 4, 2 (doublets) and 6 (triplet).

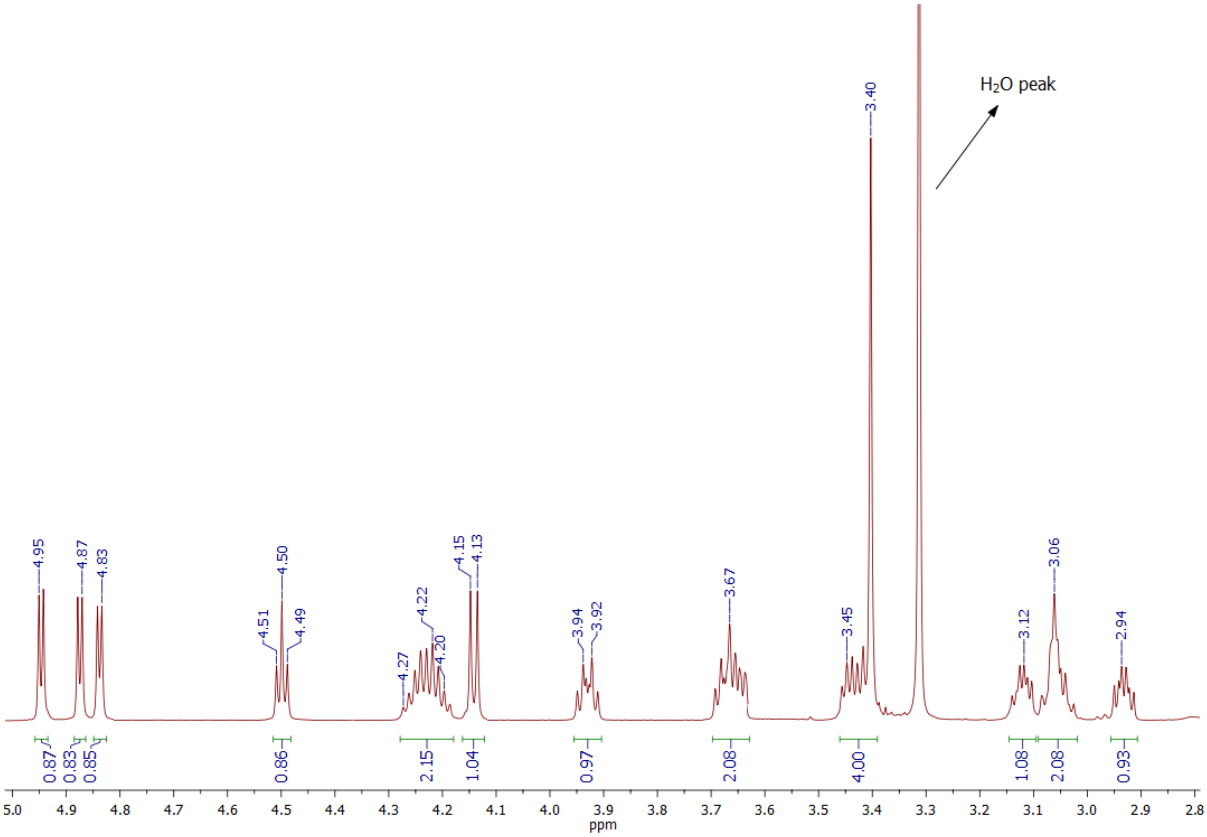

Figure 2.9: 1D ^{1}H-NMR spectrum of the glucoside-DTC ligand recorded in DMSO-*d6* at 25°C, with a 600 MHz instrument.

The resonances (ppm) and the assignments of all the protons of the glycosylated ligands are summarized **Table 2.1**. It is very interesting to note that, generally, the resonances of the equatorial protons in pyranose ring are shifted to lower fields compared to the axial ones.[20,21]

In particular, all axial methynic protons in the β-D-glucoside ligand experience the most shielded effect if compared to the β-D-galactoside and α-D-mannoside derivatives. As an example, the proton at the position 2 of the former are affected by the strongest shielding effect (2.93 ppm) with a difference of 0.66 ppm with respect to the equatorial proton in the same position of the mannoside ligand. An identical consideration can be done for the equatorial proton in C-2 of the mannoside, that is more de-shielded, and for the equatorial C-4 proton in the galactoside that resonates at lower fields with respect to the corresponding ones of the other derivatives. The shielding effect occurring for the methynic protons, is accompanied by the deshielding observed for the alcoholic ones. In fact, the hydroxylic protons resonate at higher ppm in the case of β-D-glucoside in which all the hydroxyl functions possess an equatorial configuration.

Table 2.1: δ (ppm) in DMSO-*d6* at 25°C

PROTONS (numbered as in **Figure 2.8**)	**β-D-glucoside DTC – K^+**	**β-D-galactoside DTC – K^+**	**α-D-mannoside DTC – K^+**
1 (C-*H* backbone)	4.14 (d)	4.10 (d)	4.61 (s)
2 (C-*H* backbone)	2.93 (m)	3.25 (m)	3.59 (m)
3 (C-*H* backbone)	3.11 (m)	3.25 (m)	3.30 (m)
4 (C-*H* backbone)	3.06 (m)	3.62 (m)	3.38 (m)
5 (C-*H* backbone)	3.05 (m)	3.31 (m)	3.45 (m)
6-7 (C-*H* backbone)	3.65 ; 3.44 (m)	3.46-3.52 (m)	3.63 ; 3.45 (m)
8-9 (*O*-C*H*$_2$ spacer)	3.93 ; 3.67 (m)	3.90 ; 3.67 (m)	3.75 ; 3.63 (m)
10-11(*N*-C*H*$_2$ spacer)	4.23 (m)	4.22 (t)	4.21 (m)
12 (*N*-C*H*$_3$ spacer)	3.40 (s)	3.40 (s)	3.40 (s)
13 (C$_6$-O*H*)	4.50 (t)	4.56 (t)	4.38 (t)
14 (C$_4$-O*H*)	4.87 (d)	4.31 (d)	4.52 (d)
15 (C$_3$-O*H*)	4.95 (d)	4.80 (m)	4.65 (d)
16 (C$_2$-O*H*)	4.83 (d)	4.64 (m)	4.67 (d)

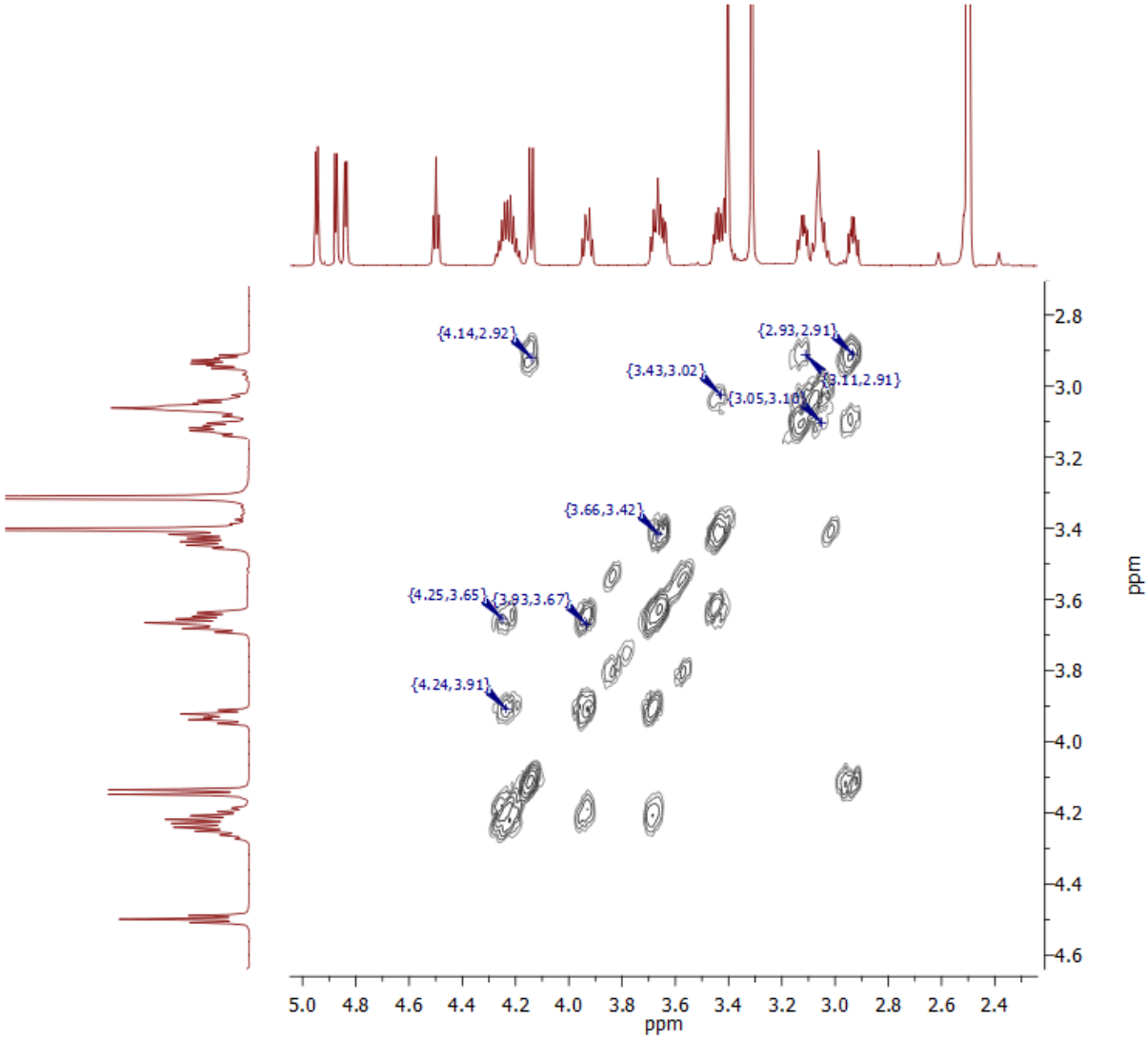

Figure 2.10: 2D $^{1}H\,^{1}H$-COSY NMR spectrum of the β-D-glucoside-DTC ligand recorded in DMSO-*d6* at 25°C, with a 600 MHz instrument.

In the $^{1}H^{1}H$-COSY NMR spectrum reported in **Figure 2.10** the correlation between the protons of the carbohydrate backbone and the ethylic spacer are shown.

2.5.2 FT-IR characterization

The FT-IR spectra of all dithiocarbamato ligands have been collected (**Supporting Information D**) in the medium (4000-600 cm^{-1}) wavenumbers domain. The diagnostic absorptions are reported in **Table 2.2** and are compared to those of the dimethyl dithiocarbamato molecule which, similarly to glycoside analogs, bears two alkyl linear substituents in α position with respect to the N-CSS moiety.

Table 2.2: main IR absorbption bands (cm^{-1}) of the dimethyl dithiocarbamate and the three glycosylic ligands (*s*: strong, *m*: medium, *w*: weak and *br*: broad).

Compound	ν(N-CSS) (m)	ν_{as}(S-C-S) (m)	ν_{as}(C-O) (s)	ν(O-C-O) (w)	ν(C-H sp^3) (m)	δ(C-H sp^3) (m)	ν(C-C) (m)	ν(OH) (br)
Dimethyl DTC	1486	962	-	-	-	-	-	-
β-D-Glucoside DTC	1481	953	1077-1033	898	2926	1424 1377	1286 1259 1210	3392
β-D-Galactoside DTC	1481	952	1077-1143	892	2931 2890	1422 1377	1287 1258 1210	3365
α-D-Mannoside DTC	1480	955	1083-1055	882	2929	1413 1377 1353	1280 1258 1210	3393

Two main IR-regions must be taken into account when characterizing dithiocarbamato derivatives, both ligand salts and metal-DTC complexes. First, the spectral region 1100-1550 cm^{-1} wherein the ν(N-CSS) band can be found and its position depends strongly on the extent of the double character of the N-C bound. In the case of a more pronounced single-bond-form (dithiocarbamic resonance structure – **Figure 1.13**), the band is located at 1250÷1350 cm^{-1}, whereas it is found at higher wavenumbers (1640-1690 cm^{-1}) if the DTC ligand contains a basically double C=N bond (thioureidic form).

In the case of the glycosylated dithiocarbamates, the N-CSS band can be recognized at about 1480 cm^{-1} for all the three synthetized ligands, denoting a prononced double bond character. As a comparison, the same vibrational frequency for the dimethyl dithiocarbamate falls at 1486 cm^{-1}, demonstrating an excellent correlation between the simplest aliphatic ligand and the functionalized ones.

The second diagnostic region spans from 800 to 1100 cm^{-1}, and it is ascribable to the asymmetric stretching $\nu_a(CSS)$[22,23], that can be recognized at about 953-955 cm^{-1} for the ligands under investigation. Once again, an optimum correlation with the same absorption for the dimethyl dithiocarbamate at 962 cm^{-1} is visible.

Afterwards, other areas of the spectrum can provide precious information about the carbohydrate moiety. Also in this case, the spectral regions that are important for the structural characterization of polysaccharides are two and are called "sugar region" (1200-950 cm^{-1}) and "anomeric region" (950-750 cm^{-1}).[24,25] The highly overlapping intense bands of C-O and C-C stretching vibrations in glycosidic bonds and pyranosic ring predominate in the former region as shown in **Table 2.2**. On the contrary, the "anomeric region" contains weaker bands of more diagnostic skeletal vibrations sensitive to the nature of the substituent in the acetal group and the anomeric structure. In particular, it is well known that O-glycosides in β- anomeric form give rise to a weak band related to the O-C-O stretching between 950 and 890 cm^{-1}, whereas α-anomers present a similar absorption at lower wavenumbers (from 890 to 750 cm^{-1}).[26] As a matter of fact, these bands are clearly visible in the FT-IR spectra of the synthetized ligands, demonstrating the stereoselectivity of the glycosylation reaction that lead to the formation of β-anomers for glucoside and galactoside derivatives (ν(OCO)= 898 and 892 cm^{-1}), and α-stereoisomers in the case of mannosides (ν(OCO)= 882 cm^{-1}).

2.5.3 UV-Vis characterization

Electronic absorption studies were carried out for the synthetized dithiocarbamato ligands by means of UV-Vis spectrophotometry in deionized water (500-190 nm) at 25 °C. The three spectra are very similar, as expected, and show intense bands at 283, 254 and 206 nm (**Figure 2.11**).

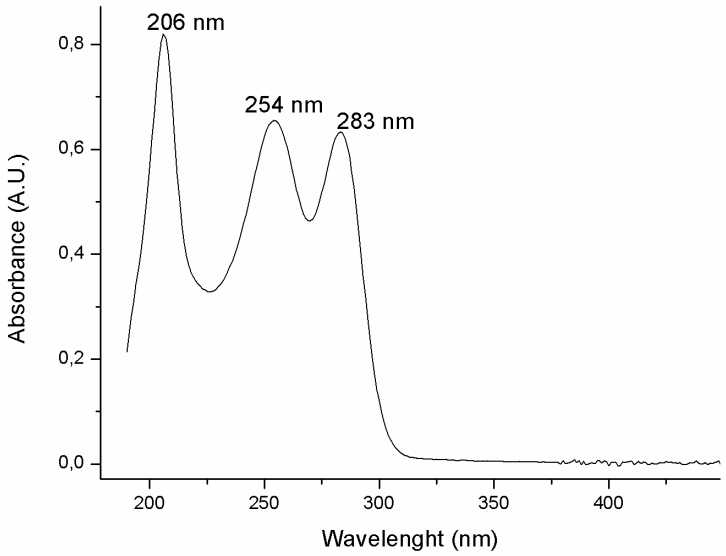

Figure 2.11: UV-Vis absorption spectra (500-190 nm) of a H_2O solution containing O-ethyl,2-(N-methylamino)-β-glucopyranosyl dithiocarbamato potassium salt (K^+-glucosideDTC) at a concentration of 7.5 μM.

As well as Band I in **Table 1.4** (regarding the absorption of Au-DTC complexes in **Chapter 1**), the most energetic band, that is observable at 206 nm, is not undoubtedly ascribed in the literature to a particular electronic transition and it is still the subject of debate: sometimes, it has been assigned either to an intra-ligand $\pi^* \leftarrow \pi$ transition located in the -NCSS moiety[27] or to intra-ligand p ← d transitions between levels originated by sulfur atoms, and it has even been not ascribed in most cases.[28] On the contrary, bands at 254 nm and 283 nm correspond to the intra-ligand $\pi^* \leftarrow \pi$ transition mainly located in the -NCS and -SCS moieties, respectively. These bands are clearly observable also in the UV spectra of Au(III) dithiocarbamato complexes. The absorptions associated to the glycosylic moiety, in particular to the acetal function, usually fall in the range 400-200 nm but unfortunately, as characterized by a small molar extinction coefficient, are fully covered by the DTC-related bands.

2.6 Au(III) complexes with glycosylated dithiocarbamates

After the synthesis and characterization of the three DTC ligands, the subsequent step was the complexation reaction with Au(III) ions. It is worth highlighting that, contrary to the PipeDTC, glycosyl conjugated dithiocarbamates lead to the formation of more hydrophilic compounds, thus making necessary some modifications in the synthetic pathways described

in **Chapter 1**. In detail, a total of six Au(III) complexes have been synthetized both with stoichiometric metal to ligand ratio [1:1] and [1:2] (**Figure 2.12**). In particular, regarding the di-halo neutral complexes, only the di-bromo derivatives were obtained from the corresponding Au(I) di-nuclear compounds via oxidative addition of Br_2. Subsequently, adding one equivalent of DTC ligand to a solution containing the 1:1 glycosyl-conjugated complex did not lead to the selective formation of ionic [1:2] compound (as for the Pipe-DTC complexes), but a mixture of different species was detected by TLC. As a matter of facts, this novel class of dithiocarbamato ligands possess four hydroxyl groups that can interact with the Au(III) ion (that is a quite hard metal centere for the Pearson's Hard-Soft theory) obtaining several byproducts. Moreover, the insolubility of this class of neutral 1:1 compounds in dichloromethane forces the use of methanol as solvent in which the reagent (1:1 complex) is not stable (after light irradiation) due to the rearrangement equilibrium. The only synthetic pathway, among those presented in **Chapter 1**, which permits to synthetize the [1:2]Cl compounds in good purity, is starting from $[Au^{III}PPh_3Cl_3]$ as reagent (see **Figure 1.10**, **Chapter 1**) which was optimized successfully for all the three glycoconjugated ligands.

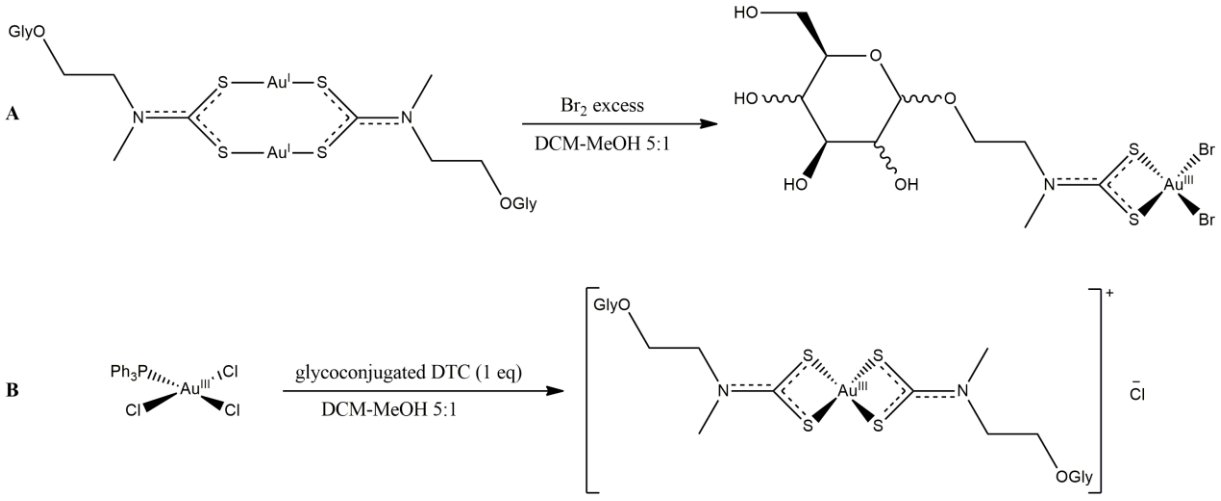

Figure 2.12: Schematic representation of the synthetic pathways exploited for the synthesis of Au(III) complexes. In particular, the route A is related to the synthesis of 1:1 di-bromo compounds *via* oxidative addition from the Au(I) complex, whereas the route B represents the selective production of the [1:2]Cl derivatives. The glycosydic structure is sometimes abbreviated as -OGly.

- Synthesis of di-nuclear glycosyl dithiocarbamato gold(I) complex, [2:2] stoichiometric ratio

0.3 mmol of [Au^{I}(THT)Cl], prepared as described elsewhere[29] were dissolved under magnetic stirring in 30 mL of acetone in a 100 mL round-bottom flask. 1 eq. of glycosylated dithiocarbamato ligand, previously dissolved in 10 mL of MeOH, was added dropwise to this clear solution. A flocculent dark yellow precipitate formed readily. The stirring was continued for 10 minutes, then the solid was filtered, washed with acetone (2 x 10 mL) and dried under vacuum. The product, obtained with high yield, was soluble in DMSO and slightly soluble in MeOH.

- Synthesis of di-bromo glycosyl dithiocarbamato gold(III) complexes

In a 50 mL double-necked round-bottom flask filled with 24 mL of a CH_2Cl_2-MeOH 5:1 solution, 0.1 mmol of [Au^{I}DTC]$_2$ complexes were suspended and the mixture was refluxed under vigorous stirring. After 20 minutes, the suspension became homogeneous and an excess of Br_2 (previously diluted in 5 mL of CH_2Cl_2) was added in one portion. The color of the yellow mixture converted prior to green, then red and the yellow suspended solid readily went into solution. In the case of glucosyl dithiocarbamato complex, a flocculent orange solid formed few minutes after the addition of the halogen. The solid was then filtered, washed with dichloromethane (3 x 10 mL), diethyl ether (2 x 10 mL) and dried under vacuum. In the other two cases, the products remained in solution. Then, the solution was cooled, the solvent half-reduced by rotatory evaporator and an orange solid was collected by precipitation with diethyl ether, both for D-galactoside and D-mannoside derivatives. All 1:1 glycosylated complexes were soluble in DMSO and MeOH.

Di-bromo, O-ethyl,2-(N-methylamino)-β-glucopyranosyl gold(III) dithiocarbamate

Aspect: orange fluffy solid

Yield: 81 %

^{1}H-NMR (DMSO-d6, 600 MHz): δ (ppm) = 4.20 (d, 1H), 2.92-2.96 (m, 1H), 3.12-3.14 (m, 1H), 2.98-3.02 (m, 1H), 3.12-3.14 (m, 1H), 3.69 (m, 1H), 3.43 (m, 1H), 3.88-4.04 (m, 2H), 3.88-4.04 (m, 2H), 3.41 (s, 3H), 4.50 (t, 1H), 4.96 (d, 1H), 5.08 (d, 1H), 5.93 (d, 1H).

Medium FT-IR (KBr): $\tilde{\nu}$ (cm^{-1}) = 1576 (ν_a, N-CSS); 1075 (ν_a, CO); 991 (ν_a, CSS); 901 (ν, OCO).

Far FT-IR (nujol): $\tilde{\nu}$ (cm^{-1}) = 568 (ν_s, CSS); 484 (ν_a, Au-C); 418 (ν_a, Au-S); 271 (ν_a, Au-Br); 218 (ν_s, Au-Br).

Di-bromo, O-ethyl,2-(N-methylamino)-β-galactopyranosyl gold(III) dithiocarbamate

Aspect: orange fluffy solid

Yield: 87 %

^{1}H-NMR (DMSO-d6, 600 MHz): δ (ppm) = 4.14 (d, 1H), 3.20-3.27 (m, 1H), 3.20-3.27 (m, 1H), 3.63 (m, 1H), 3.33-3.35 (m, 1H), 3.38-3.57 (m, 2H), 3.86-4.06 (m, 2H), 3.86-4.06 (m, 2H), 3.39 (s, 3H), 4.58 (t, 1H), 4.92 (d, 1H), 4.98 (d, 1H), 5.90 (d, 1H).

Medium FT-IR (KBr): $\tilde{\nu}$ (cm^{-1}) = 1575 (ν_a, N-CSS); 1067 (ν_a, CO); 989 (ν_a, CSS); 889 (ν, OCO).

Far FT-IR (nujol): $\tilde{\nu}$ (cm^{-1}) = 595 (ν_s, CSS); 481 (ν_a, Au-C); 414 (ν_a, Au-S); 296 (ν_a, Au-Br); 218 (ν_s, Au-Br).

Di-bromo, O-ethyl,2-(N-methylamino)-α-mannopyranosyl gold(III) dithiocarbamate

Aspect: orange fluffy solid

Yield: 72 %

^{1}H-NMR (DMSO-d6, 600 MHz): δ (ppm) = 4.65 (d, 1H), 3.58 (m, 1H), 3.19-3.22 (m, 1H), 3.34-3.37 (m, 1H), 3.43-3.47 (m, 1H), 3.66 (m, 1H), 3.43 (m, 1H), 3.37-3.98 (m, 2H), 3.74 (m, 1H), 4.04 (m, 1H), 3.40 (s, 3H), 4.52 (t, 1H), 4.89 (d, 1H), 4.91 (d, 1H), 4.87 (d, 1H).

Medium FT-IR (KBr): $\tilde{\nu}$ (cm^{-1}) = 1580 (ν_a, N-CSS); 1056 (ν_a, CO); 992 (ν_a, CSS); 882 (ν, OCO).

Far FT-IR (nujol): $\tilde{\nu}$ (cm^{-1}) = 573 (ν_s, CSS); 482 (ν_a, Au-C); 415 (ν_a, Au-S); 284 (ν_a, Au-Br); 216 (ν_s, Au-Br).

- Synthesis of bis glycosyl-dithiocarbamato gold(III) chloride complexes

The [$Au^{III}PPh_3Cl_3$] precursor was prepared and not isolated by bubbling Cl_2 into a solution containing the[$Au^{I}PPh_3Cl$] complex, as described in the **Chapter 1**.

1 eq. of the glycoconjugated DTC ligand, previously dissolved in 4 mL of dry MeOH, was added to a 4.5 mM dichloromethane solution (20 mL) of [$Au^{III}PPh_3Cl_3$] in a 50 mL round-bottom flask. The immeditely formed yellow solid was filtered, washed with dichloromethane (5 x 10 mL) and dried. Then the product was transferred in 25 mL round-bottom flask, re-dissolved in cold dry MeOH, to separate the residual KCl by filtration, and

precipitated with diethyl ether, obtaining a yellow flocculent solid. This last step was repeated several times until no more KCl was seen at the bottom of the flask after the re-dissolution of the complex in dry methanol. All the three products were soluble in H_2O, MeOH and DMSO.

Bis-[O-ethyl,2-(N-methylamino)-β-glucopyranosyl dithiocarbamato] gold(III) chloride
Aspect: yellow amorphous powder
Yield: 76 %
Anal. Calc. for $C_{20}H_{36}AuClN_2O_{12}S_4$ (MW = 857.19 g·mol^{-1}): C 28.02; H 4.23; N 3.37; S 14.96. Found: C 28.16; H 4.31; N 3.00; S 14.28.
^{1}H-NMR (DMSO-d6, 600 MHz): δ (ppm) = 4.20 (d, 1H), 2.94-2.98 (m, 1H), 3.09-3.17 (m, 1H), 3.00-3.06 (m, 1H), 3.09-3.17 (m, 1H), 3.68 (m, 1H), 3.43 (m, 1H), 3.88-4.06 (m, 2H), 3.88-4.06 (m, 2H), 3.43 (s, 3H), 4.54 (t, 1H), 5.06 (d, 1H), 5.09 (d, 1H), 5.01 (d, 1H).
Medium FT-IR (KBr): $\tilde{\nu}$ (cm^{-1}) = 1565 (ν_a, N-CSS); 1076 (ν_a, CO); 987 (ν_a, CSS); 897 (ν, OCO).
Far FT-IR (nujol): $\tilde{\nu}$ (cm^{-1}) = 554 (ν_s, CSS); 486 (ν_a, Au-S); 386 (ν_s, Au-S).
ESI-MS m/z, $[M\text{-}Cl]^+$ found (calc.): 821.09 (821.08).

Bis-[O-ethyl,2-(N-methylamino)-β-galactopyranosyl dithiocarbamato] gold(III) chloride
Aspect: yellow amorphous powder
Yield: 71 %
Anal. Calc. for $C_{20}H_{36}AuClN_2O_{12}S_4$ (MW = 857.19 g·mol^{-1}): C 28.02; H 4.23; N 3.37; S 14.96. Found: C 27.94; H 4.10; N 3.12; S 14.51.
^{1}H-NMR (DMSO-d6, 600 MHz): δ (ppm) = 4.15 (d, 1H), 3.20-3.27 (m, 1H), 3.20-3.27 (m, 1H), 3.63 (m, 1H), 3.33-3.37 (m, 1H), 3.48-3.55 (m, 2H), 3.86-4.05 (m, 2H), 3.86-4.05 (m, 2H), 3.43 (s, 3H), 4.58 (t, 1H), 4.40 (d, 1H), 4.90 (d, 1H), 4.76 (d, 1H).
Medium FT-IR (KBr): $\tilde{\nu}$ (cm^{-1}) = 1564 (ν_a, N-CSS); 1072 (ν_a, CO); 954 (ν_a, CSS); 891 (ν, OCO).
Far FT-IR (nujol): $\tilde{\nu}$ (cm^{-1}) = 528 (ν_s, CSS); 480 (ν_a, Au-S); 386 (ν_s, Au-S).
ESI-MS m/z, $[M\text{-}Cl]^+$ found (calc.): 821.09 (821.08).

Bis-[O-ethyl,2-(N-methylamino)-α-mannopyranosyl dithiocarbamato] gold(III) chloride
Aspect: yellow amorphous powder

Yield: 70 %

Anal. Calc. for $C_{20}H_{36}AuClN_2O_{12}S_4$ (MW = 857.19 g·mol^{-1}): C 28.02; H 4.23; N 3.37; S 14.96. Found: C 28.21; H 3.98; N 3.15; S 14.36.

^{1}H-NMR (DMSO-d6, 600 MHz): δ (ppm) = 4.66 (d, 1H), 3.59 (m, 1H), 3.19-3.22 (m, 1H), 3.34-3.38 (m, 1H), 3.43-3.46 (m, 1H), 3.66 (m, 1H), 3.43 (m, 1H), 3.37-3.97 (m, 2H), 3.75 (m, 1H), 4.04 (m, 1H), 3.43 (s, 3H), 4.52 (t, 1H), 4.80-4.82 (d, 1H), 4.65 (d, 1H), 4.80-4.82 (d, 1H).

Medium FT-IR (KBr): $\tilde{\nu}$ (cm^{-1}) = 1564 (ν_a, N-CSS); 1054 (ν_a, CO); 973 (ν_a, CSS); 880 (ν, OCO).

Far FT-IR (nujol): $\tilde{\nu}$ (cm^{-1}) = 528 (ν_s, CSS); 481 (ν_a, Au-S); 384 (ν_s, Au-S).

ESI-MS m/z, $[M-Cl]^+$ found (calc.): 821.09 (821.08).

2.7 Introduction to Cu(II) dithiocarbamato complexes

A further aim of this Ph.D. work is focused on the synthesis and the in vitro evaluation of novel copper(II) complexes with glycoconjugated dithiocarbamato ligands. In particular, molecules of the type $[Cu^{II}(DTC)_2]$ with cyclic alkyl dithiocarbamates already synthetized in our group, showed a very promising antineoplastic activity toward several human tumor cell lines, with IC_{50} values in the nM range.[30] Unfortunately, these coordination compounds are not soluble in water and, some of them experience a slight solubility even in DMSO.

With these preliminary information, it seems clear that a step forward in this research area is now required, with the primary attention in increasing the solubility of such complexes and targeting them selectively into the cancer site, in order to reduce toxicity and exploit their great potential only toward the malignant tissues. Before starting to describe the syntheses and the *in vitro* results regarding the Cu(II) glycosylated complexes, a description of the chemistry of this interesting metal and its biological properties is necessary.

2.7.1 Copper: an essential element for live beings

Copper is the 29th element of the periodic table with a [Ar]3d^{10}4s^1 configuration and belongs to the 11th group and the 1st row of transition metals. Copper presents four oxidation states: Cu(I), Cu(II), Cu(III) and rarely Cu(IV). Although Cu(II) is the most stable oxidation state, copper is the only metal of the first row to show also a quite satisfying stability in the +1 oxidation state.[31]

The metal has a wide range of available redox potentials, thus can form adducts with many classes of ligands bearing different donor atom sets and endowed with distinct properties in terms of electronic, steric and chelation effects. At the same time, both the nature of the ligands and the easy switch between the two main oxidation states +1 and +2 allow remarkable modifications in the geometry of the related complex, with no high energy requirements.[32] For example, a distorted octahedral Cu(II) complex can smoothly turn into a tetrahedral Cu(I) species. It is worth noting that all these features make the Cu(I)/Cu(II) complexes much less predictable from the structural point of view than other first-row transition metal counterparts.[33] The chemistry of copper is mainly represented by the +2 oxidation state especially in solution. With a $3d^9$ electronic configuration cupric compounds are paramagnetic and susceptible to Jahn-Teller distortion in an octahedral coordination.[34] Thereby, all Cu(II) compounds should virtually be blue or green despite there are some exceptions generally represented by strong ultraviolet bands (charge-transfer bands) tailing off into the blue-end of the visible spectrum and, hence, they appear red or brown.[35] According to the "hard and soft acids and bases" (HSAB) theory of Pearson, the cupric ion is regarded as a borderline metal, therefore capable of being tightly coordinated by both soft and hard ligands, even if it prefers nitrogen donor atoms.[36] Furthermore, Cu(II) can adopt different coordination numbers, most commonly 4, 5 and 6 and associated with distinct coordination geometries, respectively i) tetrahedral/ square planar, ii) trigonal bipyramidal/ square-based pyramidal and iii) octahedral.[37]

One of the most important difference between copper and gold ions, is that the former plays an important role in the homeostasis of living beings as endogenous metal. In this regard, its involvement in biological pathways started about 1.7 billion years ago with the increase of atmosphere O_2 concentration to a significant value.[38] In fact, the biologically-essential iron was oxidized to Fe(III), thus leading to the precipitation of hydroxides and making its use more energy-demanding. On the other hand, the insoluble Cu(I) turned into the more soluble and bioavailable Cu(II) ion.[39] In other words, the larger and larger amount of O_2 produced by cyanobacteria and other prokaryotic organisms favoured the onset of the Cu(II)/Cu(I) catalytical pair in biological systems. Therefore, it is not surprising that copper plays a key role in many enzymes and proteins involved in reactions with oxygen as a substrate, as well as in the degradation or transformation of its side products (*i.e.*, O_2^-, NO_2^-, NO·or N_2O).[41] For

instance, the Cu(II)/Cu(I) couple can be found in the hemocyanin (oxygen carrier found in the hemolymph of most mollusks and some arthropods, **Figure 2.13**), in the superoxide dismutase (catalyst of the dismutation of reactive O_2^- radical into both O_2 and H_2O_2) and in many other oxidoreductase and hydroxylase enzymes (i.e., tyrosinase, ascorbate oxidase, dopamine-β-hydroxylase).[42]

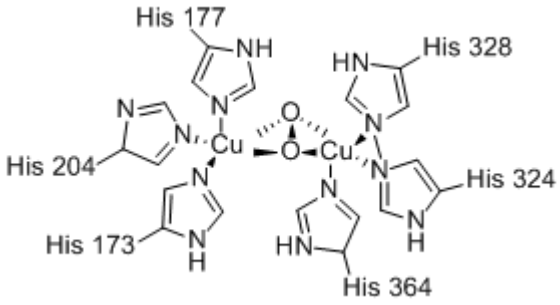

Figure 2.13: Dinuclear μ-η^2:η^2 peroxo copper(II) active site of oxyhemocyanin from *Limulus Polyphemus*, from a single-crystal X-ray determination.[43]

Furthermore, copper is also involved, as catalytic center, in many electron transfer proteins due to its ability to switch between various oxidation states and to easily twist among different coordination numbers and geometries. Although trivalent copper sites were hypothesized in the literature as possible intermediates in some enzymes,[44] further studies ruled out their presence[45] and, at the best of our knowledge, no example of the oxidation state +3 has been observed yet in copper biochemistry.[46]

In humans, copper ranks third among the most abundant transition metals and it is considered as an essential element. The body of a healthy 70-kg adult contains less than 110 mg of Cu, mainly found in the liver (10 mg), brain (8.8 mg), blood (6 mg), skeleton (bone marrow includes 46 mg) and skeletal muscles (28 mg).[47] The Recommended Dietary Allowance (RDA) for adult men and women is 0.9 mg of copper/day and the Tolerable Upper Intake level has been set at 10 mg/day,[48] since an excessive uptake results in potentially harmful free ions. Copper is indeed a potent source of free radicals and reactive oxygen species (ROS).[49] Copper is primarily absorbed in the small intestine and then delivered mainly to the liver wherein it is incorporated into ceruloplasmin and, hence, released into the blood. Ceruloplasmin is the main vector in the serum carrying about 70% of the total copper, followed by albumin with 12-18%.[30] Afterwards, copper is uptaken by the eukaryotic cells as Cu(I) by the hCTR copper transporter proteins.[50] All the members of this family show

similar structures consisting of three transmembrane helices, with a hydrophilic N-terminus, usually rich in methionine residues towards the extracellular matrix and a number of conserved Cys/His residues at the C-terminus in the cytoplasm.[51] The suggested model of action of these proteins envisages firstly the coordination of the cuprous ion by the methionine-rich motifs at the extracellular N-terminus and, then, a series of copper-exchange reactions between specific Cu(I) binding sites exploiting well-defined conformational changes.[52-54] Once inside the cytosol, Cu(I) is coordinated and vehicled by different soluble proteins, called copper chaperones, by a currently unknown mechanism. First of all, the chaperones for superoxide dismutase (CCS) deliver copper to the antioxidant enzyme Cu/Zn superoxide dismutase (SOD1).[55] On the other hand, the Cox17 (cytochrome c oxidase copper chaperone) is proposed to transport this metal ion to Sco1 (cytochrome c oxidase assembly protein) in the inner mitochondrial membrane, which may then transfer copper to the cytochrome c oxidase (COX) subunit 2 CuA site.[56]

Differently, the human Atox1 (Antioxidant-1) transfers Cu(I) to the mitochondrial membrane-bound metal transporting P1B-type ATPases, respectively ATP7A and ATP7B, in the trans-Golgi system for the ultimate incorporation into ceruloplasmin.[57] Finally, the intracellular excess of copper is removed by metallothioneins, thus avoiding acute hepatitis owing to the production of ROS.[58] Alterations of this tightly-regulated homeostasis can lead to peculiar disorders, including Alzheimer (AD), PRION diseases (PrPD), amyotrophic lateral sclerosis (ALS), Menkes' disease (MD) and Wilson's disease (WD).[48,49] In particular, the latter two are characterized by a mutation in ATP7A and ATP7B genes (encoding for Menkes MNKP and Wilson WNDP proteins) which causes the deficiency (MD) or the accumulation (WD) of copper in the tissues, respectively.[59,60] Vice versa, the metabolism of this redox-active metal center becomes profoundly altered also in cancer cells, with many types of tumors presenting high serum and tissue levels of Cu.[61]

2.7.2 Copper and cancer: the role of the metal in angiogenesis and possible therapies

The involvement of endogenous metals in cancer metabolism has been studied for several decades.[62]

Numerous papers report copper levels being aberrant in cancerous tissues of tumor-bearing mice and in cancer patients.[63] Although the mechanisms implicated in increasing the copper concentration in the serum of cancer patients have not been elucidated yet, it is undoubtedly the importance of copper as a key component of many cellular functions and modulator of cellular signaling, and not surprisingly, it is involved in cancer development and progression processes.[64] Among them, the most crucial process influenced by copper-altered homeostasis is angiogenesis and concerns in the migration, proliferation and differentiation of endothelial cells to form new blood vessels.[65] As presented in **Introduction**, **Section 1**, this is a crucial step in cancer growth, as most tumors cannot get larger than 2-3 mm without forming new blood vessels. Since angiogenesis is regulated by the so-called vascular endothelial growth factors (VEGFs), studies performed in mice by Kang and coworkers showed that the supplementation of copper promotes VEGF expression and hence, the angiogenesis itself.[66] Moreover, copper affects transcriptional activity of hypoxia-inducible transcription factor-1 (HIF-1). It can inhibit the process of HIF-1 degradation, thus favoring its accumulation and activation, which leads to an overproduction of VEGF.[67,68] Finally, in an interesting work, after treating cells with VEGF, authors proved by X-ray fluorescence microscopy that copper moves from the intracellular milieu to the extracellular matrix, so highlighting again the relationship between VEGF and copper.[69]

The concept that tumor microenvironment is associated with high levels of copper, due to its involvement in angiogenesis and tumor cell growth, opened intriguing perspectives in the development of antitumor drugs based on metal chelators or Cu-based coordination compounds.[70-71] Historically, copper chelating agents (*i.e.*, trientine, tetrathiomolybdate "TM", and D-penicillamine) were developed to treat the Wilson's disease, by eliminating the excess of copper from the body.[72] However, even if a number of clinical trials investigated the anticancer activities of this group of chelating agents, no improvement in patients' survival was recorded, rather it was associated with a marked reduction of bioavailable

copper in serum, thus pointing out that copper chelation alone is insufficient to kill malignant cell.[73]

As aforementioned, the great need of copper in growing tissues provided scientists with the rationale for developing Cu-coordination compound.[70,74] Copper (I/II) complexes are redox active, frequently labile, and atypical in their preference for distorted coordination geometries. In general, Cu(I) prefers ligands having soft donor atoms such as phosphorous, carbon, sulfur and aromatic amines, and the coordination is almost invariably tetrahedral. Few literature papers reported copper(I) complexes involving phosphine and heterocyclic carbene ligands and showed a micromolar cytotoxic activity in vitro when tested against different human cancer cell lines.[70,74] Concerning the Cu(II) derivatives, the coordination number varies from four in square planar or tetrahedral geometries, to five in square pyramidal and six in octahedral coordination compounds. This reflects in a wide range of selectable ligands and donor atoms (*i.e.*, N, O, S, halides).[74] As discussed for the +1 oxidation state, also Cu(II)–based compounds proved biologically active, and a possible biological target was identified for some of them. The Cu(II)-TACN complex (TACN= 1,4,7-triazacyclononane, **Figure 2.14A**) acts as a "molecular scissor", cleaving supercoiled DNA under both aerobic and anaerobic conditions, producing fragments that cannot be enzymatically re-ligated.[75] Differently, $CuCl_2$ was found to inhibit Topo I (topoisomerase I, an enzyme that plays an important role in the DNA replication),[76] whereas copper derivatives of thiosemicarbazones (TSC) of the type [Cu(TSC)Cl] (**Figure 2.14B**) were potent antitumor agents able to inhibit Topo II.[77] Finally, the recently investigated $[Cu(DTC)_2]$ (DTC= PDT, DEDT), synthetized in our research group, showed inhibition of the proteasome chymotrypsin-like activity (essential for many fundamental cellular processes, including cell cycle, apoptosis, angiogenesis and differentiation), blocking proliferation of breast cancer cells and inducing apoptosis.[78]

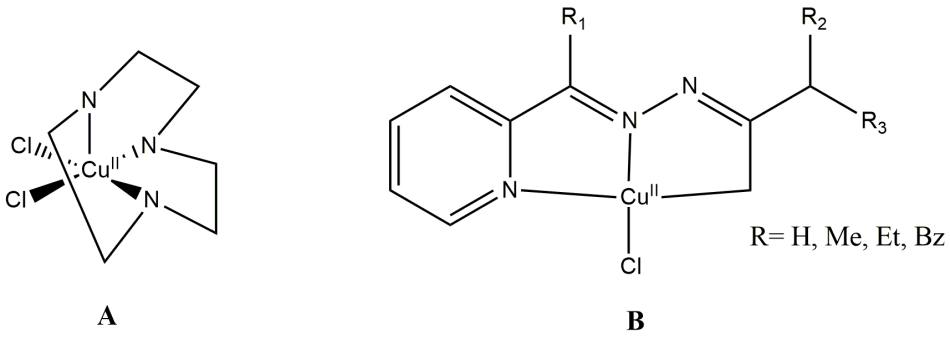

Figure 2.14: Some Cu(II) derivatives for which a possible target was identified: A) the "DNA-scissor" Cu(II)-TACN complex [$CuCl_2$(TACN)] (TACN= 1,4,7-triazacyclononane) and B) the thiosemicarbazone (TSC) derivative [Cu(TSC)Cl] acting as inhibitor of Topo II.

2.7.3 Copper(II) dithiocarbamates as anticancer agents

Copper dithiocarbamates (DTC) were first explored in the late 1960s, when they were investigated for their electrochemical and structural peculiarities.[79,80] The easy access to different oxidation states of this transition metal, led to the isolation of different Cu-DTC complexes involving Cu(I), Cu(II) or Cu(III) metal centers.[81,82] Notwithstanding, only in the 1990s the cytotoxic properties of this class of compounds were disclosed, demonstrating the cytotoxic effect of a Cu-PDT complex formed in situ (**Figure 2.15A**) on thymocytes in vitro experiments.[83] Indeed, during previous studies, researchers observed that the administration of pyrrolidine dithiocarbamate as sodium salt had an antioxidant effect due to the inhibition of the oxidative activation of the transcription factor NFκB (a cellular component with a key role in the activation of immunity system in case of oxidative stress).[84]These observations candidated dithiocarbamates as potent antioxidants in medicine, on the contrary Slater demonstrated that PDT was associated with a toxic prooxidant effect in thymocytes, inducing apoptotic cell shrinkage and chromatin fragmentation prior to cell lysis. This toxicity was demonstrated to be dependent on the ability of administered pyrrolidine dithiocarbamate to chelate in situ endogenous copper and transport it into the cells, and thereby generate an intracellular oxidative stress.[83]

To date, it is commonly accepted that the administration of PDT increases the cellular copper concentration and the combination of Cu and the DTC ligand exerts cytotoxic effects on cancer cells.[85,86] Other dithiocarbamates (*e.g.*, DEDT) yielded the same experimental biological result.[87] Taken together, these findings have fostered researchers to explore synthetic copper-DTC derivatives as potential anticancer agents. As previously reported in

Section 2.7.2, the $[Cu(PDT)_2]$ complex was found to be a potent proteasome inhibitor and an apoptosis inducer.[78] Moreover, PDT (as sodium salt) spontaneously binds copper, forming derivatives that have proteasome-inhibitory and apoptosis-inducing activities in breast tumor cells but not in normal/not transformed counterparts.[88] These encouraging results prompted our research group to synthetize and biologically study new Cu(II) dithiocarbamato derivatives of sarcosine esters and dimethylamine as potential chemotherapeutic agents (**Figure 2.15B**). In all compounds, the metal-to-ligand stoichiometry is 1:2 with symmetrical bidentate (chelate) coordination of the ligands. All the investigated compounds inhibited tumor cell growth in vitro in a dose-dependent manner both in wild type and in cisplatin-resistant cells of cervix carcinoma (C13 and A431Pt cell lines), with the complex $[Cu(ESDT)_2]$ (**Figure 2.15B**) resulting the most active one with IC50 < 0.5 μM in all the tested human tumor cell lines.[30]

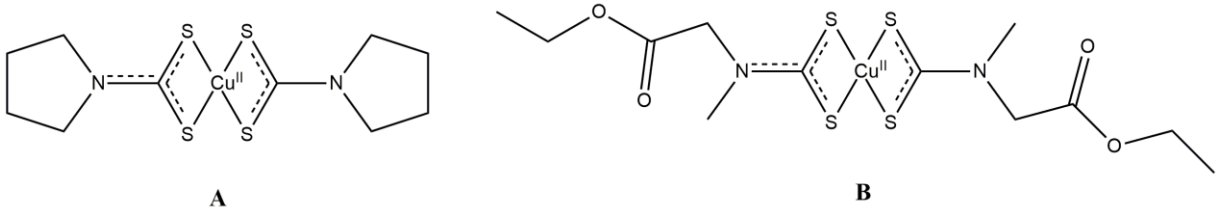

Figure 2.15: Chemical structures of two promising complexes synthetized by our group. In particular, figure A) shows the copper(II) pyrrolidine dithiocarbamato complex $[Cu(PDT)_2]$, whereas B) the $[Cu(ESDT)_2]$ derivative, bearing an ethyl-sarcosine (N-methyl glycine) dithiocarbamato as ligand.

2.8 Synthesis of glycosylated Cu(II) dithiocarbamato complexes

The synthetic pathways to obtain the Cu(II) complexes are not as challenging as for Au(III) derivatives. In fact, the copper ion, in its +2 oxidation state, tends to coordinate always two dithiocarbamato molecules in order to lose the lower-field chloride ligands and to transform into the neutral, tetracoordinated and more stable product with metal to ligand ratio 1:2. Copper(II) dithiocarbamato compounds with different M/L stoichiometries have never been presented in literature, except for the dimeric complexes of the type $[Cu^{II}Cl(DTC)]_2$ that possess two chloride as bridging ligands. In this regard, such di-nuclear derivative can be obtained by redox reaction between a Cu(I) precursor and thiuram disulfide in aprotic solvent. Thus, the formation of this sub-product is unlikely to occur in the reaction conditions used in our experiments. All reactions with glycosylated dithiocarbamates were carried out in polar solvent by mixing the $CuCl_2 \cdot 2H_2O$ precursor and the DTC ligands (**Figure 2.16**).

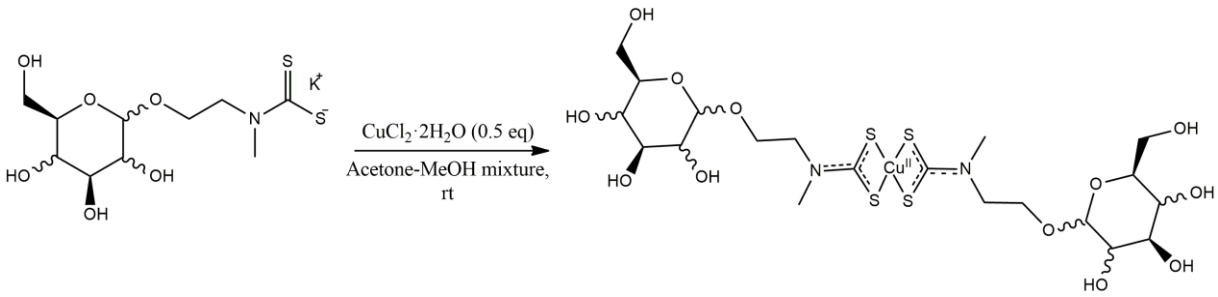

Figure 2.16: Representation of the synthetic procedure for the synthesis of Cu(II) complexes with glycosylated dithiocarbamates as ligands. The wavy bonds in the carbohydrate moieties denote the presence of both the possible stereocenters in order to offer to the reader a general depiction incorporating the structures of all the glycosyl derivatives under investigation.

2.8.1 Synthesis of glycoconjugated copper(II) dithiocarbamato complexes

0.25 mmol of $CuCl_2 \cdot 2H_2O$ were dissolved in 15 mL of acetone under stirring. in a 50 mL round-bottom flask. 2 eq. of the glycosylated dithiocarbamato ligand as potassium salt, previously dissolved in 5 mL of dry MeOH, were added dropwise, to this light green solution. The mixture initially turns dark green, due to the coordination between the excess of Cu(II) ions with the hydroxyl groups of the ligand, and then brown, with a small amount of white precipitate (KCl). The solution was filtered, the solvent volume half-reduced by means of rotatory evaporator and a brown flocculent solid was collected after precipitation with diethyl ether. Then, the product was re-dissolved in H_2O milliQ and purified via reverse phase column chromatography on C-18 functionalized silica (eluent H_2O-CH_3CN, with a gradient from 9:1 to 8:2 with 0.5% TFA), obtaining a brown powder after the lyophilization step. All the three products were soluble in water, DMSO, MeOH and slightly in EtOH.

Bis-[O-ethyl,2-(N-methylamino)-β-glucopyranosyl dithiocarbamato] copper(II)

Aspect: brown amorphous powder

Yield: 61 %

Anal. Calc. for $C_{20}H_{36}Cu_2N_2O_{12}S_4$ (MW = 688.31 g·mol^{-1}): C 34.90; H 5.27; N 4.07; S 18.63. Found: C 34.08; H 5.25; N 3.12; S 18.20.

Medium FT-IR (KBr): $\tilde{\nu}$ (cm^{-1}) = 1514 (ν_a, N-CSS); 1077 (ν_a, CO); 990 (ν_a, CSS); 897 (ν, OCO).

Far FT-IR (nujol): $\tilde{\nu}$ (cm^{-1}) = 565 (ν_s, CSS); 357 (ν_a, Cu-S); 291 (ν_s, Cu-S).

ESI-MS m/z, $[M]^+$ found (calc.): 687.05 (687.04).

Bis-[O-ethyl,2-(N-methylamino)-β-galactopyranosyl dithiocarbamato] copper(II)

Aspect: brown amorphous powder

Yield: 80 %

Anal. Calc. for $C_{20}H_{36}Cu_2N_2O_{12}S_4$ (MW = 688.31 g·mol^{-1}): C 34.90; H 5.27; N 4.07; S 18.63. Found: C 34.21; H 5.30; N 3.16; S 18.48.

Medium FT-IR (KBr): $\tilde{\nu}$ (cm^{-1}) = 1516 (ν_a, N-CSS); 1072 (ν_a, CO); 960 (ν_a, CSS); 898 (ν, OCO).

Far FT-IR (nujol): $\tilde{\nu}$ (cm^{-1}) = 542 (ν_s, CSS); 360 (ν_a, Cu-S); 290 (ν_s, Cu-S).

ESI-MS m/z, $[M]^+$ found (calc.): 687.04 (687.04).

Bis-[O-ethyl,2-(N-methylamino)-α-mannopyranosyl dithiocarbamato] copper(II)

Aspect: brown amorphous powder

Yield: 88 %

Anal. Calc. for $C_{20}H_{36}Cu_2N_2O_{12}S_4$ (MW = 688.31 g·mol^{-1}): C 34.90; H 5.27; N 4.07; S 18.63. Found: C 34.60; H 4.95; N 3.63; S 18.11.

Medium FT-IR (KBr): $\tilde{\nu}$ (cm^{-1}) = 1516 (ν_a, N-CSS); 1057 (ν_a, CO); 960 (ν_a, CSS); 884 (ν, OCO).

Far FT-IR (nujol): $\tilde{\nu}$ (cm^{-1}) = 533 (ν_s, CSS); 364 (ν_a, Cu-S); 293 (ν_s, Cu-S).

ESI-MS m/z, $[M]^+$ found (calc.): 687.04 (687.04).

2.9 Characterization of the glycoconjugated Au(III) and Cu(II) dithiocarbamato complexes

2.9.1 ^{1}H-NMR characterization

The synthetized gold (III) (either the 1:1 and [1:2] derivatives) and copper(II) complexes with glycosylated DTCs as ligands have been characterized by means of ^{1}H-NMR spectroscopy (600 MHz, 298 K) and the spectra are reported in the **Supporting Information E**. It is worth noting that all the spectra of the Au(III) complexes were acquired in DMSO-d6 as deuterated solvent and the assignments of the resonances (**Table 2.3**) were compared with those of the corresponding ligands (see **Section 2.5.1**).

Concerning the Cu(II) derivatives, taking into account the paramagnetic nature of the metal ion, a general shift and decrement of the resonances are observed. This effect, associated with the d^9 electronic configuration of the metal center, appears as a hyperfine shifts (δ) to NMR signals and the shortening of both nuclear longitudinal (T_1) and transverse (T_2) relaxation times.[89] The shifts and the low intensities were observed, in particular, for the closest protons of the ethylic spacer (H(8-9) and H(10.11)) whose signals resulted very broad, overlapping the other peaks of the carbohydrate backbone. For these reasons, they are not discussed in this characterization paragraph.

On the other hands, the spectra of the Au(III) complexes are not affected by paramagnetic disturbs and their interpretation is simpler than the Cu(II) counterparts. In particular, resonances of the protons in the Au(III) glycosylated compounds (the spectra of the glucosyl derivatives are shown in **Figure 2.17** and **Figure 2.18**, other spectra are reported in **Supporting Information E**), both with metal-ligand stoichiometry 1:1 and 1:2, are characterized by a general upshift if compared to those of ligands thanks to the electron withdrawing effect of the electronegative metal. The unique exception is detected for the protons of the spacer in α position with respect to the dithiocarbamato moiety ($H_{11\text{-}12}$) that are affected by a shielding effect of about 0.2 ppm as observed for the same protons also in the case of piperidine dithiocarbamato analogs.

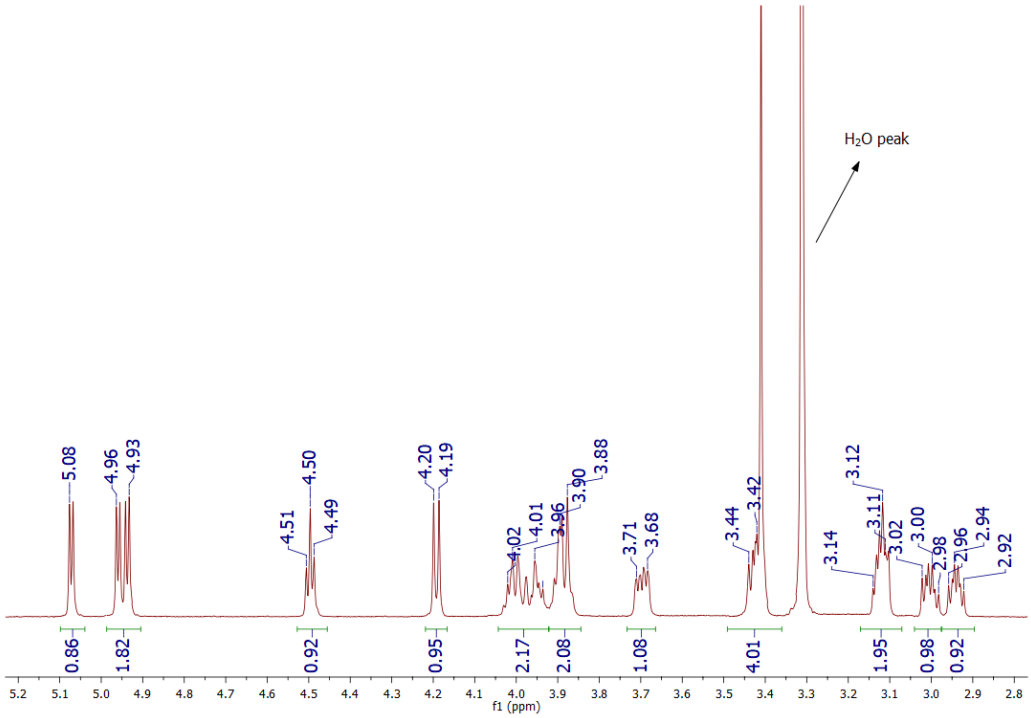

Figure 2.17: 1D ^{1}H-NMR spectrum of the [$AuBr_2$(β-D-Glucoside-DTC)] recorded in DMSO-*d6* at 25°C, with a 600 MHz instrument.

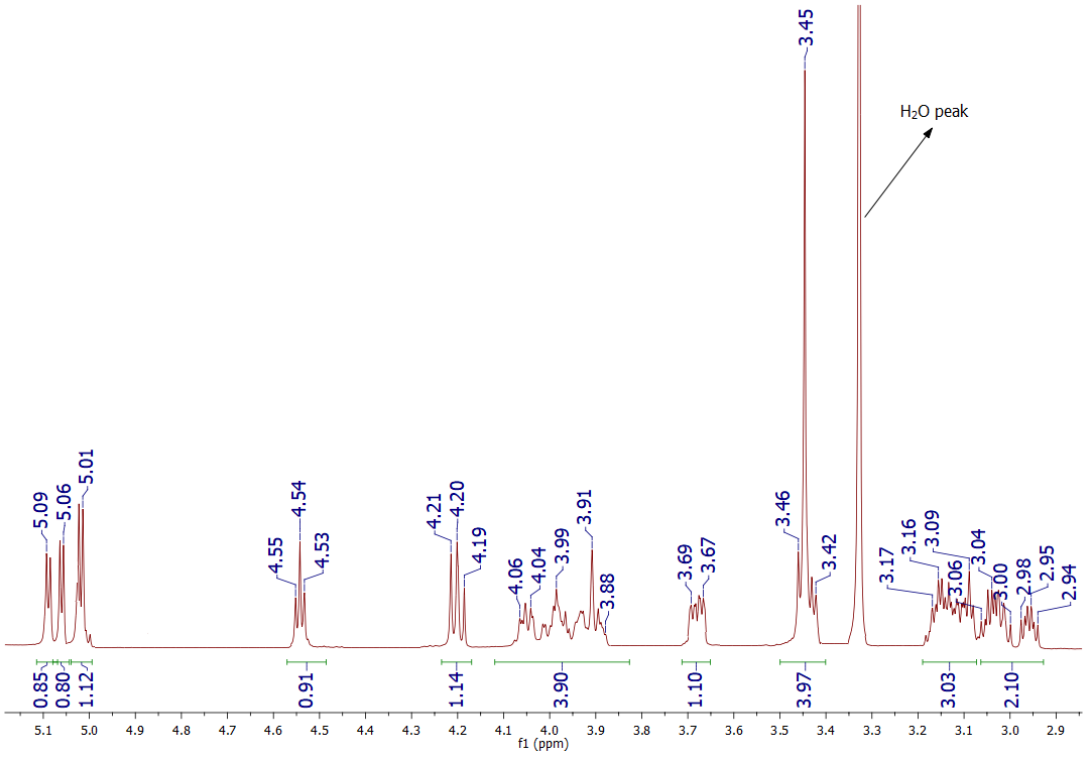

Figure 2.18: 1D ^{1}H-NMR spectrum of the [Au(β-D-Glucoside-DTC)$_2$]Cl recorded in DMSO-*d6* at 25°C, with a 600 MHz instrument.

Table 2.3: resonances (ppm) of the protons of the glycosylated ligand in the Au(III) 1:1 di-chloro complexes in DMSO-*d6* at 25°C

PROTONS (numbered as in **Figure 2.8**)	**[$Au^{III}Br_2$(β-D-glucoside DTC)]**	**[$Au^{III}Br_2$(β-D-galactoside DTC)]**	**[$Au^{III}Br_2$(α-D-mannoside DTC)]**
1 (C-*H* backbone)	4.20 (d)	4.14 (d)	4.65 (d)
2 (C-*H* backbone)	2.92-2.96 (m)	3.20-3.27 (m)	3.58 (m)
3 (C-*H* backbone)	3.12-3.14 (m)	3.20-3.27 (m)	3.19-3.22 (m)
4 (C-*H* backbone)	2.98-3.02 (m)	3.63 (m)	3.34-3.37 (m)
5 (C-*H* backbone)	3.12-3.14 (m)	3.33-3.35 (m)	3.43-3.47 (m)
6-7 (C-*H* backbone)	3.69 ; 3.43 (m)	3.48-3.57 (m)	3.66 ; 3.43 (m)
8-9 (*O*-CH_2 spacer)	3.88-4.04 (m)	3.86-4.06 (m)	3.37-3.98 (m)
10-11(*N*-CH_2 spacer)	3.88-4.04 (m)	3.86-4.06 (m)	4.04 ; 3.74 (m)
12 (*N*-CH_3 spacer)	3.41 (s)	3.39 (s)	3.40 (s)
13 (C_6-O*H*)	4.50 (t)	4.58 (t)	4.52 (t)
14 (C_4-O*H*)	4.96 (d)	4.92 (d)	4.89 (m)
15 (C_3-O*H*)	5.08 (d)	4.98 (d)	4.91 (d)
16 (C_2-O*H*)	5.93 (d)	5.90 (d)	4.87 (d)

Table 2.4: resonances (ppm) of the protons of the glycosylated ligand in the Au(III) [1:2]Cl complexes in DMSO-*d6* at 25°C

PROTONS (numbered as in **Figure 2.8**)	**[Au^{III}(β-D-glucoside DTC)$_2$]Cl**	**[Au^{III}(β-D-galactoside DTC)$_2$]Cl**	**[Au^{III}(α-D-mannoside DTC)$_2$]Cl**
1 (C-*H* backbone)	4.20 (t)	4.15 (d)	4.66 (s)
2 (C-*H* backbone)	2.94-2.98 (m)	3.20-3.27 (m)	3.59 (m)
3 (C-*H* backbone)	3.09-3.17 (m)	3.20-3.27 (m)	3.19-3.22 (m)
4 (C-*H* backbone)	3.00-3.06 (m)	3.63 (m)	3.34-3.38 (m)
5 (C-*H* backbone)	3.09-3.17 (m)	3.33-3.37 (m)	3.43-3.46 (m)
6-7 (C-*H* backbone)	3.68 ; 3.43 (m)	3.48-3.55 (m)	3.66 ; 3.43 (m)
8-9 (*O*-CH_2 spacer)	3.88-4.06 (m)	3.86-4.05 (m)	3.37-3.97 (m)
10-11(*N*-CH_2 spacer)	3.88-4.06 (m)	3.86-4.05 (m)	4.04 ; 3.75 (m)
12 (*N*-CH_3 spacer)	3.43 (s)	3.43 (s)	3.43 (s)
13 (C_6-O*H*)	4.54 (t)	4.58 (t)	4.52 (t)
14 (C_4-O*H*)	5.06 (d)	4.40 (d)	4.80-4.82 (m)
15 (C_3-O*H*)	5.09 (d)	4.90 (d)	4.65 (d)
16 (C_2-O*H*)	5.01 (d)	4.76 (d)	4.80-4.82 (m)

2.9.2 FT-IR characterization

The FT-IR spectra have been collected for all the Au(III)- as well as for Cu(II)-DTC derivatives both in the medium (4000-600 cm^{-1}) and far (600-50 cm^{-1}) wavenumber domain (**Supporting Information F** and **G**), and the diagnostic absorptions are reported in **Table 2.5**.

The spectra of metal glycosylated-DTC complexes, contain five fundamental IR-regions, corresponding to diagnostic modes of vibrations:[90,91]

- between 3500 and 2700 cm^{-1}: $\nu_{s/a}$(CH) and ν(OH) of the ligand;
- ca. 1500 cm^{-1}: ν(SSC-N), both for the Cu(II) and Au(III) derivatives;
- between 920 and 1450 cm^{-1}: ν(C-C), ν(C-O) and δ(C-H) related to the carbohydrate backbones and ν_s(C-S) in the case of Au(III) compounds;
- between 550 and 650 cm^{-1}: ν_s(C-S) for the Cu(II) complexes;
- below 420 cm^{-1}: ν(Au-S) and ν(Cu-S).

In particular, in the case of Au(III)-glycosylated dithiocarbamates, the same considerations described in the **Chapter 1** (**Section 1.4.2**) should be taken into account. In particular, the coordination of the metal ion strongly affects the SSC-N stretching frequency, which is up-shifted of ca. 80 cm^{-1} in all the investigated compounds, if compared to that of the free ligands. Moreover, the existence of the symmetric and asymmetric Au-S stretching absorptions at ca. 360-330 cm^{-1} and 420-370 cm^{-1}, for the 1:1 and 1:2 derivatives, respectively, demonstrates the coordination of the Au(III) center to the bidentate dithiocarbamato moiety of the ligand. Unfortunately, the CSS bonding mode cannot be evaluated, due to the presence of the strong bands related to the backbone vibrations which overlap the ν_a(C-S) absorption that usually falls at about 940-1060 cm^{-1}. Furthermore, a strong band is observed at 1513 cm^{-1} also for all three Cu(II)-DTC complexes, showing a N-CSS bond strength similar to that registered for the Au counterparts.[22,23] Interestingly, all the spectra of the synthetized metal complexes show a diagnostic absorption band at ca. 890 cm^{-1}, recognized as ν(OCO) vibration of the glycosidic linkage. In fact, as described in the characterization section of the free ligands, these bands can be exploited to distinguish between the α and the β anomers.[25]

Table 2.5: main IR absorption bands (expressed in cm^{-1}) of the Au(III) complexes, both the 1:1 / 1:2 derivatives, and Cu(II) glycosylated compounds.

COMPOUND	ν(N-CSS)	ν_{as}(C-O)	ν_a(CSS)	ν(O-C-O)	ν_s(CSS)	ν_a(M-S)	ν_s(M-S)	ν_a(Au-Br)	ν_s(Au-Br)
$[Au^{III}Br_2$(β-D-glucoside DTC)]	1576	1075	991	901	568	484	418	271	218
$[Au^{III}Br_2$(β-D-galactoside DTC)]	1575	1067	989	889	546	481	413	296	220
$[Au^{III}Br_2$(α-D-mannoside DTC)]	1580	1056	992	882	591	508	413	284	216
$[Au^{III}$(β-D-glucoside DTC)$_2$]Cl	1565	1076	987	897	554	486	386	-	-
$[Au^{III}$(β-D-galactoside DTC)$_2$]Cl	1564	1072	954	891	528	480	386	-	-
$[Au^{III}$(α-D-mannoside DTC)$_2$]Cl	1564	1054	973	880	528	481	384	-	-
$[Cu^{II}$(β-D-glucoside DTC)$_2$]	1514	1077	990	897	565	357	291	-	-
$[Cu^{II}$(β-D-galactoside DTC)$_2$]	1516	1072	960	898	542	352	267	-	-
$[Cu^{II}$(α-D-mannoside DTC)$_2$]	1516	1057	960	884	533	364	293	-	-

2.9.3 UV-Vis characterization

All the complexes synthetized in this Chapter were characterized also by means of UV-Vis spectrophotometry. The electronic spectra of the Au(III) 1:1 di-bromo complexes were acquired in DMSO within the range 700:250 nm, whereas, in the case of ionic Au(III) and Cu(II) derivatives, deionized water was used as solvent (range 700:290 nm). Because of the high degree of similarity between the different glycosylated ligands, only the electronic spectra of the compounds bearing the β-D-glucosyl-DTC ligand are reported (**Figure 2.19**).

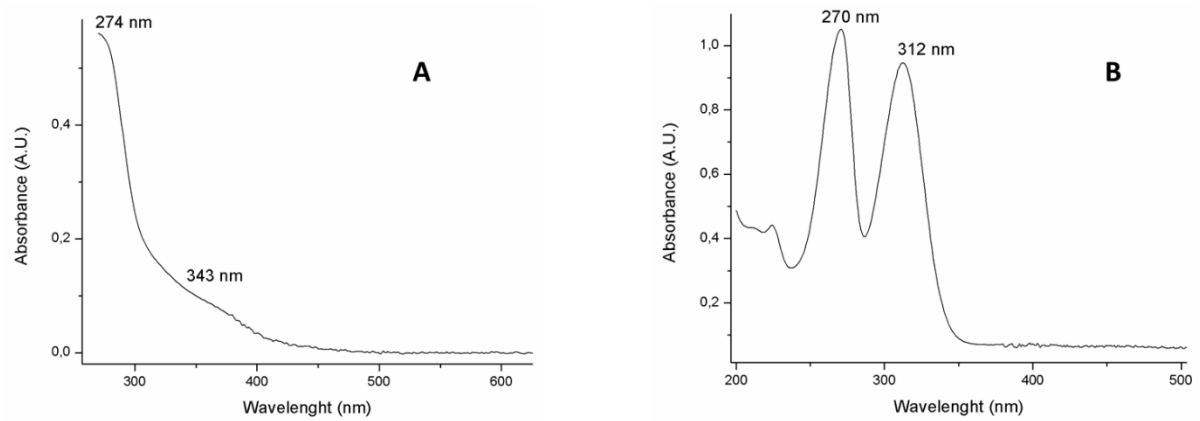

Figure 2.19: UV-Vis spectra of the two Au(III) complexes with O-ethyl,2-(N-methylamino)-β-glucopyranosyl dithiocarbamato ligand registered at 25 °C. The spectrum of the [$Au^{III}Br_2$(glucosideDTC)] 15μM in DMSO is shown on the left (A), while that of [Au^{III}(glucosideDTC)$_2$]Cl, 40μM in deionized water is on the right (B).

An exhaustive description about the nature of the absorption bands of the Au(III) glycosylated dithiocarbamato complexes, can be found in **Chapter 1** (**Section 1.4.3**), as their electronic spectra are comparable to those of the previously-discussed di-halo Au(III)-PipeDTC derivatives. Briefly, the UV-Vis spectrum of the 1:1 di-bromo derivative in **Figure 2.19A** shows two main absorption bands at 274 nm, the most intense, and 343 nm. The first is attribuible to the overlapped electronic exctitations of the -NCS and -SCS moieties, while the second is referable to an electron transfer of the type u ← g from a *4p* orbital (σ symmetry) of the bromide ligands to the lowest unfilled *5d* orbital of the metal (d_{x2-y2}). On the other hands, in the spectrum of the [1:2] compound in **Figure 2.19B** displays two intense bands at 270 nm and 312 nm related to the π* ← π intra-ligand -NCS and -SCS absorptions.

Moreover also the 1:1 di-bromo compounds synthetized in this Chapter are subjected to the rearrangement equilibrium in solution, that leads to the formation of the [1:2][$AuCl_4$] counterparts in coordinating solvents and under UV-Vis irradiation, proving the fact that the steric hindrances of the substituents on the DTC ligand are not a crucial factor in the interconversion mechanism (**Figure 2.20**).

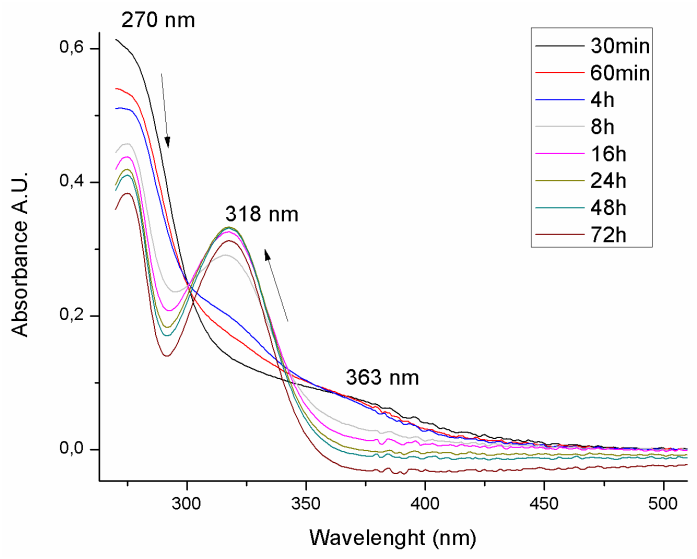

Figure 2.20: UV-Vis 72 h kinetic analysis of the rearrangement process involving the [$AuBr_2$(glucosideDTC)] complex in DMSO at 25 °C.

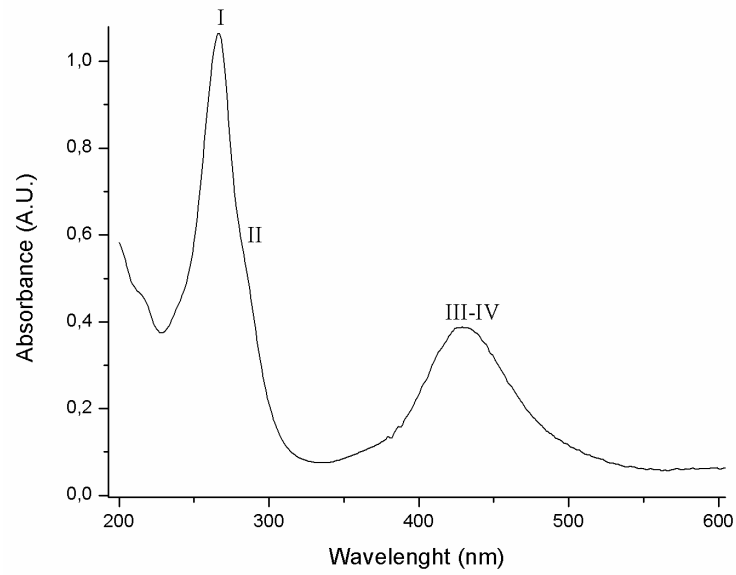

Figure 2.21: UV-Vis spectrum of the Cu(II) complexes bearing two O-ethyl,2-(N-methylamino)-β-glucopyranosyl dithiocarbamates as ligands (30μM). The acquisition was registered in saline solution at 25 °C.

Regarding the UV-Vis spectrum in H_2O of the synthesized Cu(II) glucoconjugated dithiocarbamato complex (reported in **Figure 2.21** and **Table 2.6**), it shows different bands. In particular, the band I at about 266 nm and band II (a shoulder) at around 290 nm, are ascribable to the π* ← π absorption in the -NCSS group, and the intra-ligand π* ← π transition located in the -CSS moiety, respectively.[92,93] On the other hands, the discussion

ofvthe absorption III-IV needs a brief theoretical introduction about the electronic transitions of the Cu(II) complexes. As already discussed, Cu(II) is able to form complexes with a large variety of geometries. In particular, the Jahn-Teller effect for this ion (d^9 electronic configuration) rules out regular O_h and T_d symmetries in favor of distorted structures, unless rigid and sterically-demanding ligands are present.[94] In the distorted symmetries (*i.e.*, D_{4h} and D_{2d}), three different *d-d* absorption bands could be observed in the UV-Vis range whereas octahedral and tetrahedral geometries give rise to only one electronic transition (respectively, the $E_g \leftarrow T_{2g}$ and the $T_{2g} \leftarrow E_g$).[31] Moreover, its d^9-electronic configuration allows also the use of the positive hole formalism. In this method, the excitation of the electronic hole, instead of that of electrons is taken into account, thus simplifying both the prevision and the assignment of the UV-Vis bands.[31] As a result, UV-Vis transitions are easily obtained for any geometry simply reversing the energetic order of the d orbitals (**Figure 2.22**).

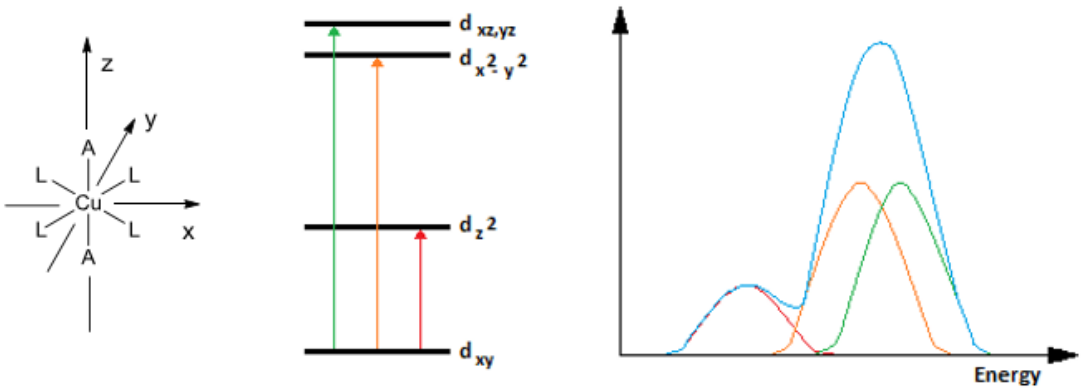

Figure 2.22: Schematic representation of *d-d* transitions for a D2h symmetry using the positive hole formalism.

Concerning Cu(II)-dithiocarbamates of aliphatic amines, their electronic spectra have been firstly rationalized by Choi using bis(di-isopropyldithiocarbamato)copper(II) in DMSO as a model compound.[95] Starting from an ideal D_{2h} geometry for the metal center, Choi and co-workers were able to calculate the energy sequence of the d-orbitals as $d_{xy} > d_z^2 > d_x^2\text{-}_y^2 > d_{xz,yz}$. Based on these findings and on the positive hole formalism, the band occurring at lower energies was attributed to a $d_z^2 \leftarrow d_{xy}$ absorption, while the $d_x^2\text{-}_y^2 \leftarrow d_{xy}$ and the $d_{xz,yz} \leftarrow d_{xy}$ transitions are detectable at higher energies and are partly overlapped, resulting in a broad band.[95]

With respect to the band intensities, *d-d* absorptions in a D_{2h} symmetry should show a low molar extinction coefficient due to their forbidden character as defined by the Laporte rules.[96] Starting from this postulate, the high intensity of the band associated with the $d_{x^2-y^2} \leftarrow d_{xy}$ and the $d_{xz,yz} \leftarrow d_{xy}$ transitions led Choi et al. to hypothesize that some kind of distortion in the D_{2h} geometry may occur. On the other hand, the Cu(II) center in a lower symmetry (C_{2v}), wherein it is lifted out of the plane of the four sulfur atoms, would make the $d_{xz,yz} \leftarrow d_{xy}$ transition allowed according to the group theory, contrary to the other two transitions, still forbidden.[95] In light of this, in the 350-600 nm region, the band III is ascribable to $d_{xz,yz} \leftarrow d_{xy}$ transition, combined with either a metal-to-ligand charge transfer (MLCT) or a ligand-to-metal charge transfer (LMCT), whereas the band IV and band V are assigned to the lowest energy *d-d* transitions $d_{x^2-y^2} \leftarrow d_{xy}$ and $d_{z^2} \leftarrow d_{xy}$, respectively.

Table 2.6: wavelengths (nm) of the most important UV-Vis absorption bands of the Au(III) and Cu(II) glycosylated-dithiocarbamato complexes with related molar absorption coefficients (*: overlapped bands).

COMPOUND	**Band I**	**Band II**	**Band III**	**Band IV**
Au^{III} 1:1 Br_2 (DMSO)	-	**274*** 37000	**274*** 37000	**343** 7333
Au^{III} 1:2 Cl (SALINE SOLUTION)	**224** 11025	**270*** 26225	**312*** 23626	-
Cu^{II} 1:2 (SALINE SOLUTION)	**265** 21260	**284** 10480	**430** 7680	**430** 7680

This theoretical discussion here reported has been drafted considering copper(II)-dithiocarbamato derivatives dissolved in non-coordinating solvents (*e.g.*, halogenated ones), hence tetracoordinate in a distorted tetrahedral geometry. However, in the case of coordinating media, such as water and DMSO, although a different coordination sphere and geometry (octahedral) is expected due to the apical coordination of the solvent molecule, no sensible spectral changes are observed with aliphatic Cu(II)-DTC complexes studied in our group on passing from apolar non-coordinating solvents to coordinating ones, both in terms of maximum wavelengths and band shapes. The only detectable change is the intensity decrement of the band II in the presence of water or DMSO, the only transition affected by the coordination of apical ligands.

2.10 LogP measurements of Au(III) and Cu(II) compounds with glucosyl-functionalized dithiocarbamato ligands

The lipophilicity of a molecule (represented as the logarithm of the *n*-octanol/water partition coefficient) often strongly correlates with its pharmacological activity and toxicity.[97] In this regard, the bi-phasic solvent system *n*-octanol/water is commonly accepted in the scientific community since it well mimics the interface water/phospholipid membrane.[98] The measurements were carried out by means of UV-Vis techniques recording the electronic spectra of the aqueous solution of the desired compound before (C_0) and after mixing it with a pre-saturated octanol solution for 2h (C_1). The evaluation of the corresponding n-octanol/water partition coefficient was carried out exploiting the following equation:

$$logP = log\frac{C_{octanol}}{C_{water}} = log\frac{C_0 - C_1}{C_0}$$

The results, reported as mean ± SD of at least three independent measurements, are presented in **Table 2.7** (only the values for the *O*-glucosyl derivatives are reported, considering the similarity of the three glycosylated ligands), and show a series of negative values indicating a strong hydrophilicity of the all synthetized compounds that is associated with their water solubility. In particular, the gold(III) compounds of the type [1:2]Cl are more hydrophilic than the copper(II) counterparts. Moreover, a Δ value of around -2.8 can be detected between the sugar-conjugated Cu(II) complex and the neutral copper derivative with piperidine dithiocarbamato as ligand. This is the first case of a Cu(II) dithiocarbamato complex with negative logP value. It is important to note that the partition coefficients of the Au(III) complexes with stoichiometric metal-to-ligand ratio 1:1 were not measured because of the rearrangement process that occurs, for this class of compounds, in the coordinating *n*-octanol/water mixture.

Table 2.7: LogP values at 25°C of selected compounds determined by UV-Vis measurements (reported as mean ± SD of at least three independent measurements).

COMPOUND	**LogP at 25°C (for glucose: -2.82 ± 0.04)[99]**
$[Cu^{II}(DTC\text{-}\beta\text{-}D\text{-}glucose)_2]$	-1.2 ± 0.1
$[Cu^{II}(pipe\text{-}DTC)_2]$	+ 1.5 ± 0.1
$[Au^{III}(DTC\text{-}\beta\text{-}D\text{-}glucose)_2]Cl$	-1.9 ± 0.1
$[Au^{III}(pipe\text{-}DTC)_2]Cl$	-1.05 ± 0.02
Cisplatin - $[Pt^{II}(Cl)_2(NH_3)_2]$	-2.21 ± 0.06 [100]

Bibliography

1. Medina, R.A.; Owen, G.I. Glucose transporters: expression, regulation and cancer. *Biol. Res.*, **2002**, *35(1)*.
2. Gaye, M.M.; Nagy, G.; Clemmer, D.E.; Pohl, N.L.B. Multidimensional Analysis of 16 Glucose Isomers by Ion Mobility Spectrometry. *Anal. Chem.,* **2016**, *88(4)*, 2335-2344.
3. Demchenko, A.V. *General Aspects of the Glycosidic Bond Formation,* in: Handbook of Chemical Glycosylation: Advances in Stereoselectivity and Therapeutic Relevance, Ed. Demchenko, A.V. Wiley-VCH Verlag GmbH & Co. KGaA. Weinheim, Germany, **2008**, 1-18.
4. Epand, R.F.; Epand, R.M.; Jung, C.Y. Ligand-modulation of the stability of the glucose transporter GLUT 1. *Protein Sci.*, **2001**, *10(7)*, 1363-1369.
5. Calvaresi, E.C.; Hergenrother, P.J. Glucose conjugation for the specific targeting and treatment of cancer. *Chem. Sci.,* **2013**, *4*, 2319-2333.
6. Fischer, E. Ueber die Glucoside der Alkohole. *Ber. Dtsch. Chem. Ges*., **1893**, *26(3)*, 2400-2412.
7. Koenigs, W.; Knorr, E. Ueber einige Derivate des Traubenzuckers und der Galactose. *Chem. Ber.*, **1901**, *34*, 957-981.
8. Igarashi, K. The Koenigs-Knorr Reaction. *Adv. Carb. Chem. Biochem.*, **1977**, *34*, 243-283.
9. Zemplen, G.; Gerecs, A. Einwirkung von Quecksilbersalzen auf Aceto-halogenzucker, IV. Mitteil.: Direkte Darstellung der Alkylbioside der α-Reihe. *Chem. Ber.*, **1930**, *63B*, 2720-2729.
10. Helferich, B.; Wedemeyer, K.F. Zur Darstellung von Glucosiden aus Acetobromglucose. *Liebigs Ann.*, **1949**, *563*,139-145.
11. Bretschneider, H.; Beran, K. Überführung ein- und zweiwertiger Phenole in acetylierteβ-d-Glucoside mit β-Pentaacetyl-D-glucose und Borfluorid. *Monatsh. Chem.*, **1949**, *80(2)*, 262-270.
12. Magnusson, G.; Noori, G.; Dahmen, J.; Frejd, T., Lave, T. BF3--Etherate Induced Formation of 2,2,2-Trichloroethyl Glycopyranosides. Selective Visualization of Carbohydrate Derivatives on TLC Plates. *Acta Chem. Scand.*, **1981**, *B35*, 213-216.
13. Adero, P.O.; Furukawa, T.; Huang, M.; Mukherjee, D.; Retailleau, P.; Bohé, L.; Crich, D. Cation Clock Reactions for the Determination of Relative Reaction Kinetics in Glycosylation Reactions: Applications to Gluco- and Manno-pyranosyl Sulfoxide and Trichloroacetimidate Type Donors. *J. Am. Chem. Soc.*, **2015**, *37(32)*, 10336-10345.
14. Lee, Y.S.; Rho, E.S.; Min, Y.K.; Kim, B.T; Kim, K.H. Practical β-Stereoselective O-Glycosylation of Phenols with Penta-O-Acetyl-β-D-Glucopyranose. *J. Carbohydr. Chem.*, **2001**, 20, 503–506.
15. Shie, T.H.; Chiang, Y.L.; Lin, J.J.; Li, Y.K.; Lo, L.C. Facile synthesis toward the construction of an activity probe library for glycosidases. *Carbohydr. Res.*, **2006**, *341*, 443-456.
16. Elofsson, M., Roy, S., Salvador, L.A. and Kihlberg, J. Building blocks for glycopeptide synthesis: Preparation of α-O-fucosylated fmoc serine and threonine in one step from L-fucose tetraacetate. *Tetrahedron Lett*., **1996**, *37*, 7645-7648.
17. Salvador, L.A.; Elofsson, M.; Kihlberg, J. Preparation of building blocks for glycopeptide synthesis by glycosylation of Fmoc amino acids having unprotected carboxyl groups. *Tetrahedron*, **1995**, *51*, 5643-5656.

18. Elofsson, M.; Walse, B.; Kihlberg, J. Building blocks for glycopeptide synthesis: glycosylation of 3-mercaptopropionic acid and Fmoc amino acids with unprotected carboxyl groups. *Tetrahedron Lett.*, **1991**, *32*, 7613-7616.
19. Michihata, N.; Kaneko, Y.; Kasai, Y.; Tanigawa, K.; Hirokane, T.; Higasa, S.; Yamada, H. High-Yield Total Synthesis of (−)-Strictinin through Intramolecular Coupling of Gallates. *J. Org. Chem.*, **2013**, *78(9)*, 4319-4328.
20. Nickon, A.; Castle, M.A.; Harada, R.; Berkoff, C.E.; Williams, R.O. Chemical Shifts of Axial and Equatorial α-Protons in the N.m.r. of Steroidal α-Haloketones. *J. Am. Chem. Soc.,* **1963**, *85(14)*, 2185-2186.
21. Lambert, J.B.; Goldstein, J.E. The chemical-shift difference between the axial and equatorial protons in pentamethylene heterocycles. *J. Am. Chem. Soc.*, **1977**, *99(17)*, 5689-5693.
22. Nakamoto, K.; Fujita, J.; Condrate, R.A.; Morimoto, Y. Infrared spectra of metal chelate compounds. IX. A normal coordinate analysis of dithiocarbamato complexes. *J. Chem. Phys.*, **1963**, *39*, 423-427.
23. Rao, C.N.R.; Venkataraghavan, R. The C=S stretching frequency and the "-N-C=S bands" in the infrared. *Spectrochim. Acta*, **1962**, *18*, 541-547.
24. Varma, R.; Kulkarni, S.Y.; Jose, C.I.; Pansare, V.S. Infrared-spectral characteristics of some acetylated, anomeric glycosides. *Carbohydr. Res.*, **1984**, *133(1)*, 25-32.
25. Tipson, R.S. *Infrared Spectroscopy of Carbohydrates: a review of the literature.* National Bureau of Standards Monographs. US Department of Commerce. **1968**.
26. Synytsya, S.; Novak, M. Structural analysis of glucans. *Ann. Transl. Med.*, **2014**, *2(2)*, 17-31.
27. Hadjikostas, C. C.; Katsoulos, G. A.; Shakhatreh, S. K. Synthesis and spectral studies of some new palladium(II) and platinum(II) dithiocarbimato complexes. Reactions of bases with the corresponding N-alkyldithiocarbamates. *Inorg. Chim. Acta* **1987**, *133,* 129-132.
28. Pallacani, G. C. Gold(III) complexes with dithiocarbimides, *Inorg. Chim. Acta* **1982**, *58*, 193-200.
29. Whittall, I.R.; Humphrey, M.G.; Samoc, M.; Luther-Davies, B.; Hockless, D.C.R. Organometallic complexes for non-linear optics XII. Syntheses and second-order susceptibilities of (neomenthyldiphenylphosphine) gold σ-arylacetylides: X-ray crystal structures of Au(C≡CPh) (nmdpp) and Au((E)-4,4′-C≡CC_6H_4CH=CH$C_6H_4NO_2$)(nmdpp). *J. Organomet. Chem.* **1997**, *544(2)*, 189-196.
30. Giovagnini, L.; Sitran, S.; Montopoli, M.; Caparrotta, L.; Corsini, M.; Rosani, C; Zanello, P.; Dou, Q.P.; Fregona, D. Chemical and biological profiles of novel copper(II) complexes containing S-donor ligands for the treatment of cancer. *Inorg. Chem.*, **2008**, *47(14)*, 6336-6343.
31. Cotton, F.A.; Wilkinson, G. *Advanced inorganic chemistry*, 3rd ed., **1972**, John Wiley & Sons, New York (USA).
32. Jo, M.; Seo, J.; Seo, M.L.; Choi, K.S.; Cha, S.K.; Lindoy, L.S.; Lee, S.S. Donor-set-induced coordination sphere and oxidation state switching in the copper complexes of O_2S_2X (X = S, O and NH) macrocycles. *Inorg. Chem.*, **2009**, *48(17)*, 8186.
33. Linder, M.C. Ceruloplasmin and other copper binding components of blood plasma and their functions: an update. *Metallomics*, **2016**, *8(9)*, 887.
34. Gerloch, M. The sense of Jahn-Teller distortions in octahedral Cu(II) and other transition-metal complexes. *Inorg. Chem.*, **1981**, *20(2)*, 638.
35. Kida, S.; Nishida, Y.; Sakamoto, M. Absorption band in the near-ultraviolet region observed for binuclear copper(II) complexes. *Bull. Chem. Soc. Jpn.*, **1973**, *46(8)*, 2428.
36. Pearson, R.G. Hard and soft acids and bases, HSAB, part I. *J. Chem. Ed.*, **1968**, *45*, 581.

37. Gaăzo, J.; Bersuker, I.B.; Garaj, J.; Kabešová, M.; Kohout, J.; Langfelderová, H.; Melník, M.; Serator, M.; Valach, F. Plasticity of the coordination sphere of copper(II) complexes, its manifestation and causes. *Coord. Chem. Rev.*, **1976**, *19(3)*, 253.
38. Boal, A.K.; Rosenzweig, A.C. Structural biology of copper trafficking. *Chem. Rev.*, **2009**, *109*, 4760.
39. Crichton, R.R.; Pierre, J.L. Old iron, young copper: from Mars to Venus. *BioMetals*, **2001**, *14*, 99.
40. Kaim, W.; Rall, J. Copper: A modern bioelement. *Angew. Chem. Int. Ed.*, **1996**, *35*, 43.
41. Samantha, S.; Lehnert, N. Metalloproteins: a switch for blue copper proteins? *Nat. Chem.*, **2016**, *8*, 639.
42. Kitajima, N.; Moro-oka, Y. Copper-dioxigen complexes. Inorganic and bioinorganic perspectives. *Chem. Rev.*, **1994**, *94(3)*, 737.
43. Hazes, B.; Magnus, K.A.; Bonaventura, C.; Bonaventura, J.; Dauter, Z.; Kalk K.H.; Hol, W.G.J. Crystal structure of deoxygenated Limulus polyphemus subunit II hemocyanin at 2.18 A resolution: clues for a mechanism for allosteric regulation. *Protein Sci.*, **1993**, *2*, 597-619.
44. Hamilton, G.A.; Adolf, P.K.; De Jersey, J.; DuBois, G.C.; Dyrkacz, G.R.; Libby, R.D. Trivalent copper, superoxide, and galactose oxidase. *J. Am. Chem. Soc.*, **1978**, *100*, 1899.
45. Himo, F.; Eriksson, L.A.; Maseras, F.; Siegbahn, P.E.M. Catalytic mechanism of galactose oxidase: a theoretical study. *J. Am. Chem. Soc.*, **2000**, *122*, 8031.
46. Solomon, E.I.; Heppner, D.E.; Johnston, E.M.; Ginsbach, J.W.; Cirera, J.; Qayyum, M.; Kieber-Emmons, M.T.; Kjaergaard, C.H.; Hadt, R.G.; Tian, L. Copper active sites in biology. *Chem. Rev.*, **2014**, *114*, 3659.
47. Bost, M.; Houdart, S.; Oberli, M.; kalonji, E.; Huneau, J.F.; Margaritis, I. Dietary copper and human health: current evidence and unresolved issues. *J. Trace Elem. Med. Biol.*, **2016**, *35*, 107.
48. Gaggelli, E.; Kozlowski, H.; Valensin, D.; Valensin, G. Copper Homeostasis and Neurodegenerative Disorders (Alzheimer's, Prion, and Parkinson's Diseases and Amyotrophic Lateral Sclerosis). *Chem. Rev.*, **2006**, *106*, 1995-2044.
49. Mercer, J.F.B. The molecular basis of Copper-Transport diseases. *Trends Mol. Med.*, **2001**, *7(2)*, 64-69.
50. Kim, H.; Wu, X.; Lee, J. SLC31 (CTR) family of copper transporters in health and disease. *Mol. Aspect. Med.*, **2013**, *34*, 561-570.
51. Banci, L.; Bertini, I.; Cantini, F.; Baffoni, S.C. Cellular copper distribution: a mechanistic system biology approach. *Cell. Mol. Life Sci.*, **2010**, *67*, 2563-2589.
52. De Feo, C.J.; Aller, S.G.; Siluvai, G.S.; Blackburn, N.J.; Unger, V.M. Three-dimensional structure of the human copper transporter hCTR1. *Proc. Natl. Acad. Sci. USA*, **2009**, *106*, 4237-4242.
53. Eisses, J.F.; Kaplan, J.H. The mechanism of copper uptake mediated by human CTR1: a mutational analysis. *J. Biol. Chem.*, **2005**, *280*, 37159-37168.
54. Wu, X.; Sinani, D.; Kim, H.; Lee, J. Copper transport activity of yeast Ctr1 is downregulated via its C terminus in response to excess copper. *J. Biol. Chem.*, **2009**, *284*, 4112-4122.
55. Schmidt, P.J.; Kunst, C.; Culotta, V.C. Copper activation of superoxide dismutase 1 (SOD1) in vivo. *J. Biol. Chem.*, **2000**, *275*, 33771-33776.
56. Horn, D.; Barrientos, A. Mitochondrial copper metabolism and delivery to cytochrome c oxidase. *IUBMB Life*, **2008**, *60*, 421-429.
57. Inesi, G.; Pilankatta, R.; Tadini-Buoninsegni, F. Biochemical characterization of P-type copper ATPases. *Biochem. J.*, **2014**, *463*, 167-176.

58. Ruttakay-Nedecky, B.; Nejdl, L.; Gumulec, J.; Zitka, O.; Masarik, M.; Eckschalager, T.; Stiborova, M.; Adam, V.; Kizek, R. The role of metallothionein in oxidative stress. *Int. J. Mol. Sci.*, **2013**, *14*, 6044-6066.
59. Tumer, Z. An overview and update of ATP7A leading to Menkes disease and occipital horn syndrome. *Hum. Mutat.*, **2013**, *34*, 417-429.
60. Braiterman, L.T.; Murthy, A.; Jayakanthan, S.; Nyasae, L.; Tzeng, E.; Gromadzka, G.; Woolf, T.B.; Lutsenko, S.; Hubbard, A.L. Distinct phenotype of a Wilson disease mutation reveals a novel trafficking determinant in the copper transporter ATP7B. *Proc. Natl. Acad. Sci. USA*, **2014**, *111*, E1364-E1373.
61. Turski, M.L.; Thiele, D.J. New roles for copper metabolism in cell proliferation, signaling and disease. *J. Biol. Chem.*, **2009**, *284*, 717-721.
62. Bleackley, M.R.; MacGillivray, R.T.A. Transition metal homeostasis: from yeast to human disease. *BioMetals*, **2011**, *24(5)*, 785-809.
63. Zowczak, M.; Iskra, M.; Torlinski, L.; Cofta, S. Analysis of serum copper and zinc concentrations in cancer patients. *Biol. Trace Elem. Res.*, **2001**, *82*, 1-8.
64. Denoyer, M.; Masaldan, S.; La Fontaine, S.; Carter, M.A. Targeting copper in cancer therapy: "Copper that cancer". *Metallomics*, **2015**, *7*, 1459-1476.
65. Carmeliet, P. Angiogenesis in life, disease and medicine. *Nature*, **2005**, *438*, 932-936.
66. Jiang, Y.; Reynolds, C.; Xiao, C.; Feng, W.; Zhou, Z.; Rodriguez, W.; Tyagi, S.C.; Eaton, J.W.; Saari, J.T.; Kang, Y.J. Dietary copper supplementation reverses hypertrophic cardiomyopathy induced by chronic pressure overload in mice. *J. Exp. Med.*, **2007**, *204(3)*, 657-666.
67. Li, Q.; Ding, X.; Kang, Y.J. Copper promotion of angiogenesis in isolated rat aortic ring: role of vascular endothelial growth factor. *J. Nut. Bio.*, **2014**, *25*, 44-49.
68. Rigiracciolo, D.C.; Scarpelli, A.; Lappano, R.; Pisano, A.; Santolla, M.F.; De Marco, P.; Cirillo, F.; Cappello, A.R.; Dolce, V.; Belfiore, A.; Maggiolini, M.; De Francesco, E.M. Copper activates HIF-1α/GPER/VEGF signaling in cancer cells. *Oncotarget*, **2015**, *6*, 34158-34177.
69. Finney, L.; Mandava, S.; Ursos, L.; Zhang, W.; Rodi, D.; Vogt, S.; Legnini, D.; Maser, J.; Ikpatt, F.; Olopade, O.I.; Glesne, D. X-ray fluorescence microscopy reveals large-scale relocalization and extracellular translocation of cellular copper during angiogenesis. *Proc. Natl. Acad. Sci. USA*, **2007**, *104*, 2247-2252.
70. Tardito, S.; Marchiò, L. Copper compounds in anticancer strategies. *Curr. Med. Chem.*, **2009**, *16*, 1325-1348.
71. Krajčiováa, D.; Melníka, M.; Havráneka, E.; Forgácsováa, A.; Mikušab, P. Copper compounds in nuclear medicine and oncology. *J. Coord. Chem.*, **2014**, *67(9)*, 1493-1519.
72. Das, S.K.; Ray, K. Wilson's disease: an update. *Nat. Clin. Pract. Neurol.*, **2006**, *2*, 482-493.
73. Brem, S.; Grossman, S.A.; Carson, K.A.; New, P.; Phuphanich, S.; Alavi, J.B.; Mikkelsen, T.; Fisher, J.D. Phase 2 trial of copper depletion and penicilamine as antioangiogenesis therapy of glioblastoma. *Neuro-Oncol.*, **2005**, *7*, 246-253.
74. Santini, C.; Pellei, M.; Gandin, V.; Porchia, M.; Tisato, F.; Marzano, C. Advances in copper complexes as anticancer agents. *Chem. Rev.*, **2014**, *114*, 815-862.
75. Tjioe, L.; Meininger, A.; Joshi, T.; Spiccia, L.; Graham, B. Efficient plasmid DNA cleavage by copper(II) complexes of 1,4,7 triazacyclononane ligands featuring xylyl-linked guanidinium groups. *Inorg. Chem.*, **2011**, *50(10)*, 4327-4339.
76. Seng, H.L.; Wang, W.S.; Kong, S.M.; Alan Ong, A.H.K.; Win, J.F.; Raja Abd. Rahman, R.N.Z.; Chikira, M.; Leong, W.K.; Ahmad, M.; Khoo, A.S.B.; Ng, C.H. Biological and

cytoselective anticancer properties of copper(II)-polypyridil complexes modulated by auxiliary methylated glycine ligand. *BioMetals*, **2012**, *25*, 1061-1081.

77. Zeglis, B.M.; Divilov, V.; Lewis, J.S. Role of metalation in the Topoisomerase Iiα inhibition and antiproliferation activity of a series of α-heterocyclic-N4-substituted thiosemicarbazones and their Cu(II) complexes. *J. Med. Chem.*, **2011**, *54*, 2391-2398.
78. Milacic, V.; Chen, D.; Giovagnini, L.; Diez, A.; Fregona, D.; Dou, Q.P. Pyrrolidine dithiocarbamate-zinc(II) and copper(II) complexes induce apoptosis in tumor cells by inhibiting the proteasomal activity. *Toxicol. Appl. Pharmacol.*, **2008**, *231*, 24-33.
79. Beurskens, P.T.; Cras, J.A.; Steggerda, J.J. Structures and properties of dibromo-N,N-di-n-buthyldithiocarbamato complexes of copper(III) and gold(III). *Inorg. Chem.*, **1968**, *7(4)*, 810-813.
80. Hendrickson, A.R.; Martin, R.L.; Rhode, M.N. Dithiocarbamates of Cu(I), Cu(II) and Cu(III). An electrochemical study. *Inorg. Chem.*, **1976**, *15(9)*, 2115-2119.
81. Cras, J.A.; Willemse, J.; Gal, A.W.; Hummelink-Peters, B.G.M.C. Preparation, structure and properties of compounds containing the dipositive tri-copper hexa (N,N-di-n-buthyldithiocarbamato) ion, compounds with copper in the oxidation states II and III. *Recl. Trav. Chim. Pays-Bas*, **1973**, *92*, 641.
82. van de Leemput, P.J.H.A.M.; Willemse, J.; Cras, J.A. Preparation and properties of copper dithiocarbamate complexes with copper in the oxidation states I and III. *Recl. Trav. Chim. Pays-Bas*, **1976**, *95*, 53.
83. Nobel, C.I.; Kimland, M.; Lind, B.; Orrenius, S.; Slater, A.F. Dithiocarbamates induce apoptosis in thymocytes by raising the intracellular level of redox-active copper. *J. Biol. Chem.*, **1995**, *270*, 26202-26208.
84. Schenk, H.; Klein, M.; Erdbrugger, W.; Droge, W.; Schulze-Osthoff, K. Distinct effects of thioredoxin and antioxidants on the activation of transcription factors NK-kappa B and AP-1. *Proc. Natl. Acad. Sci. USA*, **1994**, *91*, 1672-1676.
85. Furuta, S.; Ortiz, F.; Zhu Sun, X.; Wu, H.H.; Mason, A.; Momand, J. Copper uptake is required for pyrrolidine dithiocarbamate mediated oxidation and protein level increase of p53 in cells. *Biochem. J.*, **2002**, *365*, 639-648.
86. Erl, W.; Weber, C.; Hansson, G.K. Pyrrolidine dithiocarbamate-induced apoptosis depends on cell type, density and the presence of Cu^{2+} and Zn^{2+}. *Am. J. Phys. Cell Phys.*, **2000**, *278*, C1116-C1125.
87. Cen, D.; Brayton, D.; Shahandeh, B.; Meyskens, F.L.; Farmer, P.J. Disulfiram facilitates intracellular Cu uptake and induces apoptosis in human melanoma cells. *J. Med. Chem.*, **2004**, *47*, 6914-6920.
88. Daniel, K.G.; Chen, D.; Orlu, S.; Cui, Q.C.; Miller, F.R.; Dou, Q.P. Clioquinol and pyrrolidine dithiocarbamate complex with copper to form proteasome inhibitors and apoptosis inducers in human breast cancer cells. *Breast Cancer Res.*, **2005**, *7*, R897-R908.
89. Murthy, N.N.; Karlin, K.D.; Bertini, I.; Luchinat, C. NMR and electronic relaxation in paramagnetic dicopper(II) compounds. *J. Am. Chem. Soc.*, **1997**, *119*, 2156-2162.
90. Brown, D. A.; Glass, W. K.; Burke, M. A. The general use of IR spectral criteria in discussions of the bonding and structure of metal dithiocarbamates. *Spectrochim. Acta, Pt. A: Mol. Spectrosc.* **1976**, *32,* 145-147.
91. Forghieri, F.; Graziosi, G.; Preti, C.; Tosi, G. Cyclic substituted dithiocarbamates as ligands. Vanadium(III) and oxovanadium(IV, V) complexes. *Transition Met. Chem.*, **1983**, *8*, 372-376.

92. Jorgensen, C.K. Absorption spectra of transition group complexes of Sulphur-containing ligands. *J. Inorg. Nucl. Chem.*, **1952**, *24*, 1571-1585.
93. Takami, F.; Wakahara, S.; Maeda, T. The UV spectra and dissociation constants of some dithiocarbamates (1). *Tetrahedron Lett.*, **1971**, *12(28)*, 2645-2648.
94. Vedis, M.V.; Schreiber, G.H.; Gough, T.E.; Palenik, G.U. Jahn-Teller distortions in octahedral copper(II) complexes. *J. Am. Chem. Soc.*, **1969**, *91(7)*, 1859-1860.
95. Choi, S.; Menzel, E.R.; Wasson, J.R. Electronic spectra of copper(II) dithiocarbamates. *J. Inorg. Nucl. Chem.*, **1977**, *39*, 417-422.
96. Carlin, R.L. Electronic spectra of transition metal complexes. *J. Chem. Ed.*, **1963**, *40(3)*, 135.
97. Leeson, P.D.; Springthorpe, B. The influence of drug-like concepts on decision-making in medicinal chemistry. *Nat. Rev. Drug Discov.* **2007**, *6(11)*, 881-890.
98. Esteves, F.; Moutinho C.; Matos, C. Correlation between octanol/water and liposome/water distribution coefficients and drug absorption of a set of pharmacologically active compounds. *J. Liposome Res.*, **2013**, *23(2)*, 83-93.
99. Mazzobre, M.F.; Romàn, M.V.; Mourelle, A.F.; Corti, H.R. Octanol-water partition coefficient of glucose, sucrose, trehalose. *Carbohydr. Res.*, **2005**, *340*, 1207-1211.
100. Wilson, J.J.; Lippard, S.J. In Vitro Anticancer Activity of cis-Diammineplatinum(II) Complexes with β-Diketonate Leaving Group Ligands. *J. Med. Chem.*, **2012**, *55(11)*, 5326-5336.

CHAPTER THREE

IN VITRO SCREENINGS OF THE SYNTHESIZED METAL DITHIOCARBAMATES

In the preclinical development of potential new drugs, the first step is the use of cell models to assess the biological activity and cancer cell lines have been widely used for research purposes[1,2] In particular, one of the aims of this PhD work is the evaluate the activity of the different metal dithiocarbamato complexes, in order to generate proof-of-concept data for future preclinical studies. In the light of this, all the synthetized complexes presented in the **Chapter 1 and 2** have been tested for their cytotoxic activity against Human colorectal carcinoma cell line, called HCT-116. This cancer cell model has been selected since it is one of the most commonly used human cancer cell line for preclinical screening. Remarkably, the colorectal carcinoma is to date the fourth most prevalent cancer in women and men below 49 years old and the second most frequent cause of cancer death in Italy for both sexes.[3,4] Several factors such as poor-quality diet, lack of physical activity, obesity, cigarette smoking and heavy alcohol consumption are associated with an increased risk of colorectal cancer.[5] An individual with a history of adenomatous polyps or inflammatory bowel disease has an increased risk of developing colorectal cancer compared to an individual with no history of either.[6] Colorectal cancer includes malignant growths from the mucosa of the colon and rectum. Cancer cells may eventually spread to nearby lymph nodes and subsequently to more remote lymph nodes and other organs in the body like the liver and lungs, among others. The treatment, prognosis and survival rate largely depend on the stage of disease at diagnosis. Screening for colorectal cancer is particularly effective. Screening can prevent cancer from occurring as it can detect adenomatous polyps that can be successfully removed.[7] Treatment for colorectal cancer varies by tumor location and stage at diagnosis. Surgical removal of tumor and nearby lymph nodes is the most common treatment for early stage (stage I or II) colorectal cancer. For patients with late-stage disease, chemotherapy alone or in combination with radiation therapy is often administered before or after surgery. Regarding chemotherapy, the first-in-class treatment for this type of cancer consists in 5-fluorouracil (5-FU).[4] However, as the response to 5-FU first line mono-therapy is often low, it is given in combination with other cytotoxic agents, like oxaliplatin and irinotecan.[4]

For our purposes, HCT-116 cells (American Type Culture Collection, ATCC) were cultured in 75 cm^2 cell culture flasks in Low Glucose Dulbecco's modified Eagle's medium (LD-MEM), with addition of Fetal Bovine Serum (FBS) (10%), L-glutamine (5 mM), streptomycin (100 μg/mL), and penicillin (100 units/mL) (Sigma-Aldrich), and incubated at 37 °C in a 5% carbon dioxide-controlled atmosphere.

For the cytotoxicity assay, the medium was removed from the flask, and the cells washed with 6 mL of PBS, and then shook in presence of 1 mL of trypsin (Sigma-Aldrich), with 3 minutes-incubation. D-MEM was successively added, and the obtained cellular suspension seeded in 96-well microplates ($8 \cdot 10^3$ cells/well) in the growth medium (200 μL), and incubated at 37 °C in a 5% CO_2 atmosphere for 24 h to allow cell adhesion, prior to drug testing.

3.1 Sample preparation for in vitro studies

Due to a poor aqueous solubility, the 1:1 piperidine dithiocarbamato gold(III) compounds, the double-complex salts [1:2][$AuCl_2$] and [1:2][$AuCl_4$] and the 1:1 glycosylate dithiocarbamato Au(III) derivatives synthetized in this work were dissolved in DMSO (sterile-filtered, Sigma-Aldrich) just before the experiments. Moreover, the resulted solutions of the di-halo complexes were protected from light until the final dilution to the medium in order to prevent the rearrangement equilibrium. Regarding the ionic Au(III) complexes of the type [1:2]Cl and the Cu(II) glycosylated dithiocarbamates, which are water-soluble, were dissolved in saline solution (NaCl 0.9% *w/v*).

All the compounds were tested against the abovementioned cancer cell line at different micromolar concentrations to obtain the dose-response plots. Briefly, the metal derivatives were dissolved in the appropriate solvent at the concentration of 50 mM, 25 mM, 10 mM, 5 mM, 2 mM, 1 mM and 0.5 mM. Successively, one μL of each solution was dissolved in 999 μL of cell culture medium (LG-DMEM), to yield the following final concentrations of metal complex: 50 μM, 25 μM,10 μM, 5 μM, 2 μM, 1 μM and 0.5 μM. This procedure allows a DMSO concentration of 0.1% *v/v* in the growth medium, which has no effect on cell vitality.[8] After the preparation of the 96-well plates, containing 8000 cells each, the medium was removed and replaced with the fresh one containing the compounds to be studied at increasing concentrations. Triplicate conditions were established for each treatment and at least three independent experiments were carried out for each compound.

Mithocondrial cell vitality was evaluated by means of resazurin assay. This method exploits the effect of the blue dye resazurin (7-hydroxy-10oxidophenoxazin-10-ium-3-one, Sigma-Aldrich) which is oxidized by mitochondrial enzymes of metabolic active cells to the pink resorufin (7-hydroxy-3H-phenoxazin-3-one).[9] To perform the assay, the entire volume of incubation medium was removed after 72 hours from the treated wells, and 100 µL/well of a 10% resazurin solution in LG-DMEM were added and incubated for 2 hours at 37 °C. Mithocondrial vitality was determined by absorbance measurements at 590 nm as follows:

$$\%\boldsymbol{vitality} = \frac{\frac{\mathbf{1}}{\sum \boldsymbol{Abs}_{\boldsymbol{treated\ cells}}} - \frac{\mathbf{1}}{\sum \boldsymbol{Abs}_{\boldsymbol{resazurin\ blank}}}}{\frac{\mathbf{1}}{\sum \boldsymbol{Abs}_{\boldsymbol{control\ cells}}} - \frac{\mathbf{1}}{\sum \boldsymbol{Abs}_{\boldsymbol{resazurin\ blank}}}} \times \mathbf{100}$$

The control cells are those treated with cell culture medium containing only the vehicle, DMSO or saline solution) in the percentage of 0.1% *v/v*. The obtained cell viabilities have been plotted against the compound concentration to determine the IC_{50} (concentration of the test agent inducing 50% reduction in cell number compared with control cell cultures). The final IC_{50} values and their standard deviations were evaluated from the data coming from at least three independent experiments (**Table 3.1 and 3.2**). For comparison purposes, the cytotoxicity of cisplatin (dissolved in saline solution) was evaluated under the same experimental conditions. In this regard, it should be underlined that the experiments have been performed over a period of 72 hours since this is the time necessary to cisplatin to explicate its activity.

3.2 *In vitro* cytotoxicity studies of the Au(III) PipeDTC derivatives

Overall, five complexes with stoichiometric metal-to-DTC ligand ratio 1:1 and three 1:2 have been tested against HCT-116 human colorectal carcinoma cell line. Remarkably, seven of them demonstrated a good micromolar activity, higher to that of cisplatin.

Table 3.1: calculated IC_{50} values (μM) of the synthetized Au(III) complexes, compared to that of Cisplatin. The mithocondrial vitality essays were carried out against HCT-116 tumor cell line, 8000 cells/well, over 72h of exposure.

COMPOUND	**IC_{50} μM**	**standard deviation**
$[Au^{III}Cl_2(PipeDTC)]$	4.4	± 0.2
$[Au^{III}Br_2(PipeDTC)]$	2.7	± 0.3
$[Au^{III}I_2(PipeDTC)]$	1.3	± 0.2
$[Au^{III}(PipeDTC)_2]Cl$	6.24	± 0.05
$[Au^{III}(PipeDTC)_2][Au^{I}Cl_2]$	1.4	± 0.6
$[Au^{III}(PipeDTC)_2][Au^{III}Cl_4]$	1.3	± 0.7
$[Au^{III}BrCN(PipeDTC)]$	1.6	± 0.4
$[Au^{III}Me_2(PipeDTC)]$	Inactive below 75 μM	
Cisplatin – $[Pt^{II}Cl_2(NH_3)_2]$	10.2	± 0.6

The dimethyl Au(III) dithiocarbamate is the only compound that do not show any cytotoxic effect, even at a concentration of 75 μM, confirming the fact that 1:1 derivatives with organic substituent possess different electronic properties that could prevent the interaction between the complex and the biological targets. On the contrary, the cyano-bromo derivative, that is more structurally and electronically close to the di-halo complexes, is active at low micromolar concentrations.

Furthermore, as shown in the table above, the 1:1 di-halo compounds have interesting cytotoxic properties with IC_{50} values diminishing on passing from the chloro- to bromo- to iodo-complex. These results might be ascribable to the higher lipophilicity of the $[Au^{III}I_2(PipeDTC)]$ with respect to the other halogen derivatives accounting for a greater affinity with the phospholipid bilayer. It is important to note that their different tendency to establish the rearrangement equilibrium in DMSO (the iodo-complex is stable in coordinating solvents) do not seem to be correlated to the cytotoxic effect of the 1:1 complexes. On the other hands, the ionic 1:2 compounds showed a substantial difference in activity on passing from the water-soluble $[Au^{III}(PipeDTC)_2]Cl$ to the lipophilic double salts (see **Chapter 1**, **Section 1.3.3**). In particular, the former possesses an IC_{50} value of 6.25 μM, six time higher to those of $[Au^{III}(PipeDTC)_2][Au^{I}Cl_2]$ and $[Au^{III}(PipeDTC)_2][Au^{III}Cl_4]$. Comparing the activity of the double salts, it is evident that the oxidation state of the Au center in the counterion has no effects on the biological activity.

To sum up, it is possible to state that the more lipophilic is the complex, the higher are its cytotoxic properties toward cancer cell and the two classes of compounds, with 1:1 and 1:2 stoichiometric ratios, are both active in vitro, but probably toward different intracellular or extracellular targets and with different mechanisms of action.

3.3 *In vitro* cytotoxicity studies of the Au(III) and Cu(II) glycosylated-DTC derivatives

One of the aims of this Ph.D. work has been the selection of one or more Lead Compound(s) from the library of new metal dithiocarbamato complexes containing a targeting moiety, to generate proof-of-concept data for future preclinical studies. Hence, all the compounds synthesised in **Chapter 2** have been tested against HCT-116 human colorectal carcinoma cell line and the results are summarized below (**Table 3.2**).

Table 3.2: IC_{50} cytotoxicity values (μM) on HCT-116 cancer cells (72h, 8000 cell/well).

	COMPOUND	**IC_{50} (μM)**
Cu^{II}	$[Cu^{II}(pipe\text{-}DTC)_2]$	1.8 ± 0.1
	$[Cu^{II}(DTC\text{-}\beta\text{-}D\text{-}glucose)_2]$	**2.7 ± 0.4**
	$[Cu^{II}(DTC\text{-}\beta\text{-}D\text{-}galactose)_2]$	inactive (>50)
	$[Cu^{II}(DTC\text{-}\alpha\text{-}D\text{-}mannose)_2]$	inactive (>50)
Au^{III}	$[Au^{III}(pipe\text{-}DTC)_2]Cl$	6.24 ± 0.05
	$[Au^{III}(DTC\text{-}\beta\text{-}D\text{-}glucose)_2]Cl$	inactive (>50)
	$[Au^{III}(DTC\text{-}\beta\text{-}D\text{-}galactose)_2]Cl$	inactive (>50)
	$[Au^{III}(DTC\text{-}\alpha\text{-}D\text{-}mannose)_2]Cl$	inactive (>50)
	Cisplatin - $[Pt^{II}Cl_2(NH_3)_2]$	10.2 ± 0.6

From the collected biological data, it is interesting to note that the synthesized compound with a sugar pending targeting molecule show a lower cytotoxic activity compared to the alkyl non-targeted derivatives. In particular, the new Au(III) complexes of the three different monosaccharides seem to be inactive with a IC_{50} higher than 50 μM. These results might suggest that the Au(III) complexes are not good substrates for GLUT proteins, probabily due to steric hindrance, and, as a consequence, they cannot pass the phospholipid bilayer through an active transport. Moreover, the elevated hydrophilicity of the compounds can prevent also their passive penetration into cytoplasm and so their interaction with intracellular target. On

the other hands, the water-soluble Cu(II) complex with O-glucoside-linked dithiocarbamato ligand, shows a low micromolar cytotoxic activity. Intriguingly, neither the D-galactose nor the D-mannose derivatives show comparable results.

Then, the [Cu^{II}(DTC-β-D-glucose)$_2$] was chosen as lead compound. Moreover, in order to determine if the selected compound selectively target one or more transporter proteins in the cell membrane, cells were exposed for 72h to two different well-known GLUT inhibitors, that were added together with the lead compound to the culture medium in selected wells. The first is the *O-ethylidene-α-D-Glucose*, used as GLUT-1 inhibitor at a concentration of 10mM,[10,11] and the second is *Phlorizin dihydrate* that irreversibly binds the active site of SGLT transporter proteins at 1mM (see **Introduction**, **Figure 17**).[12,13] Furthermore, in order to evaluate the competitiveness with the drug (as GLUT substrate) of other carbohydrates, D-glucose at a concentration of 50 mM has been added to the medium in selected well together with the lead compound. The results of the mithocondrial vitality tests in presence of the inhibitors and the competitor are reported in **Table 3.3**.

Table 3.3: IC_{50} cytotoxicity values (μM) of [Cu^{II}(DTC-β-D-glucose)$_2$] complex on HCT-116 cancer cells (72h, 8000 cell/well), alone or in presence of inhibitors/competitor.

	INHIBITOR OR COMPETITOR			
COMPOUND	Only medium (1mM D-Glucose)	Phlorizin dihydrate (1mM) *GLUT1 inhibitor*	O-ethylidene α-D Glucose (10 mM) *SGLT inhibitor*	D-Glucose (50mM)
[Cu^{II}(DTC-β-D-glucose)$_2$]	2.7 ± 0.4	2.6 ± 0.2	2.1 ± 0.2	2.0 ± 0.1

The data highlight that no inhibition of the activity was detected after the addition of the target inhibitors or the competitor. Moreover, although minor decrements on the IC_{50} concentrations are observed, the differences between the values are too small to get information about a possible active transport involved in the mechanism of action of our copper(II) glucose derivative.

To sum up, a new class of dithiocarbamato complexes containing a carbohydrate moiety as targeting agent has been designed, synthetized, characterized and *in vitro* tested as active antitumor molecules. The synthetic conditions were optimized for three different monosaccharides and the desired complexes were obtained in good yield and purity.

Important biological results were achieved with [Cu^{II}(DTC-β-D-glucose)$_2$] compound that shows an interesting IC_{50} toward HCT-116 human colorectal carcinoma cell line. Unfortunately, the first experiments designed to obtain some important information about the targeting effect of the carbohydrate functionalization did not give any useful results. However, other important proof-of-concept experiments are planned for the next future.

Bibliography

1. Lovitt, C.J.; Shelper, T.B.; Avery, V.M. Advanced cell culture techniques for cancer drug discovery. *Biology*, **2014**, *3*, 345-367.
2. Jia, L.; Liu, X. The conduct of drug metabolism studies considered good practice (II): *in vitro* experiments, *Curr. Drug. Metab.* **2007**, *8*, 822-829.
3. AIOM and AIRTUM Associations; *I Numeri del Cancro in Italia*; Intermedia Editore: Roma, **2016**.
4. Kuipers, E.J.; Grady, W.M.; Sufferlein, T.D.L.; Sung, J.J.; Boelens, P.G.; van de Velde, C.H.J.; Watanabe, T. Colorectal cancer. *Nat. Rev. Dis. Primers*, **2015**, *1(15065)*, 10.1038/nrdp.2015.65
5. Haggar, F.A.; Boushey, R.P. Colorectal Cancer Epidemiology: Incidence, Mortality, Survival, and Risk Factors. *Clin. Colon Rectal Surg.* **2009**, *22(4)*, 191-197.
6. Bonnington, S.N.; Rutter, M.D. Surveillance of colonic polyps: Are we getting it right? *World J. Gastroenterol.* **2016**, *22(6)*, 1925-1934.
7. Bradshaw, N.; Holloway, S.; Penman, I.; Dunlop, M.G.; Porteous, M.E.M. Colonoscopy surveillance of individuals at risk of familial colorectal cancer. *Gut.* **2003**, *52(12)*, 1748-1751.
8. Da Violante, G.; Zerrouk, N.; Richard, I.; Provot, G.; Chaumeil, J.C.; Arnaud, P. Evaluation of the cytotoxicity effect of dimethyl sulfoxide (DMSO) on Caco2/TC7 colon tumor cell cultures. *Biol. Pharm. Bull.* **2002**, *25(12)*, 1600-1603.
9. O'Brien, J.; Wilson, I.; Orton, T.; Pognan, F. Investigation of the Alamar Blue (resazurin) fluorescent dye for the assessment of mammalian cell cytotoxicity. *Eur. J. Biochem.* **2000**, *267*, 5421-5426.
10. Rumsey, S.C.; Kwon, O.; Xu, G.W.; Burant, C.F.; Simpson, I.; Levine, M. Glucose Transporter Isoforms GLUT1 and GLUT3 Transport Dehydroascorbic Acid. *J. Biol. Chem.*, **1997**, *272*, 18982-18989.
11. Patra, M.; Johnstone, T.C.; Suntharalingam, K.; Lippard, S.J. A potent glucose-platinum conjugate exploits glucose transporter and preferentially accumulates in cancer cells. *Angew. Chem. Int. Ed.*, **2016**, *55(7)*, 2550-2554.
12. Malhotra, A.; Kudyar, S.; Gupta, A.K.; Kudyar, R.P.; Malhotra, P. Sodium glucose co-transporter inhibitors – A new class of old drugs. *Int. J. Appl. Basic Med. Res*., **2015**, *5(3)*, 161-163.
13. Liu, P.; Lu, Y.; Gao, X.; Liu, R.; Zhang-Negrerie, D.; Shi, Y.; Wang, Y.; Wanga, S.; Gao, Q. Highly water-soluble platinum(II) complexes as GLUT substrates for targeted therapy: improved anticancer efficacy and transporter-mediated cytotoxic properties. *Chem. Commun.*, **2013**, *49*, 2421-2423.

Concluding Remarks

During this three-years research, several complexes with dithiocarbamato ligands were synthetized, characterized and *in vitro* studied in order to test their anticancer properties. The first part of the project was focused on the detailed investigation of the solution chemistry of the Au(III) derivatives with piperidine dithiocarbamato as model ligand (metal:DTC-ligand stoichiometry 1:1 and 1:2). The first group is characterized by complexes bearing one dithiocarbamato residue and two anionic ligands in trans position which could be halides, cyanide or organometallic anions. In this work, we have obtained 5 different Au(III) 1:1 compounds, three di-halo derivatives (with two chloride, bromide and iodide substituents), one with mixed ligands, one bromide and one cyanide group respectively, and one organometallic complex, bearing two pure σ-donor methyl groups. Moreover, three different 1:2 cationic complexes were synthetized, differing each other by the nature of the anionic counterion. In fact, it could be a simple halide, such as chloride, or a complex itself. In the latter case, the obtained compounds are called "double-complex salts" (DCS). As a matter of facts, two different DCS were isolated, one with the linear $[Au^{I}Cl_2]^-$ counterion and the other with the square planar $[Au^{III}Cl_4]^-$ counterion. Intriguingly, as a result of the detailed investigation of their solution chemistry, we were able to characterize for the first time two distinct equilibria that connect the 1:1 di-halo species with the $[1:2][Au^{III}X_4]$ ones, by means of UV-Vis spectroscopy. In particular, it was found that, if the 1:1 di-chloro and di-bromo complexes are dissolved in coordinating solvents (*e.g.*, DMSO, alcohols and water) and irradiated by light, a rearrangement process takes place, converting the neutral complex into two equivalents of the ionic and better-solvated $[1:2][Au^{III}X_4]$ counterpart. The role played by the light irradiation in the whole process was investigated keeping a DMSO solution containing the 1:1 di-halo complex in dark, evaluating its UV-Vis spectrum after 72 hours from the initial dissolution and comparing the obtained data with those registered for an equimolar solution under light irradiation. No changes in the diagnostic bands were recorded over 72 h in dark, while, for the irradiated solution, a gradual transformation of the absorptions was detected in the same time lapse. At the end of the process (quantitative after 72 h) the final spectrum perfectly overlaps that of the $[1:2][Au^{III}X_4]$ complex in the same solvent.

On the contrary, if the [1:2][$Au^{III}X_4$] compounds are dissolved in a non-coordinating solvent, such as $CHCl_3$, CH_2Cl_2 or CH_3CN, the opposite equilibrium becomes energetically favored, transforming the ionic derivative into 0.5 equivalents of the neutral one. In this circumstance, the light irradiation is not necessary to prompt the equilibrium toward the products. At the best of our knowledge, this is one of the rare examples of dynamic and tunable inorganic system ever detected.

A mechanistic investigation is also presented in this work, highlighting the crucial role of the solvent in the rearrangement process which probably interact with the metal center, due to its coordinating ability, through the empty $6p_z$ orbital, triggering the formation of a bridged intermediate between the two Au(III) ions that decompose into the products.

Further investigations managed us to better understand the role of the opposite-ligands in the 1:1 complexes in the rearrangement process. In particular, the 1:1 di-iodo complex seemed to be perfectly stable in coordinating solvents under light irradiation, probably thanks to the extremely polarizable nature of the two iodides that are able to electronically stabilize the metal ion, preventing its interaction with the solvent. On the other hands, the lower reduction potential of the iodine with respect to gold(III), eases the reduction of the complex forming Au(I)-DTC derivatives and I_2 as products after about 72 h upon dissolution. Also the Au(III) 1:1 complex bearing a bromide and a cyanide as trans ligands undergoes the rearrangement process in coordinating solvent, forming the stable [1:2][$Au^{III}Br_2CN_2$]. On the other hands, the organometallic dimethyl derivative seems to be perfectly stable in all solvents, probably due to the instability of the [$Au^{III}Me_4$] anion and the σ-donor nature of the alkyl ligands which are not able to act as bridging ligands, as required in the rearrangement mechanism.

All the synthetized complexes were tested in vitro toward the HCT-116 human colorectal carcinoma cell line. With the exception of the [$Au^{III}Me_2$(PipeDTC)] compound, they showed interesting IC_{50} values, in the low micromolar range. In particular, the hydrophobicity of the complexes seems to be correlated with a higher activity.

The second part of the Ph.D. research work was focused on the synthesis, characterization and biological evaluation of novel bio-conjugated Au(III) and Cu(II) complexes with the aim of selectively deliver the cytotoxic metal-dithiocarbamato moiety into the tumor tissue, accumulating the anticancer payload into malignant cells. In order to reach this goal, carbohydrates were chosen as targeting agents, exploiting the Warburg effect, that stimulates

the majority of the neoplastic cells to overexpress the glucose-transporter proteins (in particular GLUTs) in their phospholipid bilayer. Taking into account the versatility of the GLUT proteins wich possess a high binding constant for different monosaccharides, we decided to functionalize the dithiocarbamato moiety with three different carbohydrates: D-glucose, D-galactose and D-mannose. On the whole, nine different complexes were synthetized, functionalizing the C-1 position of the sugars with a secondary-amine-pending spacer through a glycosylation reaction. After the transformation of the amines into dithiocarbamates, we isolated and characterized the corresponding ligands. Then, we prepared six Au(III) derivatives, three with metal:DTC-ligand stoichiometry 1:1, each of those bearing a different monosaccharide, and three complexes of the type [1:2]Cl. Moreover, also three neutral Cu(II) [1:2] coordination compounds were obtained. In particular, the Au(III) [1:2] and Cu(II) derivatives are water-soluble with a negative logP (-1.9 and -1.2, respectively). Except the 1:1 compounds, which undergo rearrangement process (like the corresponding piperidine dithiocarbamato complexes), all other bio-conjugated coordination compounds are stable in saline solution. Intriguingly, only [Cu^{II}(DTC-β-D-glucose)] complex is active toward the HCT-116 cells with a IC_{50} around 2.7 μM. The inactivity of the other synthetized Au(III) products is probably due to the high hydrophilicity of such molecules imparted by the carbohydrate moiety that prevent them to interact with phospholipidic membrane of cancerous cells.

The [Cu^{II}(DTC-β-D-glucose)] derivative was also tested as GLUT1 and SGLT substrate, adding the corresponding protein inhibitor into the cell culture medium. In addition, the competition between the investigated complex and D-glucose was evaluated. Unfortunately, no inhibition of the activity was detected in all the performed experiments. Therefore, other biological tests to better elucidate the mechanism of action of this compound are planned for the next future.

The data collected in this work along with other research results have led our group to file two Italian Patent applications (filing date: December 2nd, 2016) titled “Composti di coordinazione, sintesi, nanoformulazione ed uso degli stessi in oncologia” (102016000122363; 102016000122406). On the basis of these achievements, at the end of the 3rd -PhD year, the bureaucratic procedures to found a new startup company have been accomplished (approved by the Department of Chemical Sciences of the University of

Padova, in date January 25th, 2017 and by the Spin-Off Committee of the University of Padova in date April 5th, 2017) to transfer the acquired knowledge into advanced preclinical testing.

SUPPORTING INFORMATION

Supporting Information A: **1H-NMR spectra of the synthetized piperidine dithiocarbamato ligand and Au(III) complexes**

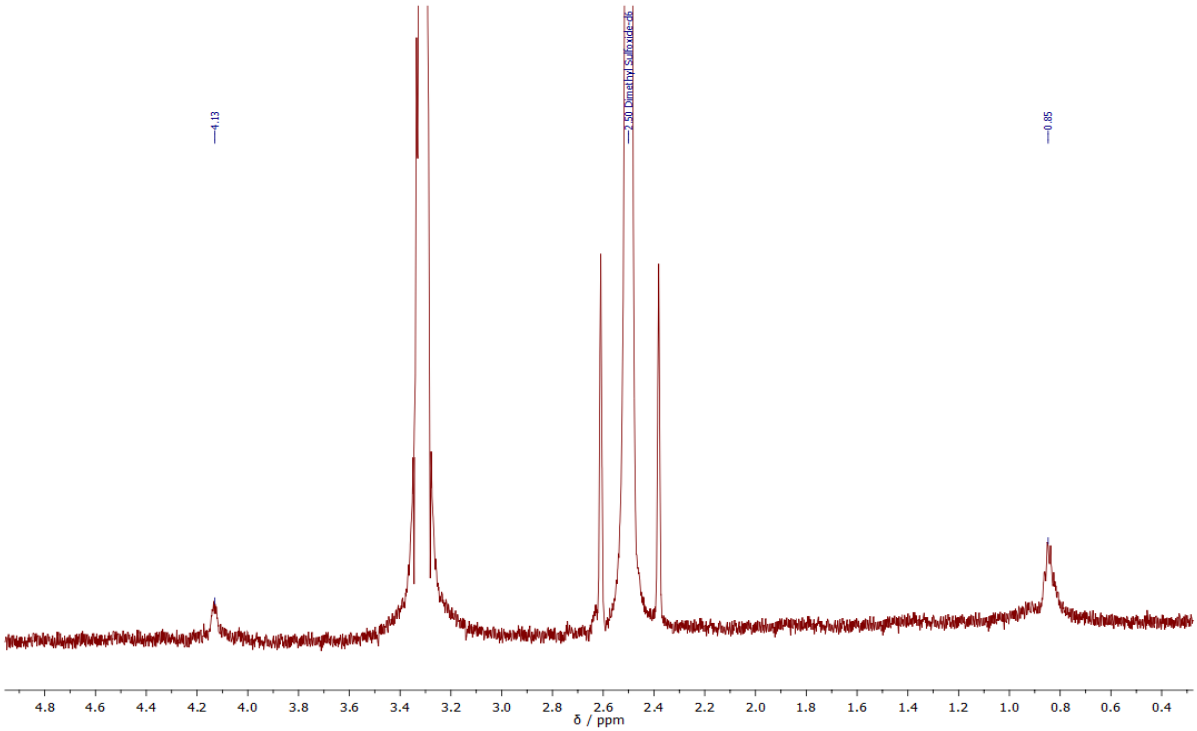

Figure A1. ^{1}H-NMR (DMSO-d6, 300 MHz) spectrum of bis(piperidine dithiocarbamate)digold(I), [Au_2(PipeDTC)$_2$].

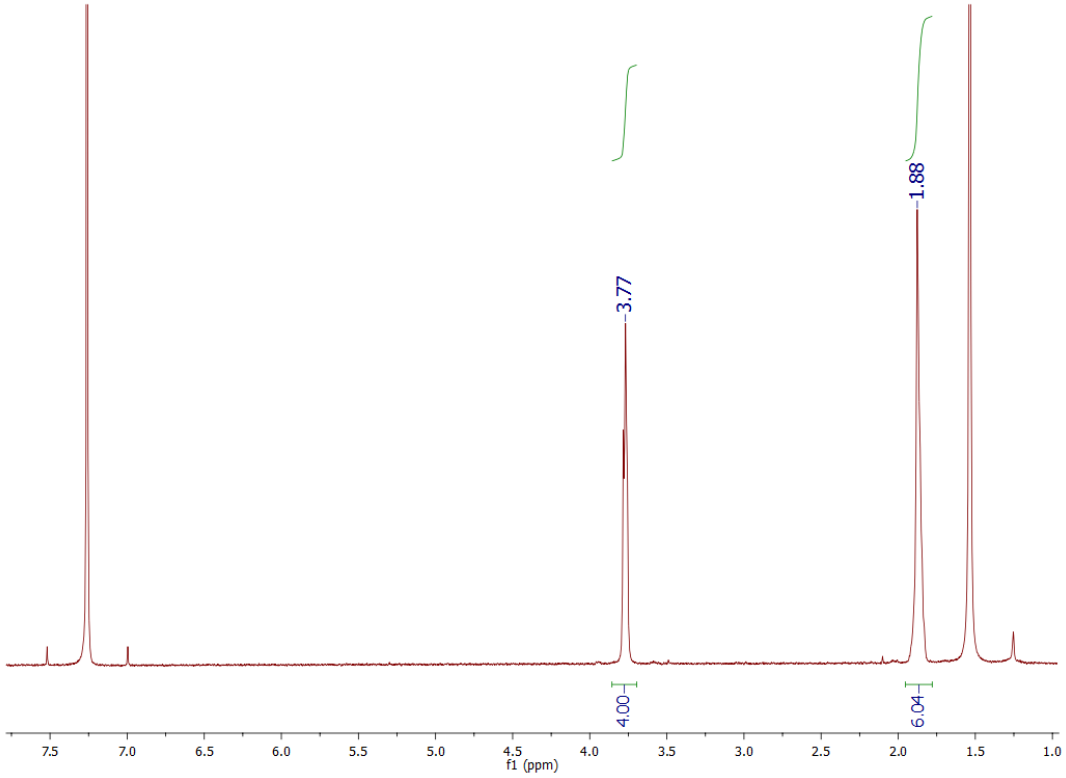

Figure A2. ^{1}H-NMR ($CDCl_3$, 600 MHz) spectrum of dichloro(piperidine dithiocarbamate)gold(III), [$AuCl_2$(PipeDTC)].

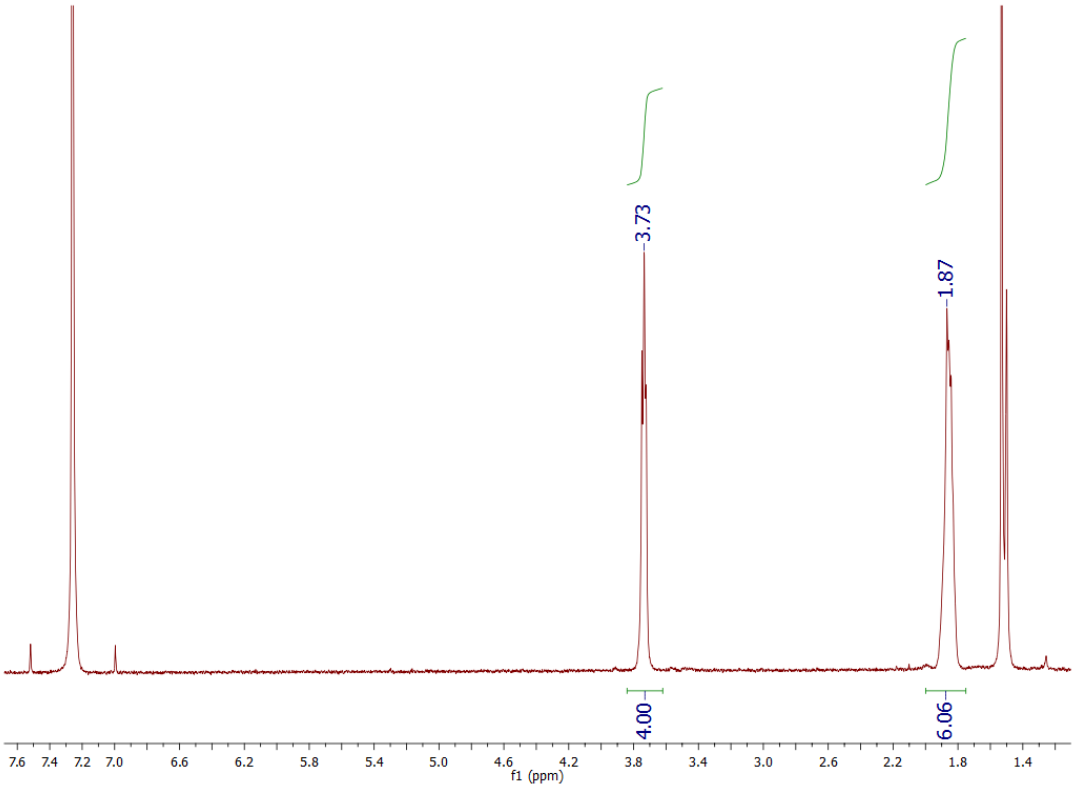

Figure A3. ^{1}H-NMR ($CDCl_3$, 600 MHz) spectrum of dibromo(piperidine dithiocarbamate)gold(III), [$AuBr_2$(PipeDTC)].

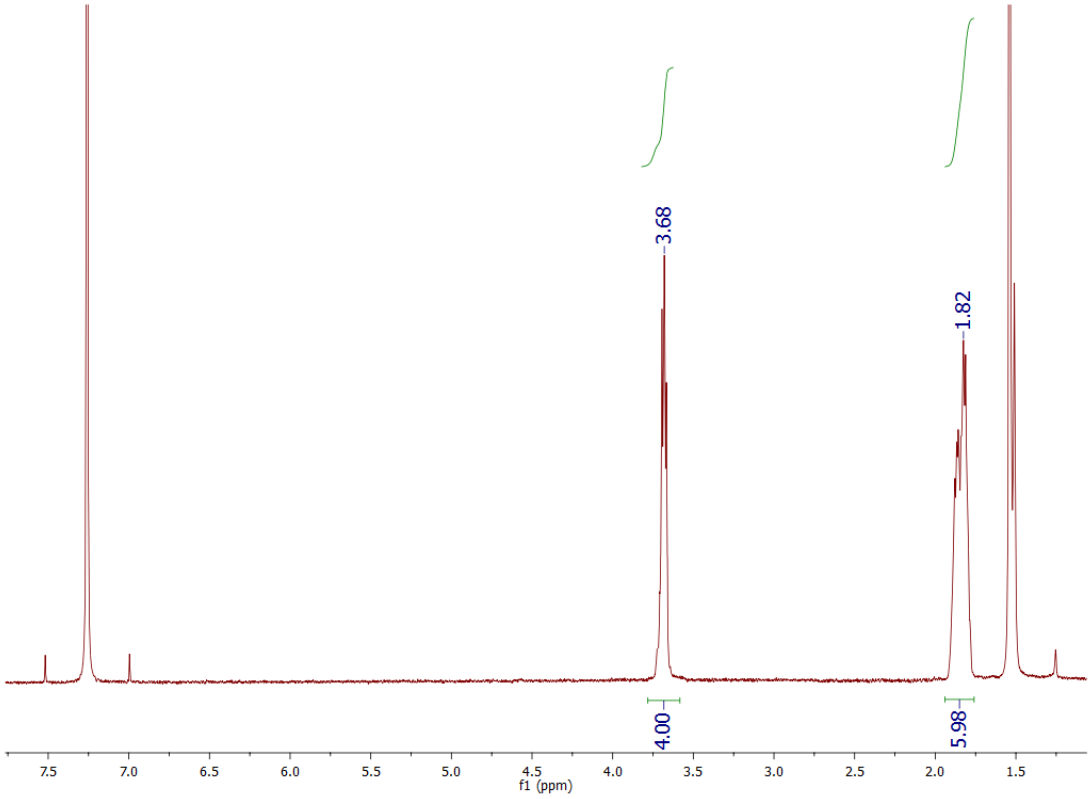

Figure A4. ^{1}H-NMR ($CDCl_3$, 600 MHz) spectrum of diiodo(piperidine dithiocarbamate)gold(III), [AuI_2(PipeDTC)].

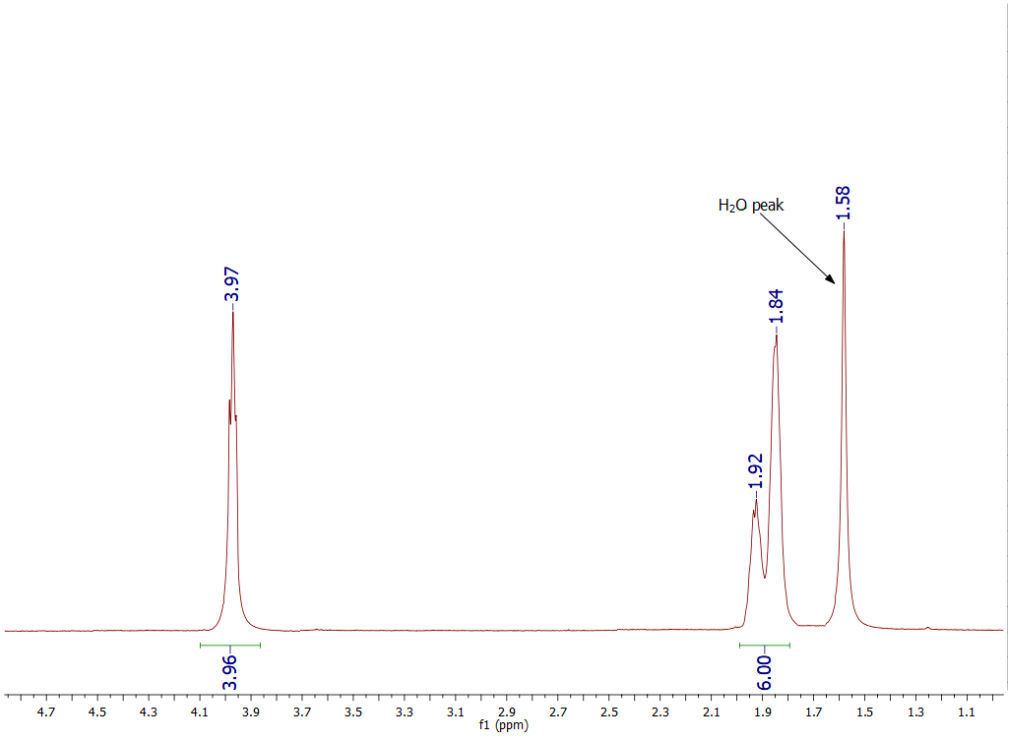

Figure A5. ^{1}H-NMR ($CDCl_3$, 600 MHz) spectrum of bis-(piperidine dithiocarbamate)gold(III) chloride, [Au(PipeDTC)$_2$]Cl.

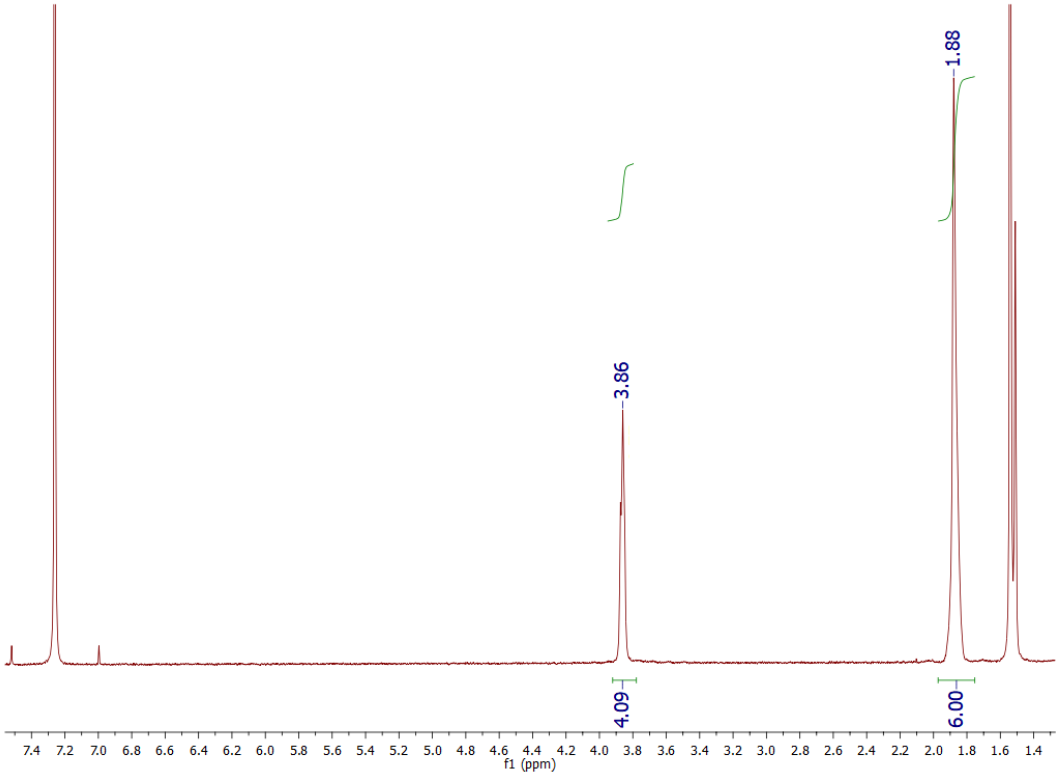

Figure A6. ^{1}H-NMR ($CDCl_3$, 600 MHz) spectrum of bis-(piperidine dithiocarbamate)gold(III) dichloro aurite(I), $[Au(PipeDTC)_2][AuCl_2]$.

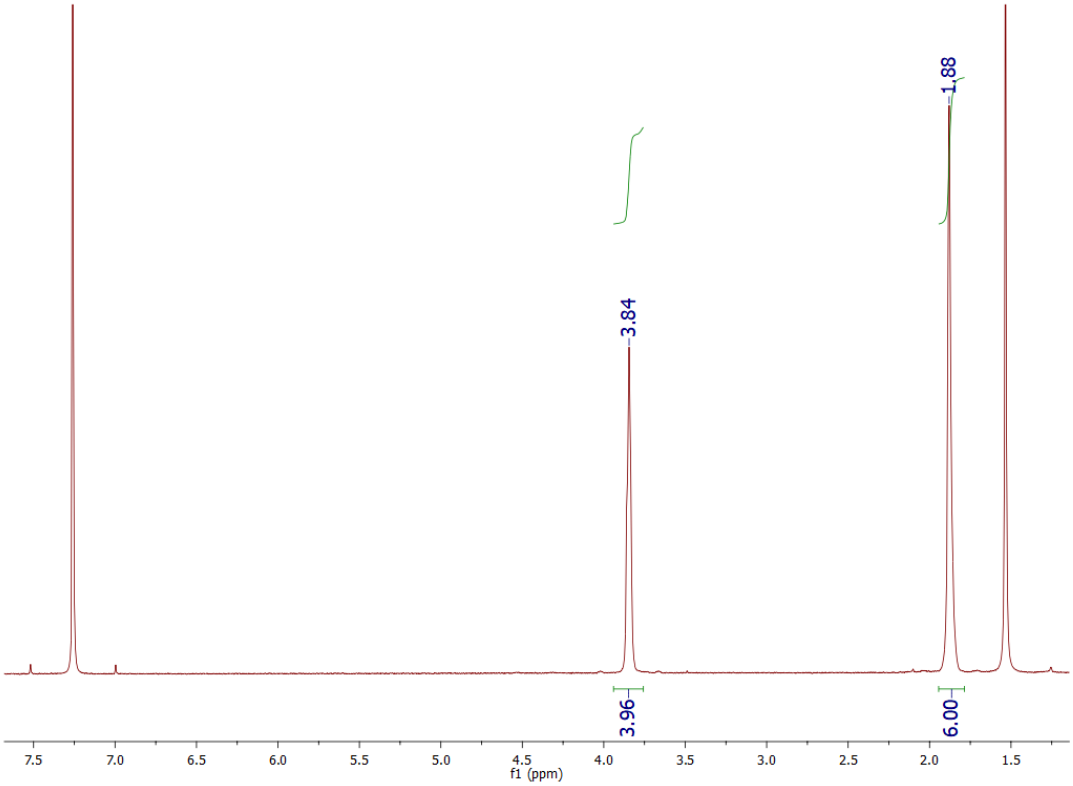

Figure A7. ^{1}H-NMR ($CDCl_3$, 600 MHz) spectrum of bis-(piperidine dithiocarbamate)gold(III) tetrachloro aurate(III), $[Au(PipeDTC)_2][AuCl_4]$.

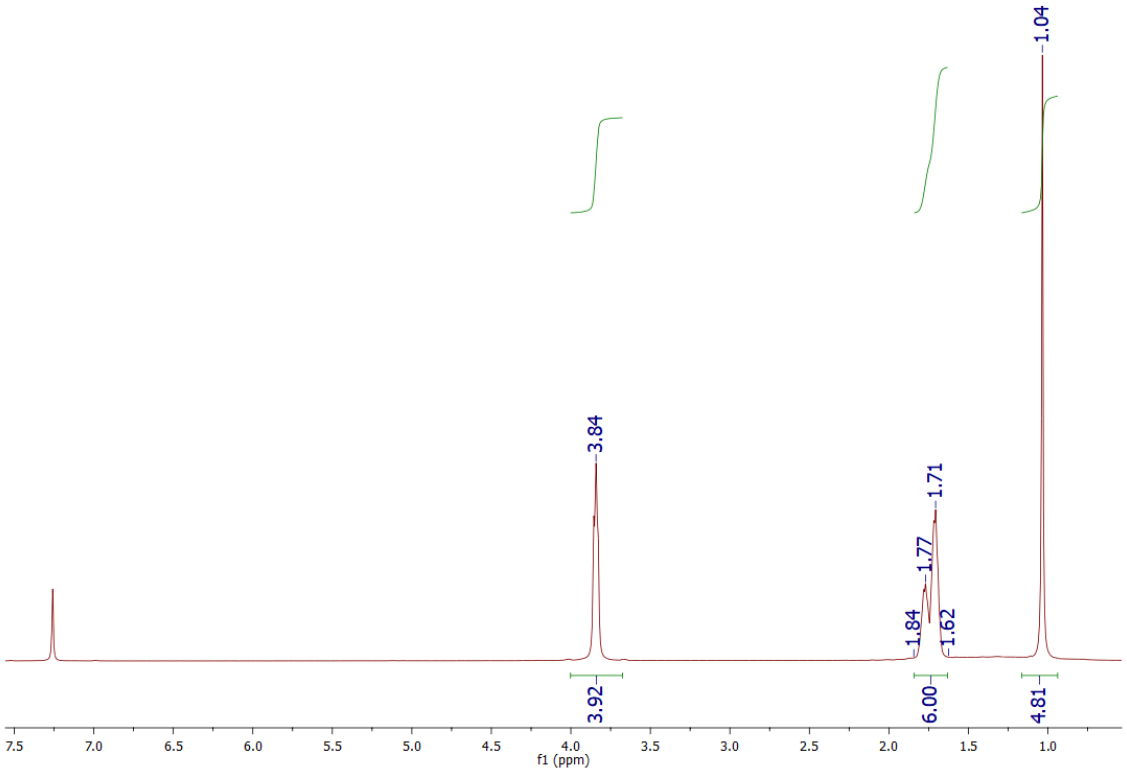

Figure A8. ^{1}H-NMR ($CDCl_3$, 600 MHz) spectrum of dimethyl(piperidine dithiocarbamate)gold(III), [$AuMe_2$(PipeDTC)].

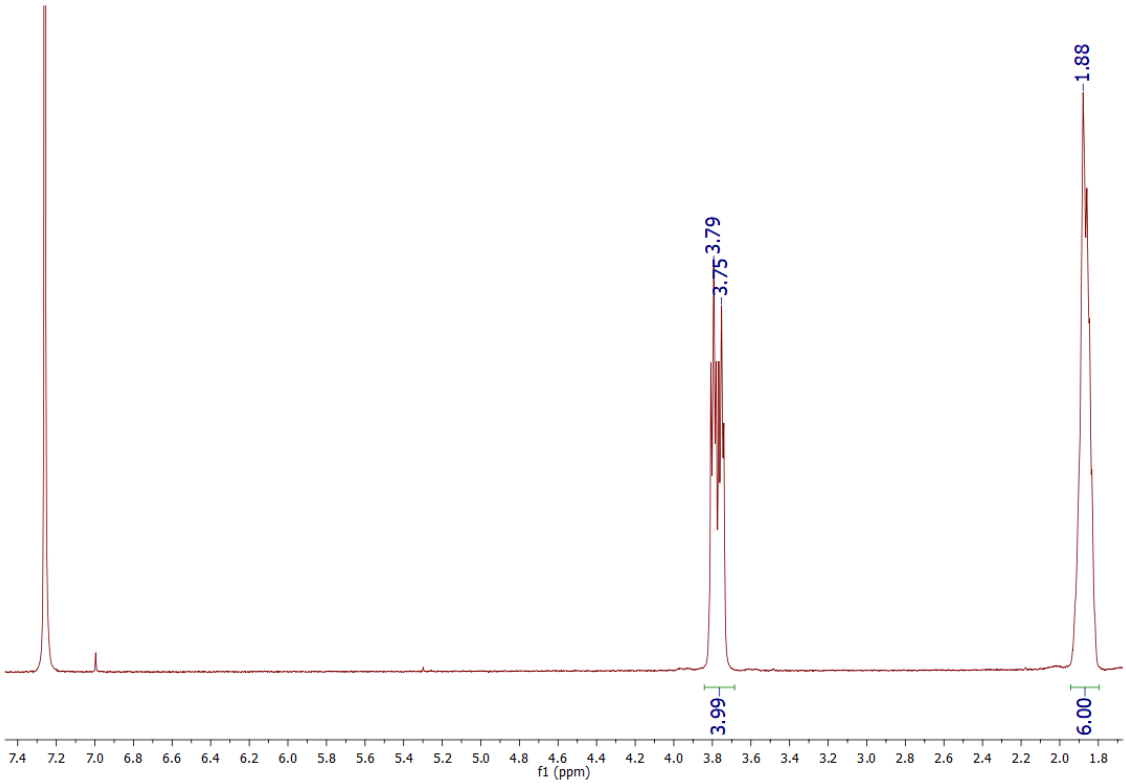

Figure A9. ^{1}H-NMR ($CDCl_3$, 600 MHz) spectrum of bromocyano(piperidine dithiocarbamate)gold(III), [AuBrCN(PipeDTC)].

Supporting Information B: FT-IR spectra of the synthetized piperidine dithiocarbamato ligand and Au(III) complexes

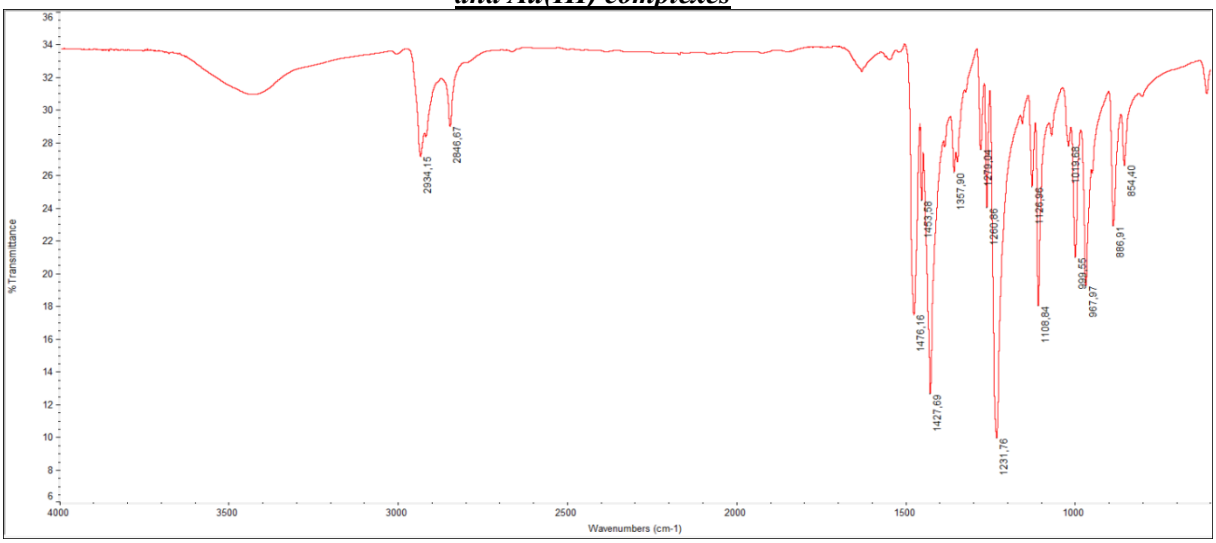

Figure B1. Medium FT-IR (4000-600 cm^{-1}, KBr) spectrum of bis(piperidine dithiocarbamate)digold(I), $[Au_2(PipeDTC)_2]$.

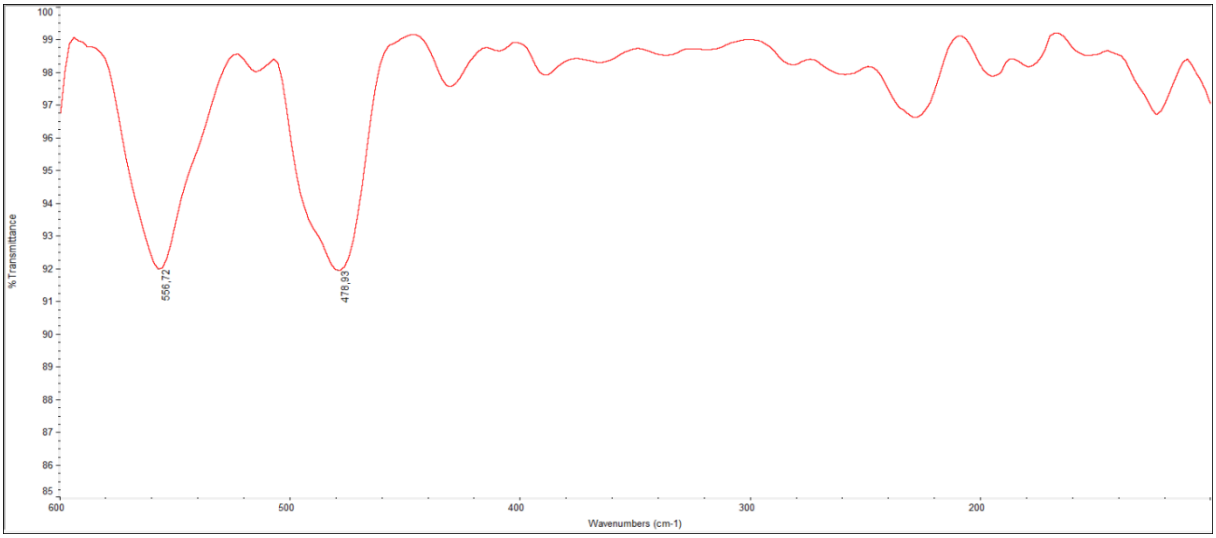

Figure B2. Far FT-IR (600-100 cm^{-1}, nujol) spectrum of bis(piperidine dithiocarbamate)digold(I), $[Au_2(PipeDTC)_2]$.

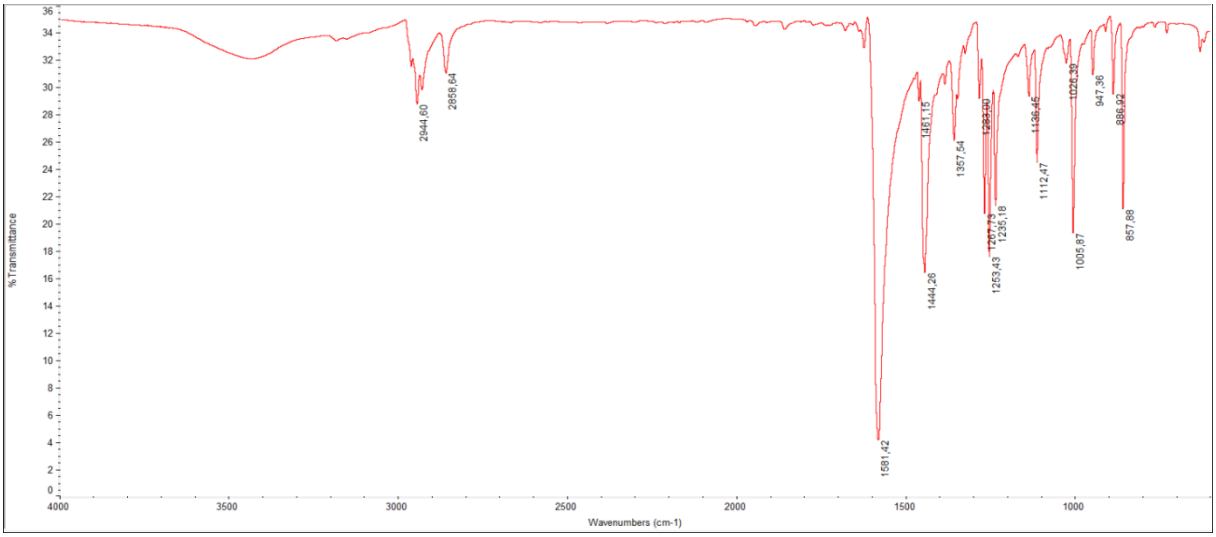

Figure B3. Medium FT-IR (4000-600 cm^{-1}, KBr) spectrum of dichloro(piperidine dithiocarbamate)gold(III), [$AuCl_2$(PipeDTC)].

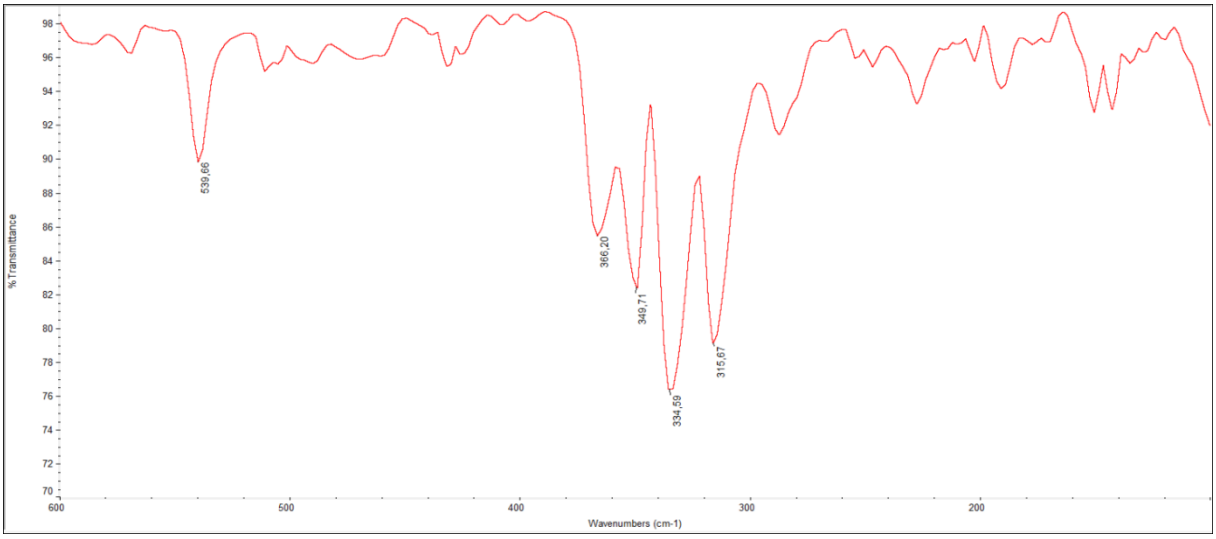

Figure B4. Far FT-IR (600-100 cm^{-1}, nujol) spectrum of dichloro(piperidine dithiocarbamate)gold(III), [$AuCl_2$(PipeDTC)].

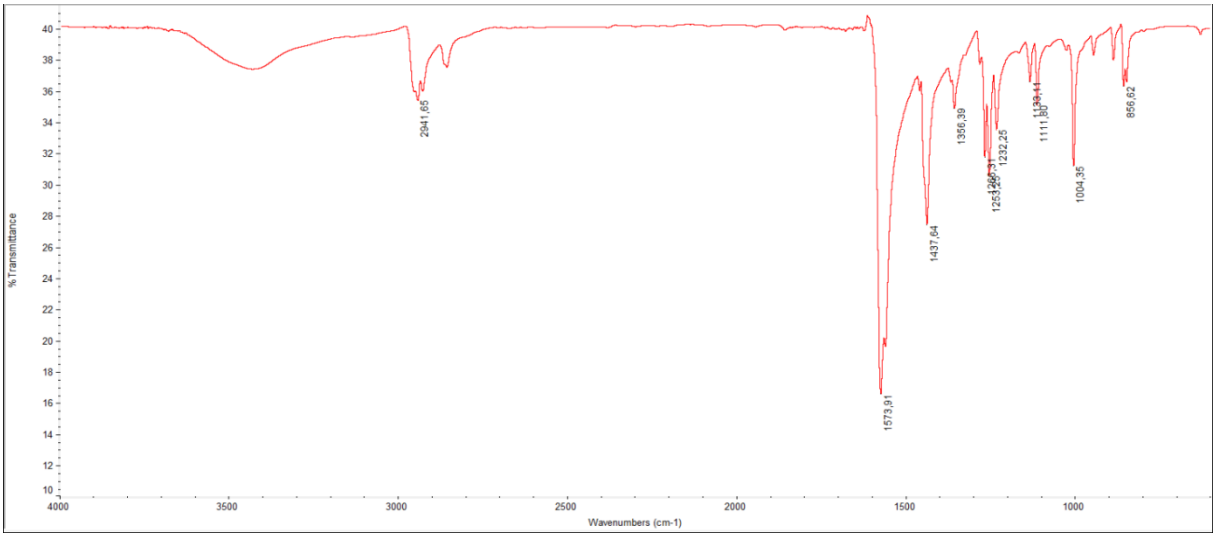

Figure B5. Medium FT-IR (4000-600 cm^{-1}, KBr) spectrum of dibromo(piperidine dithiocarbamate)gold(III), [$AuBr_2$(PipeDTC)].

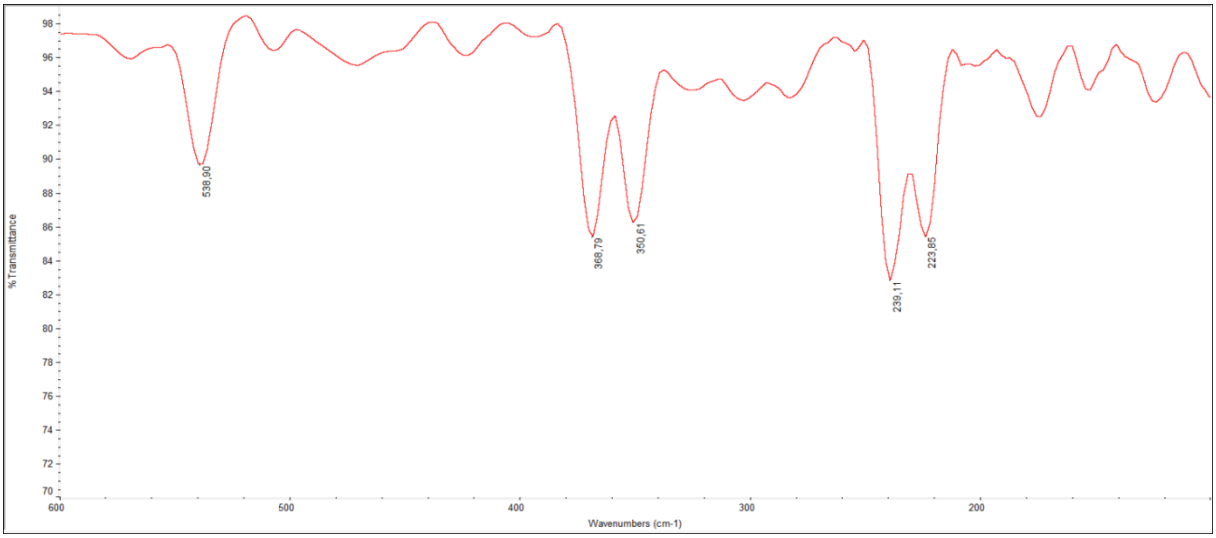

Figure B6. Far FT-IR (600-100 cm^{-1}, nujol) spectrum of dibromo(piperidine dithiocarbamate)gold(III), [$AuBr_2$(PipeDTC)].

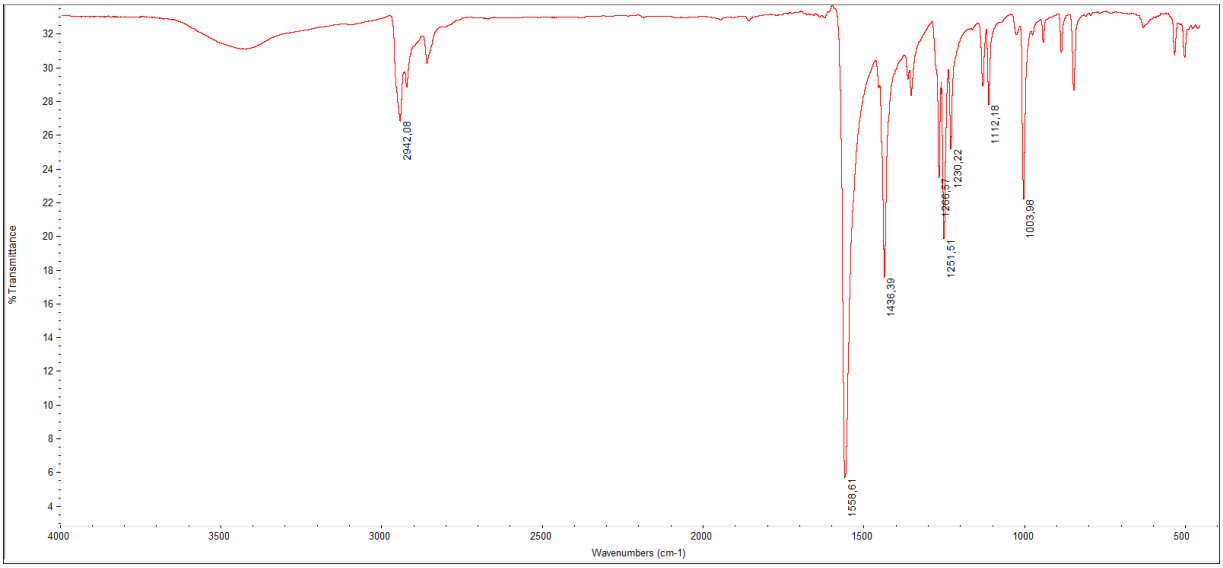

Figure B7. Medium FT-IR (4000-600 cm^{-1}, KBr) spectrum of diiodo(piperidine dithiocarbamate)gold(III), [AuI_2(PipeDTC)].

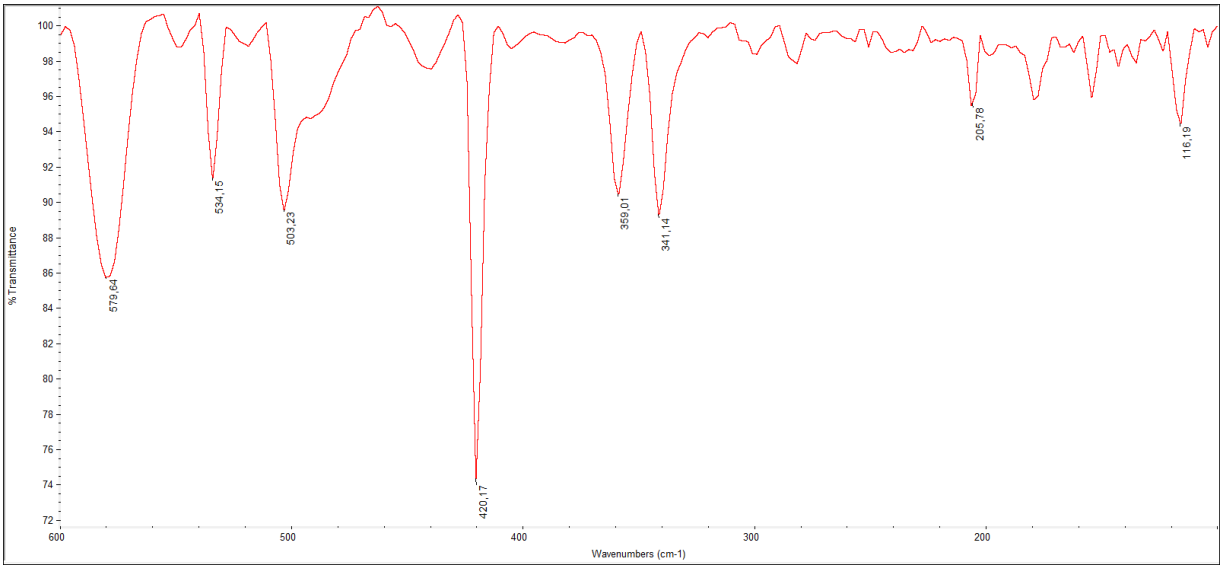

Figure B8. Far FT-IR (600-100 cm^{-1}, nujol) spectrum of diiodo(piperidine dithiocarbamate)gold(III), [AuI_2(PipeDTC)].

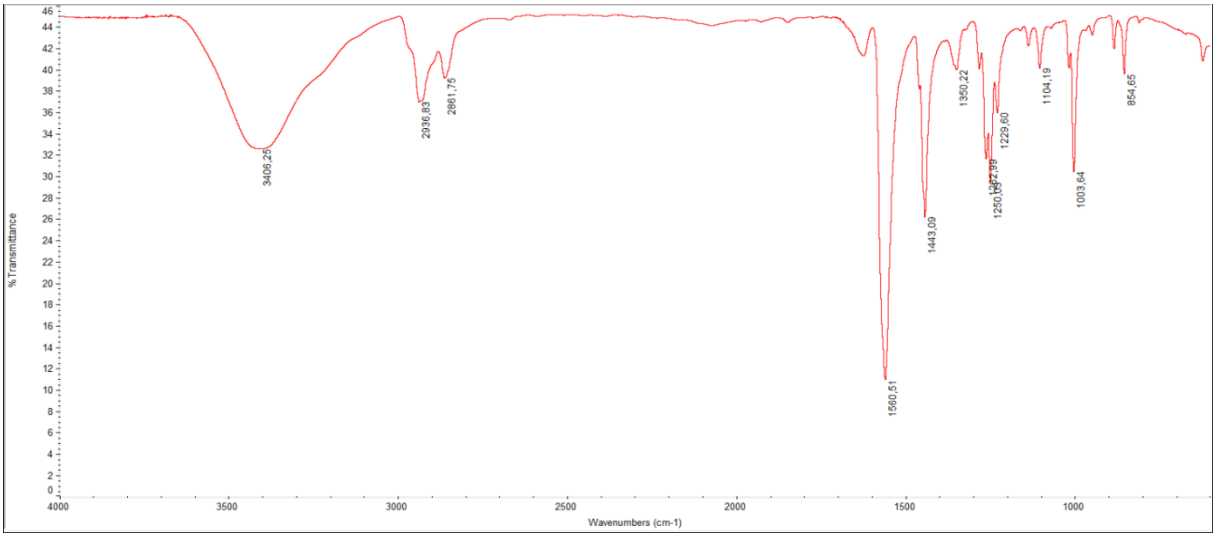

Figure B9. Medium FT-IR (4000-600 cm^{-1}, KBr) spectrum of bis(piperidine dithiocarbamate)gold(III) chloride, $[Au(PipeDTC)_2]Cl$.

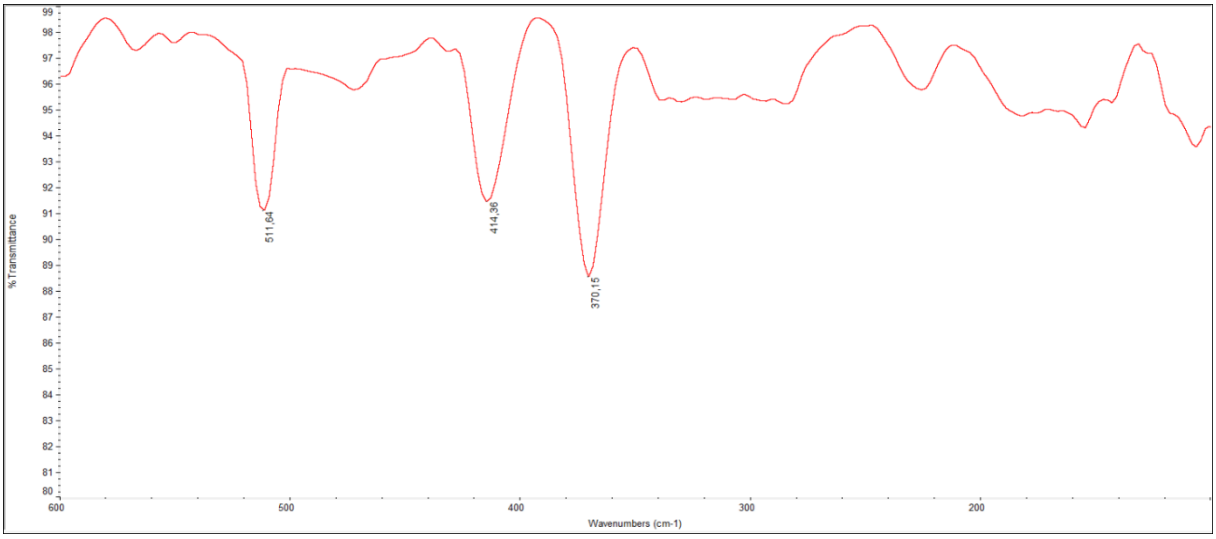

Figure B10. Far FT-IR (600-100 cm^{-1}, nujol) spectrum of bis(piperidine dithiocarbamate)gold(III) chloride, $[Au(PipeDTC)_2]Cl$.

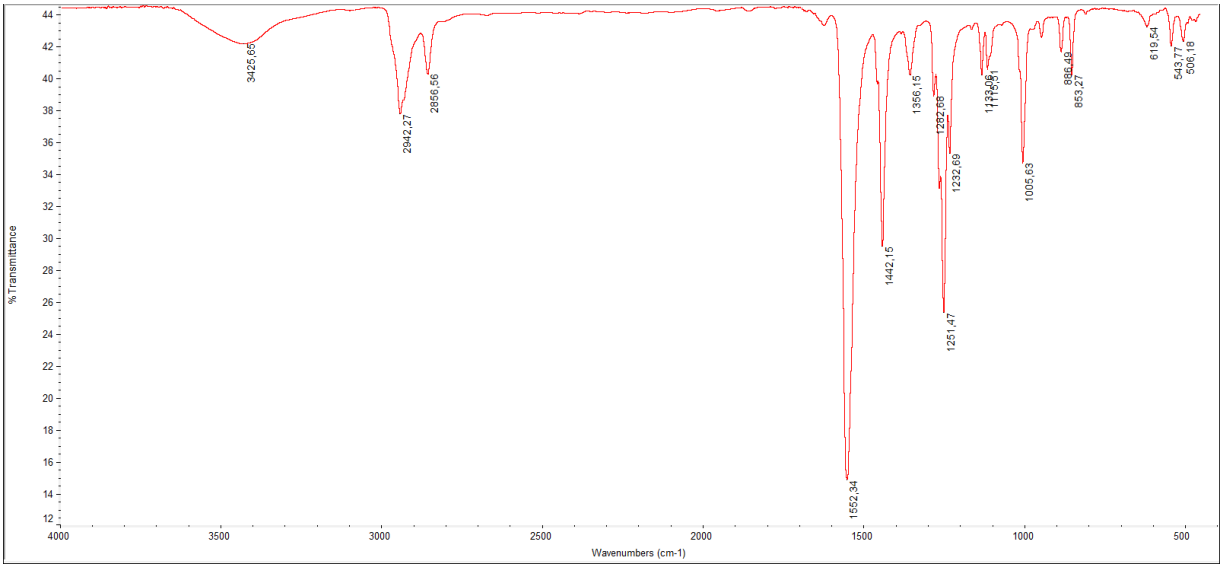

Figure B11. Medium FT-IR (4000-600 cm^{-1}, KBr) spectrum of bis(piperidine dithiocarbamate)gold(III) dichloroaurite, $[Au(PipeDTC)_2][AuCl_2]$.

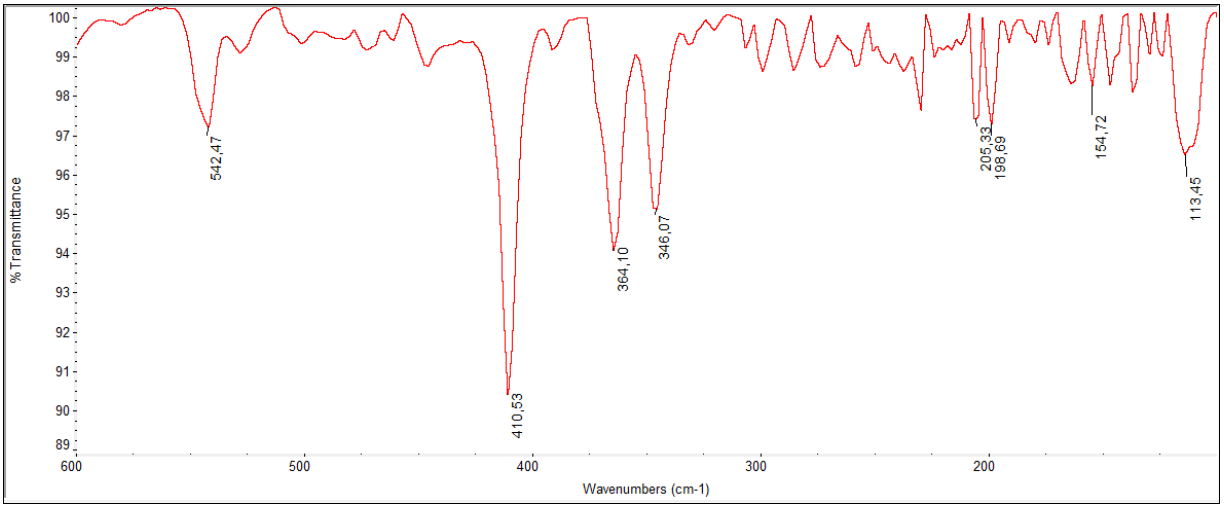

Figure B12. Far FT-IR (600-100 cm^{-1}, nujol) spectrum of bis(piperidine dithiocarbamate)gold(III) dichloroaurite, $[Au(PipeDTC)_2][AuCl_2]$.

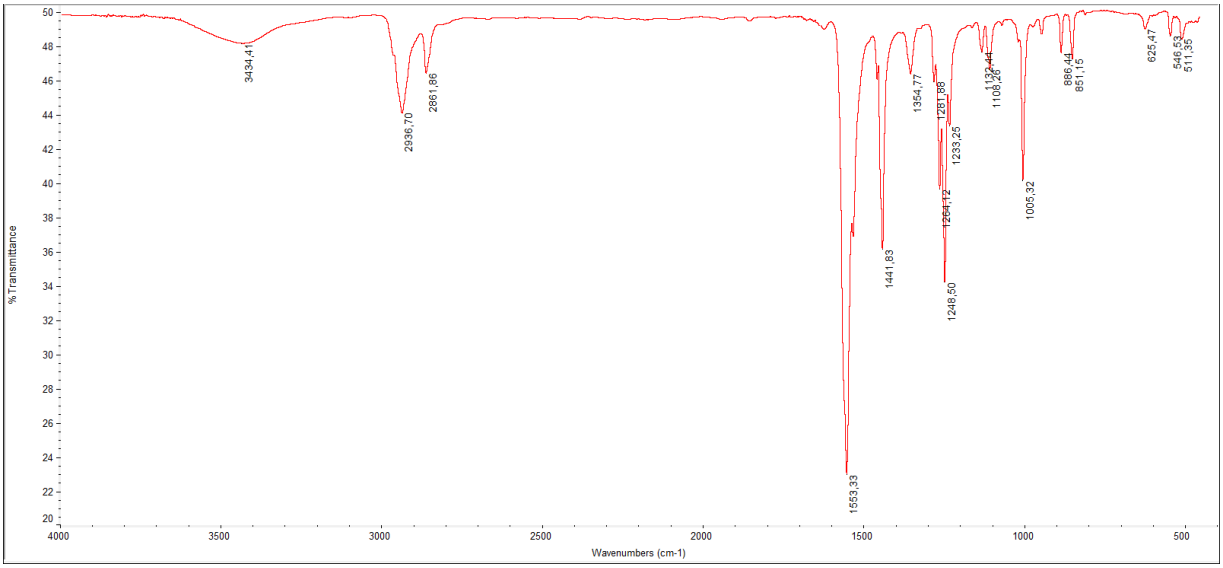

Figure B13. Medium FT-IR (4000-600 cm^{-1}, KBr) spectrum of bis(piperidine dithiocarbamate)gold(III) chloride, $[Au(PipeDTC)_2][AuCl_4]$.

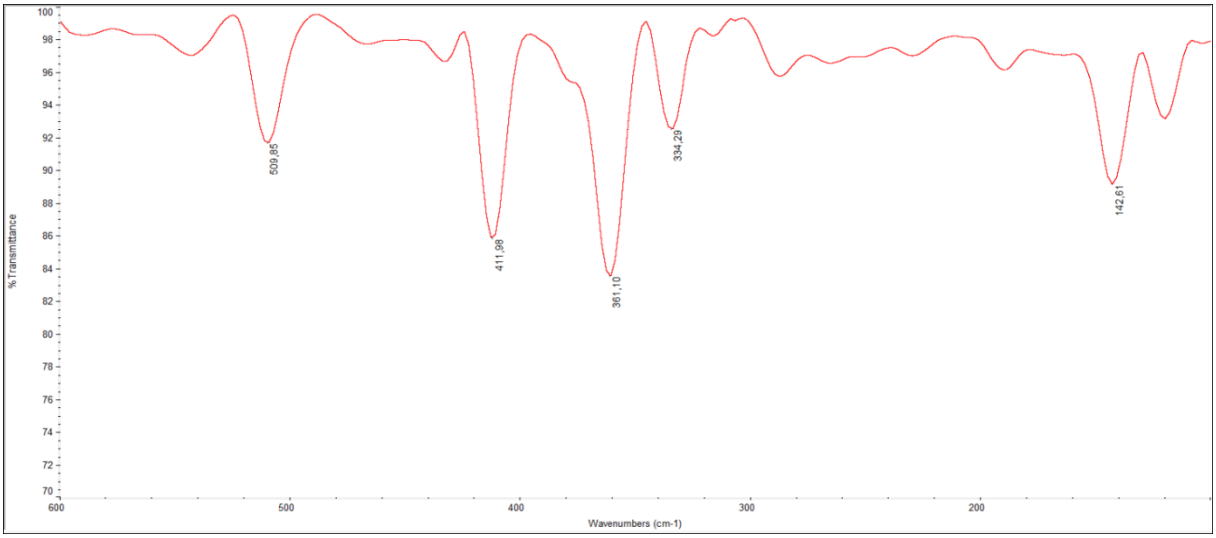

Figure B14. Far FT-IR (600-100 cm^{-1}, nujol) spectrum of bis(piperidine dithiocarbamate)gold(III) tetrachloroaurate, $[Au(PipeDTC)_2][AuCl_4]$.

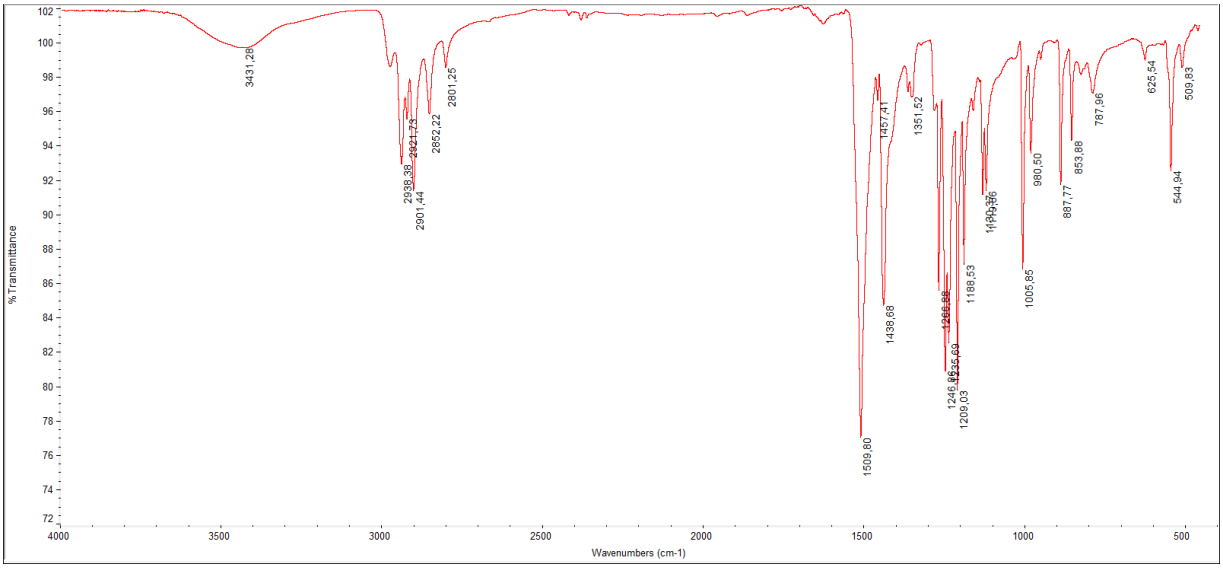

Figure B15. Medium FT-IR (4000-600 cm^{-1}, KBr) spectrum of dimethyl(piperidine dithiocarbamate)gold(III), [$AuMe_2$(PipeDTC)].

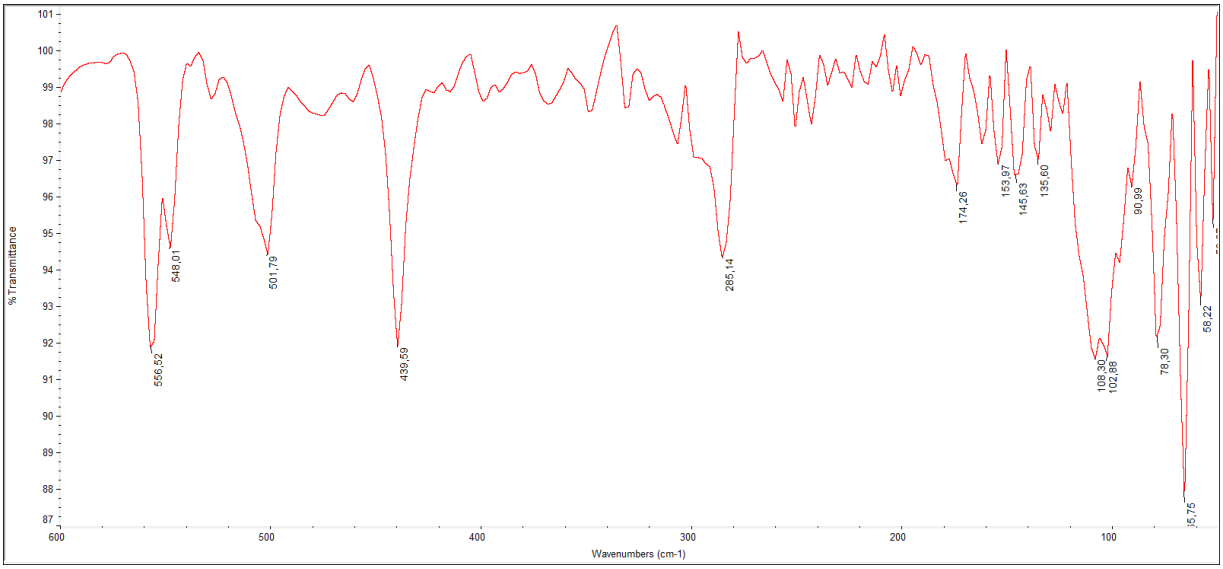

Figure B16. Far FT-IR (600-100 cm^{-1}, nujol) spectrum of dimethyl(piperidine dithiocarbamate)gold(III), [$AuMe_2$(PipeDTC)].

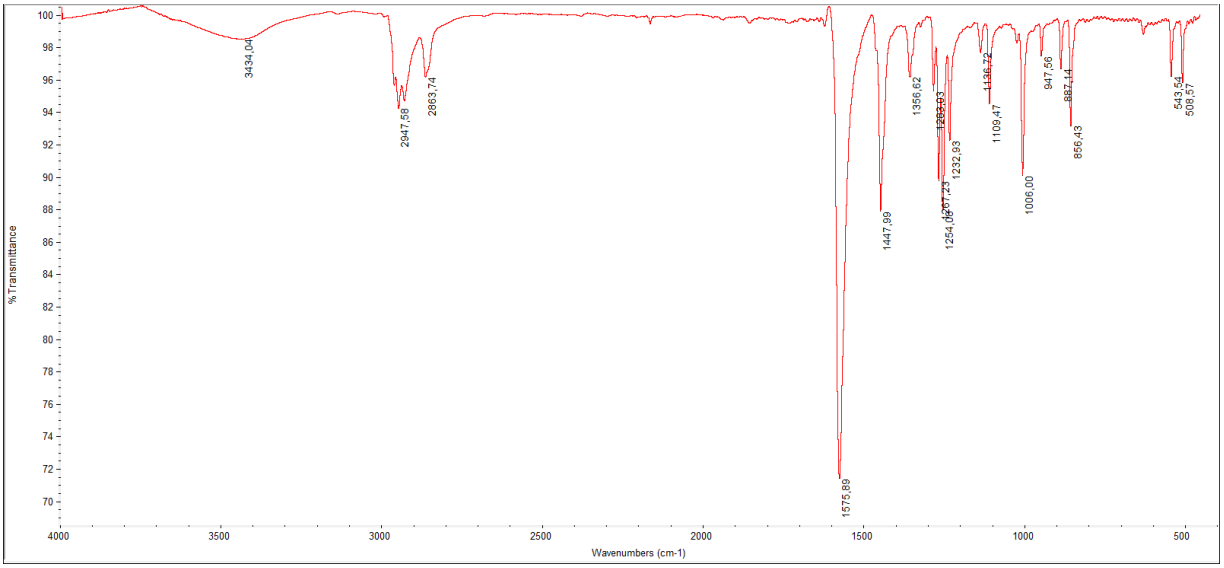

Figure B17. Medium FT-IR (4000-600 cm^{-1}, KBr) spectrum of bromocyano(piperidine dithiocarbamate)gold(III), [AuBrCN(PipeDTC)].

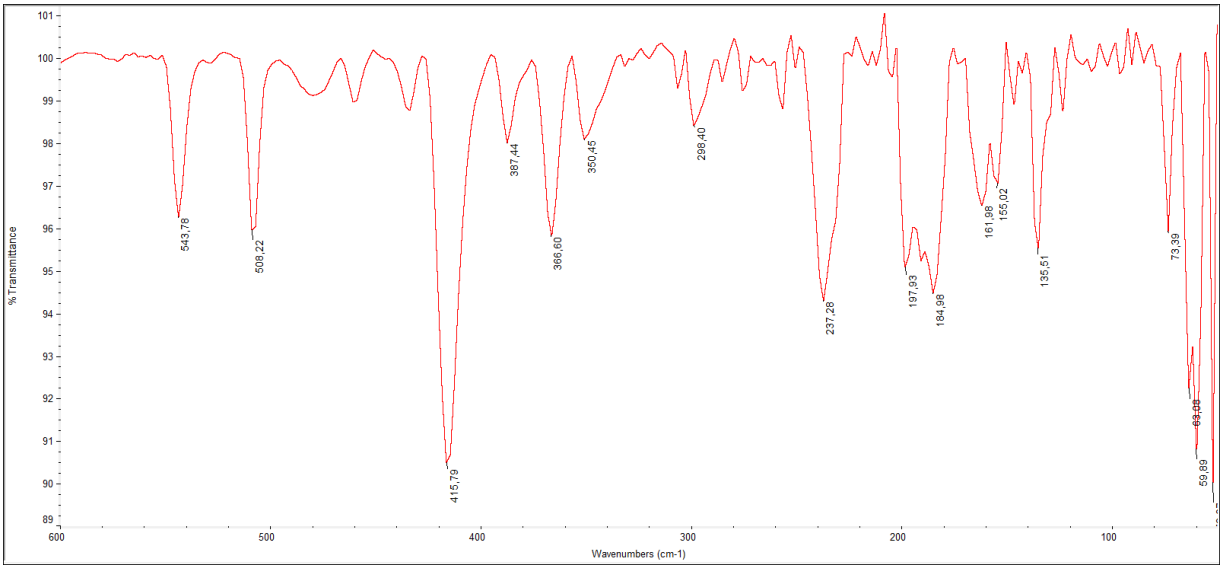

Figure B18. Far FT-IR (600-100 cm^{-1}, nujol) spectrum of bromocyano(piperidine dithiocarbamate)gold(III), [AuBrCN(PipeDTC)].

Supporting Information C: UV-Vis spectra of the synthetized piperidine dithiocarbamato Au(III) complexes.

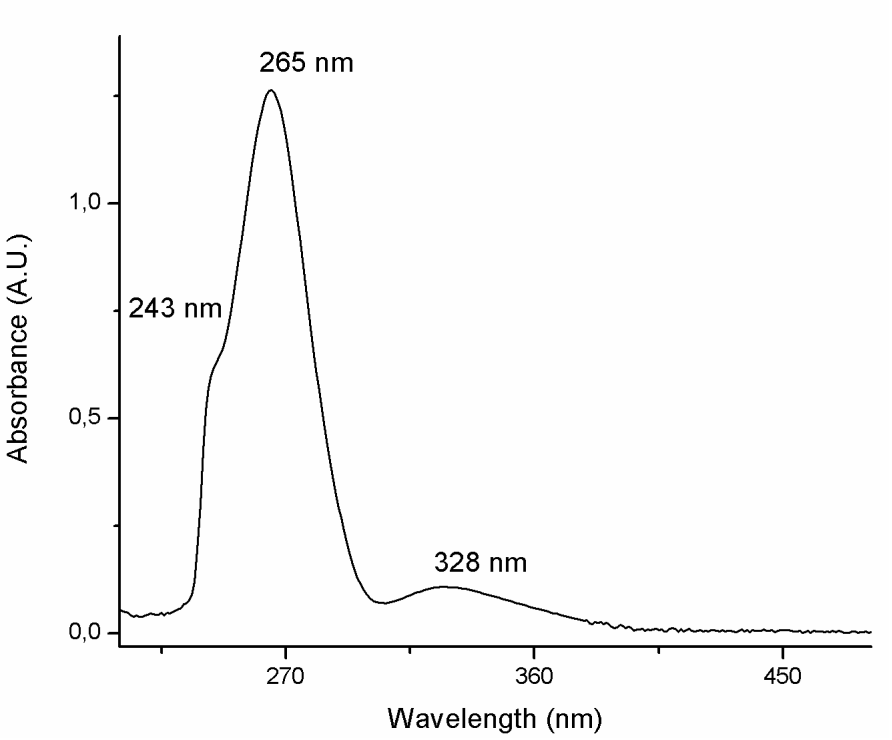

Figure C1. UV-Vis spectrum (CH_3Cl, 190-500 nm) of a 30μM solution of the dichloro(piperidine dithiocarbamate)gold(III), [$AuCl_2$(PipeDTC)].

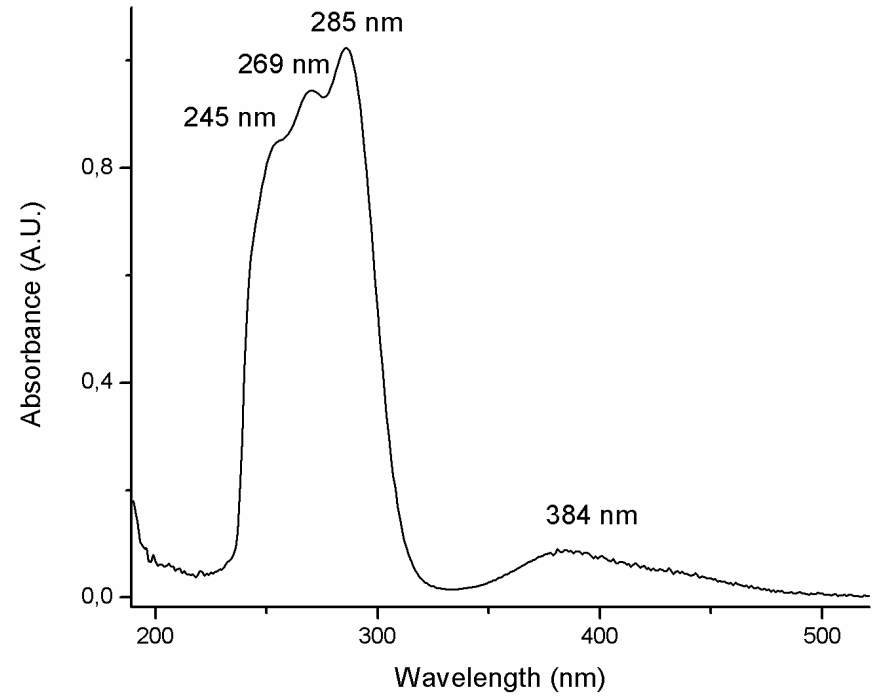

Figure C2. UV-Vis spectrum (CH_3Cl, 190-500 nm) of a 30μM solution of the dibromo(piperidine dithiocarbamate)gold(III), [$AuBr_2$(PipeDTC)].

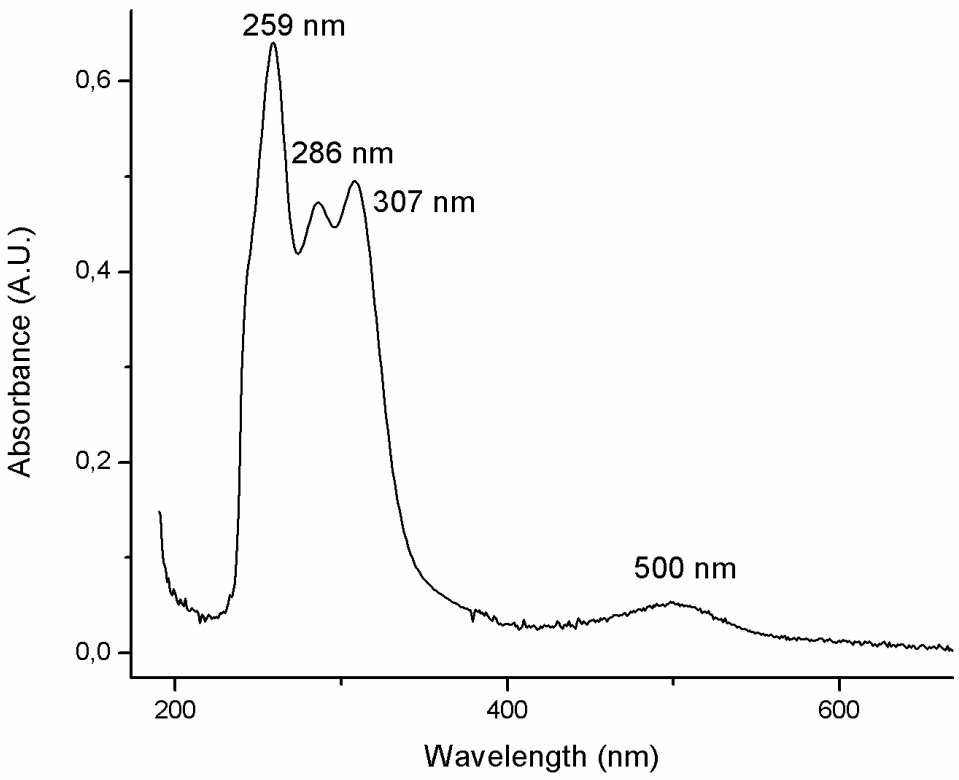

Figure C3. UV-Vis spectrum (CH_3Cl, 190-500 nm) of a 30μM solution of the diiodo(piperidine dithiocarbamate)gold(III), [AuI_2(PipeDTC)].

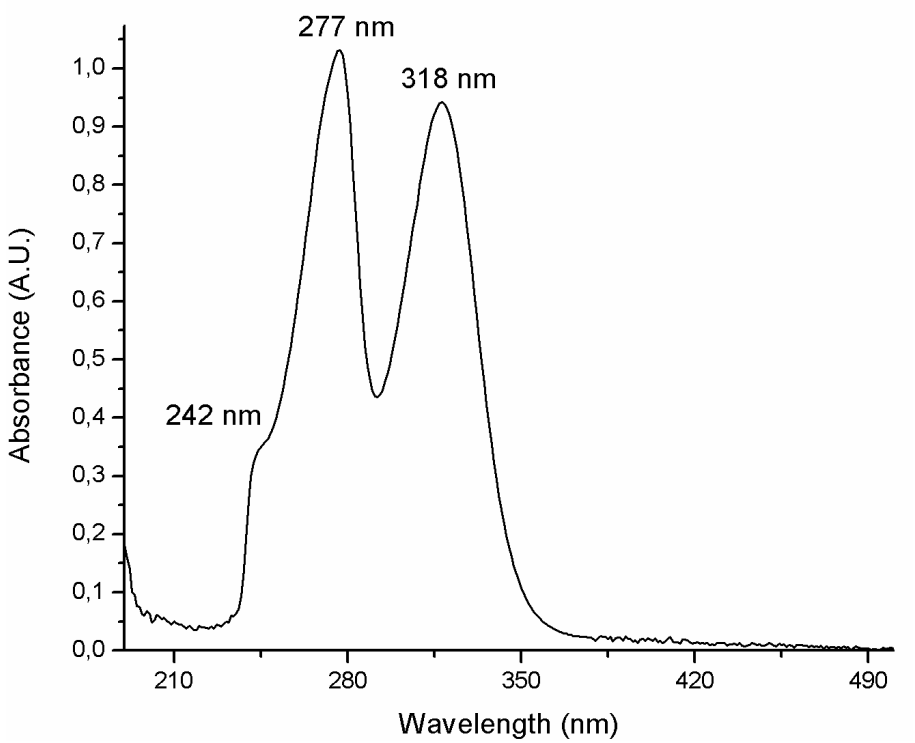

Figure C4. UV-Vis spectrum (CH_3Cl, 190-500 nm) of a 30μM solution of the bis(piperidine dithiocarbamate)gold(III) chloride, [Au(PipeDTC)$_2$]Cl.

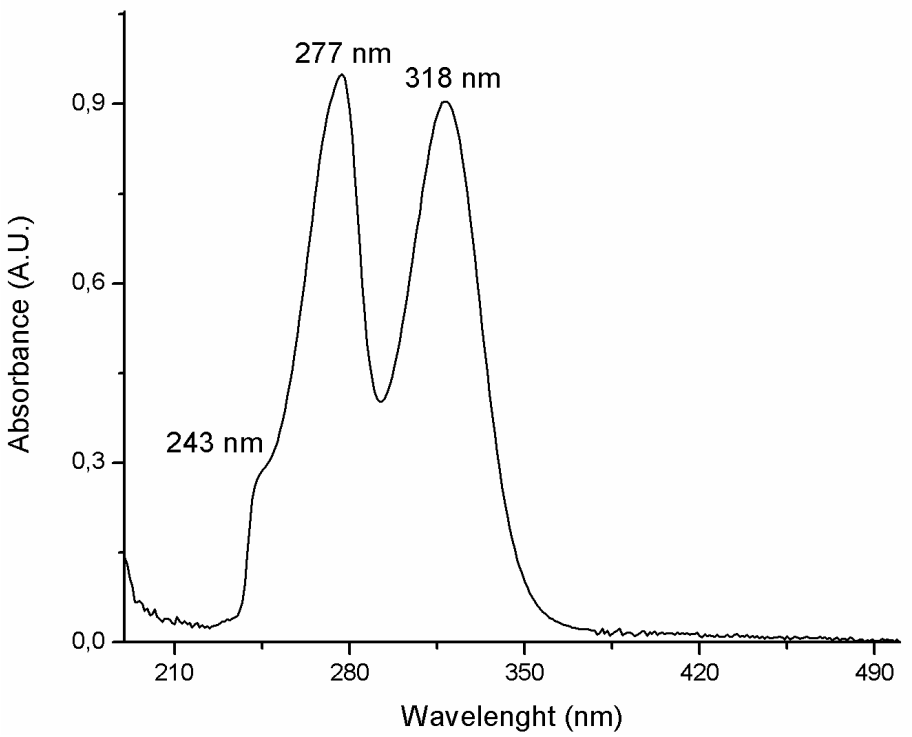

Figure C5. UV-Vis spectrum (CH_3Cl, 190-500 nm) of a 30μM solution of the bis(piperidine dithiocarbamate)gold(III) dichloroaurite, $[Au(PipeDTC)_2][AuCl_2]$.

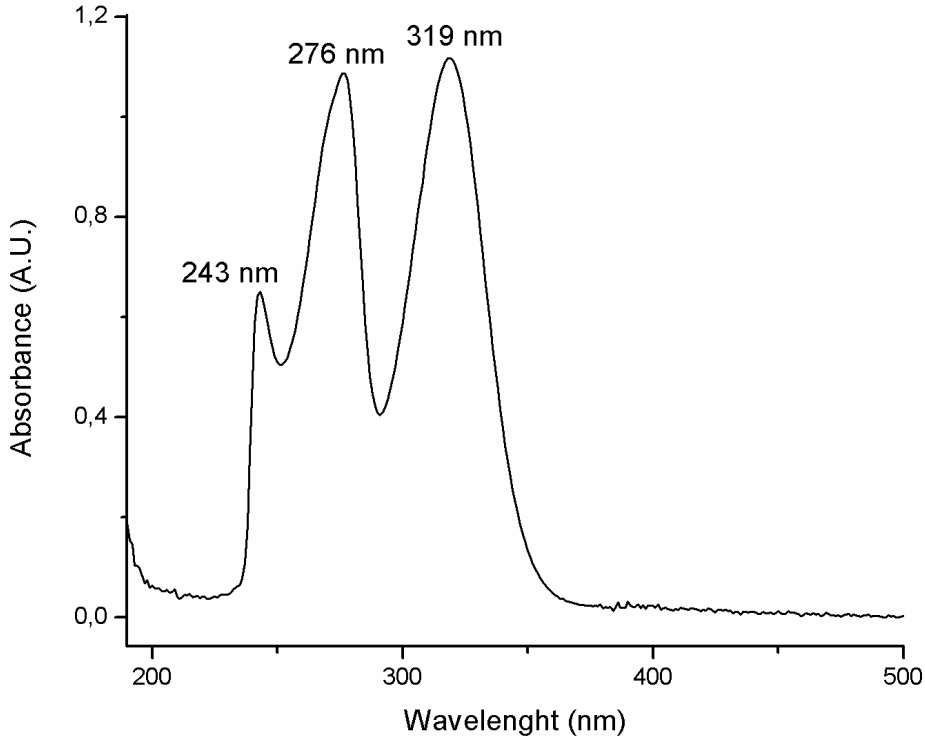

Figure C6. UV-Vis spectrum (CH_3Cl, 190-500 nm) of a 30μM solution of the bis(piperidine dithiocarbamate)gold(III) tetrachloroaurate, $[Au(PipeDTC)_2][AuCl_4]$.

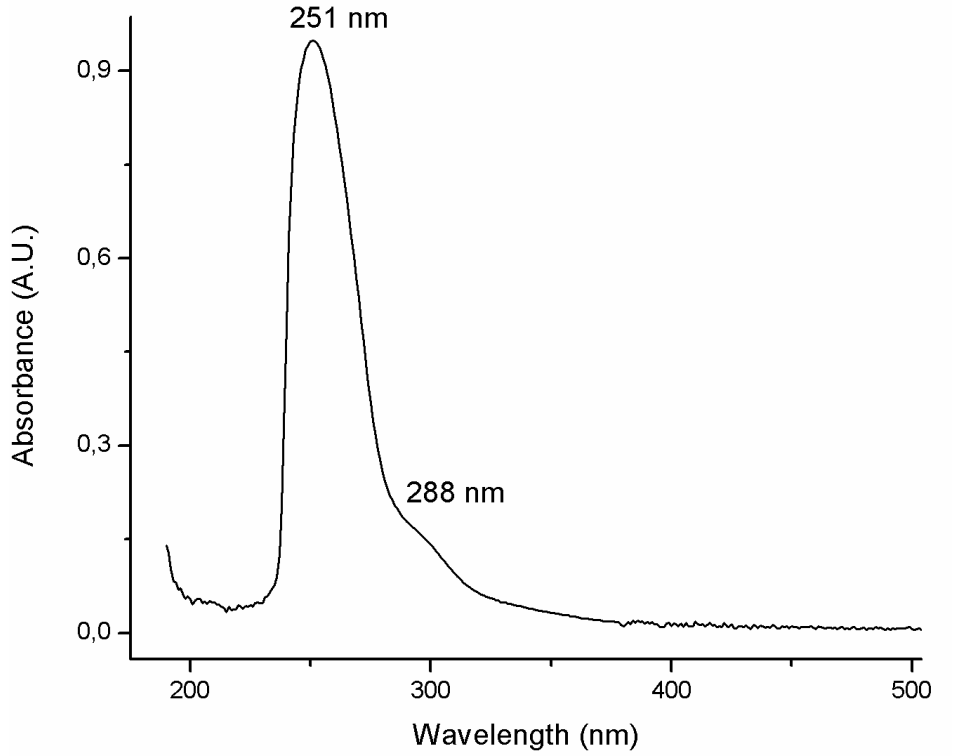

Figure C7. UV-Vis spectrum (CH_3Cl, 190-500 nm) of a 1μM solution of dimethyl(piperidine dithiocarbamate)gold(III), [$AuMe_2$(PipeDTC)].

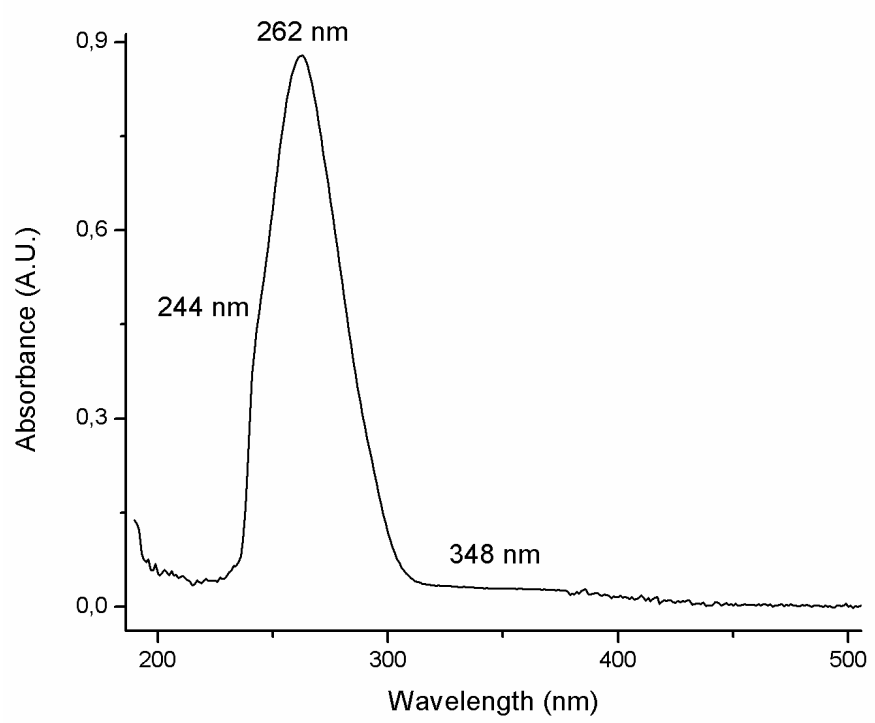

Figure C8. UV-Vis spectrum (CH_3Cl, 190-500 nm) of a 30μM solution of the bromocyano(piperidine dithiocarbamate)gold(III), [AuBrCN(PipeDTC)].

Supporting Information D: NMR and FT-IR spectra of the synthetized glycosylated dithiocarbamato ligands.

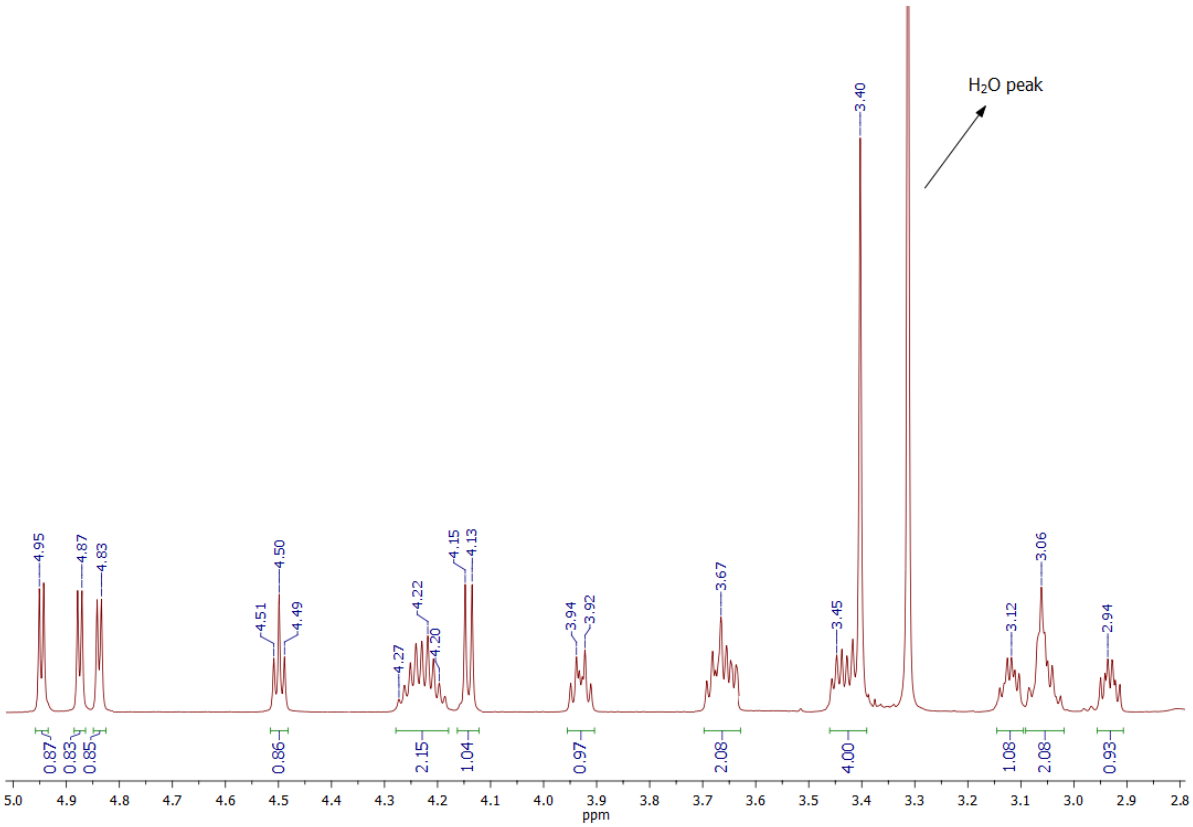

Figure D1. ^{1}H-NMR (DMSO-d6, 600 MHz) spectrum of O-ethyl, N-methyl, β-D-glucopyranosyl dithiocarbamato, potassium salt.

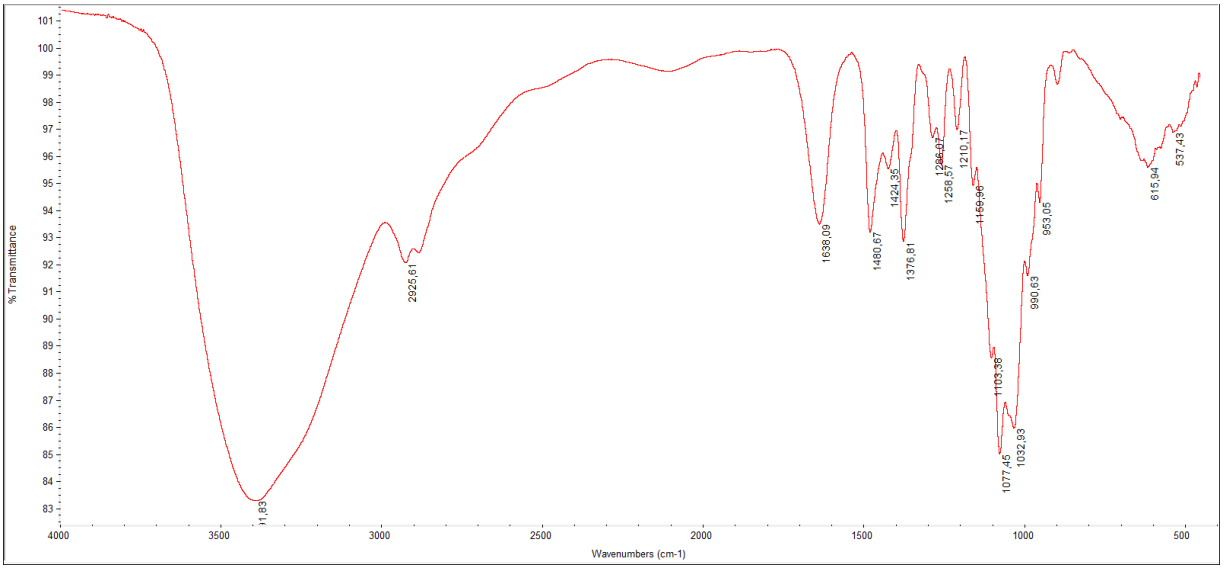

Figure D2. Medium FT-IR (4000-500 cm^{-1}) spectrum of O-ethyl, N-methyl, β-D-glucopyranosyl dithiocarbamato, potassium salt.

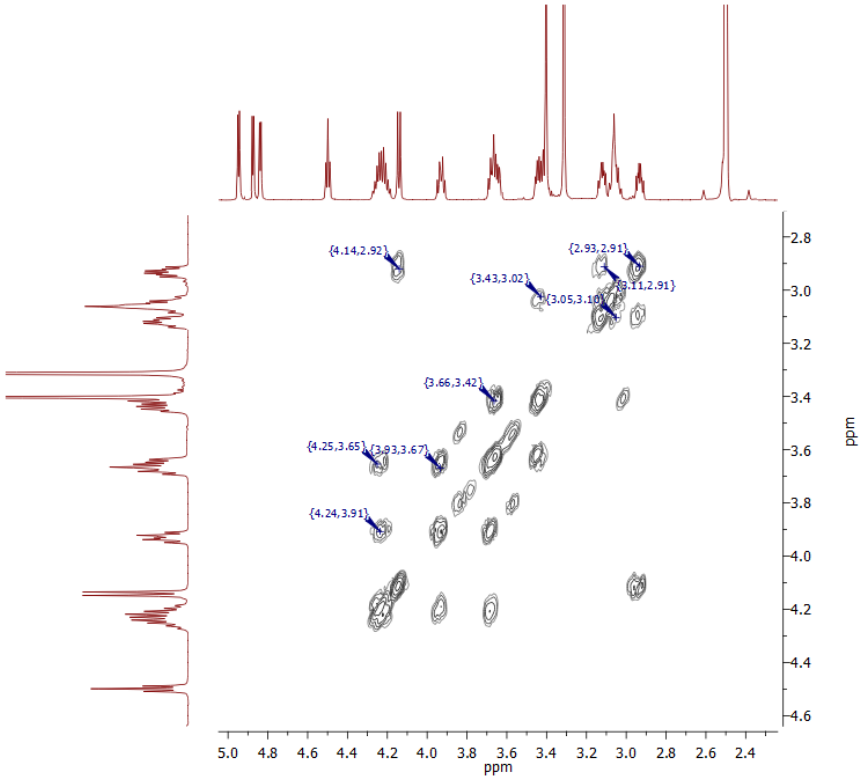

Figure D3. COSY 2D ^{1}H-^{1}H-NMR (DMSO-d6, 600 MHz) spectrum of O-ethyl, N-methyl, β-D-glucopyranosyl dithiocarbamato, potassium salt.

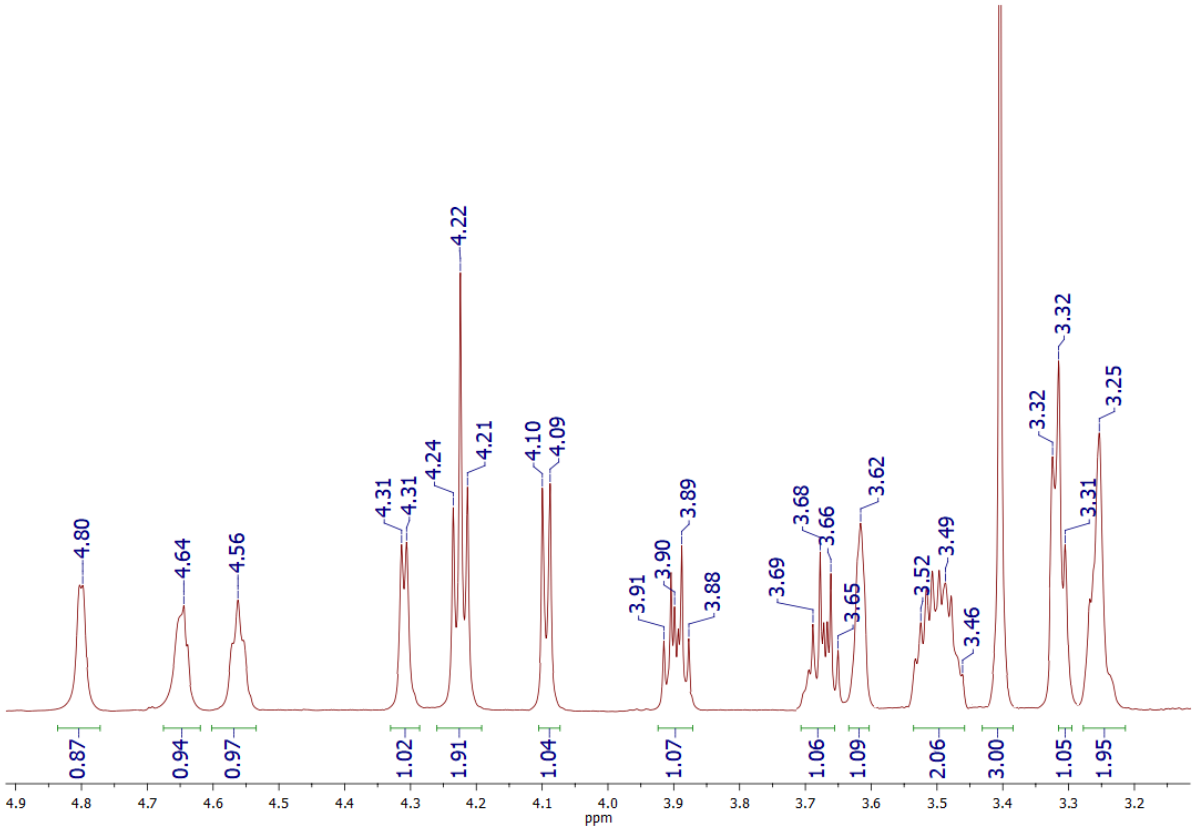

Figure D4. ^{1}H-NMR (DMSO-d6, 600 MHz) spectrum of O-ethyl, N-methyl, β-D-galactopyranosyl dithiocarbamato, potassium salt.

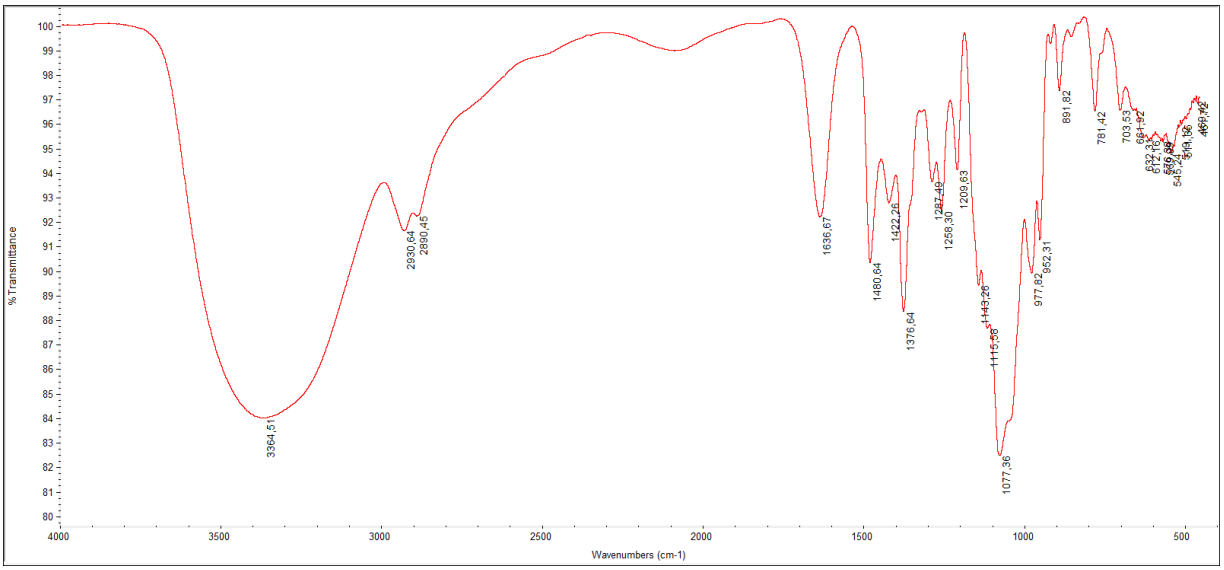

Figure D5. Medium FT-IR (4000-500 cm^{-1}) spectrum of O-ethyl, N-methyl, β-D-galactopyranosyl dithiocarbamato, potassium salt.

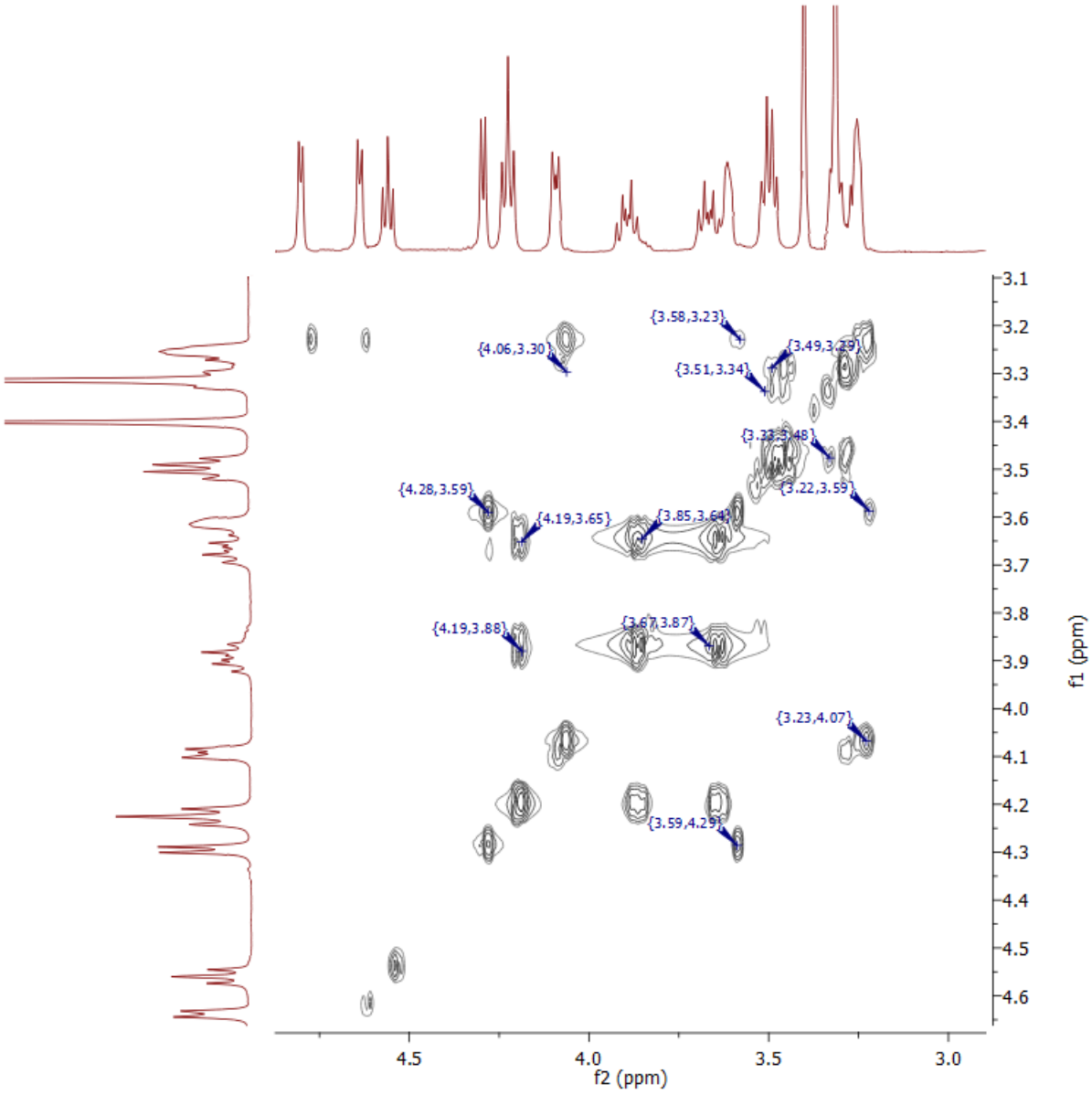

Figure D6. COSY 2D ^{1}H-^{1}H-NMR (DMSO-d6, 600 MHz) spectrum of O-ethyl, N-methyl, β-D-galactopyranosyl dithiocarbamato, potassium salt.

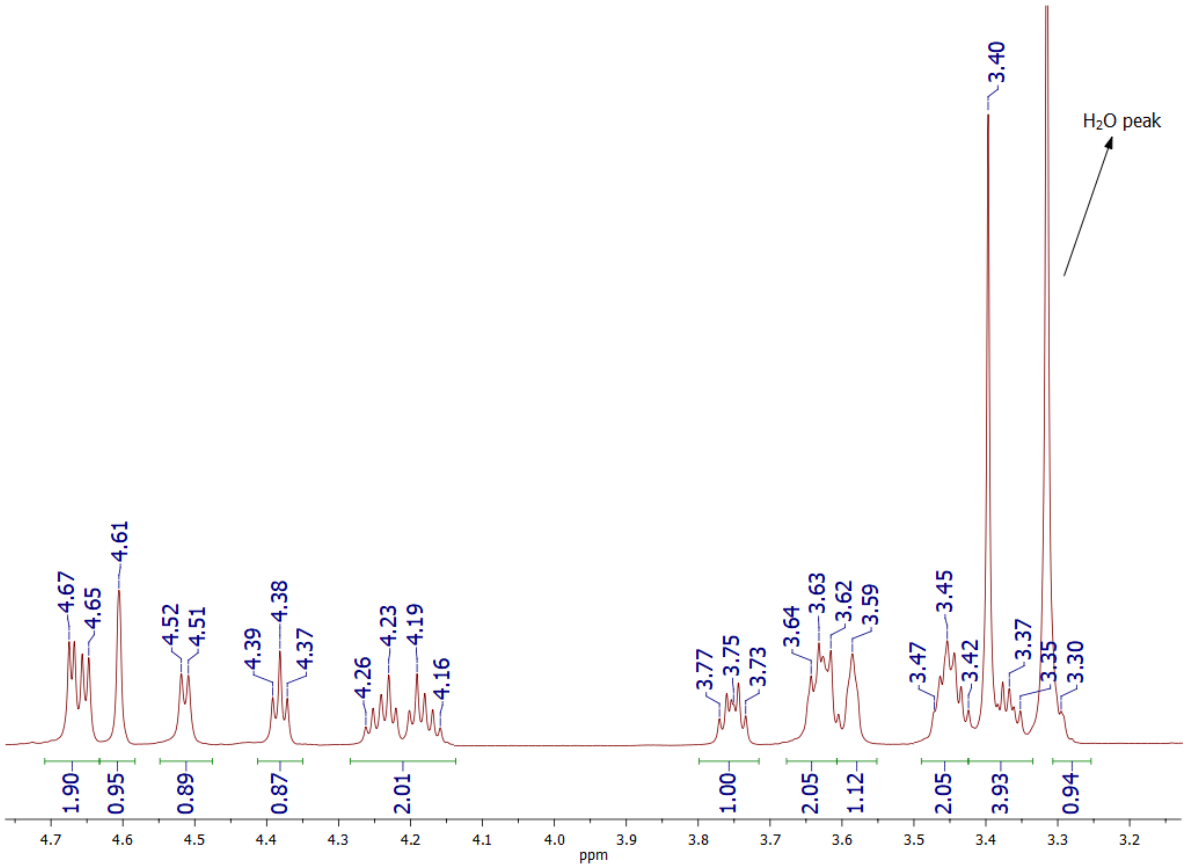

Figure D7. ^{1}H-NMR (DMSO-d6, 600 MHz) spectrum of O-ethyl, N-methyl, α-D-mannopyranosyl dithiocarbamato, potassium salt.

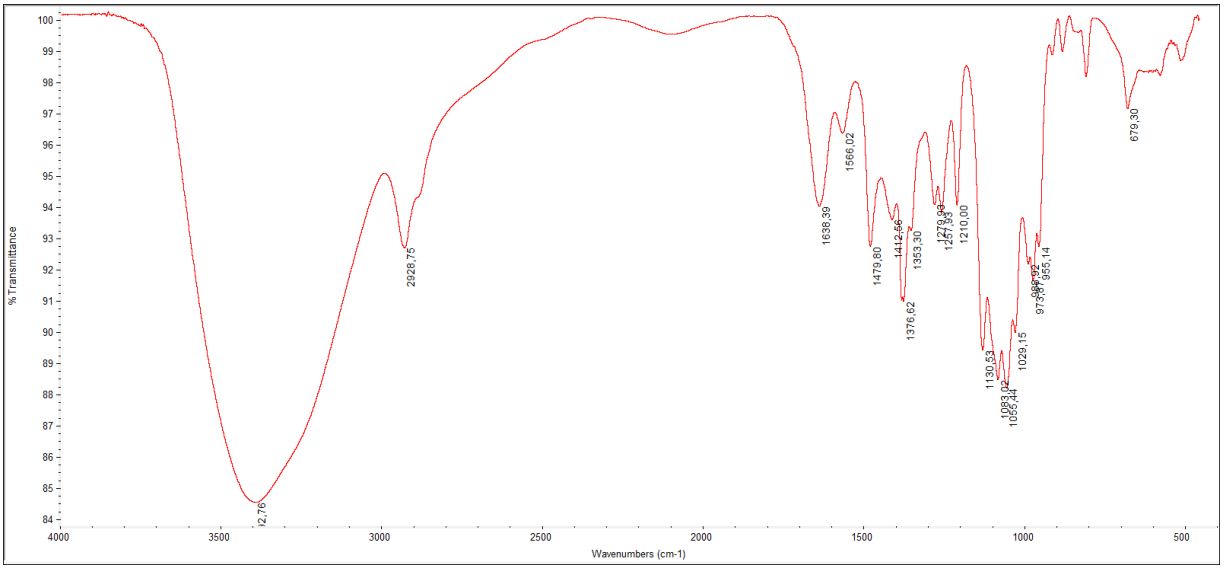

Figure D8. Medium FT-IR (4000-500 cm^{-1}) spectrum of O-ethyl, N-methyl, α-D-mannopyranosyl dithiocarbamato, potassium salt.

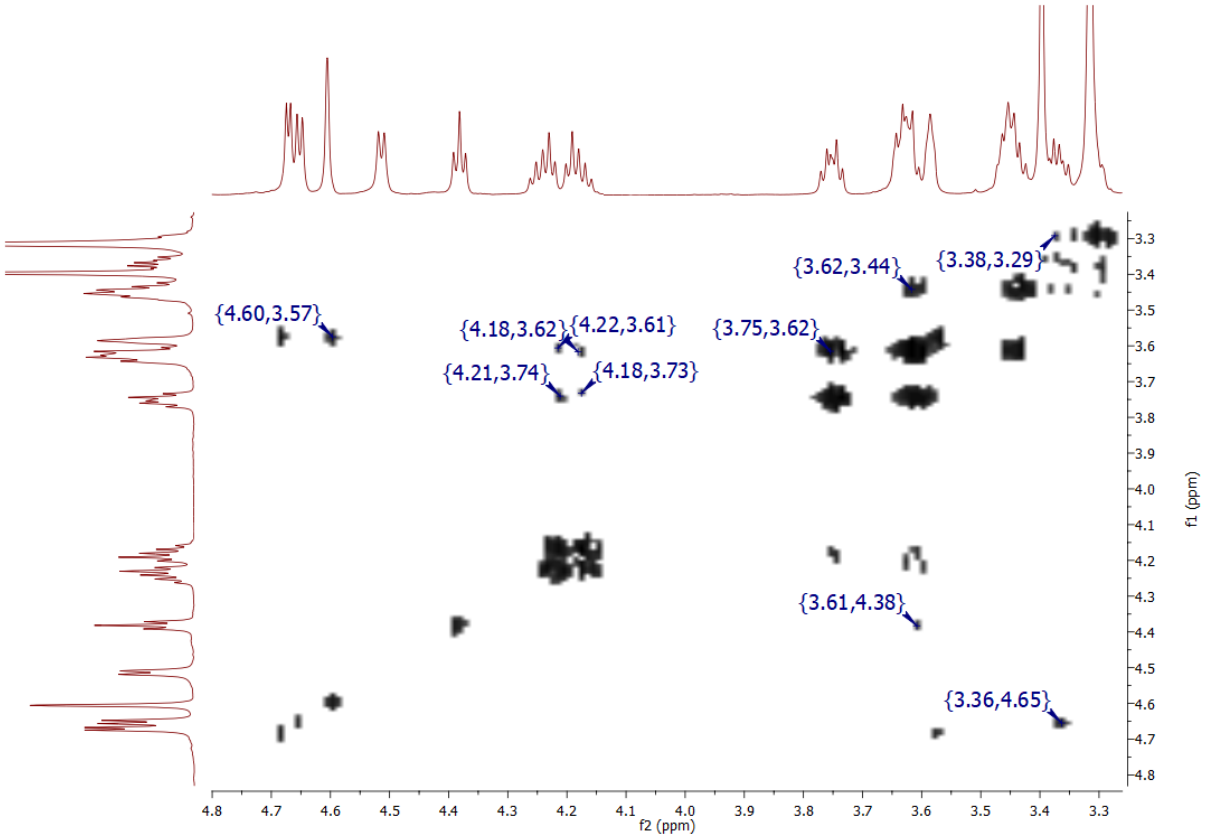

Figure D9. COSY 2D ^{1}H-^{1}H-NMR (DMSO-d6, 600 MHz) spectrum of O-ethyl, N-methyl, α-D-mannopyranosyl dithiocarbamato, potassium salt.

Supporting Information E: ^{1}H-NMR spectra of the synthetized glycosylated dithiocarbamato Au(III) complexes

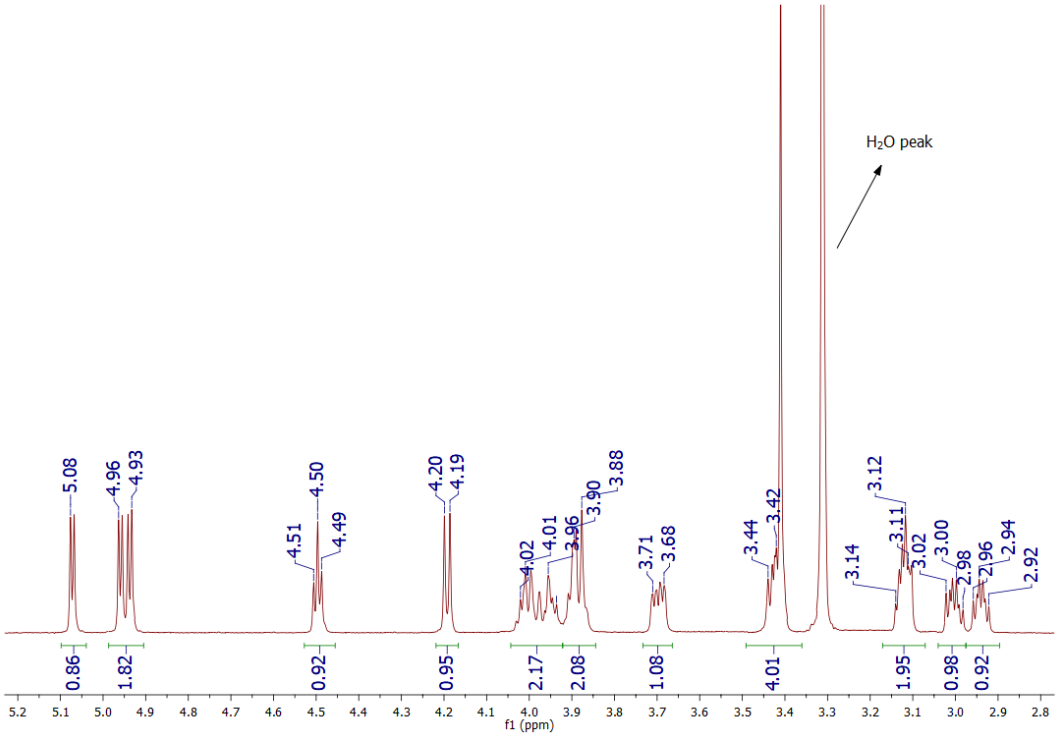

Figure E1. ^{1}H-NMR (DMSO-d6, 600 MHz) spectrum of dibromo (O-ethyl, N-methyl, β-D-glucopyranosyl dithiocarbamato) gold(III), [$AuBr_2$(β-D-glucosideDTC)].

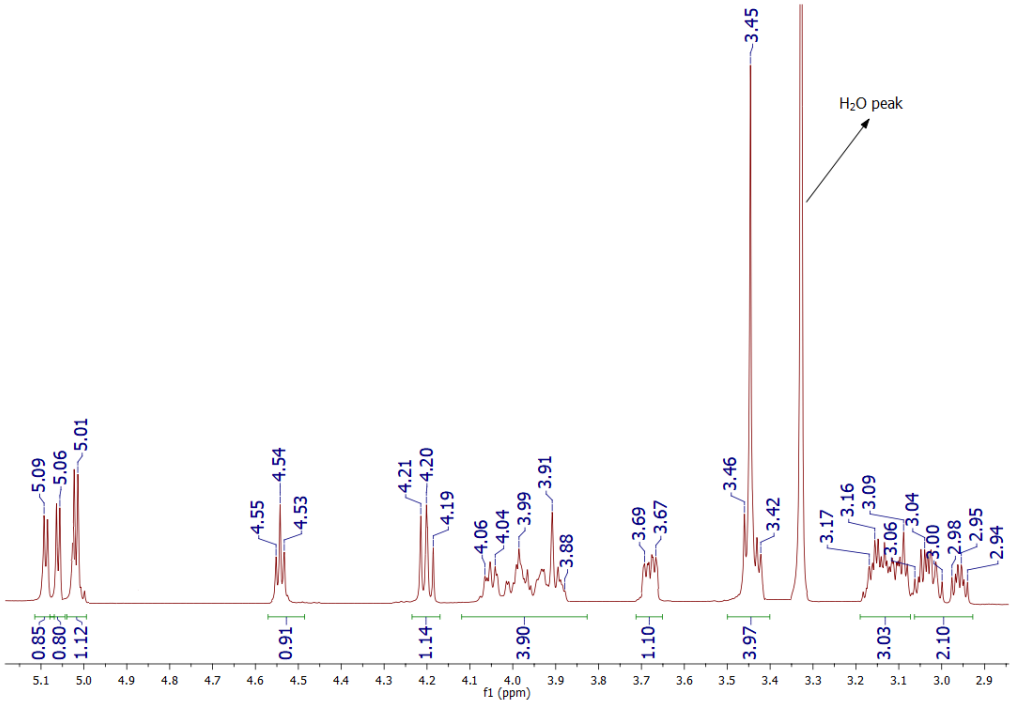

Figure E2. ^{1}H-NMR (DMSO-d6, 600 MHz) spectrum of bis(O-ethyl, N-methyl, β-D-glucopyranosyl dithiocarbamato) gold(III) chloride, [Au(β-D-glucosideDTC)$_2$]Cl.

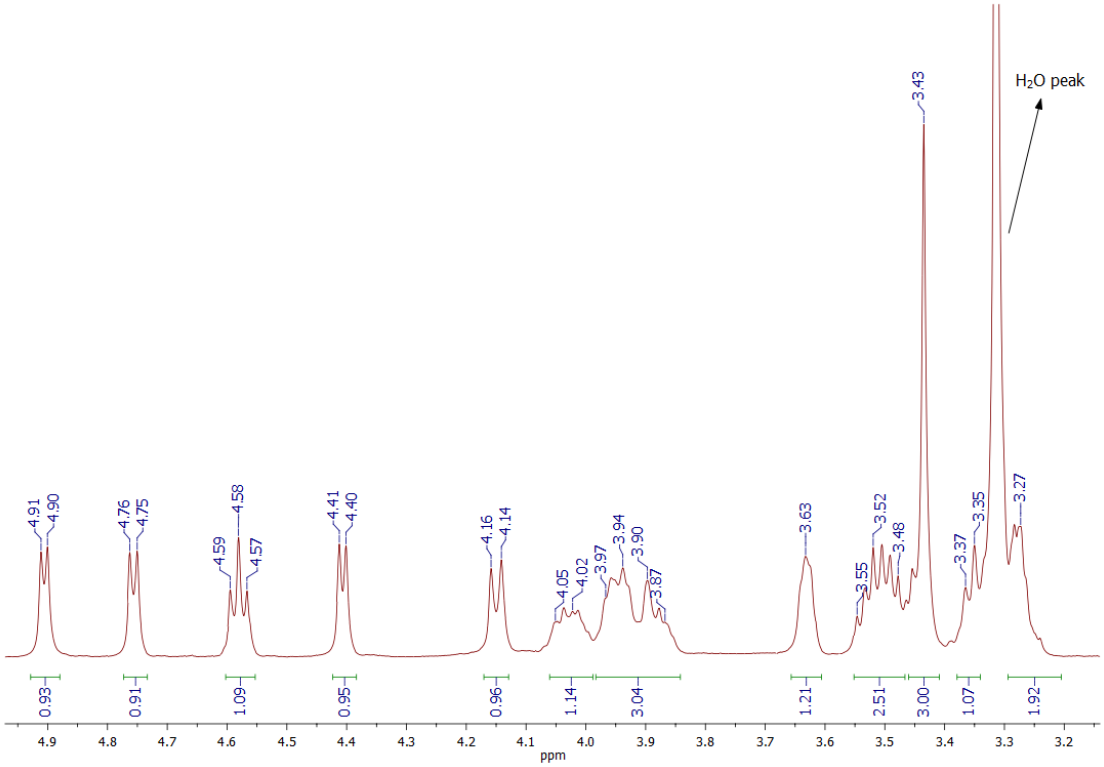

Figure E3. [1]H-NMR (DMSO-d6, 600 MHz) spectrum of bis(O-ethyl, N-methyl, β-D-galactopyranosyl dithiocarbamato) gold(III) chloride, [Au(β-D-galactosideDTC)$_2$]Cl.

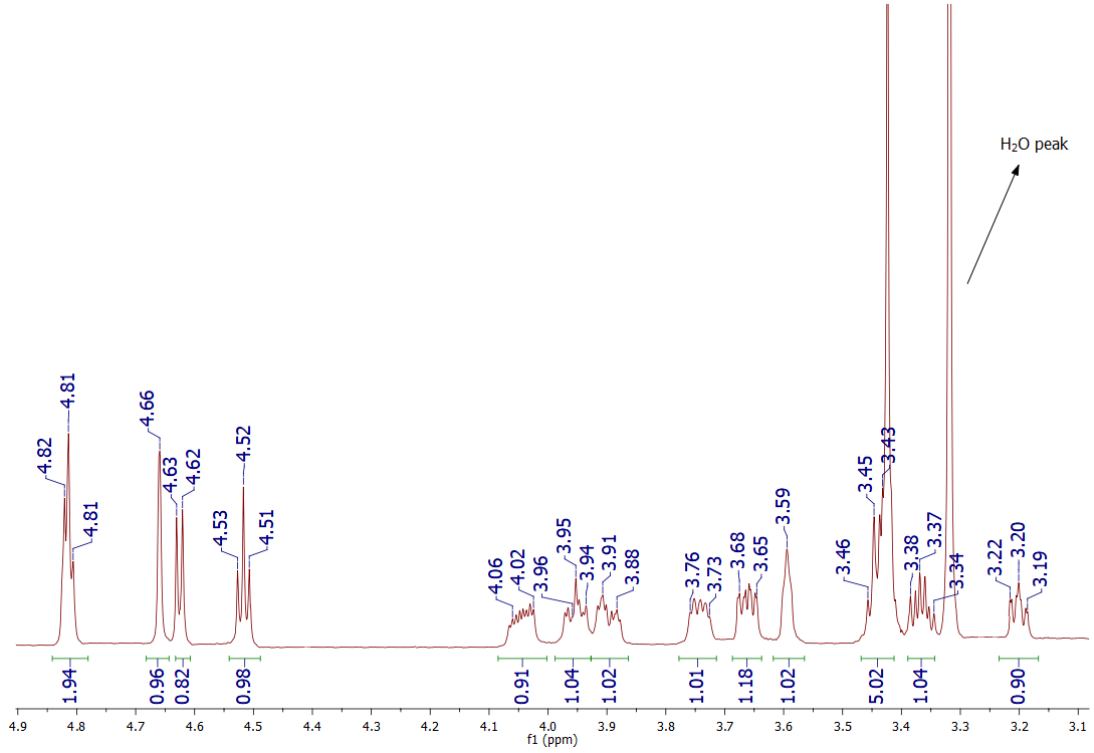

Figure E4. [1]H-NMR (DMSO-d6, 600 MHz) spectrum of bis(O-ethyl, N-methyl, α-D-mannopyranosyl dithiocarbamato) gold(III) chloride, [Au(α-D-mannosideDTC)$_2$]Cl.

Supporting Information F: FTIR spectra of the synthetized glycosylated dithiocarbamato Au(III) complexes

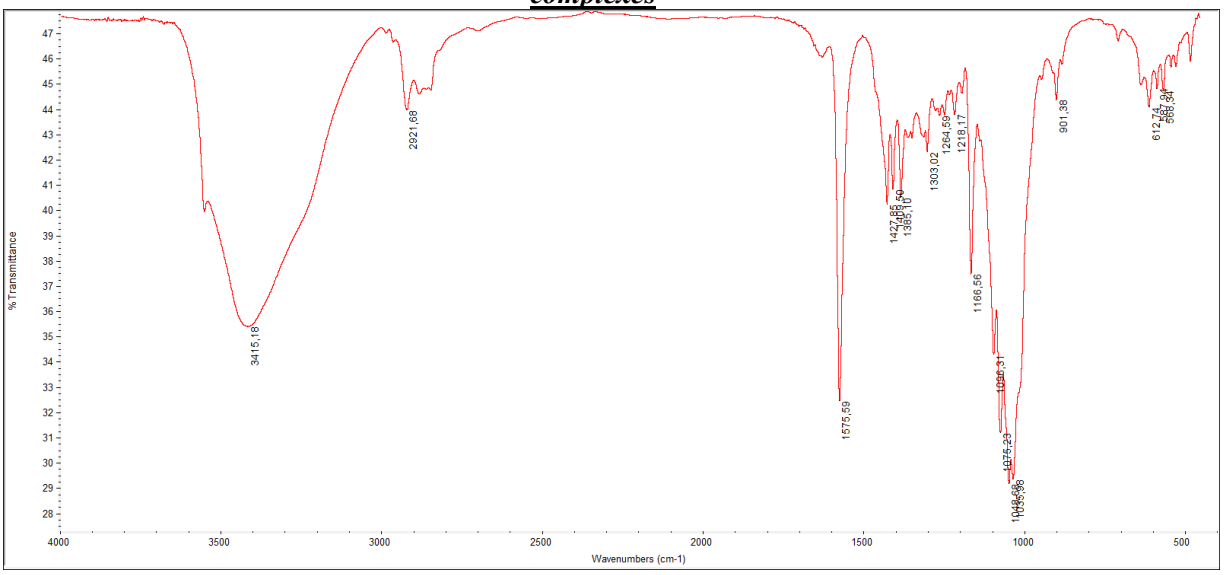

Figure F1. Medium FT-IR (4000-500 cm^{-1}) spectrum of dibromo (O-ethyl, N-methyl, β-D-glucopyranosyl dithiocarbamato) gold(III), [$AuBr_2$(β-D-glucosideDTC)].

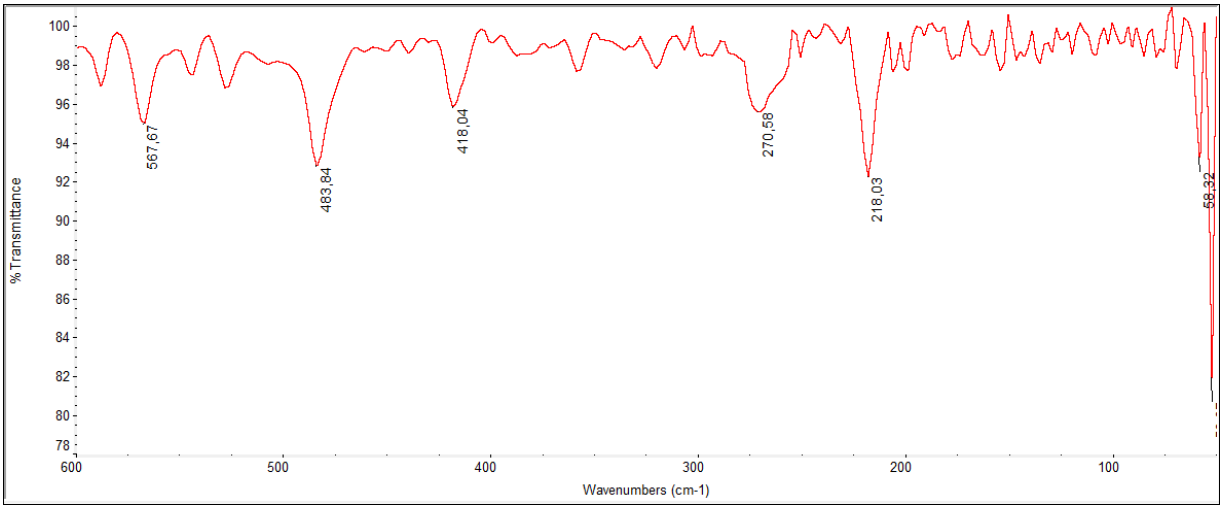

Figure F2. Far FT-IR (600-100 cm^{-1}, nujol) spectrum of dibromo (O-ethyl, N-methyl, β-D-glucopyranosyl dithiocarbamato) gold(III), [$AuBr_2$(β-D-glucosideDTC)].

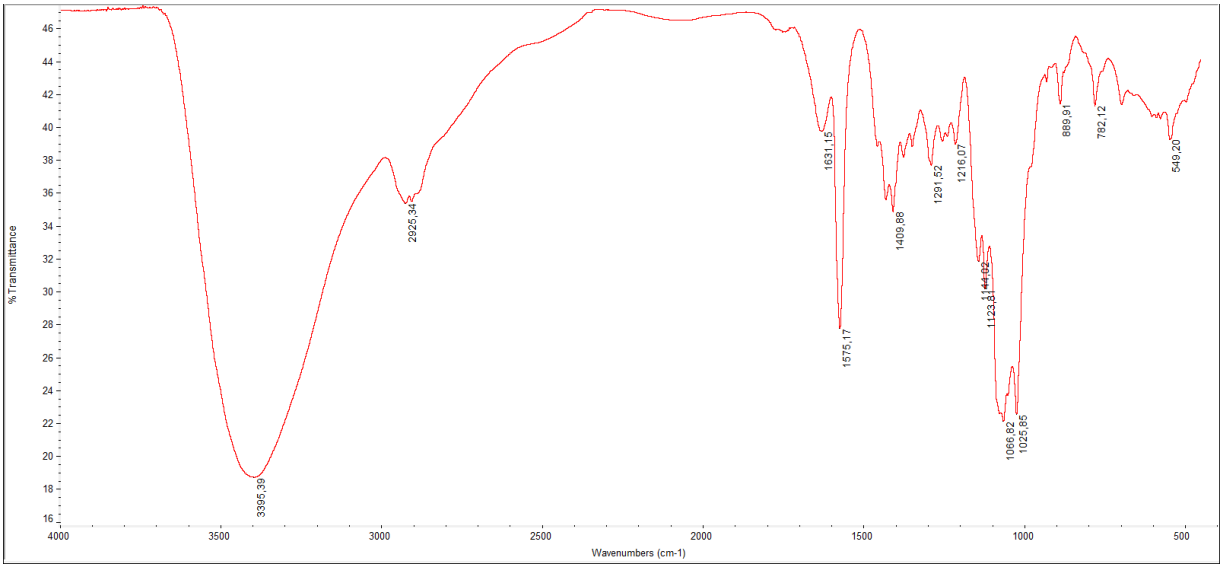

Figure F3. Medium FT-IR (4000-500 cm^{-1}) spectrum of dibromo (O-ethyl, N-methyl, β-D-galactopyranosyl dithiocarbamato) gold(III), [$AuBr_2$(β-D-galactosideDTC)].

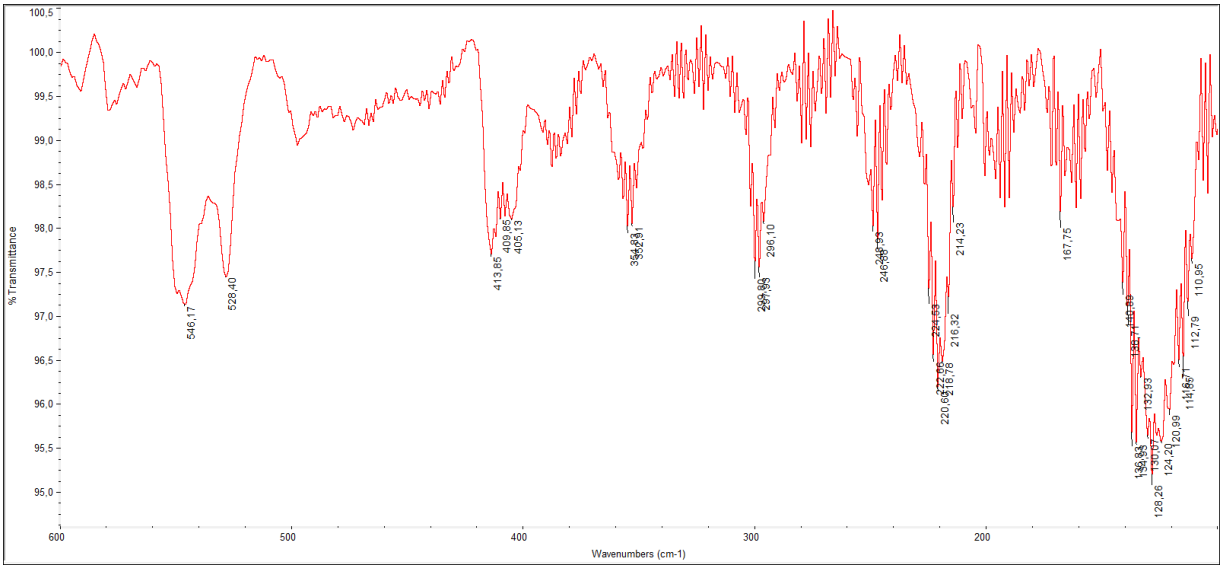

Figure F4. Far FT-IR (600-100 cm^{-1}, nujol) spectrum of dibromo (O-ethyl, N-methyl, β-D-galactopyranosyl dithiocarbamato) gold(III), [$AuBr_2$(β-D-galactosideDTC)].

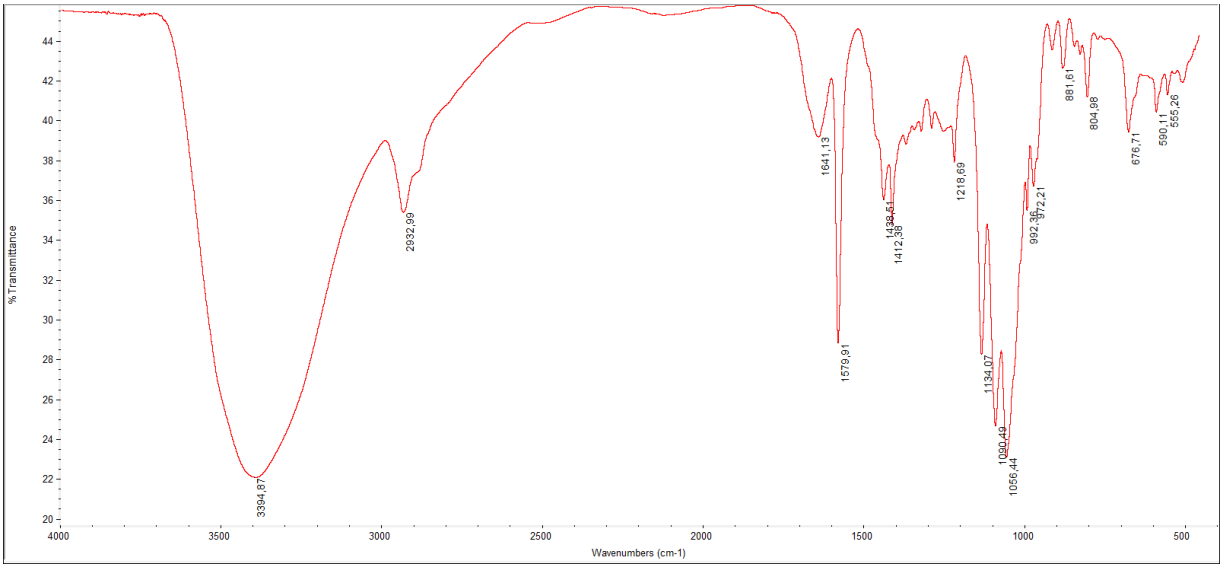

Figure F5. Medium FT-IR (4000-500 cm^{-1}) spectrum of dibromo (O-ethyl, N-methyl, α-D-mannopyranosyl dithiocarbamato) gold(III), [$AuBr_2$(α-D-mannosideDTC)].

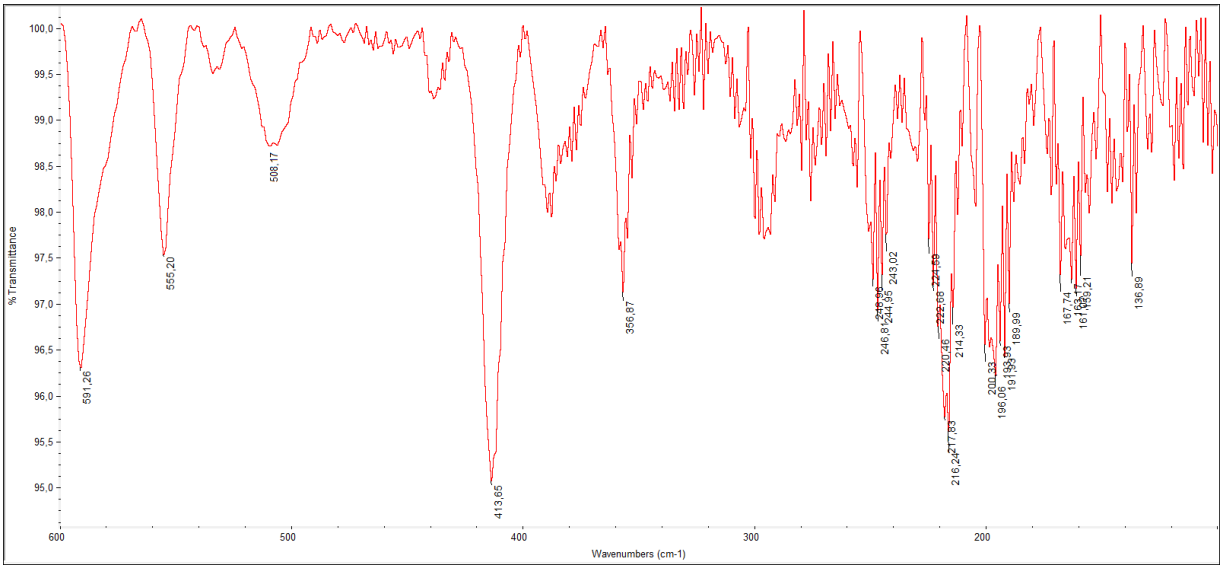

Figure F6. Far FT-IR (600-100 cm^{-1}, nujol) spectrum of dibromo (O-ethyl, N-methyl, α-D-mannopyranosyl dithiocarbamato) gold(III), [$AuBr_2$(α-D-mannosideDTC)].

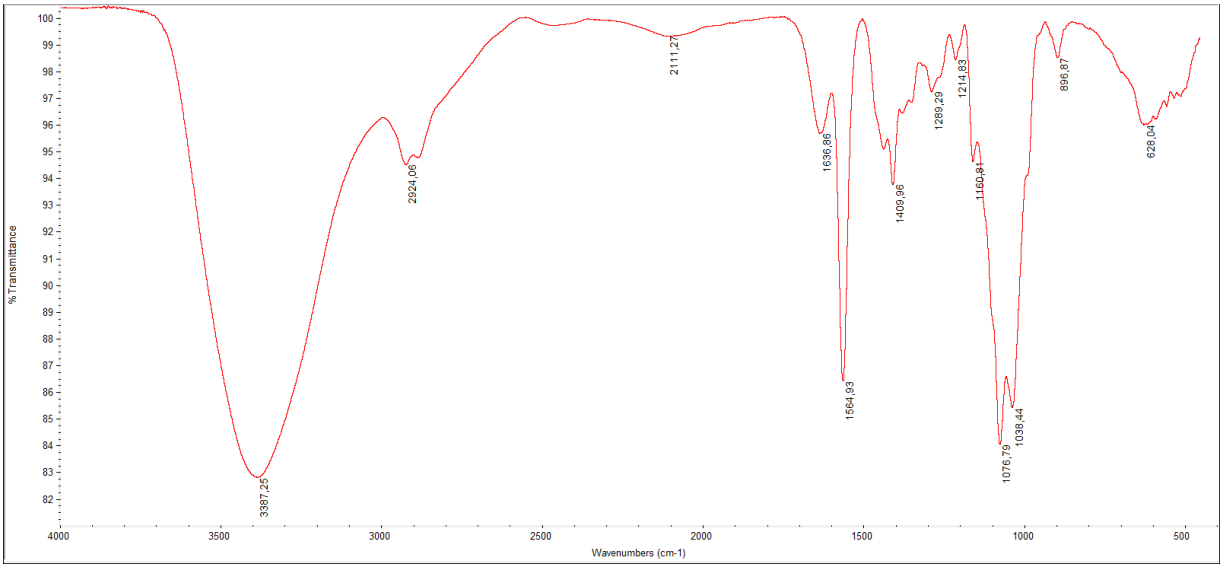

Figure F7. Medium FT-IR (4000-500 cm^{-1}) spectrum of bis(O-ethyl, N-methyl, β-D-glucopyranosyl dithiocarbamato) gold(III) chloride, $[Au(\beta\text{-D-glucosideDTC})_2]Cl$.

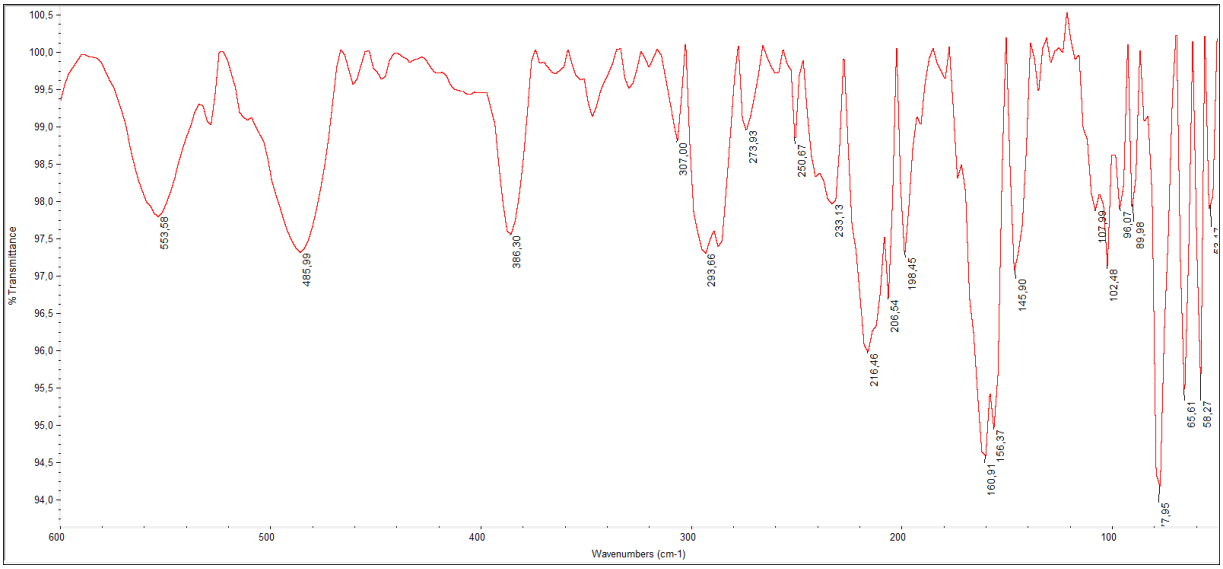

Figure F8. Far FT-IR (600-100 cm^{-1}, nujol) spectrum of bis(O-ethyl, N-methyl, β-D-glucopyranosyl dithiocarbamato) gold(III) chloride, $[Au(\beta\text{-D-glucosideDTC})_2]Cl$.

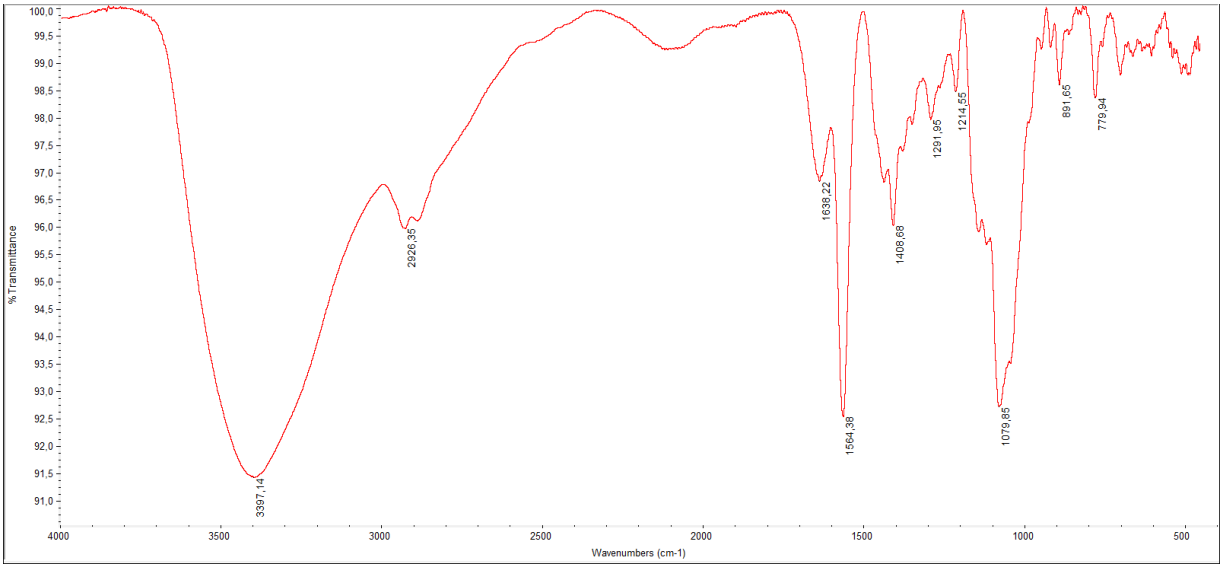

Figure F9. Medium FT-IR (4000-500 cm^{-1}) spectrum of bis(O-ethyl, N-methyl, β-D-galactopyranosyl dithiocarbamato) gold(III) chloride, $[Au(\beta\text{-D-galactosideDTC})_2]Cl$.

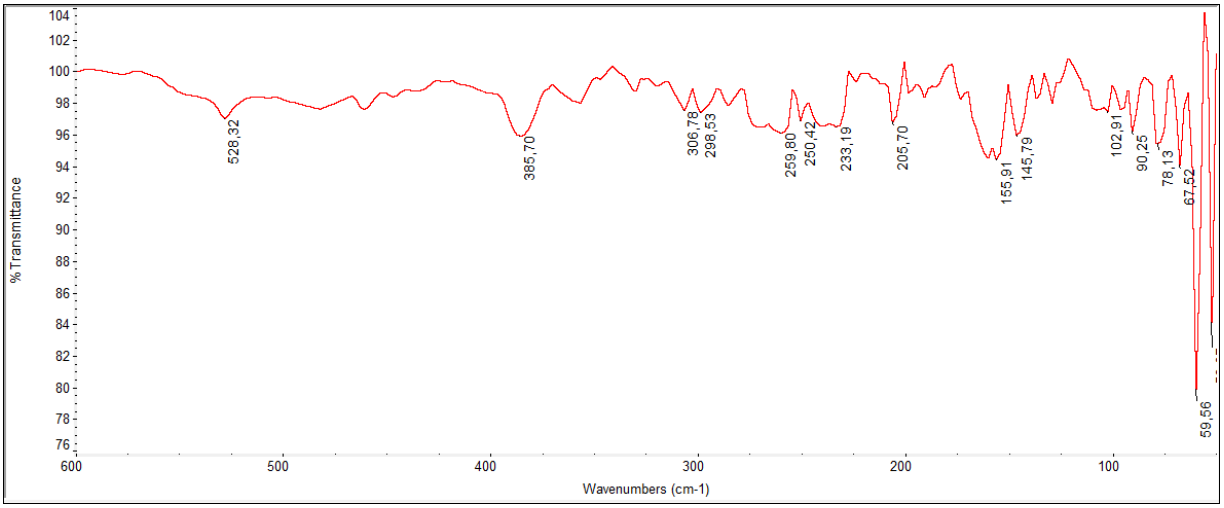

Figure F10. Far FT-IR (600-100 cm^{-1}, nujol) spectrum of bis(O-ethyl, N-methyl, β-D-galactopyranosyl dithiocarbamato) gold(III) chloride, $[Au(\beta\text{-D-galactosideDTC})_2]Cl$.

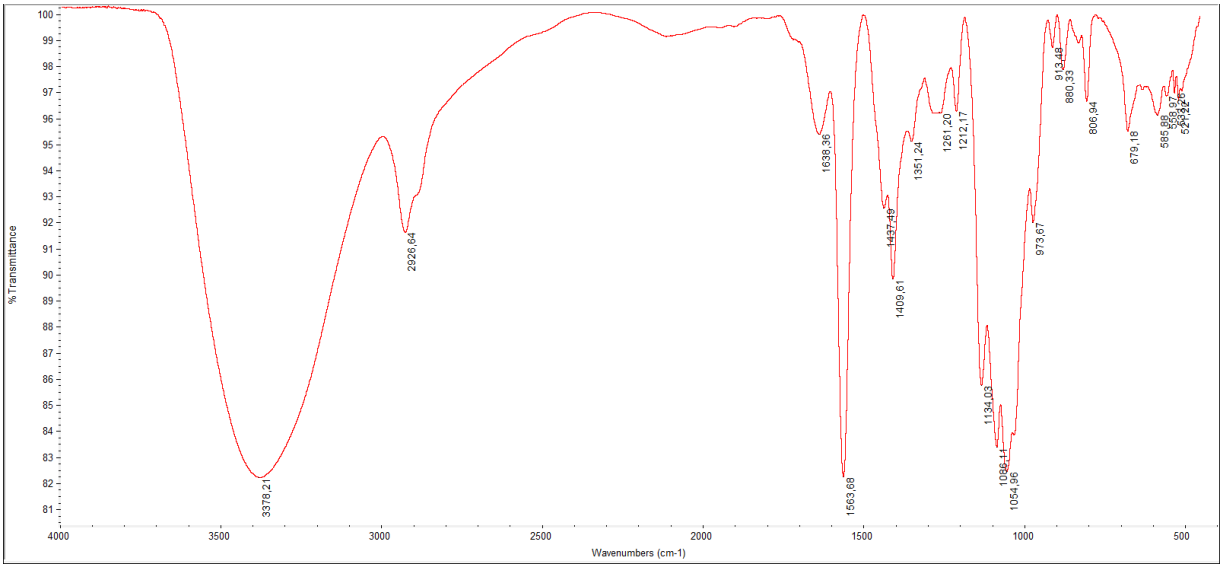

Figure F11. Medium FT-IR (4000-500 cm^{-1}) spectrum of bis(O-ethyl, N-methyl, α-D-mannopyranosyl dithiocarbamato) gold(III) chloride, $[Au(\alpha\text{-D-mannosideDTC})_2]Cl$.

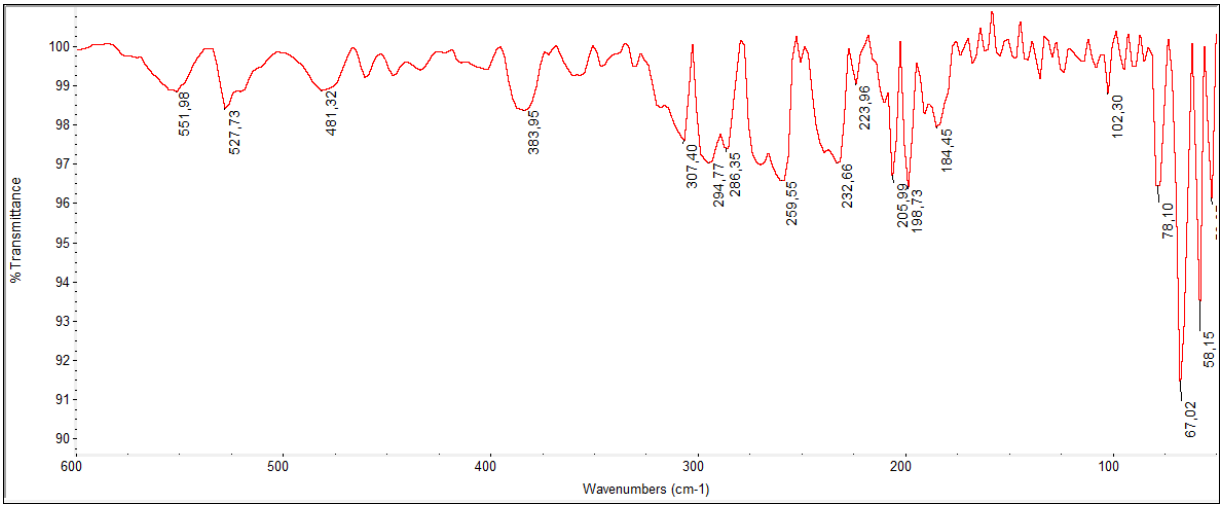

Figure F12. Far FT-IR (600-100 cm^{-1}, nujol) spectrum of bis(O-ethyl, N-methyl, α-D-mannopyranosyl dithiocarbamato) gold(III) chloride, $[Au(\alpha\text{-D-mannosideDTC})_2]Cl$.

Supporting Information G: FTIR spectra of the synthetized glycosylated dithiocarbamato Cu(II) complexes

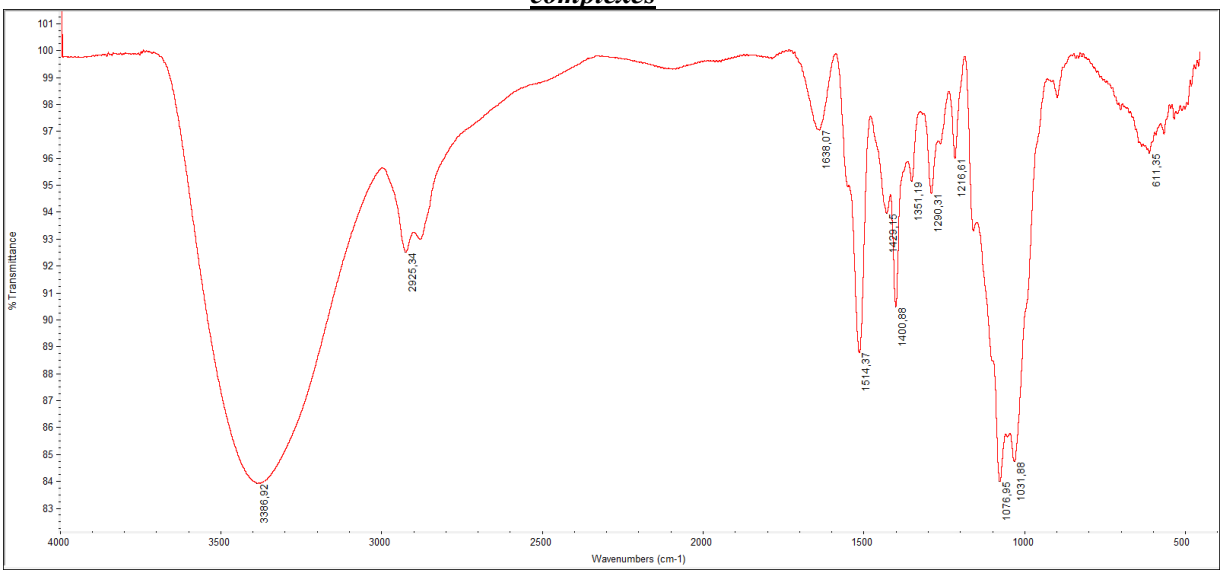

Figure G1. Medium FT-IR (4000-500 cm^{-1}) spectrum of bis(O-ethyl, N-methyl, β-D-glucopyranosyl dithiocarbamato) copper(II), [Cu(β-D-glucosideDTC)$_2$].

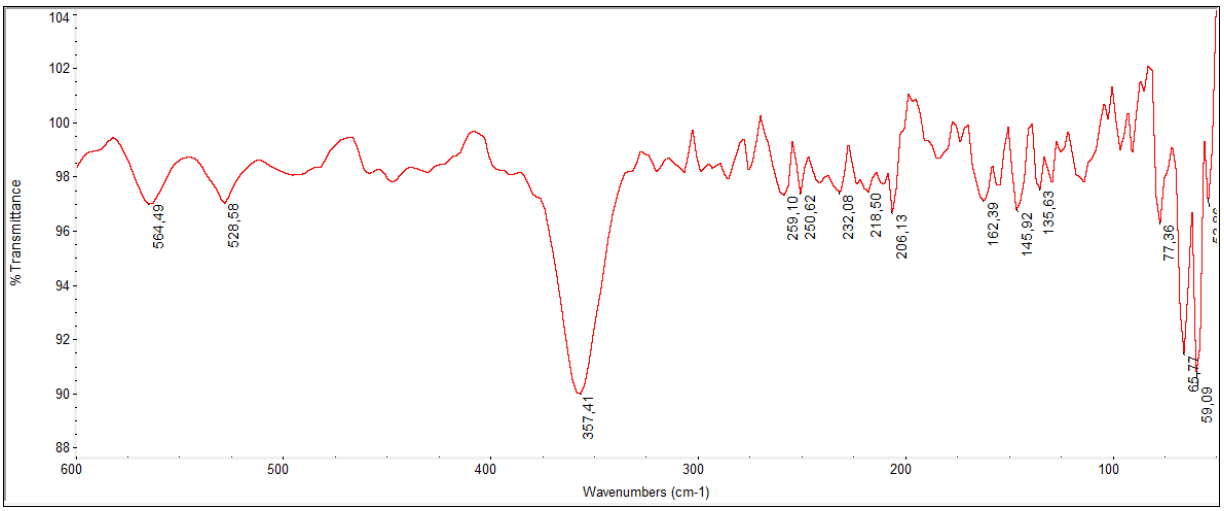

Figure G2. Far FT-IR (600-100 cm^{-1}, nujol) spectrum of bis(O-ethyl, N-methyl, β-D-glucopyranosyl dithiocarbamato) copper(II), [Cu(β-D-glucosideDTC)$_2$].

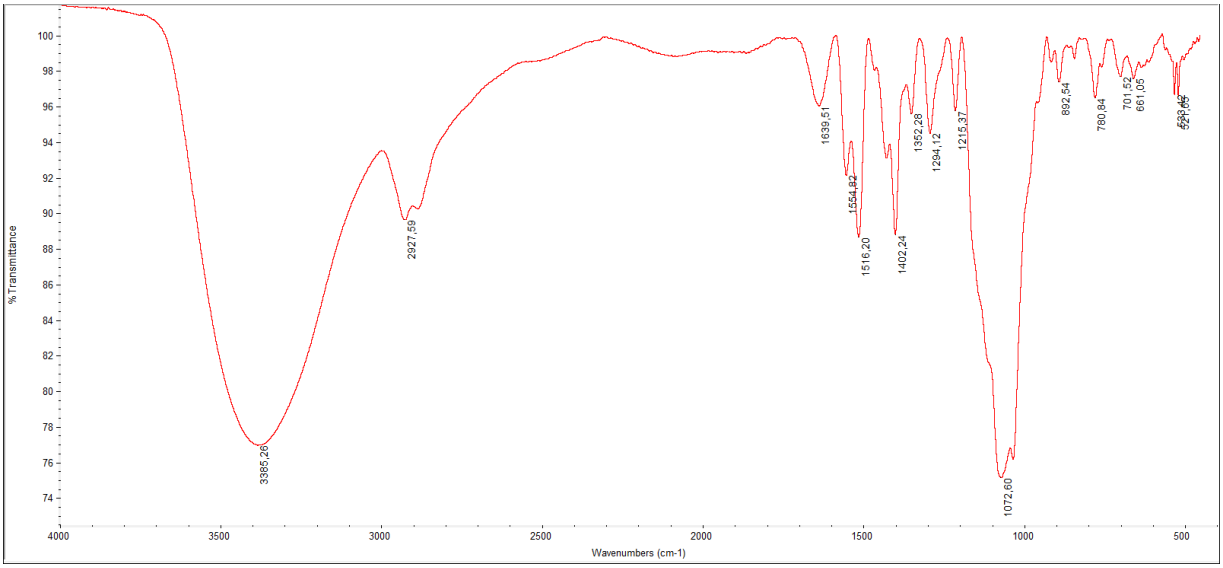

Figure G3. Medium FT-IR (4000-500 cm^{-1}) spectrum of bis(O-ethyl, N-methyl, β-D-galactopyranosyl dithiocarbamato) copper(II), [Cu(β-D-galactosideDTC)$_2$].

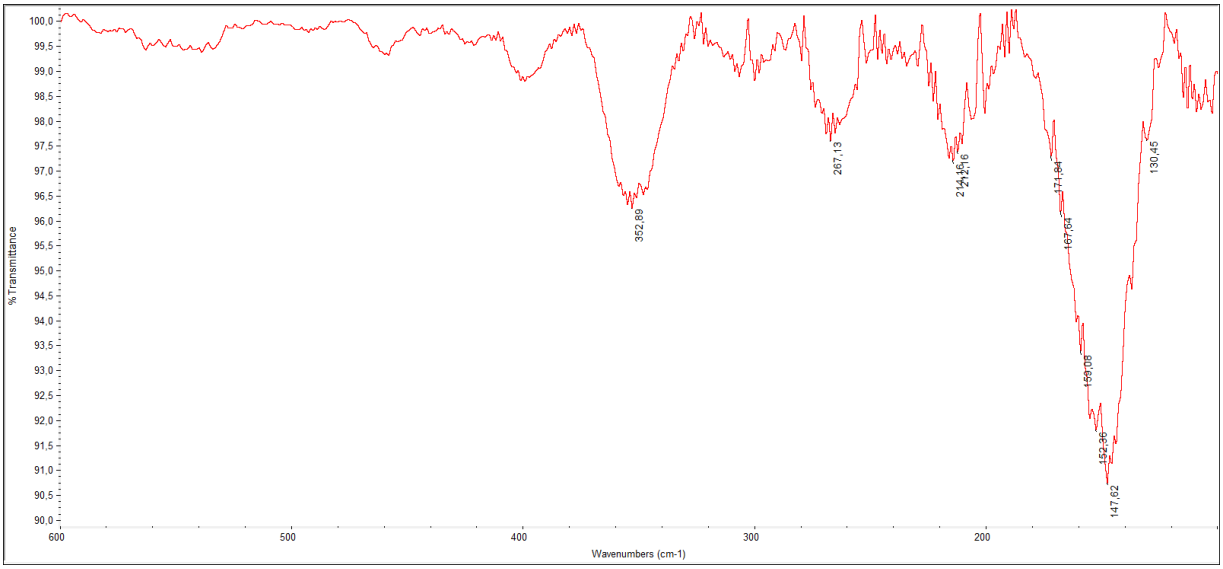

Figure G4. Far FT-IR (600-100 cm^{-1}, nujol) spectrum of bis(O-ethyl, N-methyl, β-D-galactopyranosyl dithiocarbamato) copper(II), [Cu(β-D-galactosideDTC)$_2$].

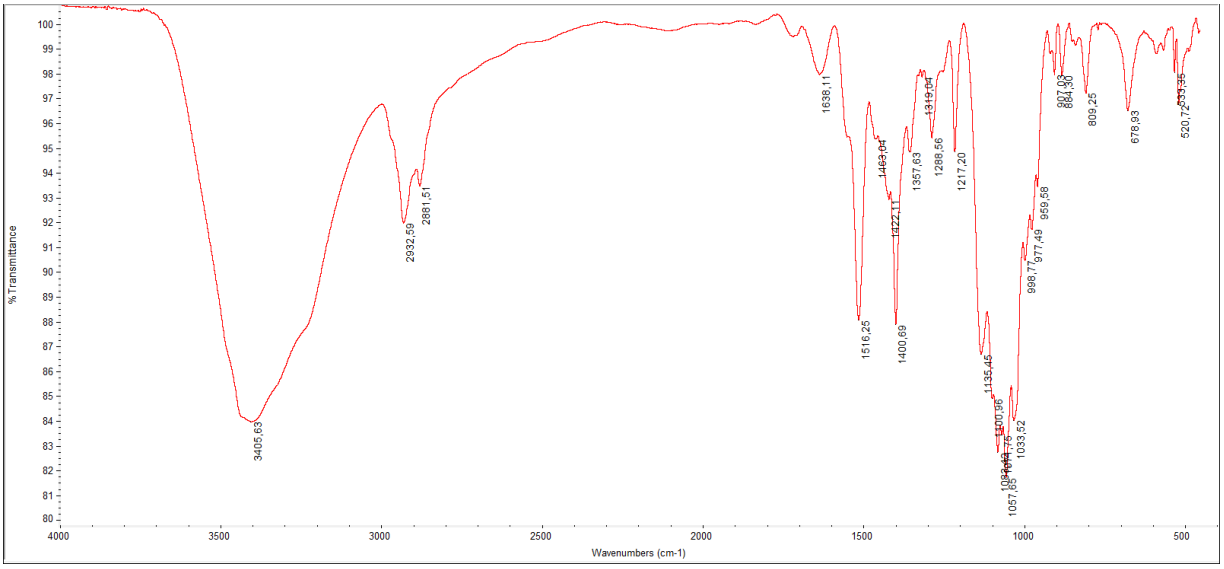

Figure G5. Medium FT-IR (4000-500 cm^{-1}) spectrum of bis(O-ethyl, N-methyl, α-D-mannopyranosyl dithiocarbamato) copper(II), [Cu(α-D-mannosideDTC)$_2$].

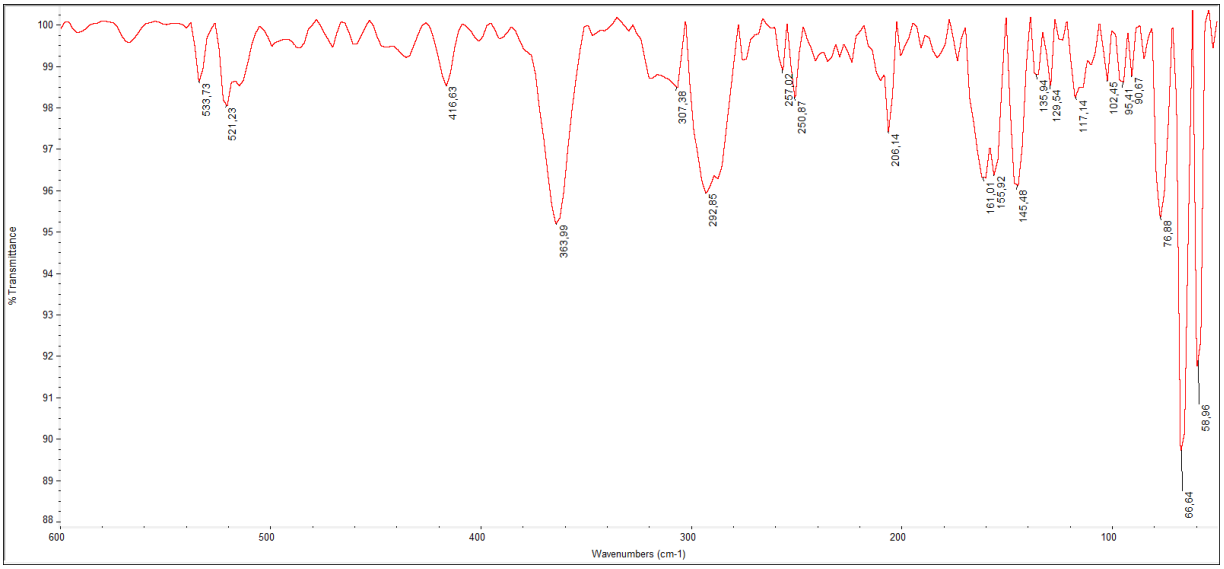

Figure G6. Far FT-IR (600-100 cm^{-1}, nujol) spectrum of bis(O-ethyl, N-methyl, α-D-mannopyranosyl dithiocarbamato) copper(II), [Cu(α-D-mannosideDTC)$_2$].

Congress Participations, Communications and Publications during the Ph.D. Studies

Congress participations

- 11th International Symposium in Biomedical Polymers and Regenerative Medicine, *FBPS 2015*, July 8th-11th 2015, Riva del Garda (Italy)
- 1st International Symposium on Clinical and Experimental Metallodrugs In Medicine: Cancer Chemotherapy *(1st CEMM)*, December 11th-13th 2015, Honolulu, Hawaii (USA).
- 3rd Liver Gymnasium - pre-meeting. Padova (Italy), September 22th 2016.
- European School of Medicinal Chemistry *(ESMEC 2017),* July 2th-6th 2017, Urbino (PU), Italy.

Conference proceedings

- C. Nardon, N. Pettenuzzo, M. Paro, D. Fregona, "Novel inorganic chemotherapeutics for cancer treatment", Proc. 6th European Conference on Chemistry for Life Sciences (6th ECCLS), Lisbon (Portugal), June 10th-12th 2015 (oral).
- R. Luisetto, C. Nardon, F. Lette de Oliveira, N. Bassi, L. Brustolin, N. Pettenuzzo, D. Fregona, L. Punzi, A. Doria, "Studio pilota sull'efficacia di una formulazione micellare contenente un complesso di Au(III) nel trattamento dell'artrite sperimentale da collagene nel topo", Congresso Nazionale SIR (Società Italiana Reumatologia), Rimini (Italy), November 25th-28th 2015 (oral).
- M. Beggio, R. Luisetto, C. Nardon, F. Lette de Oliveira, N. Bassi, L. Brustolin, N. Pettenuzzo, A. Ghirardello, D. Fregona, A. Doria, "Efficacy of a micellar formulation of Au(III) complex in collagen induced arthritis", 10th International Congress on Autoimmunity, Leipzig (Germany), April 6th-10th 2015 (poster).
- N. Pettenuzzo, L. Brustolin, C. Nardon, D. Fregona, "An excellence in medicinal inorganic chemistry: a portrait of the gold(I/III) complexes patented for theraputic purposes from 2010 to 2015", Proc. 1st International Symposium on "Clinical and experimental metallodrugs in medicine: cancer chemotherapy", Honolulu (HI), USA, December 12th-15th 2015 (poster).

- C. Nardon, L. Brustolin, N. Pettenuzzo, D. Fregona, "Exploring new strategies to overcome the drug Death Valley in oncology", 2nd International Conference on "Clinical Sciences and Drug Discovery", July 27th-29th 2016, Dundee (Scotland) (oral).
- C. Nardon, N. Pettenuzzo, L. Brustolin, D. Fregona, "The current horizon of gold-based therapeutics: from chemical features to benefits", XLVI Congresso Nazionale della Divisione di Chimica Inorganica della Società Chimica Italiana, Padova (Italy), September 13th-17th 2016 (oral).
- C. Nardon, L. Brustolin, N. Pettenuzzo, S. Scintilla, A. Accardo, G. Morelli, S. Salmaso, P. Caliceti, D. Fregona, "Natural and synthetic macromolecules as carriers for metal-based anticancer chemotherapeutics: an in vitro and in vivo survey", Convegno Nazionale della Divisione di Chimica dei Sistemi Biologici della Società Chimica Italiana – Verona (Italy), September 21th-23th 2016 (oral).
- L. Brustolin, C. Nardon, N. Pettenuzzo, S. Quarta, P. Pontisso, D. Fregona, "Groundbreaking metalbased anticancer agents in the treatment of hepatocellular carcinoma", 3rd Liver Gymnasium - premeeting, Padova (Italy), 22th September 2016 (oral).
- N. Pettenuzzo. Metal-Based Dithiocarbamato Derivatives as Targeting Anticancer Therapy: A Novel Strategy, European School of Medicinal Chemistry *(ESMEC 2017*), July 2th-6th 2017, Urbino (PU), Italy (poster).

Peer-reviewed papers

- Nardon, C.; Pettenuzzo, N.; Fregona, D. Gold complexes for therapeutic purposes: An updated Patent review (2010-2015). *Curr. Med. Chem.*, **2016**, *23(29)*, 3374-3403.
- Nardon, C.; Boscutti, G.; Gabbiani, C.; Massai, L.; Pettenuzzo, N.; Fassina, A.; Messori, L.; Fregona, D. Cell and Cell-Free Mechanistic Studies on Two Gold(III) Complexes with Proven Antitumor Properties. *Eur. J. Inorg. Chem.*, **2017**, *12*, 1737-1744.
- Tomasello, M.F.; Nardon, C.; Lanza, V.; Di Natale, G.; Pettenuzzo, N.; Salmaso, S.; Milardi, D.; Caliceti, P.; Pappalardo, G.; Fregona, D. New comprehensive studies of a gold(III) Dithiocarbamate complex with proven anticancer properties: Aqueous dissolution with cyclodextrins, pharmacokinetics and upstream inhibition of the ubiquitin-proteasome pathway. *Eur. J. Med. Chem.*, **2017**, *138*, 115-127.

Patents

- Italian patent n. 102016000122363 (Title: COMPOSTI DI COORDINAZIONE, SINTESI, NANOFORMULAZIONE ED USO DEGLI STESSI IN ONCOLOGIA); Inventors: D. Fregona, C. Nardon, L. Brustolin, N. Pettenuzzo; Filing: December 2, 2016.
- Italian patent n. 102016000122406 (Title: COMPOSTI DI COORDINAZIONE, SINTESI, NANOFORMULAZIONE ED USO DEGLI STESSI IN ONCOLOGIA); Inventors: D. Fregona, C. Nardon, L. Brustolin, N. Pettenuzzo; Filing: December 2, 2016.

Participation to national and international events on Innovation

- OneStart (World's largest healthcare accelerator) European Business Bootcamp: member of the research team ranked among the 40 Semifinalists starting from 750 teams. London (UK), February 5th-6th 2016.
- OneStart Final Phase (World's largest healthcare accelerator): member of the research team ranked among the 10 Finalists starting from 750 teams. From February to May 2016 constantly supervised by two Pharma mentors by conference calls followed by exams and drawing up of a Business Plan. The Top-10 exam and the Final Gala held in London (UK) on 12th May, 2016.
- StartCup Veneto, Ed. 2017: member of the research team selected as one of the 10 Finalist team among 90; Organized by the Universities of Padova, Verona and Venezia. Padova (IT), July 10th, 2017.
- StartCup Veneto, Ed. 2017: member of the research team selected as the Winner of the competition among 90 participants; Organized by the Universities of Padova, Verona and Venezia. Verona (IT), October 26th, 2017.